The Fanconi anemia pathway and HELQ work alongside dormant replication origins to suppress replication-associated genome instability

A DISSERTATION SUBMITTED TO THE FACULTY

OF THE UNIVERSITY OF MINNESOTA

BY

SPENCER WILLIAM LUEBBEN

IN PARTIAL FULFILLMENT OF THE REQUIREMENTS

FOR THE DEGREE OF

DOCTOR OF PHILOSOPHY

Naoko Shima, Ph.D.

Advisor

In the Month of July, Year 2014.

Acknowledgements

I would first like to wholeheartedly thank my adviser, Dr. Naoko Shima, for all of her guidance during the past five years. Her love for science and enthusiasm for my own projects has made these studies every bit as rewarding as I had hoped. She has taught me to put forth my best effort in everything and has made me a much better person.

I must also thank Dr. Tsuyoshi Kawabata, who was an outstanding co-worker to have throughout my graduate career. His continual willingness to teach and help me in my projects was essential in basically all aspects of my work. I thank all undergraduate researchers (especially Katie Haberle, Susan Yeung, Wai Long Lee, Hannah Fuher and Naomi Do) for all of their help in genotyping mice and assisting with my experiments.

I thank all of my committee members, Drs. Duncan Clarke, David Largaespada, Alexandra Sobeck, Anindya Bagchi, Kaylee Schwertfeger and York Marahrens for all their guidance. Dr. Sobeck's help to polish our manuscripts and provide helpful discussions about FA pathway function are especially appreciated. I thank all my classmates for being awesome friends and helping me so much through the first years of the program. I thank the entire GCD department and the staff of the MCDB&G program for making my graduate studies possible. A special thanks goes out to Sue Knoblauch for her continual assistance in keeping me on track for graduation.

Finally, I sincerely thank my wife, family and friends for their love and support throughout my lifetime.

Dedication

This dissertation is dedicated to my Lord and Savior, Jesus Christ, through whom all things are possible.

Abstract

DNA replication is continually impeded by endogenous lesions that cause the stalling of replication forks. If left unchecked, this threatens the integrity of the genome and may be a driver of cancer development. Utilizing the *Mcm4*^{chaos3} mouse model, we found that dormant replication origins, which act as backup initiation sites, play a critical role in the recovery of stalled replication forks. A reduced number of dormant origins in these mice led to persistently stalled forks, incomplete replication and the mis-segregation of sister chromatids in mitosis, causing elevated genome instability.

Mcm4$^{chaos3/chaos3}$ cells also displayed intrinsic activation of the Fanconi anemia (FA) pathway, suggesting that it too plays a functional role in fork progression. Indeed, disruption of FA pathway activation in the *Mcm4*$^{chaos3/chaos3}$ background led to an even higher number of persistently stalled forks. Furthermore, we discovered that a lack of dormant origins also leads to delayed replication, as seen by extremely late DNA synthesis. Accordingly, concomitant loss of both mechanisms led to heightened genomic instability, causing mice to either die shortly after birth or exhibit accelerated tumorigenesis.

Finally, we investigated if *HELQ* is perhaps another FA gene by characterizing the first *Helq* mutant mouse model (*Helq*^{gt}). *Helq*$^{gt/gt}$ cells/mice displayed modest FA-like phenotypes such as interstrand crosslink hypersensitivity and hypogonadism, but not defects in homologous recombination repair. Rather, HELQ was found to work in parallel to the FA protein FANCC to suppress replication-associated genome instability.

Table of Contents

List of Tables

CHAPTER II: Stalled Fork Rescue via Dormant Replication Origins in Unchallenged S Phase Promotes Proper Chromosome Segregation and Tumor Suppression

CHAPTER III: A Concomitant Loss of Dormant Origins and FANCC Exacerbates Genome Instability by Impairing DNA Replication Fork Progression

CHAPTER IV: *Helq* Acts in Parallel to *Fancc* to Suppress Replication-associated Genome Instability

List of Figures and Movies

CHAPTER II: Stalled Fork Rescue via Dormant Replication Origins in Unchallenged S Phase Promotes Proper Chromosome Segregation and Tumor Suppression

CHAPTER III: A Concomitant Loss of Dormant Origins and FANCC Exacerbates Genome Instability by Impairing DNA Replication Fork Progression

CHAPTER IV: *Helq* Acts in Parallel to *Fancc* to Suppress Replication-associated Genome Instability

CHAPTER I: Introduction

Introduction

All of the information required for the formation and maintenance of a human organism is stored in its DNA. The diploid human genome, consisting of 6 billion base pairs spread out over 23 pairs of chromosomes, resides in all the nuclei of the trillions of cells that make up the human body. Despite this complexity, research throughout the past few decades has provided fascinating insights into how the cell is able to accurately duplicate (DNA replication) and maintain (DNA repair) the integrity of all this genetic information throughout our lifetimes. Such information is vital to our understanding of human health, as even a single mutation in the genetic code can lead to birth defects, genetic disorders or the development of cancer.

Replication is made more difficult due to the fact that the DNA can be damaged by a number of both exogenous environmental agents as well as endogenous chemical alterations during DNA metabolism[1]. Damaged sites cannot be processed by the high-fidelity replicative polymerases and if found on the leading strand template, on which synthesis is continuous, the replication fork can stall. If left in this state, large regions of the genome could go unreplicated and be lost in subsequent daughter cells. This would lead to the loss of significant amounts of genetic information that could wreck havoc on the integrity of the genome.

To guarantee that replication is complete, cells possess many strategies for the recovery of stalled forks[2]. One solution that seems most simple is to newly initiate DNA synthesis at a nearby adjacent region of the DNA. This is achieved through the firing of

dormant replication origins that exist in excess throughout the genome. However, if dormant origins are unavailable or prove inappropriate for certain lesions, specialized proteins can be recruited to help the fork progress past the lesion. For example, error-prone translesion synthesis (TLS) polymerases can be temporarily recruited to directly bypass the lesion by inserting any base across from the damaged site. In addition, a homology-directed mechanism can replicate past the lesion in an error-free manner by temporarily switching the template to the newly-synthesized sister chromatid strand. This requires the homologous recombination (HR) machinery. Members of the Fanconi anemia (FA) pathway may play a key role in regulating these latter two mechanisms, though exactly how this occurs remains elusive.

This chapter will provide pertinent background information regarding how these mechanisms promote the complete replication of the genome. First, we will discuss how cells separate the events of "origin licensing" from "origin firing" to achieve precisely one new copy of the DNA after replication. Importantly, excess ("dormant") origins produced through the licensing process are needed to fully complete replication and prevent tumors in mice. We will also discuss how certain regions of the genome called common fragile sites (CFSs) are intrinsically difficult to replicate due to a lack of origins and thus depend on the FA pathway for their stability. Multiple lines of evidence suggest that the FA pathway plays a critical role in the recovery of spontaneously stalled forks, and loss of this pathway leads to the human cancer susceptibility disease Fanconi anemia. Finally, the potential role of a candidate FA gene, *HELQ*, will also be explored. Together, this body of information shows how cells utilize a multi-layered system,

including dormant origins and the FA pathway, to ensure complete replication and prevent chromosome instability that may otherwise lead to cancer.

DNA replication: origin licensing and origin firing

In order for replication to commence, the DNA double helix must initially be opened at special starting loci called replication origins. In bacteria, such as *E. coli*, this occurs at a single, sequence-specific element. A single pair of replication forks initiated at this site is sufficient to replicate the entire circular genome. However, the human genome is about 700 times larger than the *E. coli* genome and replication forks proceed about 20-fold more slowly. It would therefore take at least 20 days to achieve one round of replication if there were only one origin per chromosome[3].

In order to efficiently replicate larger and more complex genomes, mammalian cells activate approximately 30,000-50,000 origins at each S phase[4]. Accordingly, shorter distances between activated origins means less time to complete replication. However, this brings the added complexity of making sure that the DNA is fully replicated without activating the same origins more than once, which would lead to re-replication[5]. Eukaryotic cells solve this problem by temporally separating DNA replication into two sequential steps of "origin licensing" and "origin firing". While origin licensing determines all origin sites exclusively during the late M and early G1 phases, origins can only be activated to fire upon entry into S phase, during which licensing is inhibited.

Origin licensing entails the formation of pre-replicative complexes (pre-RCs) at prospective origin sites. This begins when a six-membered origin recognition complex (ORC) binds to origin loci. In the budding yeast *Saccharomyces cerevisiae*, this occurs exclusively at regions containing a specific sequence element called an autonomously replicating sequence (ARS)[6]. In other eukaryotes, however, there are no clear origin consensus sequences and the ORC proteins, though evolutionarily conserved, don't maintain their sequence specificity. Rather, origins appear to be determined by a complex combination of general sequence elements (AT-rich regions), chromatin context and transcriptional activity[3].

Once ORC is bound to origin sites, two proteins called cell division cycle 6 (CDC6) and chromatin licensing and DNA replication factor 1 (CDT1) work together to load the heterohexameric MCM2-7 complexes onto the chromatin[7-13]. Comprised of the essential, conserved and structurally related minichromosome maintenance proteins 2 through 7, MCM2-7 is a core component of the replicative helicase[14-19]. These proteins derive their name from the original screen performed in budding yeast for mutants that were unable to fully replicate and thereby maintain mini-chromosomes containing a single origin[20]. As they will later travel with bidirectional replication forks, MCM2-7 complexes are loaded onto the chromatin as double hexamers[21-23]. At this point, any locus containing a pair MCM2-7 hexamers is considered licensed (complete pre-RC) and is competent to initiate firing if activated[24-26]. It is now understood that a single ORC can load several MCM2-7 double hexamers onto origin sites, and it is estimated that there is anywhere from a 10- to 40-fold excess of origins that are normally licensed compared to

the number of ORC-bound sites or the number of functional origins[24,27,28]. Because this vastly exceeds the number of origins which are sufficient to complete replication[29,30], researchers originally referred to this phenomenon as the "MCM paradox"[31]. The significance of such excess or "dormant" origins will be discussed in detail below.

Three overall mechanisms are at work in eukaryotic cells to make sure that origin licensing is restricted to the late M and early G1 phases. First, S and M phase specific cyclin-dependent kinases (CDKs) function to degrade or re-localize several pre-RC components during S phase and mitosis[32-35]. The other two mechanisms involve the regulation of CDT1, which can either be bound and inhibited by the protein Geminin[36-40] or targeted for proteolytic degradation by the CUL4/DDB1 ubiquitin ligase[41-43]. Because the anaphase-promoting complex/cyclosome (APC/C), which causes ubiquitin-mediated degradation of Geminin and mitotic cyclins, is active during G1 phase[36,44] and because CUL4-DDB1-dependent degradation of CDT1 requires chromatin-bound PCNA[45,46], these three inhibitory mechanisms are inactive in G1 phase so that licensing can occur.

Once cells enter into S phase, licensed origins (or pre-RCs) are then converted to pre-initiation complexes (pre-ICs) through the recruitment of several "firing factors". Cell division cycle 45 (CDC45) and the GINS complex (GINS stands for "Go, Ichi, Nii and San" or "5, 1, 2 and 3" in Japanese) combine with MCM2-7 to form the CMG helicase, the complete replicative helicase essential for replication initiation as well as elongation[47-54]. This requires a host of other factors, including the kinases CDC7-DBF4 (DDK) and CDK. While DDK phosphorylates multiple MCM subunits[55-58], CDK

phosphorylates RECQL4 and Treslin, which work together with TOPBP1 to promote the interaction of CDC45 and GINS with MCM2-7[59-63]. Other factors such as MCM10[64,65], GEMC1[66], DUE-B[67] and Idas[68] also appear to be required for initiation in higher eukaryotes, with MCM10 playing an additional role in elongation[64,69].

After pre-ICs have formed, initiation complexes can be completed through the recruitment of the replicative polymerases and other replisome components. Origins can then be fired to generate bidirectional replication forks. Because MCM2-7 hexamers travel with each fork as the replicative helicases[70,71] this returns fired origins to the unlicensed state. Inactive MCM2-7 complexes and other pre-RC components are then passively displaced from the chromatin as active replisomes pass through them[30,72,73]. All origins do not fire at once, but are activated throughout S phase (early to late) in a distinct program determined by both chromatin context[74-76] and the availability of limiting firing factors[77-81].

Dormant replication origins

As mentioned previously, eukaryotic cells license an excessive number of potential origins compared to the number that are needed to complete replication under normal conditions. Still, early studies indicated that reduced MCM levels compromised both origin licensing and genome stability in yeast[82,83], suggesting that excess origins might have an important function after all.

In light of the fact that new origins cannot be licensed once S phase begins, it was proposed that this excessive licensing protects cells from the possibility of incomplete replication under conditions of replicative stress. In 2006, Woodward et al. analyzed DNA replication kinetics in *Xenopus laevis* egg extracts in which the chromatin was manipulated to be either "minimally licensed" or "maximally licensed"[30]. While minimally licensed chromatin replicated poorly in the presence of low levels of replication inhibitors, maximally licensed chromatin was able to maintain complete replication by activating additional origins that would have otherwise remained dormant (hence the name "dormant origins"). Furthermore, the authors showed that treatment of *Caenorhabditis elegans* with a small interfering RNA (siRNA) targeting *MCM7* caused a drastic hypersensitivity to the replication inhibitor hydroxyurea (HU)[84], indicating a physiologically important role of dormant origins in normal replication. This led the authors to propose a model in which dormant origins can be seen as a method of stalled fork rescue, ensuring that no region of the genome gets left unreplicated.

Shortly after this, two studies using human cancer cell lines provided clear evidence that dormant origins play a similar role in mammalian cells[25,26]. Up to 50% depletion of MCM2-7 complexes in these cells had little effect on replication kinetics in unperturbed conditions, but co-treatment with replication inhibitors induced chromosome instability and cell death. This suggested a role of dormant origins in preserving genomic stability only in the context of replicative stress.

How exactly dormant origins are activated under stressful conditions was confusing for many years due to the actions of the ATR (ataxia telangiectasia mutated and Rad3-related) kinase. In response to stalled forks, such as those induced by replication stress, ATR and its downstream effector CHK1 were reported to actually inhibit the firing of additional origins[85-88]. This apparent contradiction was eventually resolved in 2010, when it was demonstrated that ATR/CHK1 prevent the global firing of new replication clusters while simultaneously stimulating the local firing of dormant origins in clusters where replication has already begun[89]. This allows cells to efficiently redirect their limited replication resources to active clusters until full replication is achieved[90]. How cells are able to distinguish between local and global origins remains a mystery, though several models have been proposed[91].

Mcm mutant mouse models

The critical role of dormant origins in preserving genomic stability in normal, physiological conditions did not become clear until the characterization of several *Mcm* mutant mouse models. Using a *N*-ethyl-*N*-nitrosourea (ENU) mutagenesis screen for chromosome instability mutants[92], Shima et al. identified *chaos3* (chromosome aberrations occurring spontaneously 3), a mutant allele of the *Mcm4* gene[93]. This allele was found to harbor a point mutation encoding a single amino acid substitution (F345I) in the MCM4 protein. This change was found to significantly reduce overall MCM levels in mouse embryonic fibroblasts (MEFs) homozygous for *chaos3* (*Mcm4*$^{chaos3/chaos3}$),

leading to a lower number of dormant origins. *Mcm4*$^{chaos3/chaos3}$ MEFs also showed an increased number of chromosome breaks after treatment with aphidicolin (APH), an inhibitor of the replicative polymerases α, δ and ε[94-96]. Most striking, however, was the observation that nearly all *Mcm4*$^{chaos3/chaos3}$ females succumbed to mammary tumors with a mean latency of 12 months, suggesting for the first time that dormant origins play a critical role in tumor suppression. Importantly, these findings proved consistent with regards to other MCM subunits, as a hypomorphic *Mcm2* allele in mice also leads to decreased dormant origin usage and tumorigenesis[97,98].

Additional intriguing insights emerged when our lab later discovered that all MEFs derived in a C57BL/6J background display intrinsically lower origin densities when compared to other backgrounds[99], suggesting that such replication kinetics are genetically controlled. *Mcm4*^{chaos3} homozygosity in this context was sufficient to make the active origin density even lower and caused semi-lethality in mice. These findings match well with another group that found that incremental increases or decreases in the amount of chromatin-bound MCMs can modify the phenotypes of *Mcm4*$^{chaos3/chaos3}$ mice[100]. Namely, decreased MCM levels led to accelerated tumor onset or lethality while increased MCM levels significantly delayed tumorigenesis. Together, these findings indicate that it is likely the amount of MCM2-7 complexes loaded on the chromatin that directly impacts genome stability, cell viability and tumor suppression.

A lack of active origins induces fragility at CFSs

In every human genome, there exist certain loci called common fragile sites (CFSs) that are highly prone to chromosome breakage simply due to the fact that they are intrinsically difficult to replicate. These loci were originally identified as sites where gaps, breaks or constrictions formed on metaphase chromosomes under conditions of mild replicative stress, such as APH treatment[101]. Breakage at these sites was termed CFS "expression" and hundreds of such loci have since been identified in the human genome[102].

What makes CFSs particularly difficult to replicate? There seems to be multiple correct answers to this question, none of which are mutually exclusive and may depend on the individual locus or cell type being studied[103,104]. Early studies reported that AT-rich sequences, due to their ability to form secondary structures, can impede the replication machinery and thereby induce fragility in a subset of CFSs[105-108]. The presence of large genes[104,109] and intrinsically late replication timing[110-112] also appear to correlate with fragility. Then in 2011, two very elegant studies provided striking new evidence that fragility at the FRA3B and FRA16C loci were due to either a paucity of replication initiation events[103] or an inability to activate additional origins after fork stalling[108], respectively. These contexts sound very much like a reduction in the number of dormant origins, and indeed, the latter study found an increase in the expression of several CFSs upon knockdown of *MCM3*[108].

The role of the FA pathway in CFS stability

Perhaps unsurprisingly, factors required for the stability of stalled replication forks, such as ATR and CHK1, have been shown to induce CFS expression when absent[113-115]. This also includes the Fanconi anemia (FA) proteins[116], which play a necessary role in fork stabilization/protection[117-119]. In 2005, cells deficient for FA pathway components were shown to display higher frequencies of CFS expression under conditions of replication stress[116]. Treatment with low doses of replication inhibitors induced robust mono-ubiquitination and nuclear localization of FANCD2, key measures of FA pathway activation[120]. Together with the fact that FA pathway activation occurs during normal S phase[117,121], these data strongly implicated the FA pathway in responding to spontaneously stalled forks.

In 2009, it was observed that low levels of APH treatment robustly induced the focus formation of the FA proteins FANCD2 and FANCI at CFSs throughout the G2/M phases[122]. This led the authors to propose that FANCD2/FANCI mark sites of unresolved replication intermediates that go unrecognized by normal checkpoint processes. As these cells progressed into anaphase, it was found that such FANCD2/FANCI foci actually flank structures called DNA ultra-fine bridges (UFBs)[122,123]. UFBs are thin threads of DNA caught between segregating chromosomes that can only be visualized by staining for the BLM or PICH proteins[124,125]. While such structures may be resolved through the actions of PICH/BLM and the FA proteins, they might also represent a pathogenic consequence of under-replicated loci. CFS sequences were also reported to be present in

micronuclei (MN)[122], implicating unresolved replication intermediates in chromosome mis-segregation as well. Finally, another group found that under-replicated loci at CFSs could manifest as a newly identified form of chromosome instability called 53BP1 nuclear bodies (53BP1-NBs)[126]. Though not yet well understood, it was observed that CFSs can "rupture" during their passage through mitosis and are then "shielded" by the 53BP1 protein in the subsequent G1 phase daughter nuclei. Together, these studies reveal that UFBs, MN and 53BP1-NBs are all useful markers of unresolved replication intermediates and may be sources of replication-associated genomic instability. Notably, FA mutant cells have been shown to exhibit increased frequencies of MN[123], 53BP1-NBs[127] and UFBs[128].

Fanconi anemia

The FA pathway derives its name from the human disease Fanconi anemia, a rare genetic disorder that occurs in approximately 1 in every 100,000 births[129]. The disease is characterized at the clinical level by congenital abnormalities, hypogonadism, bone marrow failure (BMF) and a heightened predisposition to cancer, particularly acute myeloid leukemias and squamous cell carcinomas of the head, neck or ano-genital regions[130,131]. It is genetically heterogeneous with 16 different complementation groups having been identified to date, including *FANCA*, *FANCB*, *FANCC*, *FANCD1*/*BRCA2*, *FANCD2*, *FANCE*, *FANCF*, *FANCG*, *FANCI*, *FANCJ*/*BRIP1*/*BACH1*, *FANCL*, *FANCM*, *FANCN*/*PALB2*, *FANCO*/*RAD51C*, *FANCP*/*SLX4* and, most recently,

FANCQ/*ERCC4*[130,132,133]. For a subset of patients, no complementation group has yet been assigned, indicating that other FA genes are yet to be identified.

At the cellular level, FA patient cells display a slight accumulation in G2 phase of the cell cycle with increased numbers of spontaneous chromosome aberrations[134,135]. But the hallmark of these cells is an exquisite hypersensitivity to agents that produce DNA interstrand crosslinks (ICLs), such as mitomycin C (MMC), cisplatin and diepoxybutane[136]. ICLs create a covalent bond between the two DNA strands so that they cannot be opened for either replication or transcription. This makes them extremely toxic to replicating cells and potent chemotherapeutic agents[137]. ICL-inducing agents also cause a drastic increase in chromosome breaks and radial structures in FA cells, and are thus used as the standard method of FA diagnosis[138,139].

Because of this, the molecular details of FA pathway activation have largely been determined by studying its role in ICL repair. The canonical FA pathway is described as having three main tiers. The first includes the 8 members of the FA core complex (FANCA, -B, -C, -E, -F, -G, -L and -M) and their associated co-factors (MHF1, MHF2, FAAP20, FAAP24 and FAAP100)[131,140]. Upon fork stalling, these proteins function together as an E3 ubiquitin ligase, of which FANCL is the catalytic subunit[141], to mono-ubiquitinate the second tier proteins FANCD2 and FANCI. This action allows for the recruitment of FANCD2/FANCI to the chromatin and is considered the key step for pathway activation[120,142,143]. Proteins comprising the third tier are not needed for FANCD2/FANCI mono-ubiquitination and are therefore called the downstream

members. These include FANCD1, -N, -J, -O, -P and -Q. Several of these factors are known to have integral roles in HR and heterozygous mutations in *FANCD1, FANCN, FANCJ,* and *FANCO* cause susceptibility to breast and ovarian cancers[144-149]. Mono-ubiquitinated FANCD2/FANCI coordinates these factors to process the damaged fork. In the case of ICL repair, this involves the excision of the ICL by nucleases[150-154], bypassing the lesion via TLS polymerases[150,151], and finally repair of the newly created DNA double strand break (DSB) by HR using the sister chromatid[155].

Given that APH treatment also robustly induces FA pathway activation[116,122,123], the FA pathway may coordinate similar DNA repair mechanisms for the processing of non-ICL stalled forks. This would explain its association with unresolved replication intermediates and its requirement for CFS stability. Such a role would also seem to be more pertinent to physiological conditions, as ICLs are apparently very rare in the endogenous cellular environment[156]. Therefore, understanding how the FA pathway works at spontaneously stalled forks appears essential for solving the enigmatic connection between FA pathway function and the clinical phenotypes of the disease. It is currently thought that cancer predisposition in FA patients stems from increased chromosome instability, but how exactly this occurs or what the tumor-driving events are remains enigmatic. Additionally, the FA pathway plays a specialized role in the survival/maintenance of hematopoietic stem cell populations[157], but if this is due to a specific repair function of the FA pathway in these cells is unknown. A pair of recent studies may have provided part of the answer by revealing important roles of the FA pathway in aldehyde metabolism[158,159]. *Fancd2* homozygous null mutant mice that were

deprived of aldehyde dehydrogenase 2 (ALDH2) activity either experienced embryonic lethality or succumbed to acute lymphoblastic leukemias at very early ages. These findings suggest that aldehydes, which are present in the endogenous cellular environment and can form both crosslink and non-crosslink DNA damage[160-162], may be linked to the phenotypes observed in FA patients.

The generation of several FA mutant mouse models has also led to a greater understanding of the genetics underlying FA. All models to date have faithfully recapitulated the cellular ICL hypersensitivity and hypogonadism seen in FA patients, the latter stemming from a reduced number of primordial germ cells[163,164]. Surprisingly, however, these models show subtle, if any phenotypes regarding other developmental abnormalities, overt BMF or cancer predisposition[165,166]. In fact, the most common developmental abnormality observed apart from hypogonadism is an increased incidence of microphthalmia in a C57BL/6J genetic background[167-170]. These findings suggest that certain differences in the murine genetic model may mask the role of the FA pathway in physiological conditions.

Another strategy that may help us to better understand FA pathway function is to identify the yet unassigned complementation groups of FA. One compelling candidate FA gene is *HELQ* (previously known as *HEL308*), which encodes the DNA repair helicase HELQ. The *Drosophila melanogaster* ortholog of *HELQ* was first identified in a screen for ICL hypersensitive mutants[171]. It was later found to be required for meiotic DSB repair[172], suggesting a role in HR. Similar functions were shown for the *C. elegans*

ortholog[173,174], with ICL resistance being epistatic to the *FANCD2* ortholog in this organism[173]. Knockdown of *HELQ* in human cells was shown to confer MMC hypersensitivity as well as decreased HR efficiency, the latter being epistatic to knockdown of *FANCD2*[175]. Finally, GFP-tagged HELQ was found to co-localize with RAD51 and FANCD2 foci at stalled replication forks in human cells[176]. However, up to this point there had been no mutant model system in which to study HELQ's role in genome stability or its connection to the FA pathway in mammalian cells.

Replication stress is linked to genomic instability and cancer

While genomic instability has long been known to be a hallmark of cancer cells[177], how it is formed and whether it is a significant driver of tumor progression were not well understood for decades. The mutator hypothesis originally proposed that precancerous cells acquire mutations in important "caretaker genes" that are necessary for genomic stability[178,179]. The loss of such genes, it was thought, might lead to an increased mutation frequency that could drive cancer progression. This seems to be the case for many hereditary cancers[180], such as mutations in FA genes. However, large-scale sequencing studies later revealed that caretaker gene mutations are extremely rare in sporadic cancers[181-184]. Rather, the most commonly mutated genes included *TP53* and major oncogenes/tumor suppressor genes that regulate cell proliferation.

In 2005, a pair of studies made a surprising discovery when they found that precancerous lesions actually exhibit a highly activated DNA damage response (DDR),

including phosphorylation of ATM, CHK2, histone H2AX and p53[185,186]. This correlated with an increased number of DSBs as well as an increased loss of heterozygosity of CFS loci. A short time later, it was shown that oncogene-induced senescence occurs via this same mechanism[187,188]. This led to the oncogene-induced replication stress model[189], which suggests that activated oncogenes, while driving excessive proliferation, also cause perturbed replication kinetics (replication stress). This leads to a higher number of forks stalling and eventually collapsing to form DSBs, particularly at CFSs with reduced origin densities. This in turn hyper-activates the DDR, which serves as a major anti-tumor barrier by inducing p53-mediated cell cycle arrest, senescence or apoptosis. In this context, late-stage mutations inactivating the ATM-CHK2-p53 checkpoint axis can lead to the uncontrolled proliferation of cells with severely perturbed replication and rampant genomic instability. The fact that CFSs are a major source of the chromosomal rearrangements seen in tumors supports this model[104,190,191].

Summary

In summary, cells license an excess of potential origins for DNA replication prior to entering S phase. While only a small subset of these origins is needed to complete replication under normal conditions, dormant origins can be activated as backups when needed. Certain genomic loci called CFSs lack a sufficient number of active origins and therefore depend on the FA pathway for their stability during replication. In this way, both dormant origins and the FA pathway work in parallel to maintain fork

stability/progression and suppress chromosome instability that might otherwise lead to cancer.

How exactly a loss of dormant origins might confer chromosome instability and tumorigenesis in the *Mcm4*^{chaos3} mutant mouse model had been a mystery. In **CHAPTER II**, our studies reveal that MEFs homozygous for *Mcm4*^{chaos3} exhibit a ~60% decrease in the number of chromatin-bound MCMs, leading to a substantial loss of dormant origins. We found that this led to an elevated number of persistently stalled forks, indicating that dormant origins play a pivotal role in stalled fork recovery *even in unchallenged S phase*. Unresolved replication intermediates in these cells persisted even into M phase, as indicated by an increased number of FANCD2 foci in early M phase, suggesting that a number of lesions are not fully replicated upon mitotic entry. This correlated with a higher frequency of chromosome non-disjunction in *Mcm4*$^{chaos3/chaos3}$ cells, leading to elevated levels of MN, aneuploidy and chromosome breaks. These findings suggest that stalled fork recovery mediated by dormant origins is required to suppress multiple forms of chromosome instability that could promote tumorigenesis.

An intrinsically high number of FANCD2 foci in *Mcm4*$^{chaos3/chaos3}$ cells suggested an important function of the FA pathway in stalled fork recovery when dormant origins are lacking. In **CHAPTER III**, we investigated this functional interaction by disrupting the FA pathway in *Mcm4*$^{chaos3/chaos3}$ cells via a null allele of *Fancc* (*Fancc*$^{-}$). As we predicted, *Mcm4*$^{chaos3/chaos3}$*;Fancc*$^{-/-}$ MEFs displayed a much greater number of persistently stalled forks than either single mutant. However, we were also surprised to

uncover a unique role of dormant origins in replication completion. A closer examination of FANCD2 foci in *Mcm4*$^{chaos3/chaos3}$ cells revealed that DNA synthesis was still going on at these sites in early M phase, indicating delayed replication. We thus concluded that dormant origins are required to preclude the presence of long, origin-poor loci that cannot finish replicating until extremely late. Together, these collective roles of dormant origins and the FA pathway in fork progression proved essential for maintaining chromosome stability, and almost all *Mcm4*$^{chaos3/chaos3}$*;Fancc*$^{-/-}$ mice displayed perinatal lethality in an inbred C57BL/6J genetic background. Surviving mice succumbed to tumors more quickly than *Mcm4*$^{chaos3/chaos3}$ littermates, implicating both mechanisms in tumor suppression.

Finally, the role of mammalian *HELQ* in relation to the FA pathway was unknown. In **CHAPTER IV**, we describe the characterization of the first *Helq* mutant mouse model (*Helq*^{gt}). We found that mice homozygous for this allele exhibited mild forms of FA-like phenotypes such as hypogonadism and MMC sensitivity when compared to *Fancc*$^{-/-}$ mutants, despite displaying no defects in FANCD2 mono-ubiquitination. *Helq*$^{gt/gt}$ MEFs also showed no significant reduction in the levels of HR when measured *in vivo*. Rather, *Helq* was shown to play an important role in the suppression of replication-associated genome instability, as *Helq*$^{gt/gt}$*;Fancc*$^{-/-}$ double mutant cells exhibited very high levels of spontaneous MN and 53BP1-NBs. These data suggest that *Helq* acts in parallel to the FA pathway in the recovery of stalled forks.

References

1 Ciccia, A. & Elledge, S. J. The DNA Damage Response: Making It Safe to Play with Knives. *Molecular Cell* **40**, 179-204 (2010).

2 Branzei, D. & Foiani, M. Maintaining genome stability at the replication fork. *Nat Rev Mol Cell Biol* **11**, 208-219 (2010).

3 Méchali, M. Eukaryotic DNA replication origins: many choices for appropriate answers. *Nat Rev Mol Cell Biol* **11**, 728-738 (2010).

4 Huberman, J. A. & Riggs, A. D. Autoradiography of chromosomal DNA fibers from Chinese hamster cells. *Proc Natl Acad Sci U S A* **55**, 599-606 (1966).

5 Blow, J. J. & Dutta, A. Preventing re-replication of chromosomal DNA. *Nat Rev Mol Cell Biol* **6**, 476-486 (2005).

6 Bell, S. P. & Stillman, B. ATP-dependent recognition of eukaryotic origins of DNA replication by a multiprotein complex. *Nature* **357**, 128-134 (1992).

7 Coleman, T. R., Carpenter, P. B. & Dunphy, W. G. The Xenopus Cdc6 protein is essential for the initiation of a single round of DNA replication in cell-free extracts. *Cell* **87**, 53-63 (1996).

8 Cocker, J. H., Piatti, S., Santocanale, C., Nasmyth, K. & Diffley, J. F. An essential role for the Cdc6 protein in forming the pre-replicative complexes of budding yeast. *Nature* **379**, 180-182 (1996).

9 Perkins, G. & Diffley, J. F. Nucleotide-dependent prereplicative complex assembly by Cdc6p, a homolog of eukaryotic and prokaryotic clamp-loaders. *Mol Cell* **2**, 23-32 (1998).

10 Randell, J. C., Bowers, J. L., Rodriguez, H. K. & Bell, S. P. Sequential ATP hydrolysis by Cdc6 and ORC directs loading of the Mcm2-7 helicase. *Mol Cell* **21**, 29-39 (2006).

11 Nishitani, H., Lygerou, Z., Nishimoto, T. & Nurse, P. The Cdt1 protein is required to license DNA for replication in fission yeast. *Nature* **404**, 625-628 (2000).

12 Whittaker, A. J., Royzman, I. & Orr-Weaver, T. L. Drosophila double parked: a conserved, essential replication protein that colocalizes with the origin recognition complex and links DNA replication with mitosis and the down-regulation of S phase transcripts. *Genes Dev* **14**, 1765-1776 (2000).

13 Maiorano, D., Moreau, J. & Mechali, M. XCDT1 is required for the assembly of pre-replicative complexes in Xenopus laevis. *Nature* **404**, 622-625 (2000).

14 Ishimi, Y. A DNA helicase activity is associated with an MCM4, -6, and -7 protein complex. *J Biol Chem* **272**, 24508-24513 (1997).

15 Lee, J. K. & Hurwitz, J. Isolation and characterization of various complexes of the minichromosome maintenance proteins of Schizosaccharomyces pombe. *J Biol Chem* **275**, 18871-18878 (2000).

16 Schwacha, A. & Bell, S. P. Interactions between two catalytically distinct MCM subgroups are essential for coordinated ATP hydrolysis and DNA replication. *Mol Cell* **8**, 1093-1104 (2001).

17 You, Z., Ishimi, Y., Masai, H. & Hanaoka, F. Roles of Mcm7 and Mcm4 subunits in the DNA helicase activity of the mouse Mcm4/6/7 complex. *J Biol Chem* **277**, 42471-42479 (2002).
18 Kaplan, D. L., Davey, M. J. & O'Donnell, M. Mcm4,6,7 uses a "pump in ring" mechanism to unwind DNA by steric exclusion and actively translocate along a duplex. *J Biol Chem* **278**, 49171-49182 (2003).
19 Ying, C. Y. & Gautier, J. The ATPase activity of MCM2-7 is dispensable for pre-RC assembly but is required for DNA unwinding. *EMBO J* **24**, 4334-4344 (2005).
20 Maine, G. T., Sinha, P. & Tye, B.-K. Mutants of S. Cerevisiae Defective in the Maintenance of Minichromosomes. *Genetics* **106**, 365-385 (1984).
21 Remus, D. *et al.* Concerted Loading of Mcm2–7 Double Hexamers around DNA during DNA Replication Origin Licensing. *Cell* **139**, 719-730 (2009).
22 Evrin, C. *et al.* A double-hexameric MCM2-7 complex is loaded onto origin DNA during licensing of eukaryotic DNA replication. *Proceedings of the National Academy of Sciences* **106**, 20240-20245 (2009).
23 Gambus, A., Khoudoli, G. A., Jones, R. C. & Blow, J. J. MCM2-7 Form Double Hexamers at Licensed Origins in Xenopus Egg Extract. *Journal of Biological Chemistry* **286**, 11855-11864 (2011).
24 Edwards, M. C. *et al.* MCM2–7 Complexes Bind Chromatin in a Distributed Pattern Surrounding the Origin Recognition Complex in Xenopus Egg Extracts. *Journal of Biological Chemistry* **277**, 33049-33057 (2002).
25 Ge, X. Q., Jackson, D. A. & Blow, J. J. Dormant origins licensed by excess Mcm2–7 are required for human cells to survive replicative stress. *Genes & Development* **21**, 3331-3341 (2007).
26 Ibarra, A., Schwob, E. & Méndez, J. Excess MCM proteins protect human cells from replicative stress by licensing backup origins of replication. *Proceedings of the National Academy of Sciences* **105**, 8956-8961 (2008).
27 Donovan, S., Harwood, J., Drury, L. S. & Diffley, J. F. X. Cdc6p-dependent loading of Mcm proteins onto pre-replicative chromatin in budding yeast. *Proceedings of the National Academy of Sciences* **94**, 5611-5616 (1997).
28 Bowers, J. L., Randell, J. C. W., Chen, S. & Bell, S. P. ATP Hydrolysis by ORC Catalyzes Reiterative Mcm2-7 Assembly at a Defined Origin of Replication. *Molecular Cell* **16**, 967-978 (2004).
29 Cortez, D., Glick, G. & Elledge, S. J. Minichromosome maintenance proteins are direct targets of the ATM and ATR checkpoint kinases. *Proceedings of the National Academy of Sciences of the United States of America* **101**, 10078-10083 (2004).
30 Woodward, A. M. *et al.* Excess Mcm2–7 license dormant origins of replication that can be used under conditions of replicative stress. *The Journal of Cell Biology* **173**, 673-683 (2006).
31 Hyrien, O., Marheineke, K. & Goldar, A. Paradoxes of eukaryotic DNA replication: MCM proteins and the random completion problem. *BioEssays* **25**, 116-125 (2003).

32 Perkins, G., Drury, L. S. & Diffley, J. F. Separate SCF(CDC4) recognition elements target Cdc6 for proteolysis in S phase and mitosis. *EMBO J* **20**, 4836-4845 (2001).
33 Labib, K., Diffley, J. F. & Kearsey, S. E. G1-phase and B-type cyclins exclude the DNA-replication factor Mcm4 from the nucleus. *Nat Cell Biol* **1**, 415-422 (1999).
34 Nguyen, V. Q., Co, C. & Li, J. J. Cyclin-dependent kinases prevent DNA re-replication through multiple mechanisms. *Nature* **411**, 1068-1073 (2001).
35 Drury, L. S., Perkins, G. & Diffley, J. F. X. The cyclin-dependent kinase Cdc28p regulates distinct modes of Cdc6p proteolysis during the budding yeast cell cycle. *Current Biology* **10**, 231-240 (2000).
36 McGarry, T. J. & Kirschner, M. W. Geminin, an inhibitor of DNA replication, is degraded during mitosis. *Cell* **93**, 1043-1053 (1998).
37 Wohlschlegel, J. A. *et al.* Inhibition of eukaryotic DNA replication by geminin binding to Cdt1. *Science* **290**, 2309-2312 (2000).
38 Tada, S., Li, A., Maiorano, D., Mechali, M. & Blow, J. J. Repression of origin assembly in metaphase depends on inhibition of RLF-B/Cdt1 by geminin. *Nat Cell Biol* **3**, 107-113 (2001).
39 Cook, J. G., Chasse, D. A. & Nevins, J. R. The regulated association of Cdt1 with minichromosome maintenance proteins and Cdc6 in mammalian cells. *J Biol Chem* **279**, 9625-9633 (2004).
40 Lee, C. *et al.* Structural basis for inhibition of the replication licensing factor Cdt1 by geminin. *Nature* **430**, 913-917 (2004).
41 Zhong, W., Feng, H., Santiago, F. E. & Kipreos, E. T. CUL-4 ubiquitin ligase maintains genome stability by restraining DNA-replication licensing. *Nature* **423**, 885-889 (2003).
42 Higa, L. A., Mihaylov, I. S., Banks, D. P., Zheng, J. & Zhang, H. Radiation-mediated proteolysis of CDT1 by CUL4-ROC1 and CSN complexes constitutes a new checkpoint. *Nat Cell Biol* **5**, 1008-1015 (2003).
43 Hu, J., McCall, C. M., Ohta, T. & Xiong, Y. Targeted ubiquitination of CDT1 by the DDB1-CUL4A-ROC1 ligase in response to DNA damage. *Nat Cell Biol* **6**, 1003-1009 (2004).
44 Rape, M., Reddy, S. K. & Kirschner, M. W. The Processivity of Multiubiquitination by the APC Determines the Order of Substrate Degradation. *Cell* **124**, 89-103 (2006).
45 Arias, E. E. & Walter, J. C. PCNA functions as a molecular platform to trigger Cdt1 destruction and prevent re-replication. *Nat Cell Biol* **8**, 84-90 (2006).
46 Senga, T. *et al.* PCNA is a cofactor for Cdt1 degradation by CUL4/DDB1-mediated N-terminal ubiquitination. *J Biol Chem* **281**, 6246-6252 (2006).
47 Tercero, J. A., Labib, K. & Diffley, J. F. DNA synthesis at individual replication forks requires the essential initiation factor Cdc45p. *EMBO J* **19**, 2082-2093 (2000).

48 Labib, K., Tercero, J. A. & Diffley, J. F. X. Uninterrupted MCM2-7 Function Required for DNA Replication Fork Progression. *Science* **288**, 1643-1647 (2000).
49 Pacek, M. & Walter, J. C. A requirement for MCM7 and Cdc45 in chromosome unwinding during eukaryotic DNA replication. *EMBO J* **23**, 3667-3676 (2004).
50 Gambus, A. *et al.* GINS maintains association of Cdc45 with MCM in replisome progression complexes at eukaryotic DNA replication forks. *Nat Cell Biol* **8**, 358-366 (2006).
51 Moyer, S. E., Lewis, P. W. & Botchan, M. R. Isolation of the Cdc45/Mcm2–7/GINS (CMG) complex, a candidate for the eukaryotic DNA replication fork helicase. *Proceedings of the National Academy of Sciences* **103**, 10236-10241 (2006).
52 Pacek, M., Tutter, A. V., Kubota, Y., Takisawa, H. & Walter, J. C. Localization of MCM2-7, Cdc45, and GINS to the Site of DNA Unwinding during Eukaryotic DNA Replication. *Molecular Cell* **21**, 581-587 (2006).
53 Ilves, I., Petojevic, T., Pesavento, J. J. & Botchan, M. R. Activation of the MCM2-7 Helicase by Association with Cdc45 and GINS Proteins. *Molecular Cell* **37**, 247-258 (2010).
54 Zou, L. & Stillman, B. Formation of a Preinitiation Complex by S-phase Cyclin CDK-Dependent Loading of Cdc45p onto Chromatin. *Science* **280**, 593-596 (1998).
55 Masai, H. *et al.* Phosphorylation of MCM4 by Cdc7 Kinase Facilitates Its Interaction with Cdc45 on the Chromatin. *Journal of Biological Chemistry* **281**, 39249-39261 (2006).
56 Tsuji, T., Ficarro, S. B. & Jiang, W. Essential Role of Phosphorylation of MCM2 by Cdc7/Dbf4 in the Initiation of DNA Replication in Mammalian Cells. *Molecular Biology of the Cell* **17**, 4459-4472 (2006).
57 Sheu, Y.-J. & Stillman, B. Cdc7-Dbf4 Phosphorylates MCM Proteins via a Docking Site-Mediated Mechanism to Promote S Phase Progression. *Molecular Cell* **24**, 101-113 (2006).
58 Sheu, Y. J. & Stillman, B. The Dbf4-Cdc7 kinase promotes S phase by alleviating an inhibitory activity in Mcm4. *Nature* **463**, 113-117 (2010).
59 Masumoto, H., Muramatsu, S., Kamimura, Y. & Araki, H. S-Cdk-dependent phosphorylation of Sld2 essential for chromosomal DNA replication in budding yeast. *Nature* **415**, 651-655 (2002).
60 Yabuuchi, H. *et al.* Ordered assembly of Sld3, GINS and Cdc45 is distinctly regulated by DDK and CDK for activation of replication origins. *EMBO J* **25**, 4663-4674 (2006).
61 Tanaka, S. *et al.* CDK-dependent phosphorylation of Sld2 and Sld3 initiates DNA replication in budding yeast. *Nature* **445**, 328-332 (2007).
62 Zegerman, P. & Diffley, J. F. Phosphorylation of Sld2 and Sld3 by cyclin-dependent kinases promotes DNA replication in budding yeast. *Nature* **445**, 281-285 (2007).

63 Muramatsu, S., Hirai, K., Tak, Y.-S., Kamimura, Y. & Araki, H. CDK-dependent complex formation between replication proteins Dpb11, Sld2, Pol ε, and GINS in budding yeast. *Genes & Development* **24**, 602-612 (2010).

64 Merchant, A. M., Kawasaki, Y., Chen, Y., Lei, M. & Tye, B. K. A lesion in the DNA replication initiation factor Mcm10 induces pausing of elongation forks through chromosomal replication origins in Saccharomyces cerevisiae. *Molecular and Cellular Biology* **17**, 3261-3271 (1997).

65 Wohlschlegel, J. A., Dhar, S. K., Prokhorova, T. A., Dutta, A. & Walter, J. C. Xenopus Mcm10 binds to origins of DNA replication after Mcm2-7 and stimulates origin binding of Cdc45. *Molecular Cell* **9**, 233-240 (2002).

66 Balestrini, A., Cosentino, C., Errico, A., Garner, E. & Costanzo, V. GEMC1 is a TopBP1-interacting protein required for chromosomal DNA replication. *Nat Cell Biol* **12**, 484-491 (2010).

67 Chowdhury, A. *et al.* The DNA Unwinding Element Binding Protein DUE-B Interacts with Cdc45 in Preinitiation Complex Formation. *Molecular and Cellular Biology* **30**, 1495-1507 (2010).

68 Pefani, D.-E. *et al.* Idas, a Novel Phylogenetically Conserved Geminin-related Protein, Binds to Geminin and Is Required for Cell Cycle Progression. *Journal of Biological Chemistry* **286**, 23234-23246 (2011).

69 Ricke, R. M. & Bielinsky, A. K. Mcm10 regulates the stability and chromatin association of DNA polymerase-α. *Molecular Cell* **16**, 173-185 (2004).

70 Yan, H., Merchant, A. M. & Tye, B. K. Cell cycle-regulated nuclear localization of MCM2 and MCM3, which are required for the initiation of DNA synthesis at chromosomal replication origins in yeast. *Genes & Development* **7**, 2149-2160 (1993).

71 Todorov, I. T., Attaran, A. & Kearsey, S. E. BM28, a human member of the MCM2-3-5 family, is displaced from chromatin during DNA replication. *The Journal of Cell Biology* **129**, 1433-1445 (1995).

72 Krude, T., Musahl, C., Laskey, R. A. & Knippers, R. Human replication proteins hCdc21, hCdc46 and P1Mcm3 bind chromatin uniformly before S-phase and are displaced locally during DNA replication. *Journal of Cell Science* **109**, 309-318 (1996).

73 Santocanale, C. & Diffley, J. F. ORC- and Cdc6-dependent complexes at active and inactive chromosomal replication origins in Saccharomyces cerevisiae. *EMBO J* **15**, 6671-6679 (1996).

74 Gilbert, D. M. Replication timing and transcriptional control: beyond cause and effect. *Current Opinion in Cell Biology* **14**, 377-383 (2002).

75 Tabancay Jr, A. P. & Forsburg, S. L. in *Current Topics in Developmental Biology* Vol. Volume 76 (ed P. Schatten Gerald) 129-184 (Academic Press, 2006).

76 Masai, H., Matsumoto, S., You, Z., Yoshizawa-Sugata, N. & Oda, M. Eukaryotic Chromosome DNA Replication: Where, When, and How? *Annual Review of Biochemistry* **79**, 89-130 (2010).

77 Krasinska, L. *et al.* Cdk1 and Cdk2 activity levels determine the efficiency of replication origin firing in Xenopus. *EMBO J* **27**, 758-769 (2008).
78 Patel, P. K. *et al.* The Hsk1(Cdc7) Replication Kinase Regulates Origin Efficiency. *Molecular Biology of the Cell* **19**, 5550-5558 (2008).
79 Wu, P.-Y. J. & Nurse, P. Establishing the Program of Origin Firing during S Phase in Fission Yeast. *Cell* **136**, 852-864 (2009).
80 Mantiero, D., Mackenzie, A., Donaldson, A. & Zegerman, P. Limiting replication initiation factors execute the temporal programme of origin firing in budding yeast. *EMBO J* **30**, 4805-4814 (2011).
81 Tanaka, S., Nakato, R., Katou, Y., Shirahige, K. & Araki, H. Origin Association of Sld3, Sld7, and Cdc45 Proteins Is a Key Step for Determination of Origin-Firing Timing. *Current Biology* **21**, 2055-2063 (2011).
82 Lei, M., Kawasaki, Y. & Tye, B. K. Physical interactions among Mcm proteins and effects of Mcm dosage on DNA replication in Saccharomyces cerevisiae. *Molecular and Cellular Biology* **16**, 5081-5090 (1996).
83 Liang, D. T., Hodson, J. A. & Forsburg, S. L. Reduced dosage of a single fission yeast MCM protein causes genetic instability and S phase delay. *Journal of Cell Science* **112**, 559-567 (1999).
84 Slater, M. L. Effect of Reversible Inhibition of Deoxyribonucleic Acid Synthesis on the Yeast Cell Cycle. *Journal of Bacteriology* **113**, 263-270 (1973).
85 Santocanale, C. & Diffley, J. F. A Mec1- and Rad53-dependent checkpoint controls late-firing origins of DNA replication. *Nature* **395**, 615-618 (1998).
86 Shirahige, K. *et al.* Regulation of DNA-replication origins during cell-cycle progression. *Nature* **395**, 618-621 (1998).
87 Luciani, M. G., Oehlmann, M. & Blow, J. J. Characterization of a novel ATR-dependent, Chk1-independent, intra-S-phase checkpoint that suppresses initiation of replication in Xenopus. *Journal of Cell Science* **117**, 6019-6030 (2004).
88 Maya-Mendoza, A., Petermann, E., Gillespie, D. A., Caldecott, K. W. & Jackson, D. A. Chk1 regulates the density of active replication origins during the vertebrate S phase. *EMBO J* **26**, 2719-2731 (2007).
89 Ge, X. Q. & Blow, J. J. Chk1 inhibits replication factory activation but allows dormant origin firing in existing factories. *The Journal of Cell Biology* **191**, 1285-1297 (2010).
90 Toledo, Luis I. *et al.* ATR Prohibits Replication Catastrophe by Preventing Global Exhaustion of RPA. *Cell* **155**, 1088-1103 (2013).
91 Yekezare, M., Gómez-González, B. & Diffley, J. F. X. Controlling DNA replication origins in response to DNA damage – inhibit globally, activate locally. *Journal of Cell Science* **126**, 1297-1306 (2013).
92 Shima, N. *et al.* Phenotype-Based Identification of Mouse Chromosome Instability Mutants. *Genetics* **163**, 1031-1040 (2003).
93 Shima, N. *et al.* A viable allele of Mcm4 causes chromosome instability and mammary adenocarcinomas in mice. *Nat Genet* **39**, 93-98 (2007).

94 Ikegami, S. *et al.* Aphidicolin prevents mitotic cell division by interfering with the activity of DNA polymerase-alpha. *Nature* **275**, 458-460 (1978).
95 Cheng, C. H. & Kuchta, R. D. DNA polymerase epsilon: Aphidicolin inhibition and the relationship between polymerase and exonuclease activity. *Biochemistry* **32**, 8568-8574 (1993).
96 Wright, G. E., Hübscher, U., Khan, N. N., Focher, F. & Verri, A. Inhibitor analysis of calf thymus DNA polymerases α, δ and ϵ. *FEBS Letters* **341**, 128-130 (1994).
97 Pruitt, S. C., Bailey, K. J. & Freeland, A. Reduced Mcm2 Expression Results in Severe Stem/Progenitor Cell Deficiency and Cancer. *Stem Cells* **25**, 3121-3132 (2007).
98 Kunnev, D. *et al.* DNA damage response and tumorigenesis in Mcm2-deficient mice. *Oncogene* **29**, 3630-3638 (2010).
99 Kawabata, T. *et al.* A reduction of licensed origins reveals strain-specific replication dynamics in mice. *Mammalian Genome* **22**, 506-517 (2011).
100 Chuang, C.-H., Wallace, M. D., Abratte, C., Southard, T. & Schimenti, J. C. Incremental Genetic Perturbations to MCM2-7 Expression and Subcellular Distribution Reveal Exquisite Sensitivity of Mice to DNA Replication Stress. *PLoS Genet* **6**, e1001110 (2010).
101 Glover, T., Berger, C., Coyle, J. & Echo, B. DNA polymerase α inhibition by aphidicolin induces gaps and breaks at common fragile sites in human chromosomes. *Human Genetics* **67**, 136-142 (1984).
102 Mrasek, K. *et al.* Global screening and extended nomenclature for 230 aphidicolin-inducible fragile sites, including 61 yet unreported ones. *International Journal of Oncology* **36**, 929-940 (2010).
103 Letessier, A. *et al.* Cell-type-specific replication initiation programs set fragility of the FRA3B fragile site. *Nature* **470**, 120-123 (2011).
104 Le Tallec, B. *et al.* Common Fragile Site Profiling in Epithelial and Erythroid Cells Reveals that Most Recurrent Cancer Deletions Lie in Fragile Sites Hosting Large Genes. *Cell Reports* **4**, 420-428 (2013).
105 Zlotorynski, E. *et al.* Molecular Basis for Expression of Common and Rare Fragile Sites. *Molecular and Cellular Biology* **23**, 7143-7151 (2003).
106 Shah, S. N., Opresko, P. L., Meng, X., Lee, M. Y. & Eckert, K. A. DNA structure and the Werner protein modulate human DNA polymerase delta-dependent replication dynamics within the common fragile site FRA16D. *Nucleic Acids Res* **38**, 1149-1162 (2010).
107 Zhang, H. & Freudenreich, C. H. An AT-rich sequence in human common fragile site FRA16D causes fork stalling and chromosome breakage in S. cerevisiae. *Mol Cell* **27**, 367-379 (2007).
108 Ozeri-Galai, E. *et al.* Failure of Origin Activation in Response to Fork Stalling Leads to Chromosomal Instability at Fragile Sites. *Molecular Cell* **43**, 122-131 (2011).

109 Helmrich, A., Ballarino, M. & Tora, L. Collisions between Replication and Transcription Complexes Cause Common Fragile Site Instability at the Longest Human Genes. *Molecular Cell* **44**, 966-977 (2011).
110 Le Beau, M. M. *et al.* Replication of a Common Fragile Site, FRA3B, Occurs Late in S Phase and is Delayed Further Upon Induction: Implications for the Mechanism of Fragile Site Induction. *Human Molecular Genetics* **7**, 755-761 (1998).
111 Wang, L. *et al.* Allele-specific Late Replication and Fragility of the Most Active Common Fragile Site, FRA3B. *Human Molecular Genetics* **8**, 431-437 (1999).
112 Palakodeti, A., Han, Y., Jiang, Y. & Le Beau, M. M. The role of late/slow replication of the FRA16D in common fragile site induction. *Genes, Chromosomes and Cancer* **39**, 71-76 (2004).
113 Casper, A. M., Nghiem, P., Arlt, M. F. & Glover, T. W. ATR regulates fragile site stability. *Cell* **111**, 779-789 (2002).
114 Casper, A. M., Durkin, S. G., Arlt, M. F. & Glover, T. W. Chromosomal Instability at Common Fragile Sites in Seckel Syndrome. *The American Journal of Human Genetics* **75**, 654-660 (2004).
115 Durkin, S. G., Arlt, M. F., Howlett, N. G. & Glover, T. W. Depletion of CHK1, but not CHK2, induces chromosomal instability and breaks at common fragile sites. *Oncogene* **25**, 4381-4388 (2006).
116 Howlett, N. G., Taniguchi, T., Durkin, S. G., D'Andrea, A. D. & Glover, T. W. The Fanconi anemia pathway is required for the DNA replication stress response and for the regulation of common fragile site stability. *Human Molecular Genetics* **14**, 693-701 (2005).
117 Sobeck, A. *et al.* Fanconi Anemia Proteins Are Required To Prevent Accumulation of Replication-Associated DNA Double-Strand Breaks. *Molecular and Cellular Biology* **26**, 425-437 (2006).
118 Wang, L. C., Stone, S., Hoatlin, M. E. & Gautier, J. Fanconi anemia proteins stabilize replication forks. *DNA Repair* **7**, 1973-1981 (2008).
119 Schlacher, K., Wu, H. & Jasin, M. A Distinct Replication Fork Protection Pathway Connects Fanconi Anemia Tumor Suppressors to RAD51-BRCA1/2. *Cancer Cell* **22**, 106-116 (2012).
120 Garcia-Higuera, I. *et al.* Interaction of the Fanconi Anemia Proteins and BRCA1 in a Common Pathway. *Molecular Cell* **7**, 249-262 (2001).
121 Taniguchi, T. *et al.* S-phase–specific interaction of the Fanconi anemia protein, FANCD2, with BRCA1 and RAD51. *Blood* **100**, 2414-2420 (2002).
122 Chan, K. L., Palmai-Pallag, T., Ying, S. & Hickson, I. D. Replication stress induces sister-chromatid bridging at fragile site loci in mitosis. *Nat Cell Biol* **11**, 753-760 (2009).
123 Naim, V. & Rosselli, F. The FANC pathway and BLM collaborate during mitosis to prevent micro-nucleation and chromosome abnormalities. *Nat Cell Biol* **11**, 761-768 (2009).

124 Baumann, C., Körner, R., Hofmann, K. & Nigg, E. A. PICH, a Centromere-Associated SNF2 Family ATPase, Is Regulated by Plk1 and Required for the Spindle Checkpoint. *Cell* **128**, 101-114 (2007).
125 Chan, K. L., North, P. S. & Hickson, I. D. BLM is required for faithful chromosome segregation and its localization defines a class of ultrafine anaphase bridges. *EMBO J* **26**, 3397-3409 (2007).
126 Lukas, C. *et al.* 53BP1 nuclear bodies form around DNA lesions generated by mitotic transmission of chromosomes under replication stress. *Nat Cell Biol* **13**, 243-253 (2011).
127 Blackford, A. N. *et al.* The DNA translocase activity of FANCM protects stalled replication forks. *Human Molecular Genetics* **21**, 2005-2016 (2012).
128 Vinciguerra, P., Godinho, S. A., Parmar, K., Pellman, D. & D'Andrea, A. D. Cytokinesis failure occurs in Fanconi anemia pathway–deficient murine and human bone marrow hematopoietic cells. *The Journal of Clinical Investigation* **120**, 3834-3842 (2010).
129 Rosenberg, P. S., Tamary, H. & Alter, B. P. How high are carrier frequencies of rare recessive syndromes? Contemporary estimates for Fanconi Anemia in the United States and Israel. *American Journal of Medical Genetics Part A* **155**, 1877-1883 (2011).
130 Crossan, G. P. & Patel, K. J. The Fanconi anaemia pathway orchestrates incisions at sites of crosslinked DNA. *The Journal of Pathology* **226**, 326-337 (2012).
131 Kottemann, M. C. & Smogorzewska, A. Fanconi anaemia and the repair of Watson and Crick DNA crosslinks. *Nature* **493**, 356-363 (2013).
132 Bogliolo, M. *et al.* Mutations in ERCC4, Encoding the DNA-Repair Endonuclease XPF, Cause Fanconi Anemia. *The American Journal of Human Genetics* **92**, 800-806 (2013).
133 Kashiyama, K. *et al.* Malfunction of Nuclease ERCC1-XPF Results in Diverse Clinical Manifestations and Causes Cockayne Syndrome, Xeroderma Pigmentosum, and Fanconi Anemia. *The American Journal of Human Genetics* **92**, 807-819 (2013).
134 Schroeder, T. M., Anschütz, F. & Knopp, A. Spontane Chromosomenaberrationen bei familiärer Panmyelopathie. *Humangenetik* **1**, 194-196 (1964).
135 Kubbies, M., Schindler, D., Hoehn, H., Schinzel, A. & Rabinovitch, P. S. Endogenous blockage and delay of the chromosome cycle despite normal recruitment and growth phase explain poor proliferation and frequent edomitosis in Fanconi anemia cells. *Am J Hum Genet* **37**, 1022-1030 (1985).
136 Sasaki, M. S. & Tonomura, A. A high susceptibility of Fanconi's anemia to chromosome breakage by DNA cross linking agents. *Cancer Research* **33**, 1829-1836 (1973).
137 Zamble, D. B. & Lippard, S. J. Cisplatin and DNA repair in cancer chemotherapy. *Trends in Biochemical Sciences* **20**, 435-439 (1995).

138 Auerbach, A. D., Rogatko, A. & Schroeder-Kurth, T. M. International Fanconi Anemia Registry: Relation of clinical symptoms to diepoxybutane sensitivity. *Blood* **73**, 391-396 (1989).
139 Auerbach, A. D. Fanconi anemia diagnosis and the diepoxybutane (DEB) test. *Experimental Hematology* **21**, 731-733 (1993).
140 Singh, T. R. *et al.* MHF1-MHF2, a Histone-Fold-Containing Protein Complex, Participates in the Fanconi Anemia Pathway via FANCM. *Molecular Cell* **37**, 879-886 (2010).
141 Meetei, A. R. *et al.* A novel ubiquitin ligase is deficient in Fanconi anemia. *Nat Genet* **35**, 165-170 (2003).
142 Smogorzewska, A. *et al.* Identification of the FANCI Protein, a Monoubiquitinated FANCD2 Paralog Required for DNA Repair. *Cell* **129**, 289-301 (2007).
143 Sims, A. E. *et al.* FANCI is a second monoubiquitinated member of the Fanconi anemia pathway. *Nat Struct Mol Biol* **14**, 564-567 (2007).
144 Wooster, R. *et al.* Localization of a breast cancer susceptibility gene, BRCA2, to chromosome 13q12-13. *Science* **265**, 2088-2090 (1994).
145 Rafnar, T. *et al.* Mutations in BRIP1 confer high risk of ovarian cancer. *Nat Genet* **43**, 1104-1107 (2011).
146 Seal, S. *et al.* Truncating mutations in the Fanconi anemia J gene BRIP1 are low-penetrance breast cancer susceptibility alleles. *Nat Genet* **38**, 1239-1241 (2006).
147 Rahman, N. *et al.* PALB2, which encodes a BRCA2-interacting protein, is a breast cancer susceptibility gene. *Nat Genet* **39**, 165-167 (2007).
148 Tischkowitz, M. *et al.* Analysis of PALB2/FANCN-associated breast cancer families. *Proc Natl Acad Sci U S A* **104**, 6788-6793 (2007).
149 Meindl, A. *et al.* Germline mutations in breast and ovarian cancer pedigrees establish RAD51C as a human cancer susceptibility gene. *Nat Genet* **42**, 410-414 (2010).
150 Räschle, M. *et al.* Mechanism of Replication-Coupled DNA Interstrand Crosslink Repair. *Cell* **134**, 969-980 (2008).
151 Knipscheer, P. *et al.* The Fanconi Anemia Pathway Promotes Replication-Dependent DNA Interstrand Cross-Link Repair. *Science* **326**, 1698-1701 (2009).
152 Zhang, J. & Walter, J. C. Mechanism and regulation of incisions during DNA interstrand cross-link repair. *DNA Repair* **19**, 135-142 (2014).
153 Klein Douwel, D. *et al.* XPF-ERCC1 Acts in Unhooking DNA Interstrand Crosslinks in Cooperation with FANCD2 and FANCP/SLX4. *Molecular Cell* **54**, 460-471 (2014).
154 Hodskinson, Michael R. G. *et al.* Mouse SLX4 Is a Tumor Suppressor that Stimulates the Activity of the Nuclease XPF-ERCC1 in DNA Crosslink Repair. *Molecular Cell* **54**, 472-484 (2014).
155 Long, D. T., Räschle, M., Joukov, V. & Walter, J. C. Mechanism of RAD51-Dependent DNA Interstrand Cross-Link Repair. *Science* **333**, 84-87 (2011).

156 Lindahl, T. & Barnes, D. E. Repair of Endogenous DNA Damage. *Cold Spring Harbor Symposia on Quantitative Biology* **65**, 127-134 (2000).
157 Ceccaldi, R. *et al.* Bone Marrow Failure in Fanconi Anemia Is Triggered by an Exacerbated p53/p21 DNA Damage Response that Impairs Hematopoietic Stem and Progenitor Cells. *Cell Stem Cell* **11**, 36-49 (2012).
158 Langevin, F., Crossan, G. P., Rosado, I. V., Arends, M. J. & Patel, K. J. Fancd2 counteracts the toxic effects of naturally produced aldehydes in mice. *Nature* **475**, 53-58 (2011).
159 Rosado, I. V., Langevin, F., Crossan, G. P., Takata, M. & Patel, K. J. Formaldehyde catabolism is essential in cells deficient for the Fanconi anemia DNA-repair pathway. *Nat Struct Mol Biol* **18**, 1432-1434 (2011).
160 Wang, M. *et al.* Identification of DNA Adducts of Acetaldehyde. *Chemical Research in Toxicology* **13**, 1149-1157 (2000).
161 Stein, S., Lao, Y., Yang, I. Y., Hecht, S. S. & Moriya, M. Genotoxicity of acetaldehyde- and crotonaldehyde-induced 1,N2-propanodeoxyguanosine DNA adducts in human cells. *Mutat Res* **608**, 1-7 (2006).
162 Cheng, G. *et al.* Reactions of Formaldehyde Plus Acetaldehyde with Deoxyguanosine and DNA: Formation of Cyclic Deoxyguanosine Adducts and Formaldehyde Cross-Links. *Chemical Research in Toxicology* **16**, 145-152 (2003).
163 Agoulnik, A. I. *et al.* A novel gene, Pog, is necessary for primordial germ cell proliferation in the mouse and underlies the germ cell deficient mutation, gcd. *Human Molecular Genetics* **11**, 3047-3053 (2002).
164 Nadler, J. J. & Braun, R. E. Fanconi anemia complementation group C is required for proliferation of murine primordial germ cells. *Genesis* **27**, 117-123 (2000).
165 Parmar, K., D'Andrea, A. & Niedernhofer, L. J. Mouse models of Fanconi anemia. *Mutation Research/Fundamental and Molecular Mechanisms of Mutagenesis* **668**, 133-140 (2009).
166 Bakker, S. T., de Winter, J. P. & Riele, H. t. Learning from a paradox: recent insights into Fanconi anaemia through studying mouse models. *Disease Models & Mechanisms* **6**, 40-47 (2013).
167 Wong, J. C. *et al.* Targeted disruption of exons 1 to 6 of the Fanconi Anemia group A gene leads to growth retardation, strain-specific microphthalmia, meiotic defects and primordial germ cell hypoplasia. *Hum Mol Genet* **12**, 2063-2076 (2003).
168 Carreau, M. Not-so-novel phenotypes in the Fanconi anemia group D2 mouse model. *Blood* **103**, 2430 (2004).
169 Houghtaling, S. *et al.* Epithelial cancer in Fanconi anemia complementation group D2 (Fancd2) knockout mice. *Genes & Development* **17**, 2021-2035 (2003).
170 Crossan, G. P. *et al.* Disruption of mouse Slx4, a regulator of structure-specific nucleases, phenocopies Fanconi anemia. *Nat Genet* **43**, 147-152 (2011).

171 Boyd, J. B., Golino, M. D., Shaw, K. E. S., Osgood, C. J. & Green, M. M. Third-Chromosome Mutagen-Sensitive Mutants of *Drosophila Melanogaster*. *Genetics* **97**, 607-623 (1981).
172 McCaffrey, R., St Johnston, D. & González-Reyes, A. Drosophila mus301/spindle-C Encodes a Helicase With an Essential Role in Double-Strand DNA Break Repair and Meiotic Progression. *Genetics* **174**, 1273-1285 (2006).
173 Muzzini, D. M., Plevani, P., Boulton, S. J., Cassata, G. & Marini, F. Caenorhabditis elegans POLQ-1 and HEL-308 function in two distinct DNA interstrand cross-link repair pathways. *DNA Repair* **7**, 941-950 (2008).
174 Ward, J. D. *et al.* Overlapping Mechanisms Promote Postsynaptic RAD-51 Filament Disassembly during Meiotic Double-Strand Break Repair. *Molecular Cell* **37**, 259-272 (2010).
175 Moldovan, G.-L. *et al.* DNA Polymerase POLN Participates in Cross-Link Repair and Homologous Recombination. *Molecular and Cellular Biology* **30**, 1088-1096 (2010).
176 Tafel, A. A., Wu, L. & McHugh, P. J. Human HEL308 Localizes to Damaged Replication Forks and Unwinds Lagging Strand Structures. *Journal of Biological Chemistry* **286**, 15832-15840 (2011).
177 Nowell, P. C. The clonal evolution of tumor cell populations. *Science* **194**, 23-28 (1976).
178 Loeb, L. A. Mutator phenotype may be required for multistage carcinogenesis. *Cancer Res* **51**, 3075-3079 (1991).
179 Kinzler, K. W. & Vogelstein, B. Cancer-susceptibility genes. Gatekeepers and caretakers. *Nature* **386**, 761, 763 (1997).
180 Negrini, S., Gorgoulis, V. G. & Halazonetis, T. D. Genomic instability--an evolving hallmark of cancer. *Nat Rev Mol Cell Biol* **11**, 220-228 (2010).
181 Sjoblom, T. *et al.* The consensus coding sequences of human breast and colorectal cancers. *Science* **314**, 268-274 (2006).
182 Wood, L. D. *et al.* The genomic landscapes of human breast and colorectal cancers. *Science* **318**, 1108-1113 (2007).
183 Jones, S. *et al.* Core signaling pathways in human pancreatic cancers revealed by global genomic analyses. *Science* **321**, 1801-1806 (2008).
184 Parsons, D. W. *et al.* An integrated genomic analysis of human glioblastoma multiforme. *Science* **321**, 1807-1812 (2008).
185 Bartkova, J. *et al.* DNA damage response as a candidate anti-cancer barrier in early human tumorigenesis. *Nature* **434**, 864-870 (2005).
186 Gorgoulis, V. G. *et al.* Activation of the DNA damage checkpoint and genomic instability in human precancerous lesions. *Nature* **434**, 907-913 (2005).
187 Bartkova, J. *et al.* Oncogene-induced senescence is part of the tumorigenesis barrier imposed by DNA damage checkpoints. *Nature* **444**, 633-637 (2006).
188 Di Micco, R. *et al.* Oncogene-induced senescence is a DNA damage response triggered by DNA hyper-replication. *Nature* **444**, 638-642 (2006).

189 Halazonetis, T. D., Gorgoulis, V. G. & Bartek, J. An oncogene-induced DNA damage model for cancer development. *Science* **319**, 1352-1355 (2008).
190 Beroukhim, R. *et al.* The landscape of somatic copy-number alteration across human cancers. *Nature* **463**, 899-905 (2010).
191 Bignell, G. R. *et al.* Signatures of mutation and selection in the cancer genome. *Nature* **463**, 893-898 (2010).

CHAPTER II: Stalled Fork Rescue via Dormant Replication Origins in Unchallenged S Phase Promotes Proper Chromosome Segregation and Tumor Suppression

My contributions to this chapter

Figure 2

Figure 5

Figure S5

Movies S1-3

This chapter is a replicate of a publication in *Molecular Cell* (2011). Tsuyoshi Kawabata, **Spencer W. Luebben**, Satoru Yamaguchi, Ivar Ilves, Ilze Matise, Tavanna Buske, Michael R. Botchan and Naoko Shima.

Summary

Eukaryotic cells license far more origins than are actually used for DNA replication, thereby generating a large number of dormant origins. Accumulating evidence suggests that such origins play a role in chromosome stability and tumor suppression, though the underlying mechanism is largely unknown. Here, we show that a loss of dormant origins results in an increased number of stalled replication forks, even in unchallenged S phase in primary mouse fibroblasts derived from embryos homozygous for the *Mcm4*^{Chaos3} allele. We found that this allele reduces the stability of the MCM2-7 complex, but confers normal helicase activity in vitro. Despite the activation of multiple fork recovery pathways, replication intermediates in these cells persist into M phase, increasing the number of abnormal anaphase cells with lagging chromosomes and/or acentric fragments. These findings suggest that dormant origins constitute a major pathway for stalled fork recovery, contributing to faithful chromosome segregation and tumor suppression.

Graphical abstract Kawabata et al., 2011

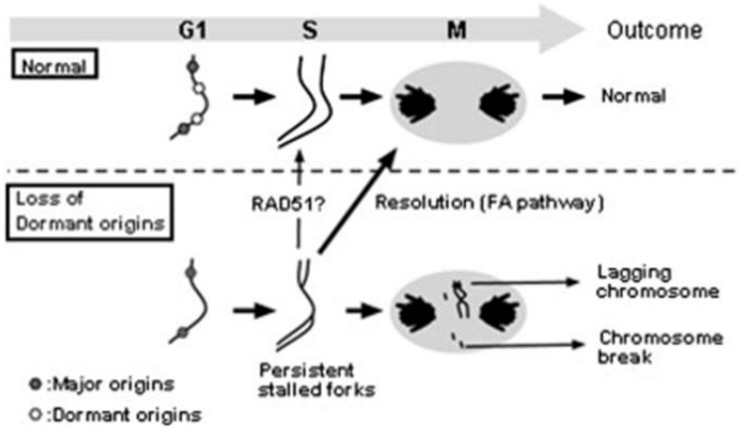

Introduction

Replication origin licensing is a prerequisite for genome duplication, as DNA synthesis in S phase initiates exclusively from licensed origins (reviewed in[1]). This process is restricted to the late M and early G1 phases, during which heterohexamers of the six minichromosome maintenance proteins (MCM2-7) are loaded onto origin recognition complex (ORC)-bound chromatin sites (reviewed in[2,3]). In the ensuing S phase, origins fire only once, when chromatin-bound *M*CM2-7 forms a replicative helicase complex (CMG complex) with cofactors CDC45 and GINS unwinding the DNA[4,5]. Active MCM2-7 complexes are then likely to travel along with ongoing replication forks, returning fired origins to the unlicensed state[6,7]. Following S phase entry, multiple factors prohibit origin relicensing, thereby preventing rereplication of DNA[8]. It should be noted that the majority of replication origins in mammalian cells are not defined by specific DNA sequences[9].

It is known that an excessive amount of MCM2-7 complex is loaded onto respective ORC-bound chromatin sites[10,11] and that these complexes are presumably competent to initiate origin firing if permitted[11-13]. So, while a huge excess of potential origins exists throughout the genome in eukaryotic cells, only a fraction of them is apparently sufficient for DNA replication[14,15]. Therefore, the role of such excess chromatin-bound MCM2-7 complexes has not been well understood.

Recent studies have investigated the role of these excess origins in human cancer cell lines[12,13]. Consistent with an overabundance of MCM2-7 complexes on chromatin,

up to 90% depletion of the MCM2-7 proteins had little effect on the densities of active origins in unperturbed S phase. However, MCM2-7-depleted cells did exhibit poor survival in the presence of low levels of the replication inhibitors aphidicolin (APH) or hydroxyurea. These findings suggest that dormant origins licensed by excess MCM2-7 complexes are most likely used as backups for "emergency" situations by increasing the number of replication forks, promoting the completion of DNA replication. However, it should be noted that the use of cancer cell lines in these studies might have hindered the ability to reveal the true role of dormant origins in vivo, as they exhibit greatly upregulated expression of the MCM2-7 proteins[16,17]. Although it was previously thought that dormant origins are essentially dispensable in unperturbed S phase[12,13], we and others have reported that a reduced level of MCM2-7 proteins causes spontaneous tumors in mice with complete penetrance[18-21], suggesting that dormant origins play an important role in such conditions. These mouse models exhibited a high level of spontaneous micronuclei in erythrocytes, a surrogate phenotype for chromosome instability[20,21]. However, it remained to be determined whether chromosome instability occurs in other types of cells in these mice and how it is generated upon a loss of dormant origins, leading to spontaneous tumorigenesis in these mice.

Here, we used the *Mcm4*^{Chaos3} allele to investigate the complex role of dormant origins in chromosome stability, as the Phe345Ile change encoded by this allele compromises the stability of the MCM2-7 complex and leads to a reduced number of dormant origins. We found that this loss of dormant origins results in an accumulation of stalled replication forks in unchallenged S phase. Furthermore, despite the activation of

Kawabata et al., 2011

multiple DNA repair pathways, a significant fraction of stalled forks persist into M phase and interfere with chromosome segregation.

Results

Chromatin-Bound MCM2-7 Protein Levels Are Significantly Reduced in *Mcm4*$^{chaos3/chaos3}$ MEFs, Resulting in a Loss of Dormant Origins

Previously, we reported that *Mcm4*^{Chaos3} homozygosity causes lower levels of the MCM2-7 proteins[21]. As these proteins exist in vast excess of the number of replication origins that fire in S phase, we investigated whether *Mcm4*^{Chaos3} homozygosity also causes lower levels of chromatin-bound MCM2-7 proteins in primary fibroblasts (MEFs) isolated from *Mcm4*$^{Chaos3/Chaos3}$ embryos. Western blots (Figure 1A) revealed an approximately 60% reduction of all components of the MCM2-7 complex on chromatin compared to wild-type cells. Chromatin immunoprecipitation followed by quantitative polymerase chain reaction also gave a similarly reduced rate of MCM2 at all specific loci examined (Figure S1A). To verify this reduced number of dormant origins in *Mcm4*$^{Chaos3/Chaos3}$ cells, we performed a DNA fiber assay using consecutive dual labeling of two kinds of modified dUTPs[22] (Figure 1B). Previous studies[12,13,19] have demonstrated that a moderate loss of the MCM2-7 complexes from chromatin has little effect on active origin density in untreated conditions. Indeed, there was no difference in the average origin-to-origin distances between wild-type and *Mcm4*$^{Chaos3/Chaos3}$ MEFs in untreated conditions (49.1 ± 2.6 kb and 49.6 ± 3.8 kb, respectively) (Figures 1C and S1B). However, in the presence of APH, which triggers dormant origin firing[12], the average origin-to-origin distance in wild-type cells was reduced to 37.4 ± 1.9 kb, significantly smaller than the 41.5 ± 0.97 kb observed in *Mcm4*$^{Chaos3/Chaos3}$ cells (Figures

1C and S1B). These findings collectively support the idea that *Mcm4*$^{Chaos3/Chaos3}$ cells have a significantly reduced number of dormant origins.

Mcm4$^{Chaos3/Chaos3}$ Cells Have an Increased Number of Spontaneously Stalled Forks

Even in unchallenged conditions, we found that *Mcm4*$^{Chaos3/Chaos3}$ cells had nearly twice as many asymmetric bidirectional forks (one fork being stalled) as wild-type cells (Figure 1D). These observations suggest that fork stalling occurs at a higher frequency in *Mcm4*$^{Chaos3/Chaos3}$ cells and may explain why they show reduced levels of replication proteins on chromatin, such as proliferating cell nuclear antigen (PCNA) and CDC45 (Figure 1A). Indeed, we found that an increased number of *Mcm4*$^{Chaos3/Chaos3}$ cells were positive for discrete, bright RPA32 foci (Figure 2A), which form at stalled replication forks[23,24]. Moreover, the frequency of *Mcm4*$^{Chaos3/Chaos3}$ cells positive for RAD17 phosphorylated at Ser645 (pRAD17)[25] was increased about 2-fold in untreated conditions (Figure 2A). RAD17 is a substrate of ATR and is involved in fork recovery[25]. It functions upstream of CHK1, a major effector kinase in the ATR pathway[26]. Previous studies reported that MCM depletion compromises checkpoint signaling in human cancer cell lines[14,27]. However, *Mcm4*$^{Chaos3/Chaos3}$ cells exhibited levels of CHK1 phosphorylation at Ser345 (pCHK1) similar to wild-type when challenged (Figure S2), suggesting that there is no major defect in the ATR-CHK1 pathway. This observation is consistent with data from a recent study using *Mcm2* hypomorphic mouse cells[19]. Despite relatively consistent detection of pRAD17 foci (Figure 2A), pCHK1 was barely detectable in

unchallenged *Mcm4*$^{Chaos3/Chaos3}$ cells (Figure S2). This may indicate that the number of stalled forks in *Mcm4*$^{Chaos3/Chaos3}$ cells is still not sufficient to induce full activation of the ATR-CHK1 pathway, allowing cell-cycle progression in the majority of *Mcm4*$^{Chaos3/Chaos3}$ cells. Stalled forks can potentially collapse, leading to the formation of double-strand breaks (DSBs). *Mcm4*$^{Chaos3/Chaos3}$ cells exhibited only a modest increase in the formation of γH2AX foci, a marker of DSBs[28], in S phase (Figure 2B, left). It should be noted that only a small percentage of S phase cells were positive for γH2AX foci regardless of genotype (Figure 2B). Thus, stalled forks appear to be stably maintained during S phase.

The Phe345Ile Change Impairs the Stability of the MCM2-7 Complex, but Not Helicase Activity

To understand what causes fork stalling in *Mcm4*$^{Chaos3/Chaos3}$ cells, we measured fork velocity using the DNA fiber technique (Figure 1B). Surprisingly, fork velocity was actually faster in *Mcm4*$^{Chaos3/Chaos3}$ cells compared to wild-type (Figure S1C). This apparently faster fork velocity could be partially explained by a lower level of fork terminations in *Mcm4*$^{Chaos3/Chaos3}$ cells due to a loss of dormant origins (see Figures S1D and S1E). The helicase functions of the MCM2-7 complex are carried out in the CMG complex ([4]; A. Costa, I.I., N. Tamberg, T. Petojevic, E. Nogales, M.R.B., and J.M. Berger, unpublished data). As the phenylalanine residue mutated in *Mcm4*$^{Chaos3/Chaos3}$ cells lies in a highly conserved domain (Figure S3A), we reconstituted the *Drosophila* CMG complex with the same mutant MCM4 to investigate its actual

helicase activity. The mutant complex was purified with a stoichiometry identical to wild-type (Figure 3A). Interestingly, the mutant CMG was slightly more efficient helicase than the wild-type CMG (Figure 3B), which may explain the faster fork speed in *Mcm4*$^{Chaos3/Chaos3}$ cells (Figures S1C and S1D). However, the consistently lower yields of the mutant CMG complex prompted us to examine the stability of the mutant MCM2-7 complex. Wild-type and mutant MCM2-7 complexes were purified and subjected to analytical fractionation. While the wild-type complexes were stable, it was clear that the mutant complexes dissociated into subfractions (Figure 3C), reflecting a suspected weaker association between MCM6 and MCM4 (Figure S3B). Similarly reduced interactions between MCM6 and MCM4 were also found in *Mcm4*$^{Chaos3/Chaos3}$ cells (Figure S3C). Therefore, these weaker associations are the most likely cause of the instability of the mutant complex, thereby contributing to a decreased amount of MCM2-7 proteins. Taken together, these data suggest that a loss of dormant origins, rather than a defect in helicase activity, is the major cause of stalled fork accumulation in *Mcm4*$^{Chaos3/Chaos3}$ cells.

Mcm4$^{Chaos3/Chaos3}$ Cells Exhibit Significantly Elevated Levels of RAD51 and BLM Foci

Stalled forks can be rescued by homology-directed repair involving RAD51[29]. We found that *Mcm4*$^{Chaos3/Chaos3}$ cells exhibit a mild increase (~2-fold) in spontaneous RAD51 foci formation (Figure 4A) and a drastic increase in foci formation for BLM helicase (Figure 4B), another protein involved in stalled fork recovery that counteracts

RAD51[30,31]. As yeast *mcm* mutants exhibit a hyperrecombination phenotype[32,33], we measured the frequency of homologous recombination (HR) events using the *FYDR* (fluorescent yellow direct repeat) transgenic locus system (Figures S4A and S4B)[34]. *Mcm4*$^{Chaos3/Chaos3}$ MEFs exhibited slightly higher frequencies of spontaneous HR events at this locus (Figures 4C and S4C), but were not significantly different from wild-type. Next, we challenged these MEFs with APH, which induces fork stalling and RAD51 foci formation (Figure 4A). Unlike treatment with a higher dose of APH (3 μM) or camptothecin (CPT), an inducer of DSBs at replication forks[35] (see Figure S2), a low dose of APH did not increase HR events (Figure 4D). Therefore, the rescue of stalled forks in *Mcm4*$^{Chaos3/Chaos3}$ cells may occur via the RAD51/BLM-mediated pathways without a significant increase in canonical HR events.

The Occurrence of Replication Intermediates Marked by FANCD2 Sister Foci in Prophase Is Markedly Enhanced in *Mcm4*$^{Chaos3/Chaos3}$ Cells, Leading to an Increased Level of Micronucleus Formation

Recent studies reported that unreplicated regions flanked by two stalled forks can persist into M phase and are marked with sister foci of FANCD2, a Fanconi anemia protein that presumably directs the resolution of such structures[36,37]. To investigate whether stalled forks are resolved before M phase entry in *Mcm4*$^{Chaos3/Chaos3}$ cells, we examined the formation of FANCD2 sister foci in prophase. While FANCD2 sister foci were very rarely found in wild-type cells, nearly 50% of *Mcm4*$^{Chaos3/Chaos3}$ cells were positive for

such foci at prophase (Figure 5A). Higher numbers of FANCD2 foci were also observed in *Mcm4*$^{Chaos3/Chaos3}$ cells throughout M phase (Figure S5A). We also found that foci formation for FANCI, a critical FANCD2-interacting protein[38,39], was drastically increased in *Mcm4*$^{Chaos3/Chaos3}$ cells as well (Figure S5B). This drastic increase in FANCD2 sister foci was associated with an elevated incidence of aberrant anaphase cells containing lagging and/or acentric chromosomes (Figure 5B). In accord with such structures in anaphase leading to micronucleus formation[37], *Mcm4*$^{Chaos3/Chaos3}$ cells also exhibited a 2-fold increase in spontaneous micronuclei MN compared to wild-type cells (Figure 5B). This is a relatively small increase compared to the 20-fold increase observed in erythrocytes, the original phenotype that led to the identification of *Mcm4*^{Chaos3} [21]. However, this can be attributed to the specific nature of erythrocytes as enucleated cells, as MN may occur more frequently in the absence of functional DNA repair and checkpoint responses in erythroblasts.

Mcm4$^{Chaos3/Chaos3}$ Cells Exhibit Chromosome Number and Structural Instability in Late M Phase

To understand the extent to which lagging chromosomes contribute to MN formation in *Mcm4*$^{Chaos3/Chaos3}$ cells, we quantitated the number of MN positive for the centromeric protein CENP-A[40]. We found that the incidence of CENP-A positive MN is significantly elevated in *Mcm4*$^{Chaos3/Chaos3}$ cells compared to wild-type (Figure 5C), indicating an increased level of aneuploidy. Since aneuploid cells are rare and may have a reduced rate

of proliferation[41], we performed interphase fluorescence in situ hybridization (FISH) using probes specific to near-centromeric regions of chromosome 16. This revealed not only a significant increase in aneuploidy in *Mcm4*$^{Chaos3/Chaos3}$ cells but also a significant increase in tetraploidy (Figure S5C). The exact mechanism responsible for tetraploidization has not been determined, but could result from cytokinesis failure (Movies S1–S3). Acentric chromosomes resulting from chromosome breaks, on the other hand, create CENP-A-negative MN, which were found in ~40% of all MN in untreated *Mcm4*$^{Chaos3/Chaos3}$ cells (compare the MN frequencies in Figures 5B and 5C). As reported previously[21], G-banding analysis of metaphase chromosomes revealed no significant increase in spontaneous breaks in *Mcm4*$^{Chaos3/Chaos3}$ cells. However, it did reveal an increase in numerical and structural aberrations in *Mcm4*$^{Chaos3/Chaos3}$ cells, such as translocations and dicentric chromosomes (Figures 5D and S5D). Therefore, it is likely that acentric fragments arise after metaphase through the conversion of unresolved replication intermediates to DSBs. Indeed, we found a >2-fold increase in the number of MN positive for γH2AX foci in *Mcm4*$^{Chaos3/Chaos3}$ cells that had just completed mitosis (Figure 5E). Interestingly, we also found a significant increase in the number of γH2AX foci in the main nuclei of *Mcm4*$^{Chaos3/Chaos3}$ cells in early G1 phase (Figure S5E). These data indicate that unresolved replication intermediates are more susceptible to collapse after metaphase, giving rise to DSBs.

The Chromosome Instability Seen in *Mcm4*$^{Chaos3/Chaos3}$ Cells Promotes the Formation of a Variety of Spontaneous Tumors

Previously, we reported that *Mcm4*$^{Chaos3/Chaos3}$ females in the C3HeB/FeJ (C3H) background develop mammary tumors only[21]. Since tumor spectrum is strongly influenced by genetic background, as seen in *Mcm2* hypomorph mice[19], we bred *Mcm4*^{Chaos3} into the C57BL/6J (B6) strain to investigate the effect of genetic background on *Mcm4*^{Chaos3} tumorigenesis. All B6 *Mcm4*$^{Chaos3/Chaos3}$ females succumbed to neoplasms by the age of 16 months with a mean latency of 12.4 months (Figure 6A and Table S1). However, unlike C3H *Mcm4*$^{Chaos3/Chaos3}$ females, B6 *Mcm4*$^{Chaos3/Chaos3}$ females were highly prone to histiocytic sarcomas. Histiocytic sarcoma is a rare malignant proliferation of macrophage-like cells in humans and mice (Figure 6B)[42,43]. We also generated 21 F1 *Mcm4*$^{Chaos3/Chaos3}$ females by crossing B6 congenic (N8) and C3H congenic (N8) mice. All F1 *Mcm4*$^{Chaos3/Chaos3}$ females developed tumors with a mean latency of 14.2 months (Figure 6A and Table S2). Histiocytic sarcomas and lymphomas were the predominant neoplasms (Figures 6B and 6C), while three mammary adenocarcinomas were also observed. These data suggest that the chromosome instability seen in *Mcm4*$^{Chaos3/Chaos3}$ cells (Figure 6D) is not restricted to mammary tumor formation but is relevant to the formation of a variety of tumors.

Discussion

In the present study, we used primary *Mcm4*$^{Chaos3/Chaos3}$ MEFs as a model to investigate the mechanism by which a loss of dormant origins confers chromosome instability. As summarized in Figure 6D, our findings suggest that a loss of dormant origins leads to the accumulation of stalled forks, ultimately resulting in incomplete DNA replication. The resulting unresolved replication intermediates are then carried over into M phase, thereby interfering with proper chromosome segregation. As a consequence, *Mcm4*$^{Chaos3/Chaos3}$ cells exhibit increased incidences of aneuploidy, chromosome breaks, translocations, and tetraploidy, all of which are commonly observed in cancer cells. Given the high tumor predisposition of *Mcm4*$^{Chaos3/Chaos3}$ mice, the chromosome instability seen in *Mcm4*$^{Chaos3/Chaos3}$ cells is likely to promote tumorigenesis. Collectively, these findings suggest that dormant origins exist in abundance because of their critical role in fork recovery in unchallenged S phase, thereby promoting chromosome stability and tumor suppression.

Even in unchallenged S phase, replication forks stall due to the presence of endogenous DNA lesions. It is currently thought that stalled forks can be recovered by (1) homology-directed repair, (2) translesion synthesis (TLS) with error-prone DNA polymerases, or (3) passive replication from an adjacent origin[44]. The use of dormant origins for stalled fork rescue can be viewed as an example of the last option, although this option originally implied rescue by adjacent major origins without any de novo firing. Our data show that the average density of active origins remains unchanged

between wild-type and *Mcm4*$^{Chaos3/Chaos3}$ cells in unchallenged S phase (Figure 1C). This observation supports the previously held notion[12] that only dormant origins in the vicinity of stalled forks are allowed to fire and are therefore not likely to be detected as clearly as major origins by DNA fiber analysis (see model in Figure S6). Further studies are needed to elucidate the molecular mechanisms responsible for the use of dormant origins for stalled fork rescue.

Among the multiple pathways for stalled fork recovery, how an appropriate pathway is chosen for spontaneously stalled forks is largely unknown. An increased frequency of spontaneously stalled forks in *Mcm4*$^{Chaos3/Chaos3}$ cells led us to hypothesize that dormant origins play a more significant role in the recovery of spontaneously stalled forks than previously anticipated[12,13]. In agreement with this hypothesis, a loss of dormant origins appears to activate homology-directed repair for the recovery of stalled forks (Figure 4A). Moreover, a recent study showed that MCM depletion in human primary lymphocytes leads to an increase in RAD51 foci formation[45]. Unlike some yeast *mcm* mutants[32,33,46], *Mcm4*$^{Chaos3/Chaos3}$ cells exhibited no significant increase in canonical HR events when measured at the *FYDR* locus. This finding is consistent with recent data[29] and can also be explained by the antirecombinogenic role of BLM[30], which also forms an elevated number of foci in *Mcm4*$^{Chaos3/Chaos3}$ cells (Figure 4B). It should be noted that this reporter assay detects only unequal recombination events with tract lengths of more than a few hundred bases. Therefore, our data cannot exclude the possibility of an increase in gene conversion events with much shorter tract lengths.

Despite the activation of homology-directed repair, stalled forks do not seem to be fully rescued, as >50% of *Mcm4*$^{Chaos3/Chaos3}$ cells exhibit FANCD2/I foci in prophase (Figures 5A and S5B), a marker of unresolved replication intermediates[36,37]. These observations suggest that dormant origins could be a preferred option for fork recovery over other pathways. This idea is quite feasible, considering the possible harmful consequences of homology-directed repair and TLS, such as genome rearrangements[47] and point mutations[48], respectively. A recent study reported that MCM depletion in human primary lymphocytes causes hyperactivation of the nonhomologous end-joining (NHEJ) pathway, resulting in an increase in the misrepair of DSBs[45]. Interestingly, we found that *Mcm4*$^{Chaos3/Chaos3}$ cells exhibited an increased incidence of translocations and dicentric chromosomes (Figures 5D and S5D). Based on our model (Figure 6D), chromosome breakage is likely to occur in late M phase. It is then possible that these broken chromosome ends are repaired by NHEJ in G1 phase, generating translocations. Taken together, these data suggest the hypothesis that the preferential use of dormant origins for stalled fork rescue occurs to prevent a possible increase in misrepair events resulting from hyperactivated DNA repair pathways.

In contrast to the commonly held idea that stalled forks eventually collapse, we found that spontaneously stalled forks are actually well preserved in S phase in primary mouse cells (Figure 2B). In fact, a fraction of stalled forks persisted into M phase, as evidenced by an increased number of FANCD2/I foci in prophase (Figures 5A and S5B). While the majority of these stalled forks are likely to be resolved by the downstream Fanconi pathway, a certain fraction of them remain unresolved, presumably physically

interconnecting sister chromatids[36,37]. Our study showed that a loss of dormant origins alone is capable of inducing such chromosome missegregation events without any exogenous replication inhibitor. The persistence of stalled forks in *Mcm4*$^{Chaos3/Chaos3}$ cells also partially activates the ATR pathway, as evidenced by a significant increase in pRAD17 foci formation (Figure 2A). This may explain why there exists a subtle but significant level of *Mcm4*$^{Chaos3/Chaos3}$ cells accumulated at the G2/M phases as described previously[21]. It should also be noted that a low level of unresolved replication intermediates apparently escape from any known cell-cycle checkpoint, as previously demonstrated[49,50].

Consistent with the role of dormant origins in tumor suppression, a recent study reported that tumor formation in *Mcm4*$^{Chaos3/Chaos3}$ mice is significantly delayed by increasing the levels of chromatin-bound MCM2-7 proteins[18]. We find that *Mcm4*$^{Chaos3/Chaos3}$ mice exhibit phenotypes very similar to what has been seen in *Mcm2* hypomorph mice[19,20], such as a modest increase in the levels of γH2AX and phosphorylated p53 (Figure S2). While it remains to be determined, *Mcm4*^{Chaos3} and *Mcm2* hypomorph mice may share essentially the same mechanism for tumorigenesis. One striking difference between these two mouse models is tumor latency; *Mcm2* hypomorph mice develop tumors much faster than *Mcm4*$^{Chaos3/Chaos3}$ mice. As discussed elsewhere[20], this difference could be attributed to the distinct roles of each component of the MCM2-7 complex. Moreover, the presence of the transgene in *Mcm2* hypomorph mice may additionally contribute to tumorigenesis by altering the expression of nearby genes.

Chromosome instability is a hallmark of cancer cells. However, how it is generated is still not well understood. We found that an increased frequency of stalled forks is sufficient to induce multiple types of chromosome instability. This idea is also consistent with an emerging hypothesis that replication stress is the major cause of the chromosome instability observed in cancer[51,52]. Since the majority of cancer-initiating events deregulate the proper G1/S transition[53], a loss of dormant origins may occur at an early stage of carcinogenesis. In this context, the findings presented in this study are highly relevant to our understanding of cancer development.

Experimental Procedures

Animals and MEFs

Mcm4^{Chaos3} was introduced into the B6 and C3H backgrounds by backcrossing seven times (N8). F1 mice were generated by crossing congenic B6 and C3H lines. All experiments involving mice were approved by the Institutional Animal Care and Use Committee (IACUC). MEFs were generated from 12.5‑14.5 dpc embryos and cultured using a standard procedure. F1 MEFs were used for all experiments unless otherwise noted.

Western Blotting and Immunofluorescence Microscopy

Western blotting and immunofluorescence staining were carried out using standard procedures. Cell fractionation was performed using the Qproteome Nuclear Protein Kit (QIAGEN, Germantown, MD). Detailed procedures are provided in Supplemental Experimental Procedures.

DNA Fiber

We used the DNA fiber protocol previously developed by Sugimura et al[22]. Briefly, ongoing forks were labeled with digoxigenin-dUTPs for 20 min and then with biotin-dUTPs for 30 min. Labeled cells were dropped onto slides, fixed, and dipped into lysis buffer. The resulting DNA fibers were released and extended by tilting the slides.

Incorporated dUTPs were then visualized by immunofluorescent detection using Anti-digoxigenin-rhodamine (Roche, Branford, CT) and streptavidin, Alexa Fluor 488 (Invitrogen, Carlsbad, CA).

HR Events at the *FYDR* Locus

HR-positive recombinant cells were detected by methods described previously[34]. Detailed procedures are provided in Supplemental Experimental Procedures.

Aberrant Anaphase and Cytokinesis-Block Micronucleus Assays

For both analyses, cells were cultured on coverslips, fixed, and stained with DAPI for fluorescence microscopy. At least 100 anaphases were scored per experiment. To score micronuclei, cytochalasin B (0.72 μg/ml) was added to block cytokinesis 16 hr before harvest. The resulting binucleated cells were scored for the presence of micronuclei. At least 200 binucleated cells were scored per experiment. For the CENP-A and γH2AX analyses, cells were subjected to antibody treatment following fixation.

Purification and Characterization of the MCM2-7 and CMG Complexes

The baculovirus vector expressing the *Drosophila melanogaster* MCM4^{Chaos3} protein was constructed by standard PCR-based site-directed mutagenesis and the Invitrogen Bac-to-Bac protocol. The conserved residue Phe349 was replaced by isoleucine in the resulting

mutant protein. The purification of the *Drosophila* CMG and MCM2-7 complexes was performed as described previously[4]. The MCM3 and Sld5 proteins carry N-terminal FLAG and HA affinity tags, respectively. For the MCM2-7 stability experiments, fractions from the Mono Q HR 5/5 column chromatography step that contained the MCM 2-7 hexameric complex were pooled and injected onto the Mono Q PC 1.6/5 column connected to the Pharmacia SMART micropurification system. The column was developed with ten column volumes of linear 300‑1100 mM potassium acetate gradient, and 20 fractions were collected and analyzed by SDS-PAGE and Coomassie brilliant blue staining. The DNA helicase assays were carried out with an M13-based circular substrate as described previously[4], except that the ATP concentration was kept at 10 mM.

Acknowledgements

We thank Kazuto Sugimura for the DNA fiber protocol and Bevin Engelward for the *FYDR* mice, as well as David Largaespada, Anja Bielinsky, and Alexandra Sobeck for their critical reading of the manuscript. We also thank LeAnn Oseth and Dr. B. Hirsch for the G-banding analyses and interpretations, as well as Andy Lane for his assistance in the live-cell imaging experiments. This study was supported by grants (to N.S.) from Susan G. Komen for the Cure (BCTR0707864) and the NCI (R01CA148806). The work at UC Berkeley was supported by the NIH grants CA R37-30490 (to M.R.B.).

Figure legends

Figure 1

Mcm4$^{Chaos3/Chaos3}$ Cells Have Reduced Amounts of the MCM2-7 Proteins on Chromatin, Resulting in a Reduced Number of Dormant Origins. (A) All components of the MCM2-7 complex are significantly reduced in *Mcm4*$^{Chaos3/Chaos3}$ cells. Reduction levels of chromatin-bound MCM2/4/7 as well as other replication proteins in *Mcm4*$^{Chaos3/Chaos3}$ (C3) cells were estimated by referencing wild-type (WT) proteins loaded in different amounts (left). In *Mcm4*$^{Chaos3/Chaos3}$ cells, the MCM3/5/6 proteins were also reduced in both the chromatin fraction and whole-cell extract (WCE) (right). Protein samples were obtained from cells cultured asynchronously. Actin and stained membranes were used as loading controls. (B) Schematic presentation of consecutive dual labeling in the DNA fiber assay. Replication forks were labeled with digoxigenin-dUTPs (dig-dUTPs, red) for 20 min followed by biotin-dUTPs (green) for 30 min. (C) There is no significant difference in the average density of active origins between wild-type and *Mcm4*$^{Chaos3/Chaos3}$ cells in untreated conditions (UNT). However, APH treatment induced a significantly lower origin density in *Mcm4*$^{Chaos3/Chaos3}$ cells ($p < 0.05$, t test). These values were determined by measuring the distances between adjacent origins as shown (left). Bars show standard error of the mean (SEM). (D) *Mcm4*$^{Chaos3/Chaos3}$ cells show a significant increase in the frequency of asymmetric forks (see image on the left). The average frequencies are shown with SEMs and are compared by χ^2 test ($p < 0.005$, see asterisk).

Figure 2

Elevated Levels of RPA, pRAD17, and γH2AX Foci Formation Are Observed in *Mcm4*$^{Chaos3/Chaos3}$ Cells. (A) An increased number of *Mcm4*$^{Chaos3/Chaos3}$ cells are positive for RPA32 and pRAD17 (Ser645) foci. Shown are the average percentages of cells positive for each marker in the untreated (UNT) and APH-treated (300 nM for 24 hr) conditions. Bars are SEMs for ten different fields obtained from two independently performed experiments. Representative images are shown on the right with a magnified view of the selected nuclei. Nuclei are stained with DAPI (blue). Scale bars are 40 μm. (B) *Mcm4*$^{Chaos3/Chaos3}$ cells show a slight increase in the formation of γH2AX foci in S phase. Shown are the average percentages of cells positive for γH2AX foci and the distribution of the number of γH2AX foci per cell in the untreated condition (left). S phase cells were detected by incorporation of dUTPs. Bars are SEMs for three independent experiments. Representative images are shown on the right. Scale bars are 10 μm.

Figure 3

The Mutant MCM2-7 Complex Is Unstable but Retains Proper Helicase Activity in the CMG Complex. (A) Silver-stained 10% SDS-polyacrylamide gels (PAGE) show purified wild-type and mutant CMG complexes. (B) An autoradiograph of a helicase assay showing the radiolabeled products separated by PAGE (top). M13 circular DNA annealed

with a radiolabeled oligonucleotide was used as a substrate. The migration of double-stranded substrate and displaced oligo is shown with arrows. The amount of protein in femtomoles in each reaction is indicated. The first two lanes show the completely denatured substrate and the substrate with no protein. The reactions were performed in duplicate and quantified as a percentage of substrate processed, as shown in the bottom graph. Error bars show standard deviations. (C) The salt elution profiles of wild-type and mutant MCM2-7 from Mono Q anion-exchange chromatography show the relative instability of the mutant complex (top). Blue and red lines show the relative absorbance at 280 nm for the wild-type and mutant gradient runs, respectively (left y axis); the gray axis indicates salt concentration (right y axis). The peak protein fractions from the mutant gradient were separated by SDS-PAGE and stained with Coomassie brilliant blue (bottom); the fraction numbers are shown above each lane. The starting stoichiometric mutant MCM2-7 complex that was loaded onto this column is shown in the first lane, and the pooled peak fractions (15 and 16) from the WT gradient are shown in the last lane.

Figure 4

An Increase in RAD51 and BLM Foci Formation in *Mcm4*$^{Chaos3/Chaos3}$ Cells Does Not Lead to a Significant Increase in Homologous Recombination Events. (A) An increased number of *Mcm4*$^{Chaos3/Chaos3}$ cells are positive for RAD51 foci. (B) BLM foci formation is drastically elevated in *Mcm4*$^{Chaos3/Chaos3}$ cells. Shown in (A) and (B) are the average percentages of cells positive for ≥2 foci in the untreated and APH-treated conditions

(left). The average number of foci per cell is also shown. Bars are SEMs for ten different fields obtained from two independently performed experiments. Representative images are shown on the right. Scale bars are 20 μm. (C) No significant increase in HR events was detected at the *FYDR* locus in *Mcm4*$^{Chaos3/Chaos3}$ cells compared to wild-type. Bars are SEMs for recombinant frequencies determined by analyzing at least 16 embryos per genotype. (D) No significant increase in HR events was detected at the *FYDR* locus in either wild-type or *Mcm4*$^{Chaos3/Chaos3}$ cells after a low dose of APH treatment. CPT and a higher dose of APH were used as positive controls. Bars are SEMs for recombinant frequencies determined by analyzing at least three independent MEF lines.

Figure 5

Mcm4$^{Chaos3/Chaos3}$ Cells Have a Drastically Increased Number of FANCD2 Sister Foci at Prophase, Preceding Abnormal Anaphase and Micronucleation. (A) An increased frequency of FANCD2 sister foci is found in *Mcm4*$^{Chaos3/Chaos3}$ cells. The average percentages of cells positive for FANCD2 sister foci (top) and the average numbers of FANCD2 sister foci per cell (bottom) are shown with SEMs. Note that the number of FANCD2 sister foci per cell increases approximately 2-fold in *Mcm4*$^{Chaos3/Chaos3}$ cells compared to wild-type cells, while nearly all cells become positive for such foci in the presence of APH. Representative images are shown on the right with a magnified view (indicated by squares). (B) An increased number of *Mcm4*$^{Chaos3/Chaos3}$ cells undergo abnormal anaphase, forming micronuclei (MN). The average frequencies of abnormal

anaphases containing lagging chromosomes and/or fragments are shown for wild-type and *Mcm4*$^{Chaos3/Chaos3}$ cells with SEMs (left, top). B6 MEFs were used for anaphase analysis. The average MN frequencies are also shown for wild-type and *Mcm4*$^{Chaos3/Chaos3}$ cells with SEMs (left, bottom). MN were detected using the cytokinesis-block micronucleus assay[54]. Representative images are shown on the right for a normal anaphase, an abnormal anaphase containing lagging chromosomes, a normal binucleated cell, and one with a micronucleus. Scale bars are 5 μm. (C) *Mcm4*$^{Chaos3/Chaos3}$ cells have an increased number of centromeric (CENP-A^{+}) MN compared to wild-type cells. The average frequencies of CENP-A^{+} MN were determined from three independently performed experiments and are shown with SEMs. Representative images are shown on the right. (D) G-banding analysis of metaphase chromosomes shows no evidence for increased chromosome breaks but does reveal an increased occurrence of translocations in *Mcm4*$^{Chaos3/Chaos3}$ cells. Representative karyotypes containing translocations are also shown (bottom). (E) *Mcm4*$^{Chaos3/Chaos3}$ cells have an increased number of γH2AX-foci-positive (γH2AX^{+}) MN compared to wild-type cells. The average frequencies of γH2AX+ MN were determined from three independently performed experiments and are shown with SEMs. Representative images are shown on the right for MN positive and negative for γH2AX (red) in binucleated cells. APH was used as a positive control (150 nM for 24 hr). Nuclei are stained with DAPI (blue). Scale bars (A, C, and E) are 10 μm.

Figure 6

Many Different Types of Spontaneous Tumors Are Observed in *Mcm4*$^{Chaos3/Chaos3}$ Mice. (A) Tumor-free survival curves for B6 and F1 *Mcm4*$^{Chaos3/Chaos3}$ (*C3*) and wild-type (WT) females. (B) Representative images of histiocytic sarcomas. A hematoxylin and eosin (H&E) stain (top) shows a diffusely hypercellular liver area with round cells (black arrowheads) smaller than hepatocytes (unfilled arrowheads). Immunohistochemistry (IHC) with Mac-2, a macrophage marker, identified these small round cells (stained brown) as histiocytes (bottom). (C) Representative images of F1 *Mcm4*^{Chaos3} gastrointestinal lymphomas, including an H&E image (top) and an IHC image with B220, a B cell marker (bottom). (D) A model for chromosome instability driven by a loss of dormant origins. A lack of dormant origins increases the frequency of unresolved replication intermediates marked with FANCD2 sister foci (red diamonds) in M phase. Although such lesions can be rescued in a Fanconi-pathway-dependent manner, a significant fraction persists into anaphase, interconnecting sister chromatids. As a result, the disjunction of sisters is disrupted and lagging chromosomes occur. This has three possible consequences: (1) Tetraploidy may occur due to cytokinesis failure, when the frequency of nondisjunction is high[55], (2) Aneuploidy could occur due to the nondisjunction of a few sisters, forming MN positive for CENP-A, or (3) Breaks may arise when unresolved replication intermediates are converted into DSBs, generating acentric fragments. In this case, MN positive for γH2AX foci would be formed. These aberrations lead to multiple types of chromosome instability, thereby contributing to tumorigenesis.

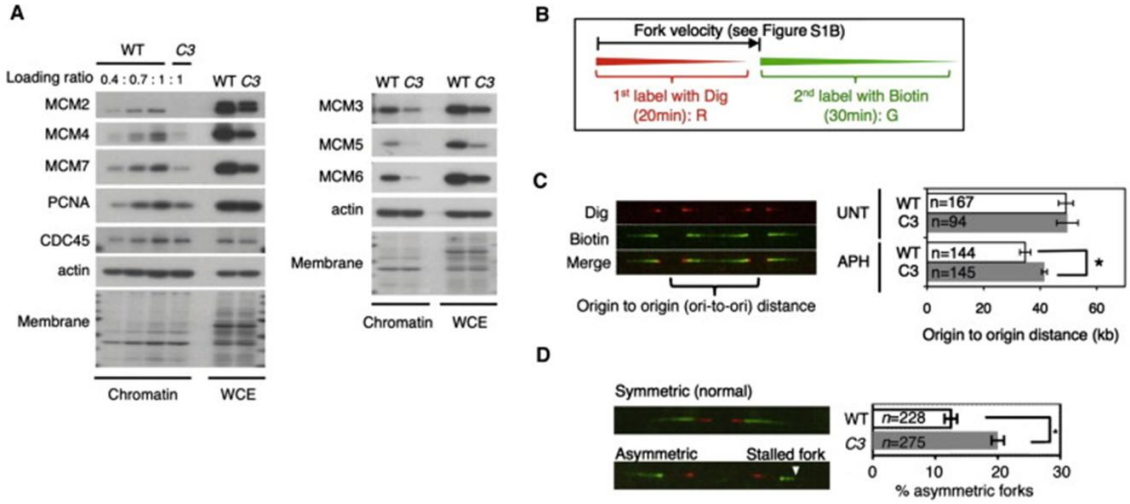
A
WT
C3
Loading ratio 0.4 : 0.7 : 1 : 1
WT C3
MCM2
MCM4
MCM7
PCNA
CDC45
actin
Membrane
Chromatin
WCE
WT C3
WT C3
MCM3
MCM5
MCM6
actin
Membrane
Chromatin
WCE
B
Fork velocity (see Figure S1B)
1st label with Dig (20min): R
2nd label with Biotin (30min): G
C
Dig
Biotin
Merge
Origin to origin (ori-to-ori) distance
UNT
APH
WT
C3
n=167
n=94
n=144
n=145
*
0
20
40
60
Origin to origin distance (kb)
D
Symmetric (normal)
Asymmetric
Stalled fork
WT
C3
n=228
n=275
0
10
20
30
% asymmetric forks

Figure 2 Kawabata et al., 2011

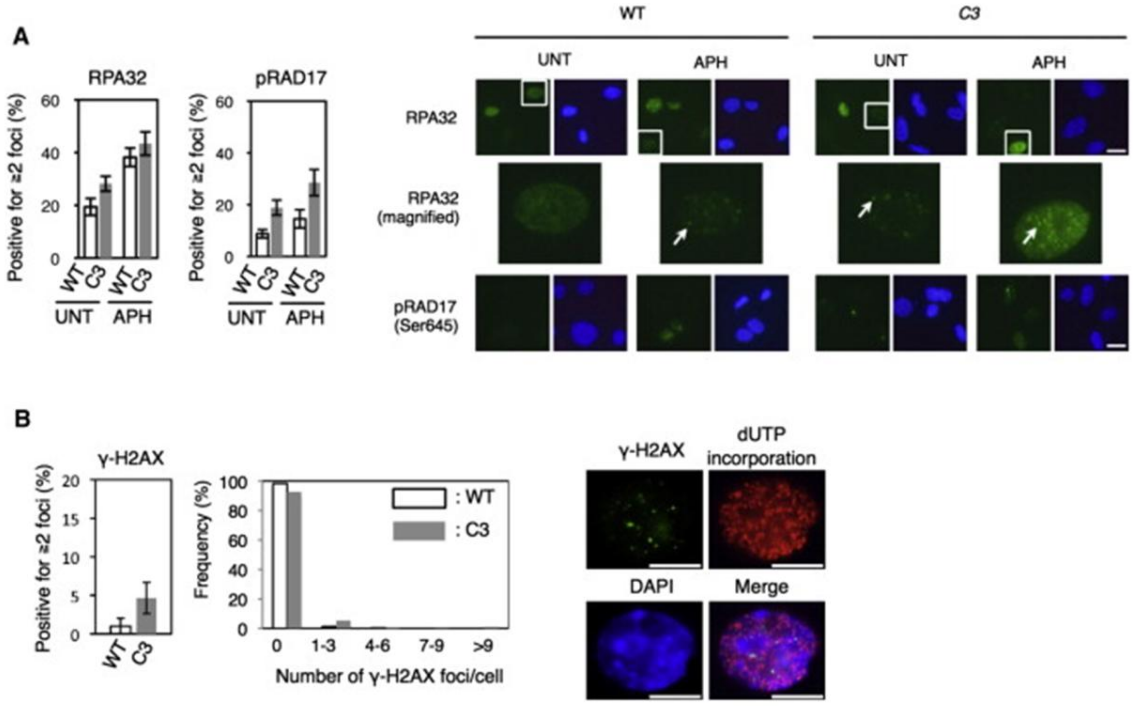

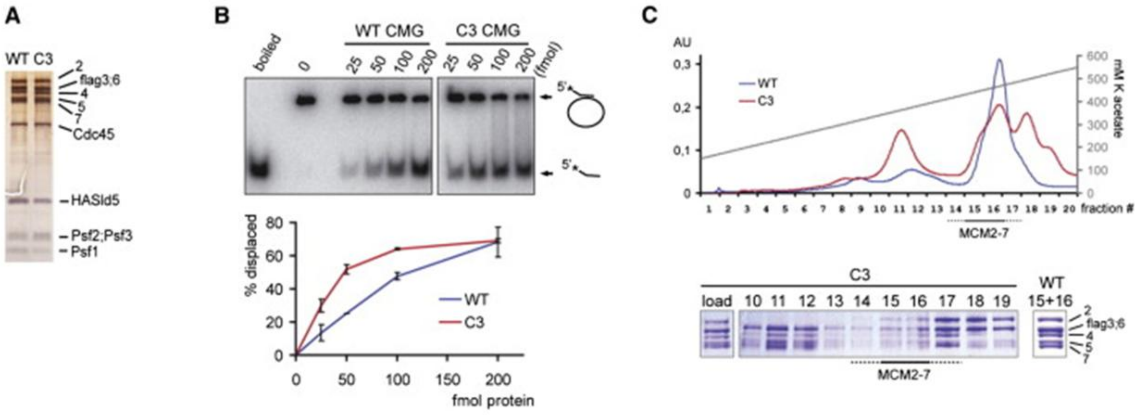
A
WT C3
2
flag3:6
4
5
7
Cdc45
HASld5
Psf2:Psf3
Psf1
B
boiled
0
WT CMG
C3 CMG
25 50 100 200
25 50 100 200
(fmol)
5'
5'
% displaced
80
60
40
20
0
0 50 100 150 200
fmol protein
WT
C3
C
AU
0,3
0,2
0,1
0
WT
C3
600 500 400 300 200 100 0
mM K acetate
1 2 3 4 5 6 7 8 9 10 11 12 13 14 15 16 17 18 19 20 fraction #
MCM2-7
C3
load 10 11 12 13 14 15 16 17 18 19
WT
15+16
2
flag3:6
4
5
7
MCM2-7

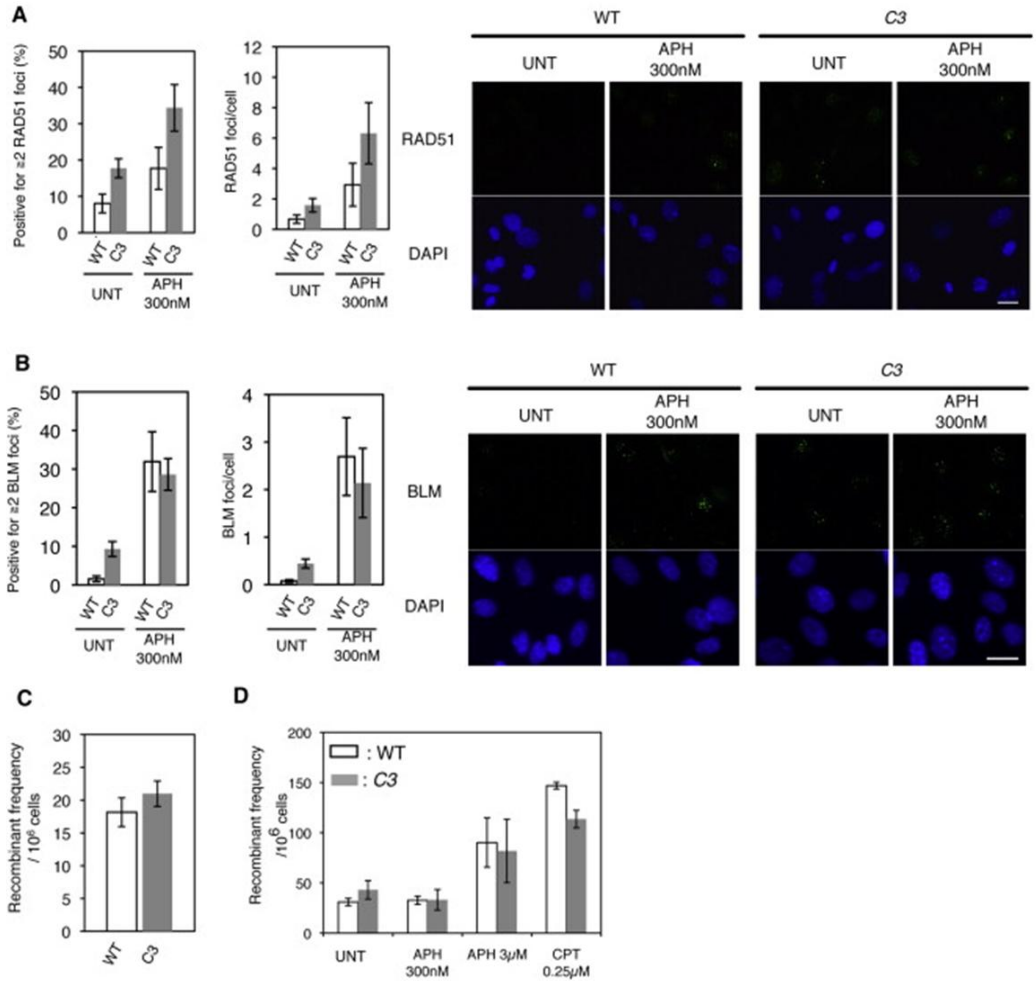
A
Positive for ≥2 RAD51 foci (%)
RAD51 foci/cell
WT
C3
UNT
APH 300nM
RAD51
DAPI
B
Positive for ≥2 BLM foci (%)
BLM foci/cell
BLM
C
Recombinant frequency / 10^6 cells
D
: WT
: C3
APH 3μM
CPT 0.25μM

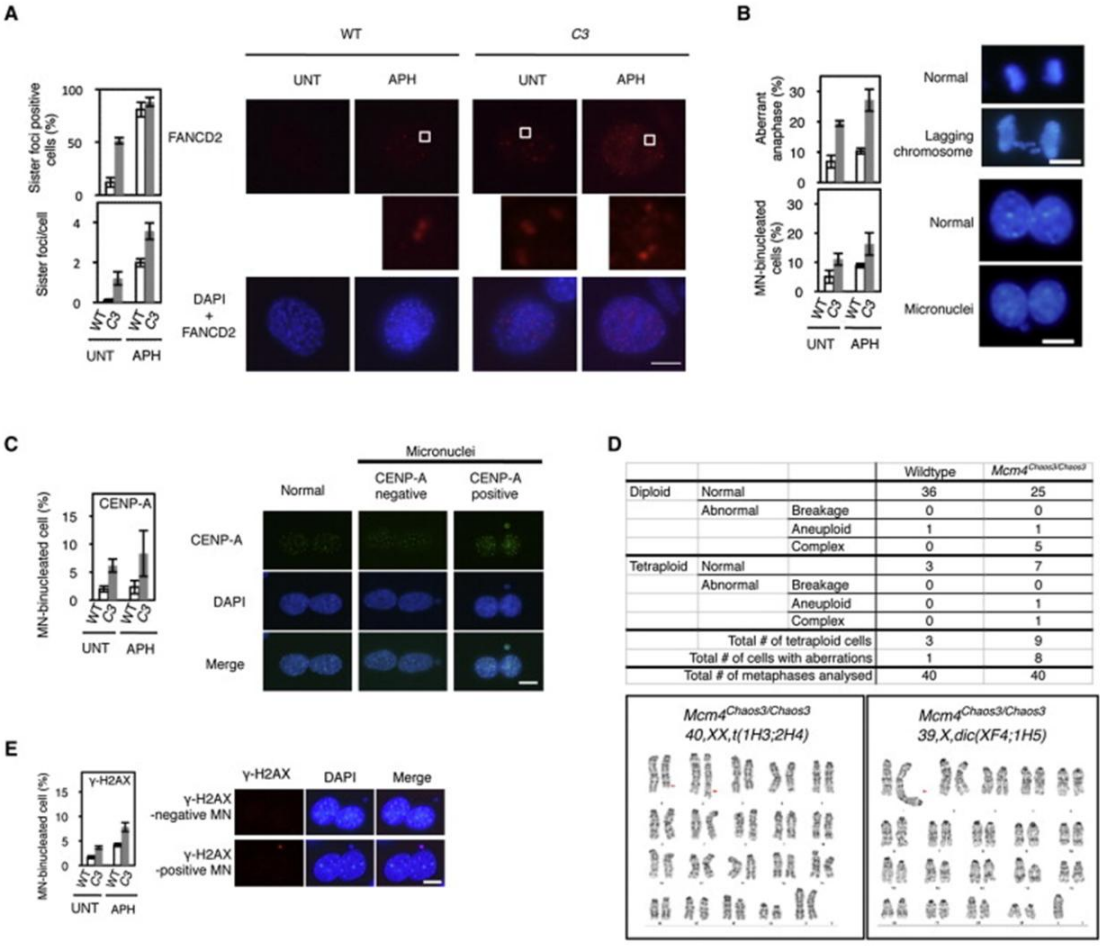

			Wildtype	*Mcm4*$^{Chaos3/Chaos3}$
Diploid	Normal		36	25
	Abnormal	Breakage	0	0
		Aneuploid	1	1
		Complex	0	5
Tetraploid	Normal		3	7
	Abnormal	Breakage	0	0
		Aneuploid	0	1
		Complex	0	1
	Total # of tetraploid cells		3	9
	Total # of cells with aberrations		1	8
	Total # of metaphases analysed		40	40

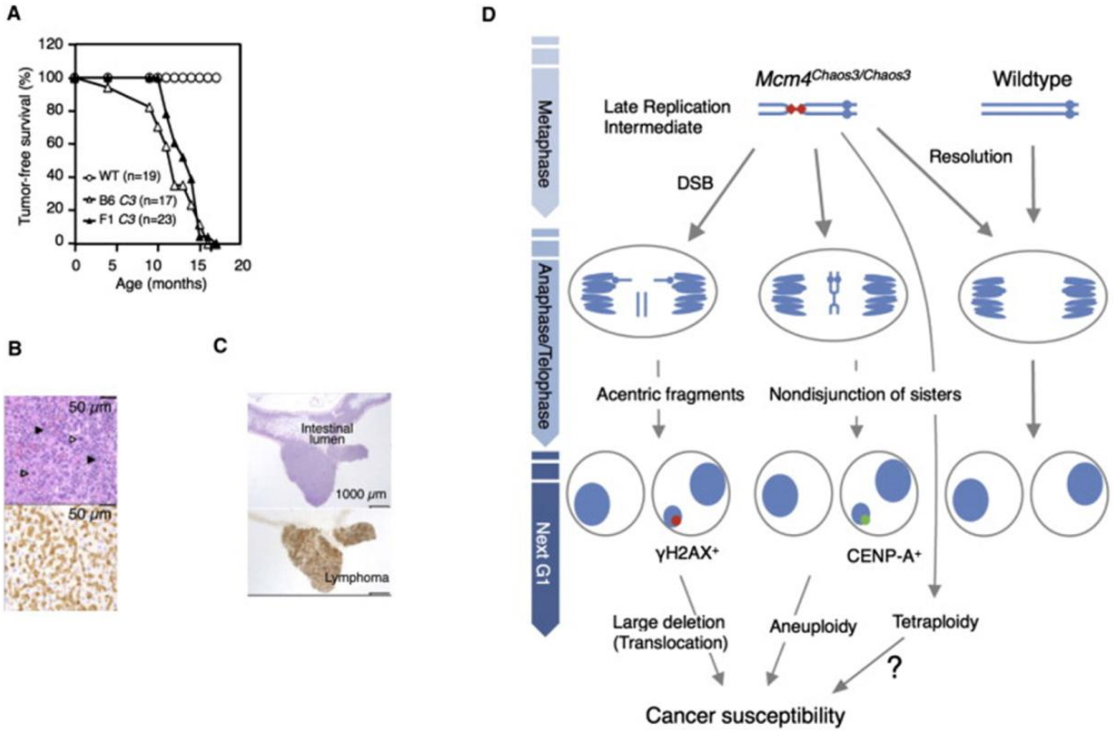
A
Tumor-free survival (%)
120
100
80
60
40
20
0
0 5 10 15 20
Age (months)
WT (n=19)
B6 C3 (n=17)
F1 C3 (n=23)
B
50 μm
50 μm
C
Intestinal lumen
1000 μm
Lymphoma
D
Metaphase
Anaphase/Telophase
Next G1
Mcm4Chaos3/Chaos3
Wildtype
Late Replication Intermediate
DSB
Resolution
Acentric fragments
Nondisjunction of sisters
γH2AX+
CENP-A+
Large deletion (Translocation)
Aneuploidy
Tetraploidy
?
Cancer susceptibility

Supplemental experimental procedures

ChIP

Sigma's Imprint Chromatin Immunoprecipitation Kit was used. Briefly, cells in an asynchronous culture were harvested. The DNA and proteins were cross-linked using 1% formaldehyde and then quenched in 0.125M glycine. After cell lysis, the nuclei were precipitated and the DNA was fragmented by sonication. A portion of the fragmented DNA was saved as an input control. For the rest of the sample, immunoprecipitation (IP) was performed with the anti-MCM2 antibody (Abcam, ab3159) that gave the best performance judged by semi-quantitative PCR results using the primer pairs specific to the rDNA locus origins[56] among all antibodies tested in our laboratory. After reversal of the cross-links and proteinase K digest, DNA was used for quantitative PCR using standard conditions.

Coimmunoprecipitation

Coimmunoprecipitation was performed using a kit (Dynabeads Co-Immunoprecipitation Kit, Invitrogen). Briefly, 3x106 cells were harvested in PBS and proteins were extracted using an extraction buffer (Buffering salts pH7.4, 110 mM KOAc, 0.5% Triton X-100, protease inhibitor; complete EDTA-free). After centrifugation (2600 x g for 5min), the supernatant was incubated with anti-MCM2 or anti-rabbit IgG antibody-bound beads,

followed by several washes. Bound proteins were released by buffer EB (Buffering salts, pH2.8) and used for western blotting.

Interphase FISH

DNA isolated from BAC clones RP23-290E4 and RP23-356A24 was used to make probes specific to regions flanking the centromere of chromosome 16[57] using the Vysis Nick Translocation kit (Abbott Molecular) as well as Green-496-dUTPs and Orange-552-dUTPs from Enzo Life Sciences. Hybridization was performed under standard conditions. Images were captured using the Axio Imager A1 (Zeiss). At least 200 nuclei were scored for the number of FISH signals per experiment. A total of >600 nuclei was observed per genotype in three sets of independently performed experiments.

Generation of MEFs

MEFs were obtained from 12.5-14.5 dpc embryos using a standard procedure. A homogenized embryo was plated onto a 10 cm dish (p0), replated onto a 15 cm dish (p1), and frozen in three vials. For experiments, one vial was thawed and the cells were cultured on a 10 cm dish for a few days (p2). The resulting 6-9 x 106 cells (p3) were then replated for experimental use.

Antibodies

For western blotting and immunocytofluorescence, we used Abcam anti-MCM antibodies (ab3159, ab4460, ab4459, ab17967, ab4458 and ab2360 for MCM2, MCM3, MCM4, MCM5, MCM6 and MCM7, respectively), anti-pan actin (Thermo Scientific; MS-1295-P1ABX), anti-RAD51 (Calbiochem; PC130) anti-CDC45, anti-FANCD2, anti-BLM, anti-FANCI (Abcam; ab56476, ab2187, ab476, and ab74332, respectively), anti-phospho-RAD17, anti-phospho-CHK1, anti-H2AX, anti-PCNA, anti-CENP-A, anti-RPA32, anti-phospho-p53, and anti-histone H3 (Cell Signaling; #3421, #2341, #2577, #2586, #2048, #2208, #9284, and #9847, respectively).

Western Blotting

Cell extracts were harvested using Laemili's sample buffer, run on 8 or 12% SDS-polyacrylamide gels, and transferred to polyvinylidene membranes. Membranes were then incubated with primary antibodies, followed by incubation with the appropriate secondary antibodies. Proteins were visualized using the Immobilon Western Chemiluminescent HRP substrate (Millipore, WBKLS0500). Cell fractionation was performed using the Qproteome Nuclear Protein Kit (Qiagen). Briefly, cells were first treated with hypotonic solution to remove cytosolic proteins, followed by incubation with a buffer containing a high concentration of salt. Histone-containing pellets were separated from soluble nuclear fractions by centrifugation and incubated with Benzonase to completely digest DNA and release proteins tightly associated with chromatin.

Immunofluorescence Microscopy

To observe discrete foci of RPA32, phospho-RAD17, BLM, and RAD51 on chromatin, cells were pretreated with 0.5% Triton X-100 in PBS for 1 minute before fixation with paraformaldehyde (PFA) for 15 minutes. After permeabilization in 0.1% Triton X-100 in PBS for 15 min, cells were subjected to treatment with the Image-iT signal enhancer (Invitrogen) before being incubated with primary antibodies. Staining with the appropriate secondary antibodies and fluorescence microscopy (Zeiss) were used to visualize foci. FANCD2, FANCI, CENP-A, and H2AX foci were visualized by the same method without the pre-extraction step. All procedures were performed at room temperature.

DNA Fiber

We used the DNA fiber protocol developed by Sugimura et al[22]. Ongoing forks were labeled with digoxigenin-dUTPs for 20 min and then with biotin-dUTPs for 30 min. To allow efficient incorporation of the dUTPs, a hypotonic buffer (10mM HEPES, 30mM KCl, pH7.4) treatment precedes each dUTP labeling step. To visualize the labeled fibers, cells were mixed with a 10-fold excess of unlabeled cells, fixed, and dropped onto slides. After cell lysis, the DNA fibers were released and extended by tilting the slides. Incorporated dUTPs were then visualized by immunofluorescent detection using anti

digoxigenin-Rhodamine (Roche) and streptavidin-Alexa-Fluor-488 (Invitrogen). Images were captured using the Axio Imager A1 (Zeiss).

HR Events at the FYDR Locus

MEFs were generated as described above. Cells at passage 2 were harvested and analyzed by the FACSCalibur (BD Biosciences) using the FL1 and FL2 channels. To determine the spontaneous recombinant frequency, at least 16 independent MEF cultures were used per genotype and at least 106 cells were analyzed per MEF line. To determine the recombinant frequency induced by replication inhibitors, MEFs were treated with APH or CPT for 24 hrs. After a 48-hr recovery period, cells were analyzed by flow cytometry.

Live Cell Imaging

0.5x106 wildtype or Mcm4Chaos3/Chaos3 MEFs were plated onto a 60 mm dish for 24 hrs and observed using the DeltaVision microscope (Applied Precision). Each dish contained standard medium supplemented with 0.25μM DRAQ5 (Sigma), a DNA dye. Each image was assembled into a movie file using the DeltaVision SoftWoRx software.

Supplemental table, figure and movie legends

Table S1

Summary of B6 *Mcm4*^{Chaos3} Tumor Histopathology

Table S2

Summary of F1 *Mcm4*^{Chaos3} Tumor Histopathology

Figure S1, Related to Figure 1

(A) Chromatin-immunoprecipitation (ChIP) data from selected loci show reduced levels of chromatin-bound MCM2 in *Mcm4*$^{Chaos3/Chaos3}$ cells. The rDNA locus contains a well-defined origin[56], and was thus used as a control. The additional four loci from chromosomes 1 and 8 were selected due to their defined replication timing with I/II, and V indicating early and late replication timing, respectively[58]. Whether or not origins are present in these loci is unknown. Reduction levels relative to wildtype were determined by quantitative PCR on ChIP'ed DNA. The averages of three experiments are shown. (B) Similar distributions of origin-to-origin distance are found between wildtype and *Mcm4*$^{Chaos3/Chaos3}$ cells (upper panel). While there was no significant difference in the distributions in the untreated conditions ($p=0.777$, Kolmogorov-Smirnov test), *Mcm4*$^{Chaos3/Chaos3}$ cells did have an increased number of origin-to-origin distances larger than 80kb ($p<0.05$, 2-test). Although aphidicolin (APH) treatment resulted in a

significant decrease in origin-to-origin distances in both genotypes, the average distance in *Mcm4*$^{Chaos3/Chaos3}$ cells was significantly larger than that of wildtype cells (lower panel, p=0.0102, t-test). (C) Fork velocity in *Mcm4*$^{Chaos3/Chaos3}$ cells is faster than that of wildtype (left, p<0.005, t-test). The distribution of fork velocity (right) in *Mcm4*$^{Chaos3/Chaos3}$ cells is also significantly different from that of wildtype cells (p<0.001, Kolmogorov-Smirnov test). This apparently faster fork velocity in *Mcm4*$^{Chaos3/Chaos3}$ cells can be explained by different levels of fork termination. Faster forks are more likely to merge together, resulting in fork termination. An increased level of stalled forks in *Mcm4*$^{Chaos3/Chaos3}$ cells might have led to a reduction in fork terminations, causing more of the faster forks to be visible for measurement. Faster forks in wildtype cells, on the other hand, might have been excluded from the measurement due to a higher level of fork terminations. To address this concern, fork velocity was re-measured using a short-pulse labeling method (10 min for dig-dUTP and 15 min for Biotin-dUTP) to reduce the frequency of fork terminations as shown in (D). (D) While fork velocity in wildtype cells is ~15% faster (left) than the data shown in (C), forks are still faster in *Mcm4*$^{Chaos3/Chaos3}$ cells (p<0.005, t-test). Note the increase in faster forks (>1.2 kb/min) in wildtype cells (right). (E) The average origin-to-origin distance remains the same after the short-pulse labeling experiments in both wildtype and *Mcm4*$^{Chaos3/Chaos3}$ cells. Therefore, a reduced number of dormant origins might have led to a lower level of fork terminations in *Mcm4*$^{Chaos3/Chaos3}$ cells.

Figure S2, Related to Figure 2

Mcm4$^{Chaos3/Chaos3}$ cells exhibit a normal checkpoint response following treatment with replication inhibitors. Increased phosphorylation of CHK1, p53 and H2AX was observed 6 hours after treatment. Note that *Mcm4*$^{Chaos3/Chaos3}$ cells (indicated as "C") have intrinsically higher levels of phospho-p53 and γ-H2AX in untreated conditions (UNT) compared to wildtype cells (indicated as "W"). However, these basal levels of phosphorylation are substantially lower than those after treatment with replication inhibitors.

Figure S3, Related to Figure 3

(A) The phenylalanine residue mutated in *Mcm4*$^{Chaos3/Chaos3}$ cells is conserved in all eukaryotes and resides at a position that affects complex stability. An alignment of the amino acid sequences from several organisms is shown with conservation levels. (B) The Phe345Ile change in *Mcm4*$^{Chaos3/Chaos3}$ cells resides at the interface between MCM4 and MCM6. The presence of a gap between MCM2 and MCM5 has been predicted for the inactive form of the MCM2-7 complex[59], and has been recently confirmed (Costa et al., in press). These two factors seem to play a role in the formation of the sub-complexes MCM2/6 (see fractions #18 & 19) and MCM4/7/3/5 (fractions #11 & 12), as seen in Fig. 3C. (C) Co-immunoprecipitation results show a robust in vivo interaction between MCM2 and MCM6 in both wildtype and *Mcm4*$^{Chaos3/Chaos3}$ cells but a somewhat weaker interaction between MCM2 and MCM4 in *Mcm4*$^{Chaos3/Chaos3}$ cells. An interaction between

MCM2 and MCM5 was very weak regardless of genotype. These data are consistent with the in vitro sub-complexes detected in Fig. 3C.

Figure S4, Related to Figure 4

(A) eYFP expression arises from homologous recombination at the FYDR locus, which contains two tandem repeats of incomplete eYFP expression cassettes. The resolution of homologous recombination between these repeats has two different outcomes at the molecular level. While gene conversion can occur as a non-crossover event (top), unequal sister chromatid exchange (SCE) can result from a crossover event (bottom). The use of both wildtype and *Mcm4*$^{Chaos3/Chaos3}$ MEFs that carry the FYDR locus in the hemizygous state allows for the detection of HR events only during and/or after this locus is replicated. (B) Recombinant cells that express eYFP are detected by flow cytometry. eYFP signals were detected using the FL1 and FL2 channels. The gate was set using cells without the FYDR locus to distinguish eYFP signals from autofluorescence. (C) Distributions of spontaneous recombinant frequencies are shown for wildtype and *Mcm4*$^{Chaos3/Chaos3}$ cells. The average frequencies are shown in Figure 4C.

Figure S5, Related to Figure 5

(A) The number of FANCD2 sister/twin-foci throughout M phase is significantly higher in *Mcm4*$^{Chaos3/Chaos3}$ cells. The average number of foci determined by three independent

experiments is shown (left). Spontaneous FANCD2 sister/twin foci, rarely observed in wildtype cells, were significantly increased in *Mcm4*$^{Chaos3/Chaos3}$ cells. Aphidicolin (APH) treatment (150 nM for 24 hrs) increased the number of foci even in wildtype cells, while *Mcm4*$^{Chaos3/Chaos3}$ cells still contained a relatively higher amount. Pro: prophase, PM: prometaphase, M: metaphase, A: anaphase. Bars indicate SEMs. Representative images of FANCD2 sister/twin foci are shown on the right. Scale bar is 10 μm. (B) *Mcm4*$^{Chaos3/Chaos3}$ cells also have a drastically increased number of FANCI foci in prophase. Much like FANCD2 foci (Figure 5A), FANCI foci were observed in more than 50% of *Mcm4*$^{Chaos3/Chaos3}$ cells in the untreated condition (UNT, left). Although APH treatment nearly saturated the formation of FANCI foci in both wildtype and *Mcm4*$^{Chaos3/Chaos3}$ cells, the number of FANCI foci per cell was still significantly higher in *Mcm4*$^{Chaos3/Chaos3}$ cells. Representative images of FANCI foci are shown on the right. Scale bar is 10 μm. (C) An increased frequency of aneuploidy in *Mcm4*$^{Chaos3/Chaos3}$ cells is revealed by interphase FISH using probes specific to near-centromeric regions of Chromosome 16 (top, left). The percentage of aneuploid cells was determined by dividing the number of cells with chromosome loss (-1) and chromosome gain (+1) signals by the total number of cells observed (see representative images of interphase FISH below). The percentage of tetraploid cells was also significantly increased in *Mcm4*$^{Chaos3/Chaos3}$ cells (top, right). Scale bar is 10 μm. (D) G-banding analysis of metaphase chromosomes shows an increased frequency of translocations in *Mcm4*$^{Chaos3/Chaos3}$ cells. The top portion includes the results for wild-type cells, while the bottom portion includes results for *Mcm4*$^{Chaos3/Chaos3}$ cells. A total of 40 chromosomes

were fully analyzed per genotype. Numbers in brackets indicate the number of cells with karyotypes shown on the left. (E) *Mcm4*$^{Chaos3/Chaos3}$ cells exhibit a significantly elevated level of twin H2AX foci formation in early G1 phase. G1 phase cells were detected as binucleated cells following a 4hr-treatment with cytochalasin B. Only binucleated cells that contained H2AX foci in both nuclei were considered positive for twin foci. Scale bar is 10 μm.

Figure S6, Related to Figure 6

The use of dormant origins may provide a simple and prompt pathway for stalled fork recovery. A speculative model of stalled fork rescue by dormant origin firing is shown. In both wildtype and *Mcm4*$^{Chaos3/Chaos3}$ cells, active origins (indicated as filled orange hexagons) fire to generate bidirectional forks. When fork stalling occurs in wildtype cells, a nearby dormant origin (open orange hexagons) immediately fires and fork progression continues. However, the lack of dormant origins in *Mcm4*$^{Chaos3/Chaos3}$ cells results in persistent fork stalling. In this model, only those in the vicinity of stalled forks are allowed to fire, causing the apparent inter-origin distances to remain unchanged between wildtype and *Mcm4*$^{Chaos3/Chaos3}$ cells, as seen in Fig 1C.

Movie S1

Normal Cytokinesis of Wild-Type MEF. Movie S1, related to Figure 5, shows a living wild-type cell in cytokinesis. Cells were cultured in the presence of DNA dye DRAQ5 (0.25 μM) and subjected to fluorescence microscopy to monitor cytokinesis. The duration of the movie is 30 min, and the time interval between captures is 2 min.

Movie S2

Normal Cytokinesis of *Mcm4*$^{Chaos3/Chaos3}$ MEF. Movie S2, related to Figure 5, shows a living *Mcm4*$^{Chaos3/Chaos3}$ cell in cytokinesis. Cells were cultured in the presence of DNA dye DRAQ5 (0.25 μM) and subjected to fluorescence microscopy to monitor cytokinesis. The duration of the movie is 22 min, and the time interval between captures is 2 min.

Movie S3

Cytokinesis Failure Resulting in Binucleated *Mcm4*$^{Chaos3/Chaos3}$ MEF. Movie S3, related to Figure 5, is of a *Mcm4*$^{Chaos3/Chaos3}$ cell in aberrant cytokinesis. Cells were cultured in the presence of DNA dye DRAQ5 (0.25 μM) and subjected to fluorescence microscopy to monitor cytokinesis. The duration of the movie is 30 min, and the time interval between captures is 2 min.

Table S1 Kawabata et al., 2011

Case	Age (mo.)	Location	Diagnosis	Immunohistochemistry
160	15	Small intestine	Lymphoma	N.D.
161	12	Small intestine	Lymphoma	N.D.
		Peripancreatic adipose tissue	Histiocytic sarcoma	Mac-2: +, CD3: -, B220: -
193	11	Adipose tissue	Histiocytic sarcoma	Mac-2: +, CD3: -, B220: -
194	16	Liver and abdominal mass	Histiocytic sarcoma	Mac-2: +
202	10	Liver	Histiocytic sarcoma	Mac-2: +
203	15	Liver	Histiocytic sarcoma	N.D.
204	14	Peripancreatic adipose tissue	Histiocytic sarcoma	N.D.
211	4	Mammary gland and subcutis	Spindle cell sarcoma	N.D.
250	15	Liver	Histiocytic sarcoma	N.D.
265	10	Liver	Histiocytic sarcoma	N.D.
311	10	Liver	Histiocytic sarcoma	N.D.
312	11	Vertebrae	Osteosarcoma	N.D.
314	11	Vertebrae	Osteosarcoma	N.D.
216	15	LN of shoulder region	Lymphoma	CD3: ±, B220: +
391	10	Thymus	Lymphoma	N.D.
388	13	Thymus	Histiocytic sarcoma	Mac-2: +
316	12	Peripancreatic mass	Histiocytic sarcoma	N.D.

LN: lymph node

Table S2 Kawabata et al., 2011

Case	Age (mo.)	Location	Diagnosis	Immunohistochemistry
328	12	Mesenteric LN	Histiocytic sarcoma	Mac-2: +
329	15	Uterus	Endometrial hemangioma	N.D.
330	15	Intestine	Lymphoma	N.D.
		Liver	Histiocytic sarcoma	Mac-2: +
331	14	Mammary gland	Adenocarcinoma	N.D.
332	10	Spleen	Round cell sarcoma	Mac2: ±, B220: ±
224	12	Intestine	Lymphoma	N.D.
		Liver, Mesenteric LN	Histiocytic sarcoma	N.D.
231	14	Intestine	Lymphoma, B cell	CD3: ±, B220: ++, Pax-5: ++
232	11	Mesenteric LN	Histiocytic sarcoma	N.D.
221	15	Spleen	Round cell sarcoma	Mac-2: ±
377	10	Uterus	Spindle cell tumor	N.D.
378	12	Uterus	Histiocytic sarcoma	N.D.
335	13	Tibia	Osteosarcoma [a]	N.D.
395	16	Liver, Ovary-uterus	Histiocytic sarcoma	N.D.
396	17	Vertebrae	Osteosarcoma [a]	N.D.
469	12	Spleen, Liver, Intramammary LN	Lymphoma	B220: +
470	17	Spleen, Liver, Mesenteric LN	Lymphoma	Mac-2: +, B220: ++
471	16	Intestine, Spleen, Thoracic nodule	Lymphoma	N.D.

436	17	Mammary gland	Adenocarcinoma	N.D.
437	7	Mammary gland	Adenocarcinoma	N.D.
438	16	Spleen, Liver, LN	Histiocytic sarcoma	N.D.
439	16	Intestine	Lymphoma	Mac-2: -, B220: +
		Thymus	Histiocytic sarcoma	Mac-2: +

LN: lymph node
[a]Diagnoses were given by X-ray.

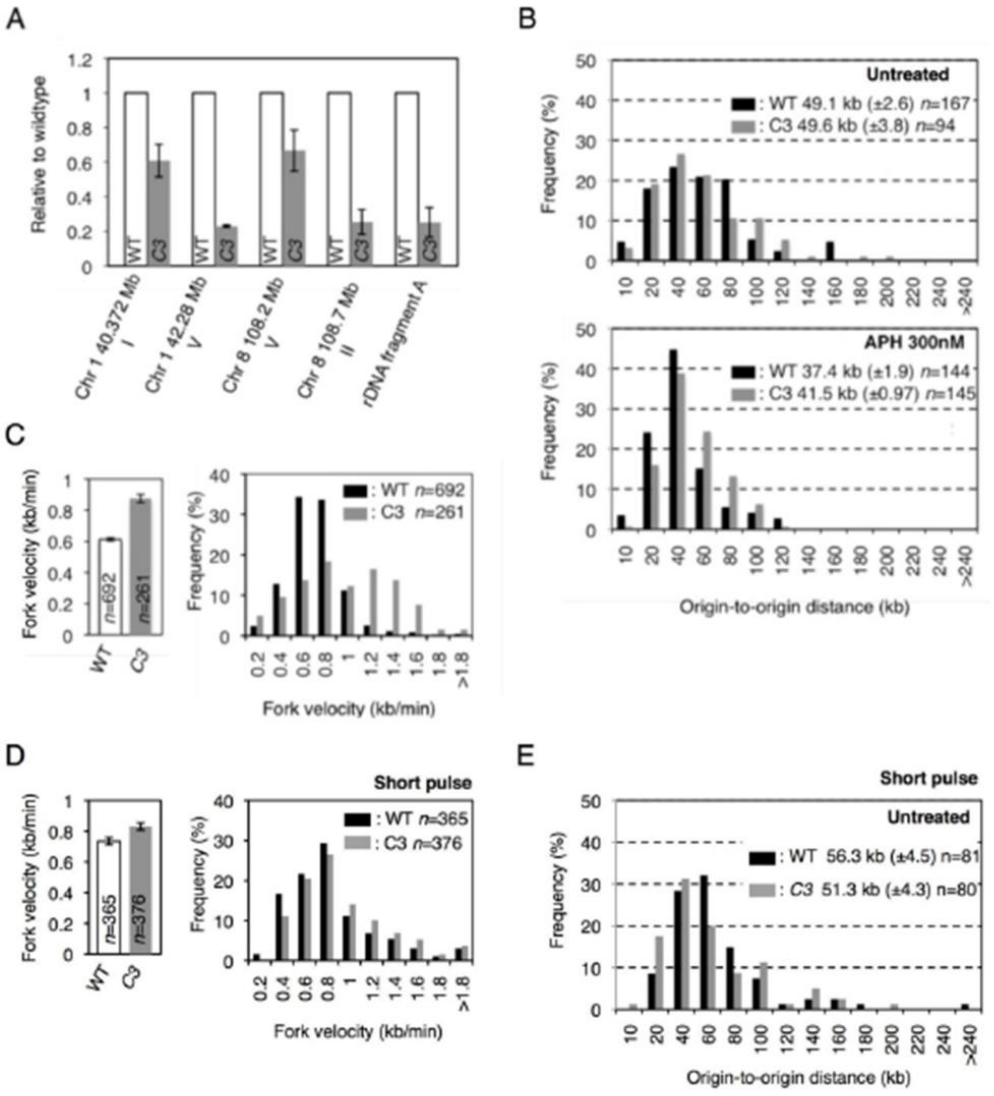
A
Relative to wildtype
WT
C3
Chr 1 40,372 Mb
I
Chr 1 42.28 Mb
V
Chr 8 108.2 Mb
V
Chr 8 108.7 Mb
II
rDNA fragment A
B
Untreated
: WT 49.1 kb (±2.6) n=167
: C3 49.6 kb (±3.8) n=94
APH 300nM
: WT 37.4 kb (±1.9) n=144
: C3 41.5 kb (±0.97) n=145
Frequency (%)
Origin-to-origin distance (kb)
C
Fork velocity (kb/min)
n=692
n=261
: WT n=692
: C3 n=261
Frequency (%)
Fork velocity (kb/min)
D
Short pulse
n=365
n=376
: WT n=365
: C3 n=376
E
Short pulse
Untreated
: WT 56.3 kb (±4.5) n=81
: C3 51.3 kb (±4.3) n=80
Frequency (%)
Origin-to-origin distance (kb)

Figure S2, related to Figure 2 Kawabata et al., 2011

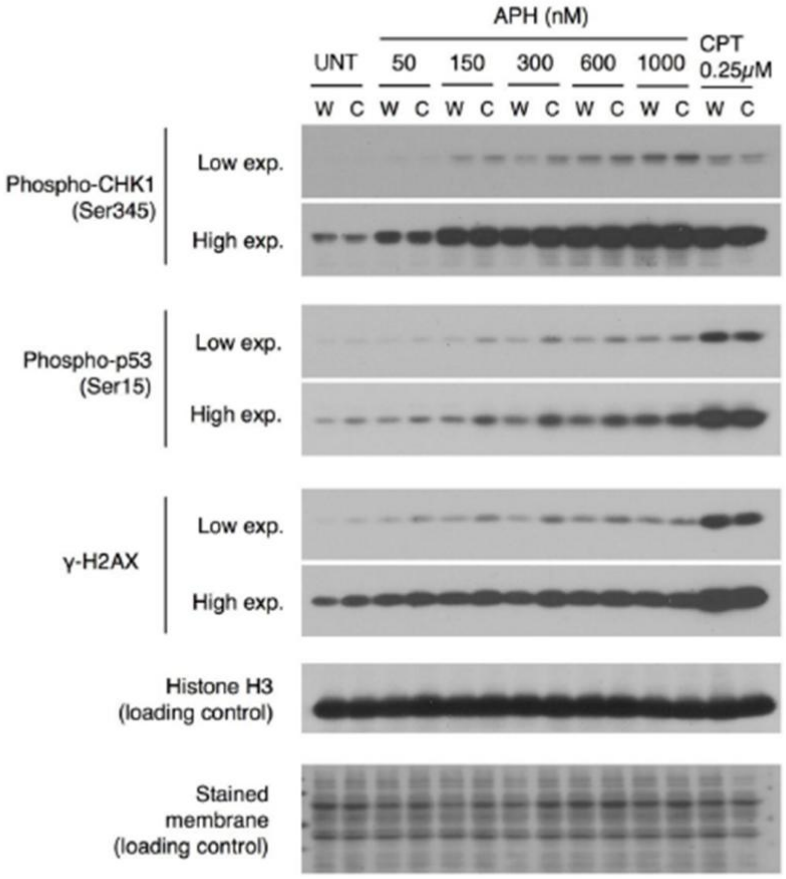

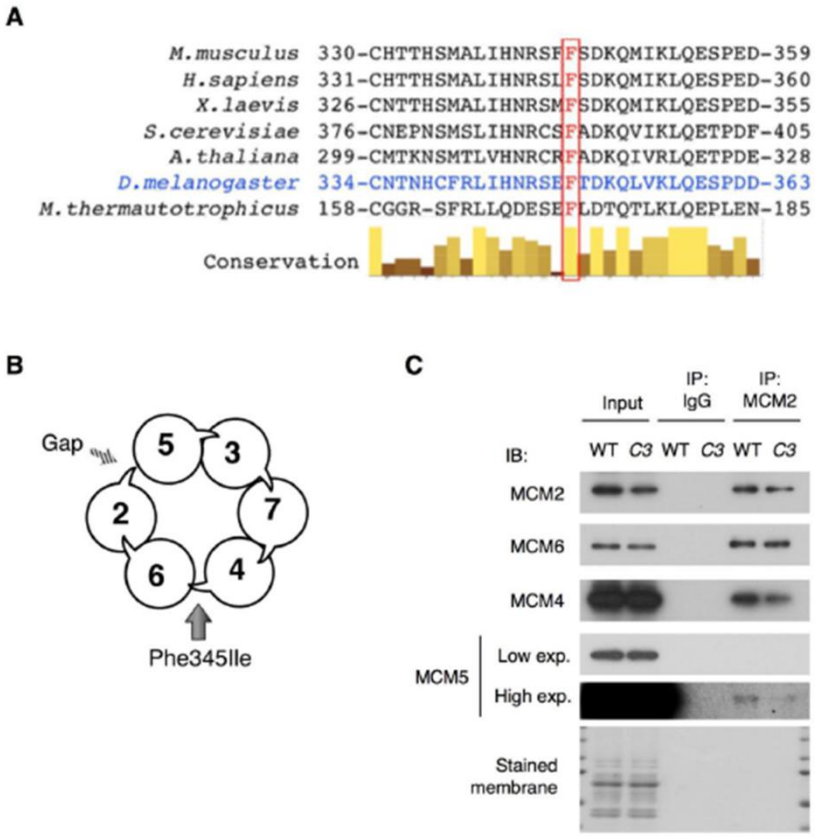
A
M.musculus 330-CHTTHSMALIHNRSFFSDKQMIKLQESPED-359
H.sapiens 331-CHTTHSMALIHNRSLFSDKQMIKLQESPED-360
X.laevis 326-CNTTHSMALIHNRSMFSDKQMIKLQESPED-355
S.cerevisiae 376-CNEPNSMSLIHNRCSFADKQVIKLQETPDF-405
A.thaliana 299-CMTKNSMTLVHNRCRFADKQIVRLQETPDE-328
D.melanogaster 334-CNTNHCFRLIHNRSEFTDKQLVKLQESPDD-363
M.thermautotrophicus 158-CGGR-SFRLLQDESEFLDTQTLKLQEPLEN-185
Conservation
B
Gap
5
3
2
7
6
4
Phe345Ile
C
Input
IP: IgG
IP: MCM2
IB:
WT C3 WT C3 WT C3
MCM2
MCM6
MCM4
MCM5
Low exp.
High exp.
Stained membrane

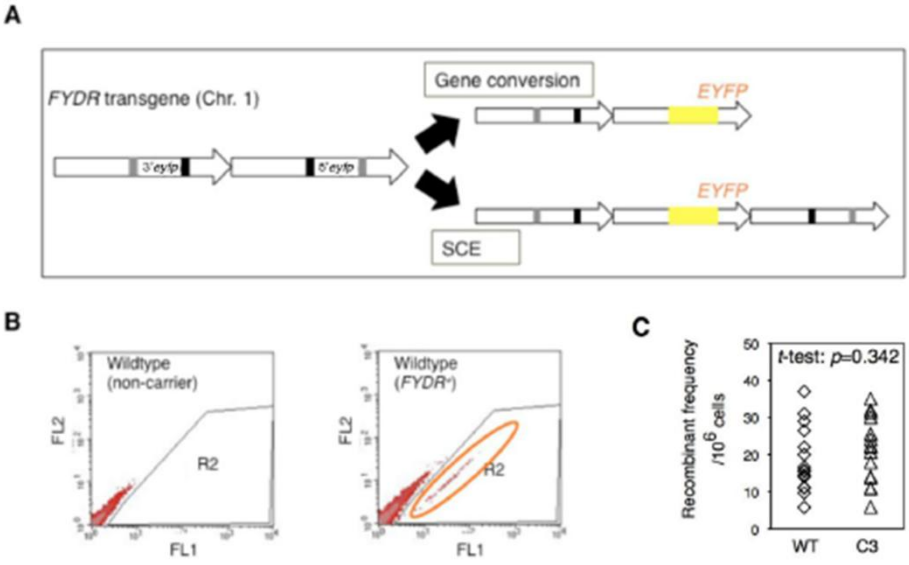
A
FYDR transgene (Chr. 1)
3'eyfp
5'eyfp
Gene conversion
EYFP
EYFP
SCE
B
Wildtype
(non-carrier)
R2
FL2
FL1
Wildtype
(FYDR+)
R2
FL2
FL1
C
t-test: p=0.342
Recombinant frequency
/10^6 cells
50
40
30
20
10
0
WT
C3

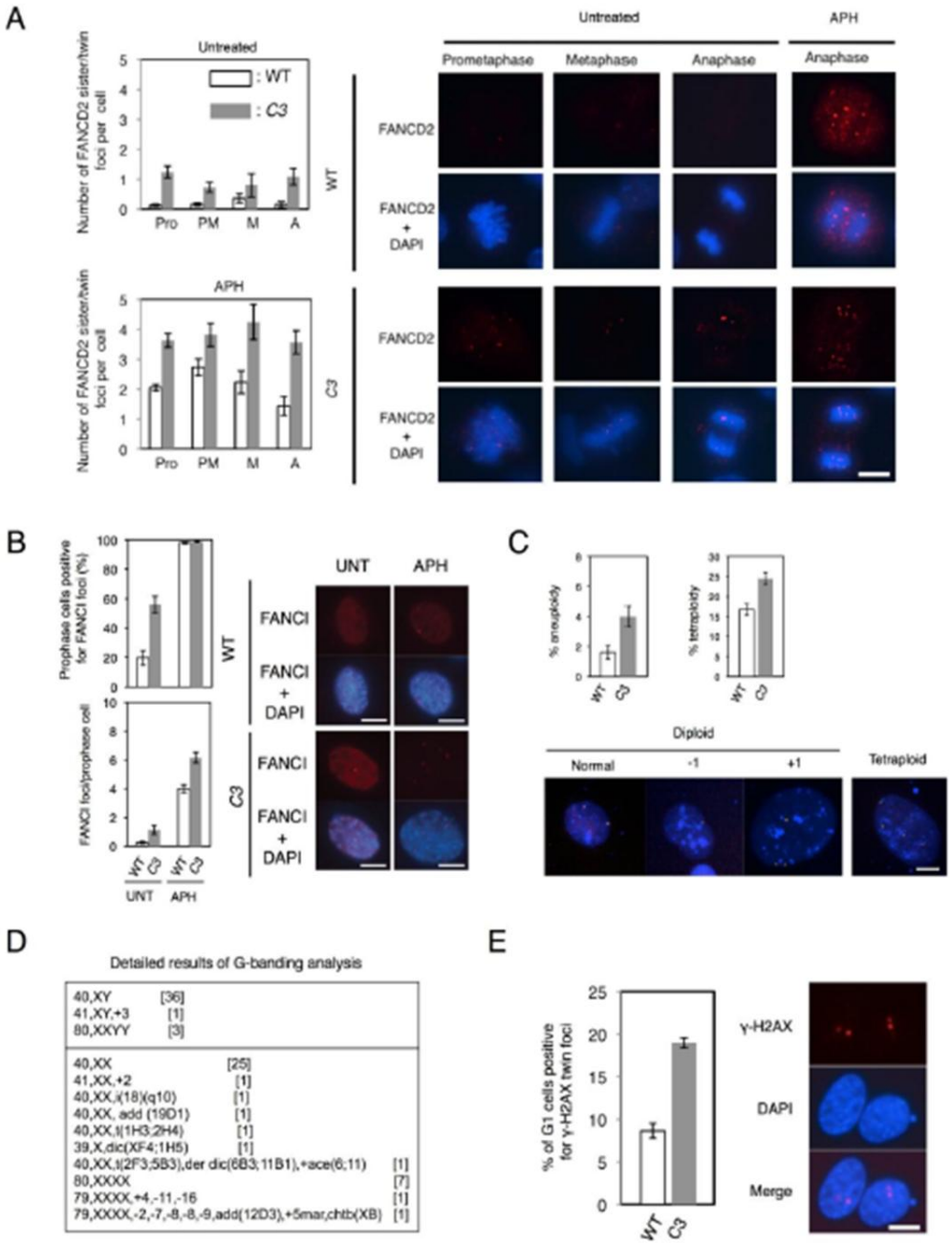
A
Untreated
APH
Prometaphase
Metaphase
Anaphase
Anaphase
Untreated
: WT
: C3
Number of FANCD2 sister/twin foci per cell
Pro
PM
M
A
WT
C3
FANCD2
FANCD2 + DAPI
B
Prophase cells positive for FANCI foci (%)
FANCI foci/prophase cell
UNT
APH
FANCI
FANCI + DAPI
C
% aneuploidy
% tetraploidy
Diploid
Normal
-1
+1
Tetraploid
D
Detailed results of G-banding analysis
40,XY [36]
41,XY,+3 [1]
80,XXYY [3]
40,XX [25]
41,XX,+2 [1]
40,XX,i(18)(q10) [1]
40,XX, add (19D1) [1]
40,XX,t(1H3;2H4) [1]
39,X,dic(XF4;1H5) [1]
40,XX,t(2F3;5B3),der dic(6B3;11B1),+ace(6;11) [1]
80,XXXX [7]
79,XXXX,+4,-11,-16 [1]
79,XXXX,-2,-7,-8,-8,-9,add(12D3),+5mar,chtb(XB) [1]
E
% of G1 cells positive for γ-H2AX twin foci
γ-H2AX
DAPI
Merge

Figure S6, related to Figure 6 Kawabata et al., 2011

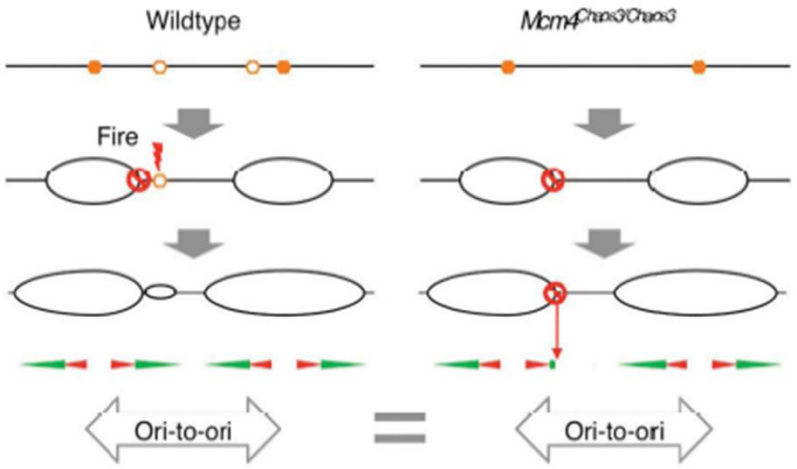

Movie S1 Kawabata et al., 2011

Movie S1 can be found online at:

http://www.sciencedirect.com/science/article/pii/S109727651100089X

Movie S2 Kawabata et al., 2011

Movie S2 can be found online at:

http://www.sciencedirect.com/science/article/pii/S109727651100089X

Movie S3 Kawabata et al., 2011

Movie S3 can be found online at:

http://www.sciencedirect.com/science/article/pii/S109727651100089X

References

1 Sclafani, R. A. & Holzen, T. M. Cell Cycle Regulation of DNA Replication. *Annual Review of Genetics* **41**, 237-280 (2007).

2 Forsburg, S. L. Eukaryotic MCM Proteins: Beyond Replication Initiation. *Microbiol. Mol. Biol. Rev.* **68**, 109-131 (2004).

3 Tye, B. K. MCM Proteins in DNA Replication. *Annual Review of Biochemistry* **68**, 649-686 (1999).

4 Ilves, I., Petojevic, T., Pesavento, J. J. & Botchan, M. R. Activation of the MCM2-7 Helicase by Association with Cdc45 and GINS Proteins. *Molecular Cell* **37**, 247-258 (2010).

5 Moyer, S. E., Lewis, P. W. & Botchan, M. R. Isolation of the Cdc45/Mcm2–7/GINS (CMG) complex, a candidate for the eukaryotic DNA replication fork helicase. *Proceedings of the National Academy of Sciences* **103**, 10236-10241 (2006).

6 Todorov, I. T., Attaran, A. & Kearsey, S. E. BM28, a human member of the MCM2-3-5 family, is displaced from chromatin during DNA replication. *The Journal of Cell Biology* **129**, 1433-1445 (1995).

7 Yan, H., Merchant, A. M. & Tye, B. K. Cell cycle-regulated nuclear localization of MCM2 and MCM3, which are required for the initiation of DNA synthesis at chromosomal replication origins in yeast. *Genes & Development* **7**, 2149-2160 (1993).

8 Blow, J. J. & Dutta, A. Preventing re-replication of chromosomal DNA. *Nat Rev Mol Cell Biol* **6**, 476-486 (2005).

9 Gilbert, D. M. In search of the holy replicator. *Nat Rev Mol Cell Biol* **5**, 848-855 (2004).

10 Bowers, J. L., Randell, J. C. W., Chen, S. & Bell, S. P. ATP Hydrolysis by ORC Catalyzes Reiterative Mcm2-7 Assembly at a Defined Origin of Replication. *Molecular Cell* **16**, 967-978 (2004).

11 Edwards, M. C. *et al.* MCM2–7 Complexes Bind Chromatin in a Distributed Pattern Surrounding the Origin Recognition Complex in Xenopus Egg Extracts. *Journal of Biological Chemistry* **277**, 33049-33057 (2002).

12 Ge, X. Q., Jackson, D. A. & Blow, J. J. Dormant origins licensed by excess Mcm2–7 are required for human cells to survive replicative stress. *Genes & Development* **21**, 3331-3341 (2007).

13 Ibarra, A., Schwob, E. & Méndez, J. Excess MCM proteins protect human cells from replicative stress by licensing backup origins of replication. *Proceedings of the National Academy of Sciences* **105**, 8956-8961 (2008).

14 Cortez, D., Glick, G. & Elledge, S. J. Minichromosome maintenance proteins are direct targets of the ATM and ATR checkpoint kinases. *Proceedings of the National Academy of Sciences of the United States of America* **101**, 10078-10083 (2004).

15 Woodward, A. M. *et al.* Excess Mcm2–7 license dormant origins of replication that can be used under conditions of replicative stress. *The Journal of Cell Biology* **173**, 673-683 (2006).

16 Ha, S.-A. *et al.* Cancer-Associated Expression of Minichromosome Maintenance 3 Gene in Several Human Cancers and Its Involvement in Tumorigenesis. *Clinical Cancer Research* **10**, 8386-8395 (2004).
17 Ishimi, Y. *et al.* Enhanced expression of Mcm proteins in cancer cells derived from uterine cervix. *European Journal of Biochemistry* **270**, 1089-1101 (2003).
18 Chuang, C.-H., Wallace, M. D., Abratte, C., Southard, T. & Schimenti, J. C. Incremental Genetic Perturbations to MCM2-7 Expression and Subcellular Distribution Reveal Exquisite Sensitivity of Mice to DNA Replication Stress. *PLoS Genet* **6**, e1001110 (2010).
19 Kunnev, D. *et al.* DNA damage response and tumorigenesis in Mcm2-deficient mice. *Oncogene* **29**, 3630-3638 (2010).
20 Pruitt, S. C., Bailey, K. J. & Freeland, A. Reduced Mcm2 Expression Results in Severe Stem/Progenitor Cell Deficiency and Cancer. *Stem Cells* **25**, 3121-3132 (2007).
21 Shima, N. *et al.* A viable allele of Mcm4 causes chromosome instability and mammary adenocarcinomas in mice. *Nat Genet* **39**, 93-98 (2007).
22 Sugimura, K., Takebayashi, S.-i., Ogata, S., Taguchi, H. & Okumura, K. Non-Denaturing Fluorescence in Situ Hybridization to Find Replication Origins in a Specific Genome Region on the DNA Fiber. *Bioscience, Biotechnology, and Biochemistry* **71**, 627-632 (2007).
23 Byun, T. S., Pacek, M., Yee, M.-c., Walter, J. C. & Cimprich, K. A. Functional uncoupling of MCM helicase and DNA polymerase activities activates the ATR-dependent checkpoint. *Genes & Development* **19**, 1040-1052 (2005).
24 Zou, L. & Elledge, S. J. Sensing DNA Damage Through ATRIP Recognition of RPA-ssDNA Complexes. *Science* **300**, 1542-1548 (2003).
25 Bao, S. *et al.* ATR/ATM-mediated phosphorylation of human Rad17 is required for genotoxic stress responses. *Nature* **411**, 969-974 (2001).
26 Wang, X. *et al.* Rad17 Phosphorylation Is Required for Claspin Recruitment and Chk1 Activation in Response to Replication Stress. *Molecular Cell* **23**, 331-341 (2006).
27 Tsao, C. C., Geisen, C. & Abraham, R. T. Interaction between human MCM7 and Rad17 proteins is required for replication checkpoint signaling. *EMBO J* **23**, 4660-4669 (2004).
28 Rogakou, E. P., Pilch, D. R., Orr, A. H., Ivanova, V. S. & Bonner, W. M. DNA Double-stranded Breaks Induce Histone H2AX Phosphorylation on Serine 139. *Journal of Biological Chemistry* **273**, 5858-5868 (1998).
29 Petermann, E., Orta, M. L., Issaeva, N., Schultz, N. & Helleday, T. Hydroxyurea-Stalled Replication Forks Become Progressively Inactivated and Require Two Different RAD51-Mediated Pathways for Restart and Repair. *Molecular Cell* **37**, 492-502 (2010).
30 Bugreev, D. V., Yu, X., Egelman, E. H. & Mazin, A. V. Novel pro- and anti-recombination activities of the Bloom's syndrome helicase. *Genes & Development* **21**, 3085-3094 (2007).
31 Davies, S. L., North, P. S. & Hickson, I. D. Role for BLM in replication-fork restart and suppression of origin firing after replicative stress. *Nat Struct Mol Biol* **14**, 677-679 (2007).

32 Gibson, S. I., Surosky, R. T. & Tye, B. K. The phenotype of the minichromosome maintenance mutant mcm3 is characteristic of mutants defective in DNA replication. *Molecular and Cellular Biology* **10**, 5707-5720 (1990).

33 Li, X. C., Schimenti, J. C. & Tye, B. K. Aneuploidy and improved growth are coincident but not causal in a yeast cancer model. *PLoS Biol* **7**, e1000161 (2009).

34 Hendricks, C. A. *et al.* Spontaneous mitotic homologous recombination at an enhanced yellow fluorescent protein (EYFP) cDNA direct repeat in transgenic mice. *Proc Natl Acad Sci U S A* **100**, 6325-6330 (2003).

35 Saleh-Gohari , N. *et al.* Spontaneous Homologous Recombination Is Induced by Collapsed Replication Forks That Are Caused by Endogenous DNA Single-Strand Breaks. *Molecular and Cellular Biology* **25**, 7158-7169 (2005).

36 Chan, K. L., Palmai-Pallag, T., Ying, S. & Hickson, I. D. Replication stress induces sister-chromatid bridging at fragile site loci in mitosis. *Nat Cell Biol* **11**, 753-760 (2009).

37 Naim, V. & Rosselli, F. The FANC pathway and BLM collaborate during mitosis to prevent micro-nucleation and chromosome abnormalities. *Nat Cell Biol* **11**, 761-768 (2009).

38 Sims, A. E. *et al.* FANCI is a second monoubiquitinated member of the Fanconi anemia pathway. *Nat Struct Mol Biol* **14**, 564-567 (2007).

39 Smogorzewska, A. *et al.* Identification of the FANCI Protein, a Monoubiquitinated FANCD2 Paralog Required for DNA Repair. *Cell* **129**, 289-301 (2007).

40 Howman, E. V. *et al.* Early disruption of centromeric chromatin organization in centromere protein A (Cenpa) null mice. *Proceedings of the National Academy of Sciences* **97**, 1148-1153 (2000).

41 Williams, B. R. *et al.* Aneuploidy affects proliferation and spontaneous immortalization in mammalian cells. *Science* **322**, 703-709 (2008).

42 Blackwell, B.-N., Bucci, T. J., Hart, R. W. & Turturro, A. Longevity, Body Weight, and Neoplasia in Ad Libitum-Fed and Diet-Restricted C57BL6 Mice Fed NIH-31 Open Formula Diet. *Toxicologic Pathology* **23**, 570-582 (1995).

43 Pileri, S. A. *et al.* Tumours of histiocytes and accessory dendritic cells: an immunohistochemical approach to classification from the International Lymphoma Study Group based on 61 cases. *Histopathology* **41**, 1-29 (2002).

44 Paulsen, R. D. & Cimprich, K. A. The ATR pathway: Fine-tuning the fork. *DNA Repair* **6**, 953-966 (2007).

45 Orr, S. J. *et al.* Reducing MCM levels in human primary T cells during the G(0)-->G(1) transition causes genomic instability during the first cell cycle. *Oncogene* **29**, 3803-3814 (2010).

46 Liang, D. T., Hodson, J. A. & Forsburg, S. L. Reduced dosage of a single fission yeast MCM protein causes genetic instability and S phase delay. *Journal of Cell Science* **112**, 559-567 (1999).

47 Lee, J. A., Carvalho, C. M. B. & Lupski, J. R. A DNA Replication Mechanism for Generating Nonrecurrent Rearrangements Associated with Genomic Disorders. *Cell* **131**, 1235-1247 (2007).

48 Prakash, S., Johnson, R. E. & Prakash, L. Eukaryotic translesion synthesis DNA polymerases: specificity of structure and function. *Annu Rev Biochem* **74**, 317-353, doi:10.1146/annurev.biochem.74.082803.133250 (2005).
49 Casper, A. M., Nghiem, P., Arlt, M. F. & Glover, T. W. ATR regulates fragile site stability. *Cell* **111**, 779-789 (2002).
50 Chan, K. L. & Hickson, I. D. On the origins of ultra-fine anaphase bridges. *Cell Cycle* **8**, 3065-3066 (2009).
51 Halazonetis, T. D., Gorgoulis, V. G. & Bartek, J. An oncogene-induced DNA damage model for cancer development. *Science* **319**, 1352-1355 (2008).
52 Negrini, S., Gorgoulis, V. G. & Halazonetis, T. D. Genomic instability--an evolving hallmark of cancer. *Nat Rev Mol Cell Biol* **11**, 220-228 (2010).
53 Sherr, C. J. The Pezcoller Lecture: Cancer Cell Cycles Revisited. *Cancer Research* **60**, 3689-3695 (2000).
54 Fenech, M. Cytokinesis-block micronucleus cytome assay. *Nat. Protocols* **2**, 1084-1104 (2007).
55 Shi, Q. & King, R. W. Chromosome nondisjunction yields tetraploid rather than aneuploid cells in human cell lines. *Nature* **437**, 1038-1042 (2005).
56 Zellner, E., Herrmann, T., Schulz, C. & Grummt, F. Site-specific interaction of the murine pre-replicative complex with origin DNA: assembly and disassembly during cell cycle transit and differentiation. *Nucleic Acids Res* **35**, 6701-6713 (2007).
57 Sotillo, R. *et al.* Mad2 overexpression promotes aneuploidy and tumorigenesis in mice. *Cancer Cell* **11**, 9-23 (2007).
58 Farkash-Amar, S. *et al.* Global organization of replication time zones of the mouse genome. *Genome Res* **18**, 1562-1570 (2008).
59 Bochman, M. L., Bell, S. P. & Schwacha, A. Subunit organization of Mcm2-7 and the unequal role of active sites in ATP hydrolysis and viability. *Mol Cell Biol* **28**, 5865-5873 (2008).

CHAPTER III: A Concomitant Loss of Dormant Origins and FANCC Exacerbates Genome Instability by Impairing DNA Replication Fork Progression

My contributions to this chapter

Figures 1-6

Table 1

Figures S1-3, S5-6

This chapter is a replicate of a publication in *Nucleic Acids Research* (2014). Spencer W. Luebben, Tsuyoshi Kawabata, Charles S. Johnson, M. Gerard O'Sullivan and Naoko Shima.

Summary

Accumulating evidence suggests that dormant DNA replication origins play an important role in the recovery of stalled forks. However, their functional interactions with other fork recovery mechanisms have not been tested. We previously reported intrinsic activation of the FA pathway in a tumor-prone mouse model (*Mcm4*^{chaos3}) with a 60% loss of dormant origins. To understand this further, we introduced a null allele of *Fancc* (*Fancc*$^{-}$), encoding a member of the FA core complex, into the *Mcm4*^{chaos3} background. Primary embryonic fibroblasts double homozygous for *Mcm4*^{chaos3} and *Fancc*$^{-}$ (*Mcm4*$^{chaos3/chaos3}$*;Fancc*$^{-/-}$) showed significantly increased levels of markers of stalled/collapsed forks compared to either single homozygote. Interestingly, a loss of dormant origins also increased the number of sites in which replication was delayed until prophase, regardless of FA pathway activation. These replication defects coincided with substantially elevated levels of genome instability in *Mcm4*$^{chaos3/chaos3}$*;Fancc*$^{-/-}$ cells, resulting in a high rate of perinatal lethality of *Mcm4*$^{chaos3/chaos3}$*;Fancc*$^{-/-}$ mice and the accelerated tumorigenesis of surviving mice. Together, these findings uncover a specialized role of dormant origins in replication completion while also identifying important functional overlaps between dormant origins and the FA pathway in maintaining fork progression, genome stability, normal development and tumor suppression.

Introduction

Origin licensing builds a fundamental basis for genome stability during eukaryotic DNA replication as it provides replication origins with the competency to fire and restricts their firing to once per S phase[1-3]. This process occurs during the late M to early G1 phases of the cell cycle, when heterohexameric complexes of the minichromosome maintenance proteins (MCM2-7), essential components of the replicative helicase, are loaded onto chromatin[4-6]. While any genomic loci bound by MCM2-7 complexes can potentially act as origins, only a small fraction of them (~10%) assemble active helicases with their co-factors to unwind the DNA and initiate genome duplication in S phase[7,8]. In fact, chromatin-bound MCM2-7 complexes exist in a large excess (10- to 20-fold) over the number of replication origins that actually fire in S phase[9-12], thereby licensing additional origins termed dormant origins. Although dormant origins represent the vast majority (>90%) of all licensed origins[13,14], their role in DNA replication has only recently been revealed. These dormant origins can be activated as "backups" under conditions of replication stress to compensate for slow fork progression and rescue stalled replication forks, thereby contributing to completion of DNA replication[13-15].

Using a mouse model called *Mcm4*^{chaos3}, we demonstrated that dormant origins also play an important role in the rescue of stalled forks even in unchallenged S phase[16]. *Mcm4*^{chaos3} is a hypomorphic allele encoding a Phe345Ile change in the MCM4 protein, a subunit of the MCM2-7 complex[17]. Cells homozygous for this allele (*Mcm4*$^{chaos3/chaos3}$) exhibit a decreased rate of assembly of the MCM2-7 complex, leading to a ~60% loss of

chromatin-bound MCM2-7 complexes[16]. This results in a significant reduction of dormant origins, causing the accumulation of stalled forks and increased levels of spontaneous micronuclei in *Mcm4*$^{chaos3/chaos3}$ cells. Reflecting intrinsic genome instability, *Mcm4*$^{chaos3/chaos3}$ mice are highly prone to spontaneous tumors[16,17]. These properties of *Mcm4*$^{chaos3/chaos3}$ mice substantiate the formerly underappreciated role of dormant origins in stalled fork recovery[18]. In our previous work[16], *Mcm4*$^{chaos3/chaos3}$ cells were also found to exhibit intrinsic activation of the Fanconi anemia (FA) pathway of DNA repair, though the functional relevance of this had yet to be determined.

FA is a rare genetic disorder characterized by congenital abnormalities, bone marrow failure and a heightened predisposition to cancer[19,20]. It is a genetically heterogeneous disease, with 16 complementation groups identified to date[19,21,22]. Our current understanding is that the products of these genes coordinately function to promote genome stability with a specialized role in the repair of DNA inter-strand crosslinks (ICLs) [20,23,24] and certain endogenous lesions[25]. Activation of the FA pathway is typically observed by mono-ubiquitination of the FANCD2 and FANCI proteins by the FA core complex (composed of at least 8 FA proteins), promoting their recruitment to chromatin and focus formation[26-29]. Even in the absence of exogenous sources of ICLs, this activation occurs in normal S phase[29,30]. Moreover, treatment of cells with a low dose of aphidicolin (APH), a polymerase inhibitor[31], robustly activates the FA pathway, indicating a role of the FA proteins during DNA replication[32]. Previous studies reported that APH-induced FANCD2/FANCI foci often form as a pair (sister foci) during the

G2/M phases, presumably flanking late replication intermediates at common fragile sites[33,34]. These chromosomal loci are prone to breakage after partial inhibition of DNA replication[35], likely due to a paucity of DNA replication origins at these sites[36,37]. As FA proteins are required for the stability of common fragile sites[32], they are likely to be involved in guiding successful replication of loci with fewer replication origins.

As *Mcm4*^{chaos3} homozygosity significantly decreases the total number of licensed origins on a genome-wide scale, it is likely to increase the number of loci lacking dormant origins or perhaps any origins. We therefore hypothesized that intrinsic activation of the FA pathway in *Mcm4*$^{chaos3/chaos3}$ cells occurs in an attempt to support replication fork progression at these sites. To test this hypothesis, we introduced a null allele of *Fancc* (*Fancc*$^{-}$), encoding a member of the FA core complex[38], into the *Mcm4*^{chaos3} background. Here, we report that loss of an intact FA pathway in *Mcm4*$^{chaos3/chaos3}$ cells severely impairs replication fork stability even in unchallenged conditions. Furthermore, a reduced number of dormant origins also increased the number of sites in which replication was delayed until prophase, regardless of FA pathway activation. This increase in late replication intermediates as well as replication delay led to highly elevated levels of genome instability in *Mcm4*$^{chaos3/chaos3}$*;Fancc*$^{-/-}$ cells and almost all *Mcm4*$^{chaos3/chaos3}$*;Fancc*$^{-/-}$ pups died shortly after birth in an inbred C57BL/6J background. While viable in a mixed genetic background, *Mcm4*$^{chaos3/chaos3}$*;Fancc*$^{-/-}$ mice still succumbed to spontaneous tumors at much younger ages than their *Mcm4*$^{chaos3/chaos3}$ littermates. These findings confirm the role of dormant origins in stalled fork recovery

while also unveiling their unique function in the complete replication of the genome, as other pathways are not able to fully compensate in their absence. Moreover, our results provide new insights into how the FA pathway functions in unchallenged conditions to promote genome stability.

Materials and methods

Mouse strains and MEFs

All experiments were performed using mice/cells derived from an inbred C57BL/6J genetic background or a C57BL/6J x C3HeB/FeJ mixed genetic background and were approved by the Institutional Animal Care and Use Committee (IACUC). MEFs were generated from 12.5-14.5 dpc embryos and cultured using standard procedures. All mice were genotyped by PCR. The primers used are available upon request.

Immunocytochemistry

Cells were grown on coverslips for two days and then fixed using 10% formalin. When RPA immunocytostaining was performed, cells were additionally pre-extracted with a 0.5% Triton X-100 in PBS solution for about 1 minute prior to fixation. For analyses involving APH treatment, cells were given doses of either 150nM or 300nM APH for 24 hours before harvest. Coverslips were then treated with the appropriate primary antibodies (4°C, overnight) and secondary antibodies (RT, 1 hour) and stained with DAPI (1 μg/ml, 10 minutes) before being mounted onto slides using Vectashield (Vector Laboratories, #H-1000) or ProLong Gold antifade reagent (Life Technologies, #P36930). The Axio Imager A1 (Zeiss) was used for fluorescence microscopy analysis and to collect all images.

Antibodies

For immunocytochemistry, immunohistochemistry and western blotting procedures, we used anti-phospho-histone H3-AlexaFluor488 conjugate, anti-phospho-histone H3, anti-RPA32, anti-γH2AX, anti-CENP-A (Cell Signaling; #9708, #9706, #2208, #2577, #2048, respectively), anti-FANCD2, anti-FANCI, anti-53BP1 (Abcam; #ab2187, #ab74332, #ab36823, respectively), anti-pan actin, anti-MPO (Thermo Scientific; #MS-1295-P1ABX, #RB-373-A1, respectively), anti-F4/80, anti-Mac-2 (Cedarlane; #CL8940AP and #CL8942AP, respectively), anti-CD-3 (Serotec; #MCA1477), anti-B220 (BD Biosciences; #550286), anti-digoxigenin (Roche; #11333062910), anti-FANCD2 (Epitomics; #2986-1), anti-PICH (Abnova; #H00054821-D01P) and Streptavidin-AlexaFluor488 conjugate antibody (Invitrogen, #S-32354). For the DNA Fiber assay, the digoxigenin-Rhodamine conjugate antibody from Roche (#11207750910) and Streptavidin-AlexaFluor488 conjugate antibody from Invitrogen (#S-32354) were used.

DNA fiber assay and cell cycle analysis

All techniques and methods of analysis used were performed as described previously[16,39].

EdU spots analysis

EdU (Life Technologies, #A10044) was added to cells at a final concentration of 20μM for 10 minutes prior to harvest. After fixation, cells were subjected to the Click-iT™

reaction using Biotin-Azide (Life Technologies, #B10184) for 1 hour at RT, according to the manufacturer's instructions. Cells were then stained with the appropriate antibodies using normal immunocytochemistry techniques.

Cytokinesis-block micronucleus assay and 53BP1 nuclear bodies analysis

The cytokinesis-block micronucleus assays and 53BP1-NBs analyses were performed as described previously[40]. Though the identification G1 nuclei for the analysis of 53BP1 nuclear bodies is typically determined by those that are cyclin A-negative[41,42], the lack of a cyclin A antibody that works well for mouse cells precluded use of this technique. As an alternative, G1 nuclei were identified as those contained within binucleated cells following cytochalasin B treatment.

DNA ultra-fine bridge analysis

To measure the levels of DNA ultra-fine bridges (UFBs), another consequence of late replication intermediates[33,34,43], anaphase cells were stained for the Pkl1-interacting checkpoint helicase (PICH) and analyzed for the presence of PICH-coated UFBs.

Results

Mcm4^{chaos3} homozygosity results in a reduced number of dormant origins and a lower active origin density in a C57BL/6J background

The phenotypes of *Mcm4*$^{chaos3/chaos3}$ and *Fancc*$^{-/-}$ mice in a C57BL/6J background have been relatively well characterized and share several similarities, including semi-lethality and a heightened predisposition to microphthalmia[39,40,44]. We therefore generated wild-type, *Mcm4*$^{chaos3/chaos3}$, *Fancc*$^{-/-}$ and *Mcm4*$^{chaos3/chaos3}$*;Fancc*$^{-/-}$ primary mouse embryonic fibroblasts (MEFs) in this inbred background to perform various types of cellular assays. First, we verified that *Mcm4*$^{chaos3/chaos3}$ and *Mcm4*$^{chaos3/chaos3}$*;Fancc*$^{-/-}$ cells have reduced levels of chromatin-bound MCM4 compared to wild-type and *Fancc*$^{-/-}$ cells, indicating a reduced number of licensed origins (Supplementary Figure S1A)[16]. Consistent with our previous work[16], *Mcm4*$^{chaos3/chaos3}$ cells exhibited higher levels of FANCD2 foci at prophase compared to wild-type cells (Supplementary Figure S1B). Expectedly, the lack of FANCC abolished FANCD2 chromatin loading to sub-detectable levels in both *Fancc*$^{-/-}$ and *Mcm4*$^{chaos3/chaos3}$*;Fancc*$^{-/-}$ cells (Supplementary Figure S1C). To understand DNA replication kinetics in these MEFs, we began our analysis with a DNA fiber assay. Previously, we reported that *Mcm4*^{chaos3} homozygosity in this inbred background not only results in a reduced number of dormant origins but also lowers the density of active origins, thereby contributing to the semi-lethality of newborn mice[39]. To verify that this was also the case for *Mcm4*$^{chaos3/chaos3}$*;Fancc*$^{-/-}$ cells, we measured origin-to-origin distances (Figure 1A and B). Compared to wild-type cells (63.3kb±3.57), significantly

longer average origin-to-origin distances were observed in *Mcm4*$^{chaos3/chaos3}$ (80.0kb±4.32, $p<0.01$) and *Mcm4*$^{chaos3/chaos3}$*;Fancc*$^{-/-}$ cells (75.0kb±3.60, $p<0.05$), indicating lower densities of active origins. While *Fancc*$^{-/-}$ cells exhibited a slightly longer average origin-to-origin distance (68.3kb±4.12), this was not statistically different from wild-type cells ($p=0.361$). To determine if overall replication fork movement was substantially altered in mutant cells, fork velocities were also measured. Average fork velocities were largely similar among the four genotypes, with only *Fancc*$^{-/-}$ and *Mcm4*$^{chaos3/chaos3}$*;Fancc*$^{-/-}$ cells exhibiting very slightly faster and slower forks, respectively (Figure 1B).

Loss of FANCC leads to a drastic increase in stalled/collapsed forks in *Mcm4*$^{chaos3/chaos3}$ cells

The FA proteins function to support replication fork stability as well as fork restart[30,45-47]. Thus, *Mcm4*$^{chaos3/chaos3}$*;Fancc*$^{-/-}$ cells lack two important fork recovery mechanisms: dormant origins and another mechanism mediated by FANCC. To investigate fork progression under these circumstances, we examined the focus formation of RPA32 (Figure 2A), a marker of stalled replication forks[48,49]. Compared to wild-type cells, slightly increased numbers of *Mcm4*$^{chaos3/chaos3}$ and *Fancc*$^{-/-}$ cells were positive for ≥5 RPA32 foci (1.2- and 1.6-fold, respectively) though only *Fancc*$^{-/-}$ cells exhibited a significant increase ($p<0.001$), similar to our previous observations[40]. The marginal increase in RPA32 foci in *Mcm4*$^{chaos3/chaos3}$ cells may be due to intrinsic upregulation of

the FA pathway, which could compensate for a loss of dormant origins in the recovery of stalled/collapsed forks, preventing the formation of such foci. Indeed, loss of FANCC in *Mcm4*$^{chaos3/chaos3}$ cells resulted in drastically increased levels of RPA32 foci (>3-fold, $p<0.001$, relative to wild-type cells). Furthermore, the number of RPA32 foci co-localizing with γH2AX foci, a marker of DNA double strand breaks[50], exhibited a similar trend with the highest increase (>3.8-fold, $p<0.001$, relative to wild-type cells) seen in *Mcm4*$^{chaos3/chaos3}$*;Fancc*$^{-/-}$ cells. These findings suggest that FANCC plays a crucial role in preventing stalled/collapsed forks, particularly in the absence of dormant origins. We then investigated the ability of *Mcm4*$^{chaos3/chaos3}$*;Fancc*$^{-/-}$ cells to progress through the cell cycle. Cell cycle analysis reproduced a typical profile of *Mcm4*$^{chaos3/chaos3}$ cells[17,39,51] including a reduced S phase fraction (24.6% vs. 28.1% in wild-type, $p<0.01$) and G2/M accumulation (24.1% vs. 21.1% in wild-type, $p<0.01$)(Figure 2B; Supplementary Figure S2). While cell cycle profiles for *Fancc*$^{-/-}$ cells were indistinguishable from *Mcm4*$^{chaos3/chaos3}$ cells, these trends were further exacerbated in *Mcm4*$^{chaos3/chaos3}$*;Fancc*$^{-/-}$ cells, in which the S phase and G2/M fractions were 19.3% and 28.0%, respectively ($p<0.001$). *Mcm4*$^{chaos3/chaos3}$*;Fancc*$^{-/-}$ cells therefore suffer from a greatly increased level of late replication intermediates, accumulating during the G2/M phases.

Despite FA pathway activation, *Mcm4*$^{chaos3/chaos3}$ cells exhibit an increase in sites of isolated DNA synthesis in early M phase

Although *Mcm4*$^{chaos3/chaos3}$ cells exhibited only a marginal increase in RPA32/γH2AX foci, they still exhibited significant G2/M phase accumulation (Figure 2B). This may therefore stem from an additional defect, such as delayed completion of DNA replication. Recent studies reported that delayed DNA replication can be identified as sites of localized DNA synthesis persisting until early M phase by pulse-labeling with EdU, a thymidine analogue (referred to as "EdU spots")[52,53]. We therefore quantified EdU spots in prophase cells after a short pulse labeling (10 min) of EdU. We also examined the co-localization of EdU spots with FANCD2 foci in wild-type and *Mcm4*$^{chaos3/chaos3}$ cells (Figure 3A), as EdU spots co-localize with FANCD2 foci[52,53] as well as FANCI foci (Supplementary Figure S3A) in early M phase. Compared to wild-type cells, a greatly elevated percentage (>3-fold, $p<0.001$) of *Mcm4*$^{chaos3/chaos3}$ cells contained prophase EdU spots even in the untreated condition (Figure 3B). Consistent with previous studies[52,53], the majority of EdU spots indeed co-localized with FANCD2 foci in either genotype, resulting in a corresponding increase in the number of *Mcm4*$^{chaos3/chaos3}$ cells positive for EdU-FANCD2 co-localizations. This was further supported by the analysis of individual EdU spots, which showed that only a minor fraction failed to co-localize with FANCD2 in either genotype (Figure 3C), possibly representing loci that are naturally late replicating. Interestingly, analysis of individual FANCD2 foci revealed an almost exclusive increase in those co-localizing with EdU spots in *Mcm4*$^{chaos3/chaos3}$ cells (Figure

3C). Consistent with previous findings[52], we also observed that treatment with a low dose of APH greatly elevated the numbers of both EdU spots and FANCD2 foci in both genotypes (Supplementary Figure 3B), yielding trends very similar to the untreated condition. Taken together, these observations indicate that the elevated number of FANCD2 foci seen in *Mcm4*$^{chaos3/chaos3}$ cells is primarily due to an increased number of sites exhibiting isolated DNA synthesis, though this activation is apparently insufficient to prevent this synthesis from being delayed until prophase. We interpret these findings as follows: a loss of dormant origins not only lowers the efficiency of stalled fork recovery but also generates long, origin-poor regions. The FA pathway can effectively compensate for the former, thus preventing the formation of RPA32/γH2AX foci as seen in *Mcm4*$^{chaos3/chaos3}$ cells (Figure 2A). In the latter case, however, it is almost inevitable that fork stalling occurs and persists more frequently in origin-poor regions, thereby delaying the completion of DNA replication in these regions until early M phase despite FA pathway activation.

<u>The FA pathway exerts its role in preventing delayed DNA replication under conditions of replication stress</u>

Based on our interpretations, activation of the FA pathway should act against the formation of EdU spots at prophase, though its effect may be limited. On the other hand, given the high level of EdU-FANCD2 co-localizations, an alternative possibility is that FANCD2 mono-ubiquitination is actually required for this isolated form of DNA

synthesis. To distinguish between these two possibilities, we repeated our pulse-labeling experiments to score prophase EdU spots in all four genotypes in the untreated conditions (Figure 4A and B). A reproducibly elevated percentage (>2-fold, $p<0.001$) of *Mcm4*$^{chaos3/chaos3}$ cells were positive for EdU spots relative to wild-type cells, whereas *Fancc*$^{-/-}$ cells displayed no significant difference from wild-type ($p=0.251$), consistent with the idea that mono-ubiquitinated FANCD2 is dispensable for this isolated DNA synthesis. Interestingly, however, a slightly increased percentage of *Mcm4*$^{chaos3/chaos3}$*;Fancc*$^{-/-}$ cells contained EdU spots compared to *Mcm4*$^{chaos3/chaos3}$ cells ($p<0.01$), suggesting that FANCC is actually required to prevent the formation of EdU spots in the absence of dormant origins. To further test the role of the FA pathway in preventing this delayed replication, we treated cells with a low dose of APH, which substantially increased the number of EdU spots in all genotypes (Figure 4C and D). A significantly increased number (1.5-fold compared to wild-type cells, $p<0.001$) of *Fancc*$^{-/-}$ cells were now positive for ≥10 APH-induced EdU spots. As APH is known to slow fork velocities[36,53], increase the frequency of fork stalling[16,54] and hyper-activate dormant origins[14,16], it seems likely that such conditions make the role of the FA pathway more crucial to sustain fork progression and prevent delayed replication. Indeed, we observed a sharp increase in the number of *Mcm4*$^{chaos3/chaos3}$*;Fancc*$^{-/-}$ cells exhibiting ≥10 APH-induced EdU spots (1.9-fold increase compared to wild-type cells, $p<0.001$), with a 2-fold higher number of APH-induced EdU spots per cell compared to all other genotypes. These data support the idea that FANCC, and potentially other components of the FA

pathway, function to prevent delayed DNA replication, particularly under conditions of replication stress.

The frequencies of spontaneous MN and 53BP1 nuclear bodies are significantly increased in *Mcm4*$^{chaos3/chaos3}$*;Fancc*$^{-/-}$ cells

Based on the above findings, we conclude that *Mcm4*$^{chaos3/chaos3}$*;Fancc*$^{-/-}$ cells suffer from two distinct defects: 1) a greatly increased level of stalled/collapsed forks due to the lack of two major fork recovery mechanisms (dormant origins and the FA pathway), and 2) an increased number of sites in which replication is delayed until early M phase. To investigate the consequences of these accumulated late replication intermediates, we first looked at the formation of MN, which occurs at an elevated frequency in *Mcm4*$^{chaos3/chaos3}$ and *Fancc*$^{-/-}$ cells[16,40]. Using the cytokinesis-block MN assay[55], we observed that *Mcm4*$^{chaos3/chaos3}$ cells reproducibly exhibited a 2.9-fold increase in spontaneous MN compared to wild-type cells ($p<0.001$, Figure 5A). *Fancc*$^{-/-}$ cells showed an even higher increase (3.5-fold, $p<0.001$), with the most severe phenotype seen for *Mcm4*$^{chaos3/chaos3}$*;Fancc*$^{-/-}$ cells (5.3-fold, $p<0.001$). If unresolved, late replication intermediates can also manifest as 53BP1 nuclear bodies (53BP1-NBs) in the subsequent G1 phase nuclei[41,42]. These structures co-localize with γH2AX and are often exquisitely symmetrical in terms of their appearance within the daughter nuclei, suggesting that they are derived from a common breakage event occurring during passage through M phase[41]. We thus measured the levels of 53BP1-NBs in G1 phase daughter nuclei contained

within binucleated cells using essentially the same protocol as the cytokinesis-block MN assay. While *Mcm4*$^{chaos3/chaos3}$ and *Fancc*$^{-/-}$ cells displayed slightly increased numbers (1.16- and 1.5-fold, respectively) of G1 nuclei positive for 53BP1-NBs ($p<0.01$ and $p<0.001$, respectively) compared to wild-type, *Mcm4*$^{chaos3/chaos3}$*;Fancc*$^{-/-}$ cells had a substantial increase in 53BP1-NBs compared to either single mutant (1.9-fold, $p<0.001$)(Figure 5B). Taken together, these findings suggest that FANCC and dormant origins coordinately function to prevent genome instability derived from late replication intermediates.

Almost all B6 *Mcm4*$^{chaos3/chaos3}$*;Fancc*$^{-/-}$ pups die right after birth

Given the additive effect of *Fancc*$^{-}$ and *Mcm4*^{chaos3} in causing genome instability, we hypothesized that B6 *Mcm4*$^{chaos3/chaos3}$*;Fancc*$^{-/-}$ mice may exhibit more severe phenotypes than either single homozygote. We therefore set up *Fancc*$^{+/-}$ heterozygous intercrosses in the *Mcm4*^{chaos3} homozygous background to obtain B6 double homozygous mutants. Among 74 newborns, the numbers of pups for the three expected genotypes were not statistically different from the expected Mendelian ratio ($p=0.640$, see Table 1). However, 13 out of 15 double homozygous (*Mcm4*$^{chaos3/chaos3}$*;Fancc*$^{-/-}$) pups died shortly after birth, revealing a strikingly high rate of perinatal lethality. We previously reported that *Mcm4*^{chaos3} and *Fancc*$^{-}$ homozygosity each cause semi-lethality in this background[39,40]. However, this cannot fully explain the high lethality of *Mcm4*$^{chaos3/chaos3}$*;Fancc*$^{-/-}$ pups, as their survival rate (13%) was substantially lower than

that of their *Mcm4*$^{chaos3/chaos3}$*;Fancc*$^{+/+}$ littermates (85%, p=7.64x10^{-15}) or of *Fancc*$^{-/-}$ mice (65%)[40]. We also noticed that *Mcm4*$^{chaos3/chaos3}$*;Fancc*$^{+/-}$ pups exhibited a decreased rate of survival (69%) at 3 weeks of age compared to *Mcm4*$^{chaos3/chaos3}$*;Fancc*$^{+/+}$ pups (p=0.00582). This *Fancc* dosage-dependent survival of *Mcm4*$^{chaos3/chaos3}$ pups supports a synthetic lethal/sickness interaction between *Mcm4*^{chaos3} and *Fancc*$^{-}$. Histopathological analyses of *Mcm4*$^{chaos3/chaos3}$*;Fancc*$^{-/-}$ pups did not reveal an apparent cause of death. Of the two *Mcm4*$^{chaos3/chaos3}$*;Fancc*$^{-/-}$ pups that survived past 3 weeks, one was euthanized for a non-tumor abscess at the age of 128 days while the other developed disseminated T-cell lymphoma in only 163 days (Supplementary Figure S4), much more quickly than the average tumor latency of about 12.4 months for *Mcm4*$^{chaos3/chaos3}$ mice in the B6 background[16]. However, due to the very high rate of perinatal lethality, it has been extremely difficult to generate additional *Mcm4*$^{chaos3/chaos3}$*;Fancc*$^{-/-}$ pups even after the expansion of mating crosses. Together, these data indicate that a concomitant loss of dormant origins and *Fancc* is incompatible with postnatal development in this inbred background.

<u>*Mcm4*$^{chaos3/chaos3}$*;Fancc*$^{-/-}$ mice are viable in a mixed genetic background but succumb to spontaneous tumors at much younger ages</u>

It is well known that phenotypic expression in mice is greatly influenced by genetic background. We therefore reasoned that performing the same intercrosses in a different genetic background would allow us to obtain viable *Mcm4*$^{chaos3/chaos3}$*;Fancc*$^{-/-}$ mice to test

their tumor predisposition. Indeed, we found *Mcm4*$^{chaos3/chaos3}$;*Fancc*$^{-/-}$ mice were viable when generated in a mixed background between C57BL/6J and C3HeB/FeJ. *Fancc*$^{-/-}$ and *Mcm4*$^{chaos3/chaos3}$;*Fancc*$^{-/-}$ mice were again born at reduced frequencies compared to the expected numbers (Supplementary Tables S1-2), but these differences were not statistically significant. While *Mcm4*$^{chaos3/chaos3}$;*Fancc*$^{-/-}$ mice did not show any apparent developmental abnormalities, they did exhibit a slightly decreased average body weight (p<0.05)(Figure 6A). A loss of dormant origins also worsened the hypogonadism phenotype of *Fancc*$^{-/-}$ mice, as *Mcm4*$^{chaos3/chaos3}$;*Fancc*$^{-/-}$ mice exhibited a smaller average testes size (p<0.05 when compared to *Fancc*$^{-/-}$ mice) with an increased number of empty seminiferous tubules (Supplementary Figure 5A and B). After verifying an enhanced level of replication-associated genome instability in *Mcm4*$^{chaos3/chaos3}$;*Fancc*$^{-/-}$ MEFs in this background (Supplementary Figure S6), we aged cohorts of wild-type, *Mcm4*$^{chaos3/chaos3}$, *Fancc*$^{-/-}$ and *Mcm4*$^{chaos3/chaos3}$;*Fancc*$^{-/-}$ mice to observe the formation of spontaneous tumors until 14 months of age. In agreement with previous findings[44,56], >95% of wild-type and *Fancc*$^{-/-}$ mice survived to the end of the study, with only one *Fancc*$^{-/-}$ mouse exhibiting tumors at necropsy (Figure 6B). As expected, the majority (~71%) of *Mcm4*$^{chaos3/chaos3}$ mice succumbed to tumors before 14 months, as did ~84% of *Mcm4*$^{chaos3/chaos3}$;*Fancc*$^{-/-}$ mice. The tumor spectrum displayed by *Mcm4*$^{chaos3/chaos3}$;*Fancc*$^{-/-}$ mice was largely similar to that of *Mcm4*$^{chaos3/chaos3}$ mice, though the entire cohort that developed tumors before 235 days succumbed exclusively to lymphosarcomas (Figure 6C and Supplementary Tables S3-4). Most of these tumors

were of T-cell origin (CD-3 positive), though B-cell tumors (B220 positive) were also observed (Supplementary Figure S7). Notably, a myeloid leukemia was seen as well. Overall, *Mcm4*$^{chaos3/chaos3}$;*Fancc*$^{-/-}$ mice exhibited an average tumor latency of 279.7 days, much shorter than the 361.9 days seen for *Mcm4*$^{chaos3/chaos3}$ mice. This difference did not reach statistical significance (Log-Rank test, p=0.264), most likely due to great variation in the latencies in individual mice and gender-specific effects in this background (Supplementary Tables S3-4) [57]. However, it should be noted that a much greater proportion of *Mcm4*$^{chaos3/chaos3}$;*Fancc*$^{-/-}$ mice (~53%) developed spontaneous tumors before 300 days of age compared to *Mcm4*$^{chaos3/chaos3}$ mice (~7%, p=1.21x10^{-19}) suggesting that a concomitant loss of dormant origins and *Fancc* can accelerate tumorigenesis.

Discussion

Exploiting the *Mcm4*^{chaos3} mouse model, we investigated the nature of FA pathway activation in the absence of dormant origins. We hypothesized that this activation occurs to compensate for the rescue of stalled forks. In agreement with our hypothesis, *Mcm4*$^{chaos3/chaos3}$*;Fancc*$^{-/-}$ cells exhibited impaired fork stability, an increased number of sites displaying delayed replication and greatly enhanced levels of genome instability. Furthermore, we found that an intact FA pathway is required in *Mcm4*$^{chaos3/chaos3}$ mice not only for promoting tumor suppression but also for supporting postnatal development under conditions in which the density of active origins is relatively low[39].

While the exact role of the FA pathway in unchallenged S phase is still largely unknown, a loss of *Fancc* in *Mcm4*$^{chaos3/chaos3}$ cells clearly revealed its function in replication fork progression as well as stability. In the absence of dormant origins, the FA core complex may facilitate translesion synthesis (TLS) to recover stalled forks[58-60]. Another recent study demonstrated a role of FANCD2 in BLM-mediated fork restart[47]. This mechanism may come into play in the absence of dormant origins. Alternatively, if no appropriate choice is available for stalled fork recovery during S phase, the FA pathway may function to stabilize stalled forks, thereby manifesting as FANCD2/FANCI foci during the G2/M phases, as proposed earlier[33]. Indeed, lack of a functional FA pathway leads to the degradation of nascent strands at stalled forks, supporting its role in fork protection[46,47,61]. Furthermore, given the increased levels of spontaneous genome

instability in *Fancc*$^{-/-}$ cells, it seems that there must be certain types of endogenous lesions that are primarily taken care of by the FA pathway rather than dormant origins. Fork recovery at such lesions may also be shared with HELQ, as double homozygosity for *Fancc*$^{-}$ and *Helq*^{gt} greatly elevates genome instability[40].

In this study, we observed that an elevated level of FANCD2 focus formation in *Mcm4*$^{chaos3/chaos3}$ cells during prophase (Supplementary Figures S1B) is primarily associated with the formation of EdU spots (Figure 3). A recent study reported that polymerase eta deficiency induces common fragile site instability and the formation of EdU spots co-localizing with FANCD2 foci in early M phase, suggesting that EdU spots most likely represent delayed DNA replication within loci where replication intermediates long persist[52]. Consistent with this idea, APH treatment predominantly induced EdU spots co-localizing with FANCD2 foci both in wild-type and *Mcm4*$^{chaos3/chaos3}$ cells (Figure 3). Despite the high rate of EdU-FANCD2 co-localizations, an intact FA pathway is apparently dispensable for this type of DNA synthesis. On the contrary, lack of a functional FA pathway actually increases the number of prophase EdU spots under conditions of replication stress, as seen in *Mcm4*$^{chaos3/chaos3}$*;Fancc*$^{-/-}$ cells in the untreated condition and both *Fancc*$^{-/-}$ and *Mcm4*$^{chaos3/chaos3}$*;Fancc*$^{-/-}$ cells in the APH-treated condition (Figure 4). These findings suggest the presence of an FA-independent mechanism(s) to support DNA synthesis at such loci until early M phase. Such mechanisms may include HELQ, which functions parallel to FANCC, as we reported very recently[40]. Moreover, it was recently shown that

the structure-specific endonucleases MUS81 and ERCC1 are also found at EdU spots along with FANCD2 but their presence on mitotic chromosomes does not depend on FANCC[53]. While the exact mechanism(s) remains to be unveiled, it was demonstrated that depletion of these endonucleases increased the formation of MN, DNA ultra-fine bridges at anaphase and 53BP1-NBs[53,62]. It will therefore be important to understand the roles of these endonucleases in the formation of EdU spots as well as the role of this late DNA synthesis in the resolution of late replication intermediates.

Mcm4$^{chaos3/chaos3}$ and *Fancc*$^{-/-}$ cells/mice are phenotypically similar, particularly in the B6 background, with respect to genome instability (Figure 5) and susceptibility to newborn lethality and microphthalmia[39,44]. However, *Mcm4*$^{chaos3/chaos3}$ mice are highly prone to spontaneous tumorigenesis while *Fancc*$^{-/-}$ mice are not. One major phenotype that was found in *Mcm4*$^{chaos3/chaos3}$ but not *Fancc*$^{-/-}$ cells was an increased number of EdU spots in prophase in the untreated condition (Figure 4B). We thus speculate that a reduction in the number of licensed origins by *Mcm4*^{chaos3} homozygosity not only causes a loss of dormant origins but also generates relatively long stretches of the genome that are devoid of any replication origins. So, fork stalling within small regions lacking dormant origins may be fully replicated by the fork rescuing actions of the FA pathway described above. However, this activity may not be sufficient in large, origin-poor loci so that completion of DNA synthesis in these regions is delayed until early M phase despite FA pathway activation, thus manifesting as a large increase in the number of EdU-FANCD2 co-localizations. It is possible that a fraction of these sites may not even

fully complete DNA replication prior to anaphase. Therefore, a combination of intrinsic chromosome instability along with an increased number of un-replicated loci could be a driving factor in spontaneous tumorigenesis in *Mcm4*$^{chaos3/chaos3}$ mice.

While several mouse models have been generated to study the FA pathway, the majority fails to recapitulate the phenotypes of human FA patients, including tumor predisposition[63,64]. We were unable to further test to what extent *Mcm4*$^{chaos3/chaos3}$*;Fancc*$^{-/-}$ mice recapitulate other phenotypes of human FA patients, such as bone marrow failure. However, we think that *Mcm4*^{chaos3} homozygosity provides a unique condition in which to understand the role of the FA proteins as well as others in genome stability in unchallenged conditions, as recently shown for ATM[57]. In particular, an FA core complex-independent role of FANCD2 in replication fork stability[61] can also be investigated in *Mcm4*$^{chaos3/chaos3}$ mice, which may clarify the role of FANCD2 in the formation of EdU spots. Very recently, the first human genetic disorder caused by a mutant *MCM4* gene was discovered[65,66]. Cells from these patients exhibit chromosome fragility much like *Mcm4*$^{chaos3/chaos3}$ cells. Due to a very limited number of patients with this disorder, however, it is not yet unknown whether they are cancer prone. Nevertheless, it is quite possible that there remain undiscovered genetic disorders caused by mutations in *MCM2-7* genes in which the physiological role of the FA pathway may become more apparent.

Acknowledgements

We thank Dr. Markus Grompe for providing us with the *Fancc*$^{-}$ mice. We thank Dr. Alexandra Sobeck for her critical reading of this manuscript. We thank Katie Haberle, Masanao Chinen, Susan Yeung and Wai Long Lee for their assistance in genotyping.

Table and figure legends

Table 1

Mcm4$^{chaos3/chaos3}$;*Fancc*$^{-/-}$ mice exhibit severe perinatal lethality in an inbred C57BL/6J background.

Figure 1

(A) A schematic of the consecutive dual labeling steps of the DNA fiber assay is shown at left. Active replication forks were labeled with digoxigenin-conjugated dUTPs (250µM, red) for 20 minutes followed by labeling with biotin-conjugated dUTPs (250µM, green) for 30 minutes. Fork velocity and origin-to-origin distances were determined as shown. A representative image of adjacent origins is shown on the right with staining for digoxigenin-dUTPs (red) and biotin-dUTPs (green). White arrowheads indicate the location of origins. The scale bar is 10 µm. (B) Box plots show the ranges observed for the origin-to-origin (ori-to-ori) distance (left) and fork velocity (right) values for each genotype. Lines within the shaded boxes indicate the medians while the "+" signs show the location of the mean. Black dots represent outliers. The tables on the right show the summaries for ori-to-ori distances (top) and fork velocities (bottom). Significance was determined by *t*-test. Asterisks denote: *p<0.05, **p<0.01 and ***p<0.001. NS means not significant. WT, C3, FAC and C3;FAC refer to wild-type, *Mcm4*$^{chaos3/chaos3}$, *Fancc*$^{-/-}$ and *Mcm4*$^{chaos3/chaos3}$;*Fancc*$^{-/-}$, respectively.

Figure 2

(A) *Mcm4*$^{chaos3/chaos3}$;*Fancc*$^{-/-}$ cells display a drastic increase in markers of persistently stalled replication forks upon exiting S phase. Shown at left are representative images of all four genotypes co-stained for RPA (green) and γH2AX (red). The average percentages of cells positive for 5 or more RPA foci (top right) or 5 or more RPA-γH2AX co-localizations (bottom right) are also shown. Error bars show the binomial error for the combined data set obtained from three independently performed experiments. The scale bar is 10 μm. Significance was determined by χ^2-test. (B) *Mcm4*$^{chaos3/chaos3}$;*Fancc*$^{-/-}$ cells experience a heightened accumulation in the G2/M phases. Shown are the average proportions of cells observed within the G1, S or G2/M phases for all four genotypes. Error bars show the standard error of the mean (SEM) for at least 5 independent replicates. Asterisks denote: *p<0.05, **p<0.01 and ***p<0.001. WT, C3, FAC and C3;FAC refer to wild-type, *Mcm4*$^{chaos3/chaos3}$, *Fancc*$^{-/-}$ and *Mcm4*$^{chaos3/chaos3}$;*Fancc*$^{-/-}$, respectively.

Figure 3

A higher number of prophase FANCD2 foci in *Mcm4*$^{chaos3/chaos3}$ cells are the result of a sharp increase in EdU spots that co-localize with FANCD2. (A) Shown are representative images of wild-type and *Mcm4*$^{chaos3/chaos3}$ cells co-stained for EdU (green)

and FANCD2 (red) in the untreated (UNT) condition. Prophase cells were identified by prominent chromatin condensation via DAPI staining (blue). The scale bar is 10 μm. (B) At top are the percentages of prophase cells positive for EdU spots (white bars) or EdU-FANCD2 co-localization events (grey bars). At bottom are the number of EdU spots (white bars) per prophase cell and the number of EdU-FANCD2 co-localization events (grey bars) per prophase cell. Error bars show the binomial error for the combined data sets obtained from three independently performed experiments. Significance was determined by χ^2-test. Asterisks denote: ***$p<0.001$. (C) Shown at top are the numbers of EdU spots with "EdU only" (white bars) as well as the number of EdU-FANCD2 co-localization events (grey bars) observed in 150 prophase cells. At bottom are the numbers of FANCD2 foci with "FANCD2 only" (black bars) as well as the number of EdU-FANCD2 co-localizations (shown again as grey bars) observed in 150 prophase cells. WT and C3 refer to wild-type and *Mcm4*$^{chaos3/chaos3}$, respectively.

Figure 4

A loss of dormant origins increases the number of EdU spots at prophase, which is further enhanced by disruption of *Fancc*. (A) Shown are representative images of all four genotypes co-stained for EdU (green) and pH3 (red). In this experiment, staining for pH3, a marker of condensed chromatin [67], was used to confirm the scoring of nuclei at prophase in addition to nuclear morphology by DAPI staining. (B) Shown are the average percentages of prophase cells positive for EdU spots (top) and the number of

EdU spots per prophase cell (bottom). (C) As in (A), with cells treated with 300nM APH for 24 hours. (D) Shown are the average percentages of prophase cells positive for 10 or more EdU spots (top) and the number of EdU spots per prophase cell (bottom). Nuclei (A,C) were stained with DAPI (blue). Scale bars (A,C) are 10 μm. Error bars (B,D) show the binomial error for the combined data sets obtained from three independently performed experiments. Significance was determined by χ^2-test. Asterisks denote: $^{**}p<0.01$ and $^{***}p<0.001$. WT, C3, FAC and C3;FAC refer to wild-type, *Mcm4*$^{chaos3/chaos3}$, *Fancc*$^{-/-}$ and *Mcm4*$^{chaos3/chaos3}$*;Fancc*$^{-/-}$, respectively.

Figure 5

Mcm4$^{chaos3/chaos3}$*;Fancc*$^{-/-}$ cells show highly elevated levels of MN and 53BP1-NBs. (A) Shown are a representative image of binucleated cell positive for a micronucleus (left), the average percentages of binucleated cells positive for MN (middle) and a distribution of the number of MN per binucleated cell (right). (B) Shown at left are representative images of a 53BP1-NB in a binucleated cell. 53BP1 staining is in red. At middle are the average percentages of individual nuclei from binucleated cells positive for 53BP1-NBs, and at right are the distributions indicating the number of 53BP1-NBs per G1 phase nucleus. All nuclei were stained with DAPI (blue). All scale bars are 10 μm. All error bars show the binomial error for the combined data sets obtained from three independently performed experiments. Significance was determined by χ^2-test. Asterisks

denote: *p<0.05 and ***p<0.001. WT, C3, FAC and C3;FAC refer to wild-type, *Mcm4*$^{chaos3/chaos3}$, *Fancc*$^{-/-}$ and *Mcm4*$^{chaos3/chaos3}$;*Fancc*$^{-/-}$, respectively.

Figure 6

(A) The average body weight of *Mcm4*$^{chaos3/chaos3}$;*Fancc*$^{-/-}$ mice derived in a C57BL/6J x C3HeB/FeJ mixed genetic background is slightly reduced. Shown are the average body weights of the four genotypes in grams. Error bars show the standard error of the means (SEMs) for at least 5 mice per genotype. Significance was determined by *t*-test. Asterisks denote: *p<0.05. (B) *Mcm4*$^{chaos3/chaos3}$;*Fancc*$^{-/-}$ mice succumb to tumors with a shorter latency than *Mcm4*$^{chaos3/chaos3}$ mice in a C57BL/6J x C3HeB/FeJ mixed genetic background. Shown are the tumor-free survival curves for all four genotypes. (C) Shown are the tumor spectrums observed for *Mcm4*$^{chaos3/chaos3}$ and *Fancc*$^{-/-}$;*Mcm4*$^{chaos3/chaos3}$ mice. WT, C3, FAC and C3;FAC refer to wild-type, *Mcm4*$^{chaos3/chaos3}$, *Fancc*$^{-/-}$ and *Mcm4*$^{chaos3/chaos3}$;*Fancc*$^{-/-}$, respectively.

Table 1 Luebben et al., 2014

Genotype (all in *Mcm4*$^{chaos3/chaos3}$)	# of pups found at birth	# of live pups at birth	# of live pups at 3 wks	% survival at 3 wks	*p* value
Fancc$^{+/+}$	20	18	17	85%	-
Fancc$^{+/-}$	39	31	27	69%	0.00582
Fancc$^{-/-}$	15	2	2	13%	7.64E-15
Total	74	51	46	62%	

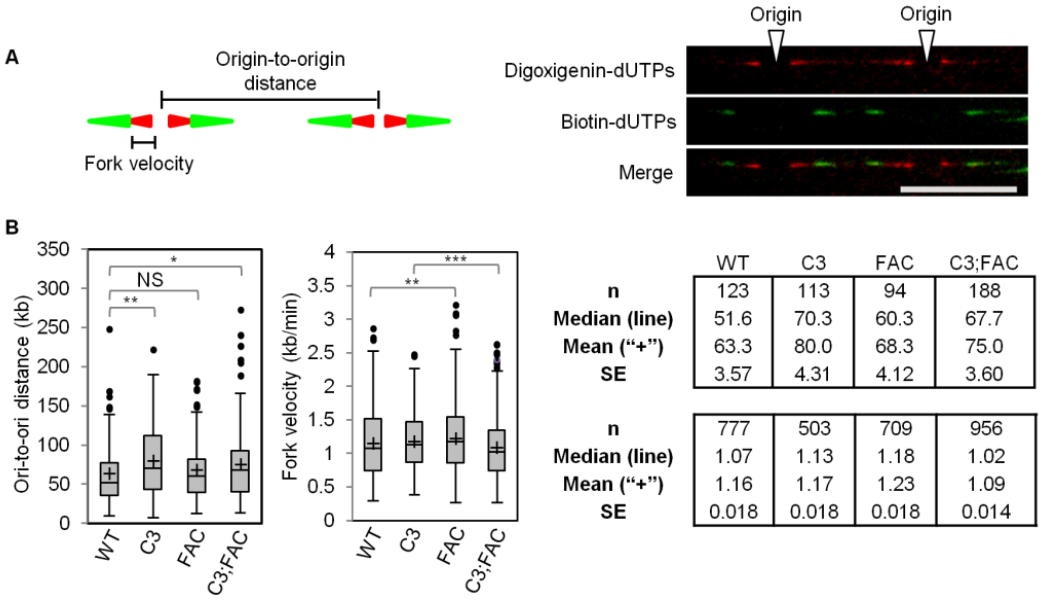

	WT	C3	FAC	C3;FAC	
n	123	113	94	188	Ori-to-ori
Median (line)	51.6	70.3	60.3	67.7	
Mean ("+")	63.3	80.0	68.3	75.0	
SE	3.57	4.31	4.12	3.60	
n	777	503	709	956	Fork velocity
Median (line)	1.07	1.13	1.18	1.02	
Mean ("+")	1.16	1.17	1.23	1.09	
SE	0.018	0.018	0.018	0.014	

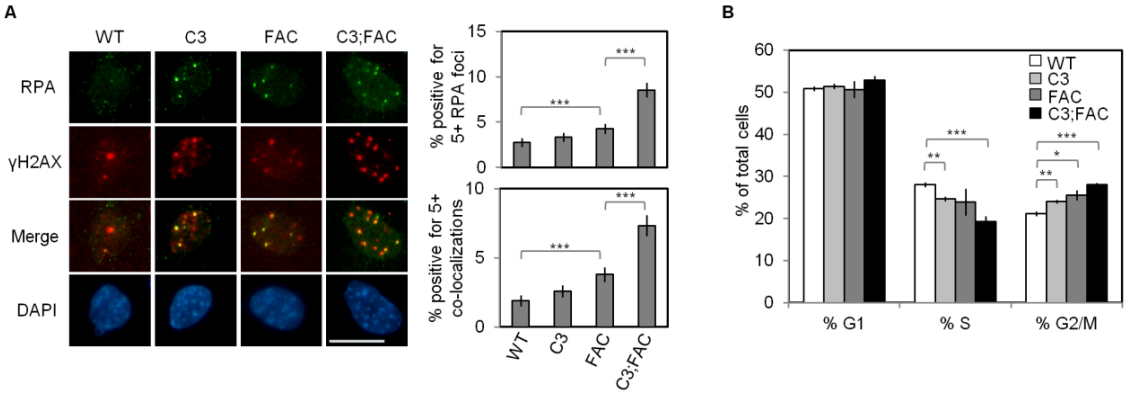
A
WT
C3
FAC
C3;FAC
RPA
γH2AX
Merge
DAPI
% positive for 5+ RPA foci
% positive for 5+ co-localizations
***
WT
C3
FAC
C3;FAC
B
% of total cells
WT
C3
FAC
C3;FAC
% G1
% S
% G2/M
**
*

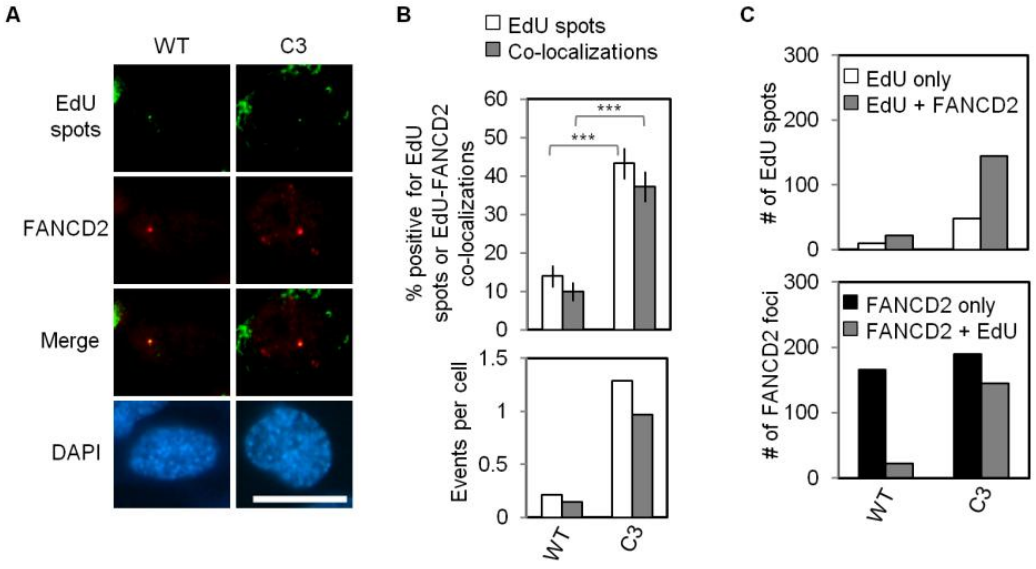
A
WT
C3
EdU spots
FANCD2
Merge
DAPI
B
EdU spots
Co-localizations
% positive for EdU spots or EdU-FANCD2 co-localizations
60
50
40
30
20
10
0
***
***
Events per cell
1.5
1
0.5
0
WT
C3
C
# of EdU spots
300
200
100
0
EdU only
EdU + FANCD2
# of FANCD2 foci
300
200
100
0
FANCD2 only
FANCD2 + EdU
WT
C3

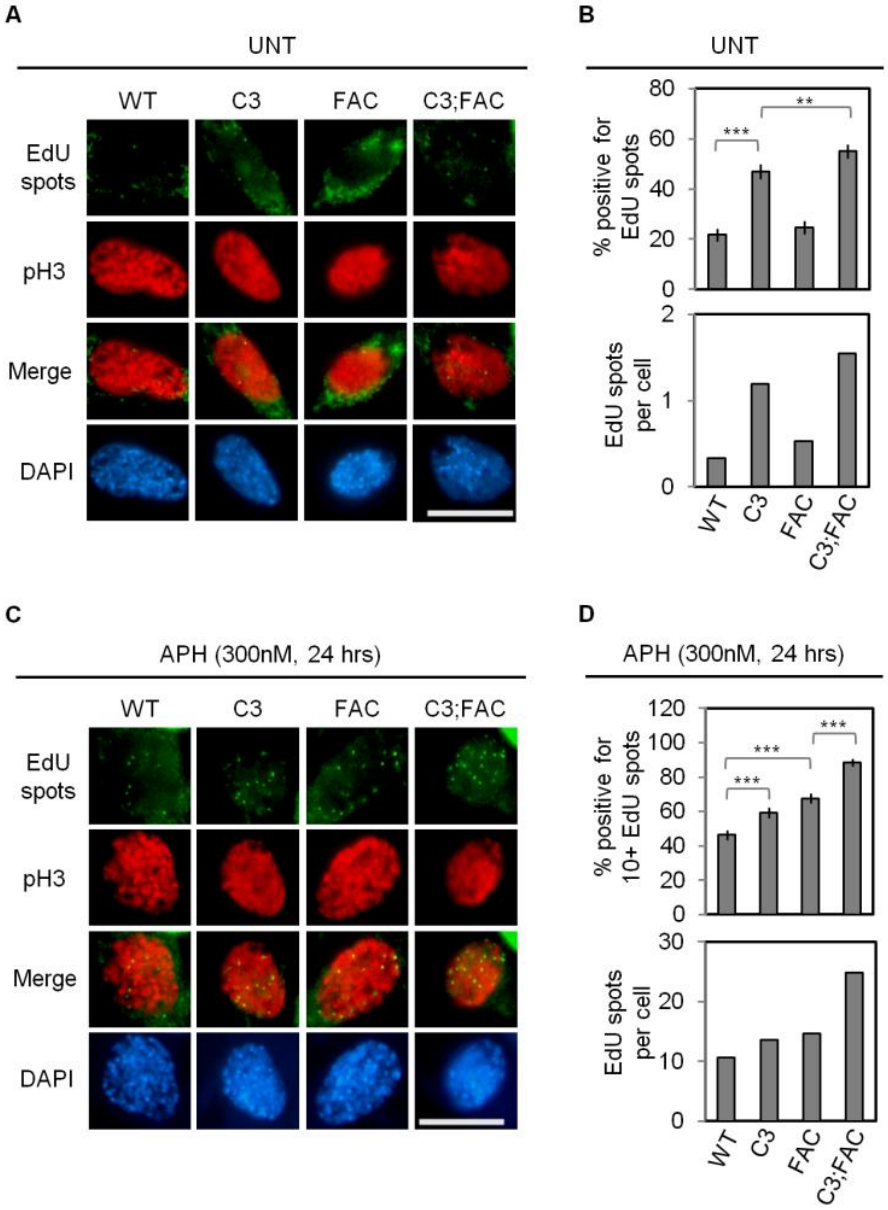
A
UNT
WT
C3
FAC
C3;FAC
EdU spots
pH3
Merge
DAPI
B
UNT
% positive for EdU spots
80
60
40
20
0
***
**
EdU spots per cell
2
1
0
WT
C3
FAC
C3;FAC
C
APH (300nM, 24 hrs)
WT
C3
FAC
C3;FAC
EdU spots
pH3
Merge
DAPI
D
APH (300nM, 24 hrs)
% positive for 10+ EdU spots
120
100
80
60
40
20
0
***
***
***
EdU spots per cell
30
20
10
0
WT
C3
FAC
C3;FAC

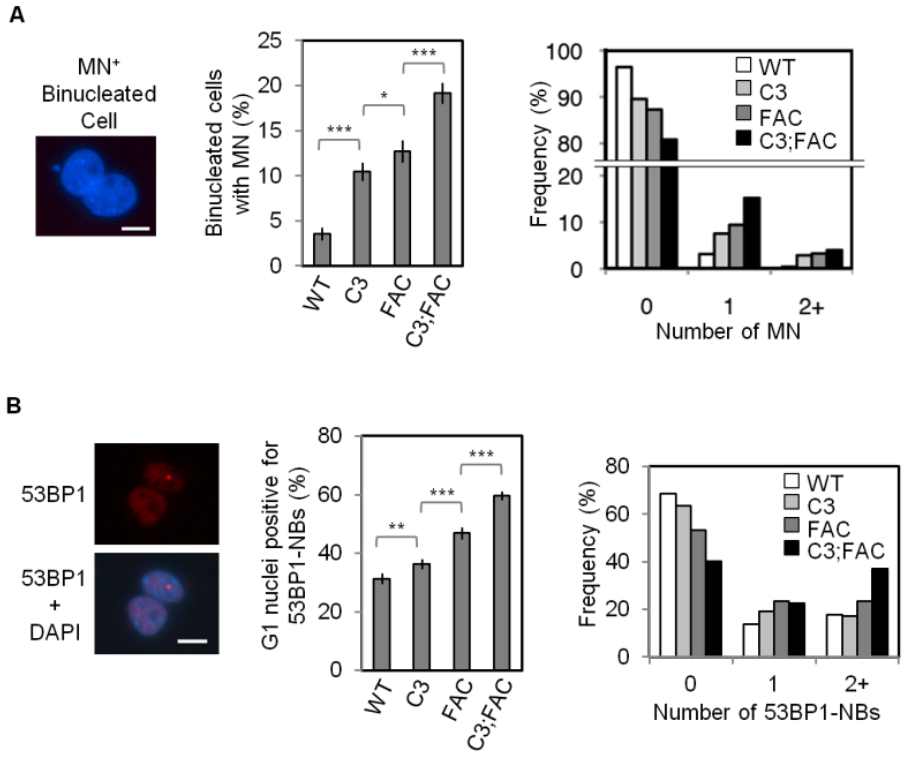
A
MN+
Binucleated
Cell
Binucleated cells
with MN (%)
25
20
15
10
5
0
***
*
***
WT
C3
FAC
C3;FAC
Frequency (%)
100
90
80
20
10
0
WT
C3
FAC
C3;FAC
0
1
2+
Number of MN
B
53BP1
53BP1
+
DAPI
G1 nuclei positive for
53BP1-NBs (%)
80
60
40
20
0
**
***
***
WT
C3
FAC
C3;FAC
Frequency (%)
80
60
40
20
0
WT
C3
FAC
C3;FAC
0
1
2+
Number of 53BP1-NBs

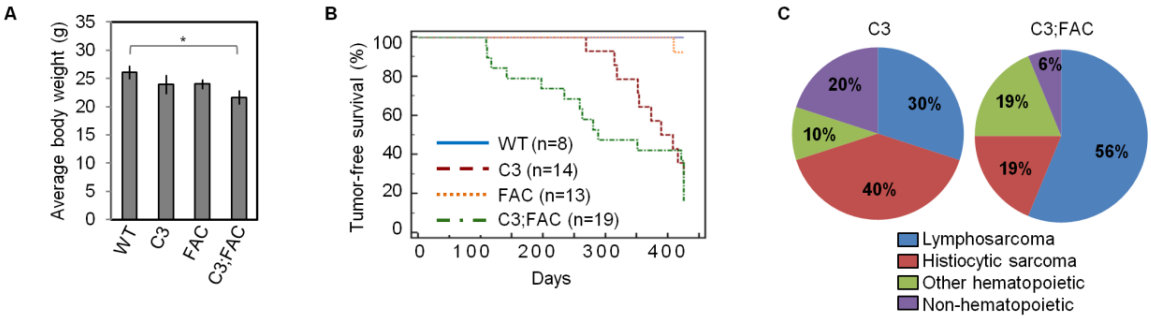
A
Average body weight (g)
35
30
25
20
15
10
5
0
*
WT
C3
FAC
C3;FAC
B
Tumor-free survival (%)
100
80
60
40
20
0
0
100
200
300
400
Days
WT (n=8)
C3 (n=14)
FAC (n=13)
C3;FAC (n=19)
C
C3
C3;FAC
20%
30%
10%
40%
6%
19%
19%
56%
Lymphosarcoma
Histiocytic sarcoma
Other hematopoietic
Non-hematopoietic

Supplementary table and figure legends

Supplementary Table S1

Fancc$^{-/-}$ mice are born at a frequency approximately equal to the expected Mendelian ratio in a C57BL/6J x C3HeB/FeJ mixed genetic background.

Supplementary Table S2

Mcm4$^{chaos3/chaos3}$*;Fancc*$^{-/-}$ mice are born at a frequency approximately equal to the expected Mendelian ratio in a C57BL/6J x C3HeB/FeJ mixed genetic background.

Supplementary Table S3

Summary of *Mcm4*$^{chaos3/chaos3}$ tumor histopathology in a C57BL/6J x C3HeB/FeJ mixed genetic background.

Supplementary Table S4

Summary of *Mcm4*$^{chaos3/chaos3}$*;Fancc*$^{-/-}$ tumor histopathology in a C57BL/6J x C3HeB/FeJ mixed genetic background.

Supplementary Figure S1

(A) Western blotting reveals a substantial reduction in the levels of MCM4 in both the total cell extracts (left) and chromatin fractions (right) of *Mcm4*$^{chaos3/chaos3}$ and *Mcm4*$^{chaos3/chaos3}$*;Fancc*$^{-/-}$ cells. Wild-type samples were also loaded in ratios of 0.4 and 0.7 as a reference for the mutants. (B) *Mcm4*$^{chaos3/chaos3}$ cells display an increased number of FANCD2 foci in prophase. Shown are the average percentages of prophase cells positive for 3 or more FANCD2 foci (top) as well as the average numbers of FANCD2 foci per prophase cell (bottom). Prophase cells were identified by prominent chromatin condensation via DAPI staining. Error bars show the binomial error for the combined data set obtained from three independent experiments. Significance was determined by χ^2-test. Asterisks denote: ***p<0.001. (C) Western blotting shows that the amount of chromatin-loaded FANCD2 is below the threshold of detection in both *Fancc*$^{-/-}$ and *Mcm4*$^{chaos3/chaos3}$*;Fancc*$^{-/-}$ cells. This was consistent in both the untreated (UNT) and APH-treated (300nM, 4 hrs) conditions. Stained membranes (A,C) were used as loading controls. WT, C3, FAC and C3;FAC refer to wild-type, *Mcm4*$^{chaos3/chaos3}$, *Fancc*$^{-/-}$ and *Mcm4*$^{chaos3/chaos3}$*;Fancc*$^{-/-}$, respectively.

Supplementary Figure S2

Representative images of cell cycle analyses are shown for all genotypes. Cell cycle analysis was performed by measuring EdU incorporation in combination with propidium iodide staining (DNA content) by flow cytometry. The FL2-H channel was used to

quantitate DNA content while the FL4-H channel was used to measure EdU incorporation. Cells were categorized according to the gates shown (R2: G1; R3: S; R4: G2/M). WT, C3, FAC and C3;FAC refer to wild-type, *Mcm4*$^{chaos3/chaos3}$, *Fancc*$^{-/-}$ and *Mcm4*$^{chaos3/chaos3}$*;Fancc*$^{-/-}$, respectively.

Supplementary Figure S3

(A) Representative images of FANCI foci co-localizing with EdU spots are shown. Wild-type cells in the untreated (UNT) or APH-treated (150nM, 24 hrs) conditions were co-stained for EdU (green) and FANCI (red). (B) Shown at left are representative images of FANCD2 foci co-localizing with EdU spots. Wild-type and *Mcm4*$^{chaos3/chaos3}$ cells were co-stained for EdU (green) and FANCD2 (red) following treatment with APH (150nM, 24 hrs). At top, middle are the average percentages of prophase cells positive for EdU spots (white bars) or EdU-FANCD2 co-localization events (grey bars). At bottom, middle are the number of EdU spots per prophase cell as well as the number of EdU-FANCD2 co-localization events per prophase cell. While the number of EdU spots and EdU-FANCD2 co-localizations were drastically increased in both genotypes after APH treatment, *Mcm4*$^{chaos3/chaos3}$ cells still showed a more severe phenotype. Shown at top, right are the numbers of EdU spots with "EdU only" (white bars) as well as the number of EdU-FANCD2 co-localization events (grey bars) observed in 150 prophase cells. At bottom, right are the numbers of FANCD2 foci with "FANCD2 only" (black bars) as well as the number of EdU-FANCD2 co-localizations (shown again as grey bars)

observed in 150 prophase cells. These data were consistent with results obtained in the untreated conditions. Error bars show the binomial error for the combined data sets obtained from three independent experiments. Significance was determined by χ^2-test. Asterisks denote: ***p<0.001. All nuclei were stained with DAPI (blue). Scale bars are 10 µm. WT and C3 refer to wild-type and *Mcm4*$^{chaos3/chaos3}$, respectively.

Supplementary Figure S4

Shown are representative images of a T-cell lymphoma from a *Mcm4*$^{chaos3/chaos3}$*;Fancc*$^{-/-}$ mouse in an inbred C57BL/6JR background, including hematoxylin and eosin (H&E) stains (left) and immunohistochemistry using the T-cell marker CD-3 (middle) and the B cell marker B220 (right). The images were taken from slightly different areas of the same liver. The scale bar is 200 µm. WT and C3 refer to wild-type and *Mcm4*$^{chaos3/chaos3}$, respectively.

Supplementary Figure S5

(A) *Mcm4*$^{chaos3/chaos3}$*;Fancc*$^{-/-}$ mice display a reduced average testes size in a C57BL/6J x C3HeB/FeJ mixed genetic background. Shown are the average percentages of total testes weight relative to total body weight. Samples were taken from mice euthanized at 6 weeks of age. Error bars show the SEMs for at least 5 mice per genotype. Significance was determined by t-test. Asterisks denote: *p<0.05, **p<0.01. (B) Histological

analysis by hematoxylin and eosin (H&E) staining shows a mosaic pattern of normal and empty seminiferous tubules in *Fancc*$^{-/-}$ and *Mcm4*$^{chaos3/chaos3}$*;Fancc*$^{-/-}$ mice, with *Mcm4*$^{chaos3/chaos3}$*;Fancc*$^{-/-}$ mice having the most severe phenotype. Scale bars are 1500 μm for the whole testis sections (top) and 75 μm for the enlarged images (bottom). WT, C3, FAC and C3;FAC refer to wild-type, *Mcm4*$^{chaos3/chaos3}$, *Fancc*$^{-/-}$ and *Mcm4*$^{chaos3/chaos3}$*;Fancc*$^{-/-}$, respectively.

Supplementary Figure S6

The number of MN, 53BP1-NBs and UFBs are also increased in *Mcm4*$^{chaos3/chaos3}$*;Fancc*$^{-/-}$ cells derived from a C57BL/6J x C3HeB/FeJ mixed genetic background. (A) Shown are the average percentages of binucleated cells positive for MN (left) and distributions indicating the number of MN per binucleated cell (right). (B) Shown are the average percentages of individual G1 nuclei from binucleated cells positive for 53BP1-NBs (left) and distributions indicating the number of 53BP1-NBs per binucleated cell nucleus (right). (C) Only *Mcm4*$^{chaos3/chaos3}$*;Fancc*$^{-/-}$ cells display a significantly increased number of PICH-coated UFBs. Shown at left are representative images of an anaphase cell positive for a PICH-coated UFB. PICH staining is in red, and chromosomes are stained with DAPI (blue). At middle are the average percentages of anaphases positive for UFBs. At right are the distributions for the number of UFBs per anaphase cell. All error bars show the binomial error for the combined data sets obtained from at least three independent experiments. Significance was determined by χ^2-test. Asterisks denote:

*p<0.05 and ***p<0.001. WT, C3, FAC and C3;FAC refer to wild-type, *Mcm4*$^{chaos3/chaos3}$, *Fancc*$^{-/-}$ and *Mcm4*$^{chaos3/chaos3}$;*Fancc*$^{-/-}$, respectively.

Supplementary Figure S7

Shown at top are representative images of lymphosarcomas from *Mcm4*$^{chaos3/chaos3}$;*Fancc*$^{-/-}$ mice, including H&E stains (left) and immunohistochemistry using the T cell marker CD-3 (middle) and the B cell marker B220 (right). The lymphosarcoma of mouse #58 is of T cell origin, while that of mouse #57 is of B cell origin. At bottom are representative images of a presumed myeloid leukemia from a *Mcm4*$^{chaos3/chaos3}$;*Fancc*$^{-/-}$ mouse (#40), including an H&E stain (left) and immunohistochemistry using the pan-macrophage marker F4/80 (middle) and the myeloid precursor marker MPO (right). Scale bars are 100 μm. C3;FAC refers to *Mcm4*$^{chaos3/chaos3}$;*Fancc*$^{-/-}$.

Fancc$^{+/-}$ x *Fancc*$^{+/-}$

Genotype	Expected	Observed
Fancc$^{+/+}$ or *Fancc*$^{+/-}$	105	112
Fancc$^{-/-}$	35	28
Total	140	140

X^2-test: p = 0.17186

Mcm4$^{chaos3/chaos3}$;*Fancc*$^{+/-}$ x *Mcm4*$^{chaos3/chaos3}$;*Fancc*$^{+/-}$

Genotype		Expected	Observed
Mcm4$^{chaos3/chaos3}$;*Fancc*$^{+/+}$ *Mcm4*$^{chaos3/chaos3}$;*Fancc*$^{+/-}$	or	73.5	81
Mcm4$^{chaos3/chaos3}$;*Fancc*$^{-/-}$		24.5	17
Total		98	98

X^2-test: p = 0.08018

Mouse #	Sex	Age (Days)	Location	Diagnosis	Immunohistochemistry
33	F	269	LN, liver, lung, spleen	Lymphosarcoma	CD3+
25	M	314	Abdomen	Myeloid or histiocytic sarcoma	CD3-; B220-; MPO-; F4/80-
32	F	318	Long bone of hind leg, ribcage	Osteosarcoma	N.D.
62810	F	352	Spleen, pancreas, liver, lung, fat pad	Lymphosarcoma	CD3-; B220-
31	F	354	LN, liver, lung, spleen	Lymphosarcoma	N.D.
26	M	373	Behind front leg	Schwannoma	N.D.
34	F	389	Abdominal fat pads, pancreas	Histiocytic sarcoma	Mac-2+; F4/80+
27	M	408	LN, thymus	Hematopoietic neoplasia	Mac-2+; F4/80-
29	M	416	Abdomen	Histiocytic sarcoma	Mac-2+; F4/80+
328	M	425	LN, pancreas	Histiocytic sarcoma	N.D.
28	M	425	N.T.F.		
56	M	425	N.T.F.		
36	F	425	N.T.F.		
37	F	425	N.T.F.		

Mouse #	Sex	Age (Days)	Location	Diagnosis	Immunohistochemistry
12910	F	109	LN, liver, lung, spleen, kidneys, thymus	Lymphosarcoma	CD3+; B220-
58	F	110	LN, liver, lung, spleen	Lymphosarcoma	CD3+
41	F	117	LN, liver, lung, spleen	Lymphosarcoma	CD3+
57	F	142	LN, liver, lung, spleen	Lymphosarcoma	B220+
44	F	197	LN, liver, lung, spleen, kidneys, thymus	Lymphosarcoma	CD3+;B220-
49	F	234	LN, liver, lung, spleen, kidneys	Lymphosarcoma	CD3-; B220-
51	F	259	Within front leg	Myeloid or histiocytic sarcoma	CD3-; B220-; MPO-; F4/80-
47	F	263	LN, liver, lung, spleen	Myelomonocytic neoplasia	MPO+; F4/80+
42	F	280	LN, liver, lung, spleen, pancreas, thymus	Lymphosarcoma; myeloid leukemia	B220+
235	M	288	Back	Schwannoma	N.D.
48	F	351	LN, liver, lung, spleen	Hematopoietic	CD3+; B220+
40	F	421	LN, liver, uterus, pancreas, spleen	Myeloid leukemia	MPO+
30	M	425	Small mass adjacent to testis	Histiocytic sarcoma	Mac-2+; F4/80+
46	F	425	LN	Lymphosarcoma	N.D.
50	F	425	Abdomen, liver, spleen	Histiocytic sarcoma	Mac-2+; F4/80+
55	M	425	LN, spleen	Lymphosarcoma	CD3+; B220+
43	M	425	N.T.F.		
52	M	425	N.T.F.		
45	F	425	N.T.F.		

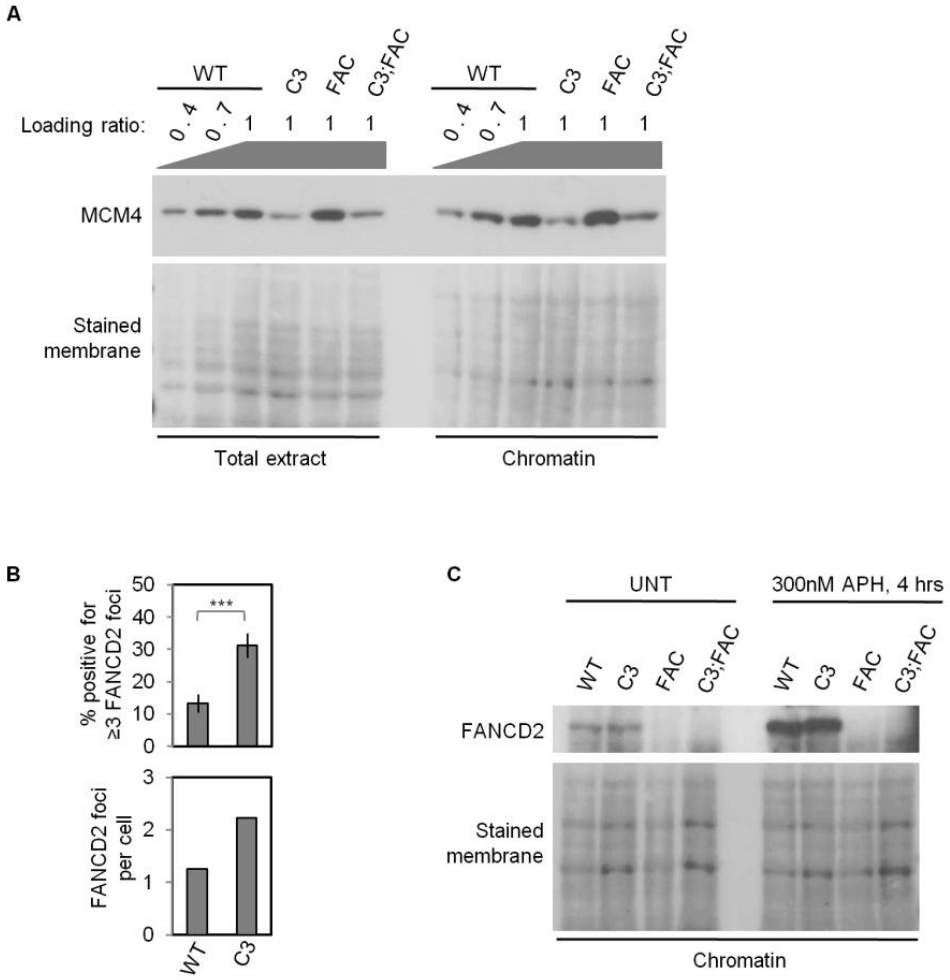
A
WT
C3
FAC
C3;FAC
WT
C3
FAC
C3;FAC
Loading ratio:
0.4
0.7
1
1
1
1
0.4
0.7
1
1
1
1
MCM4
Stained membrane
Total extract
Chromatin
B
% positive for ≥3 FANCD2 foci
50
40
30
20
10
0
***
FANCD2 foci per cell
3
2
1
0
WT
C3
C
UNT
300nM APH, 4 hrs
WT
C3
FAC
C3;FAC
WT
C3
FAC
C3;FAC
FANCD2
Stained membrane
Chromatin

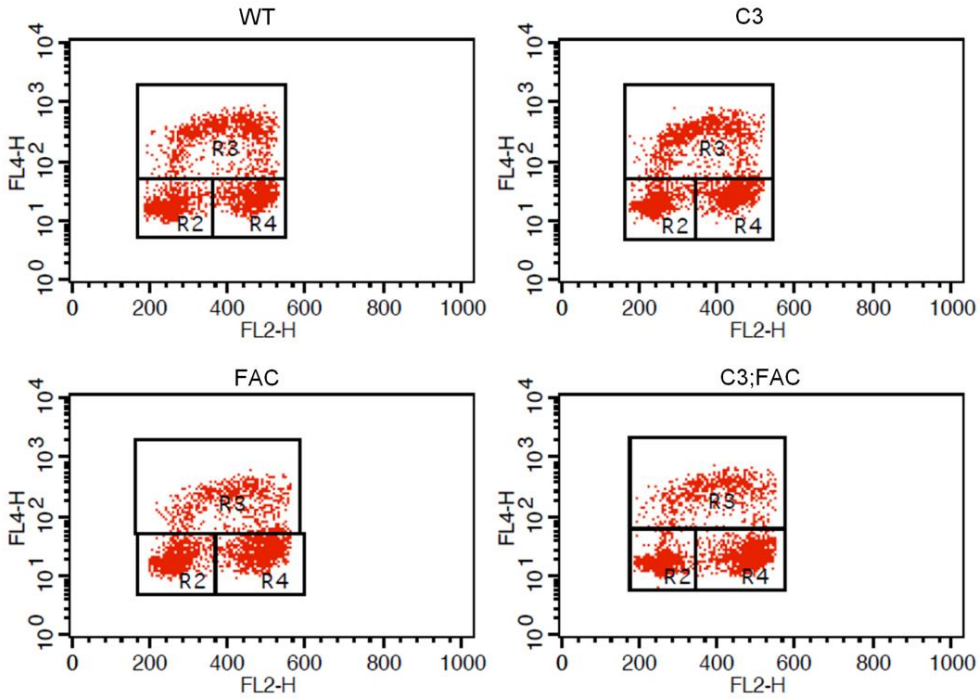
WT
C3
FAC
C3;FAC
FL4-H
FL2-H
R2
R3
R4
0
200
400
600
800
1000
10^0
10^1
10^2
10^3
10^4

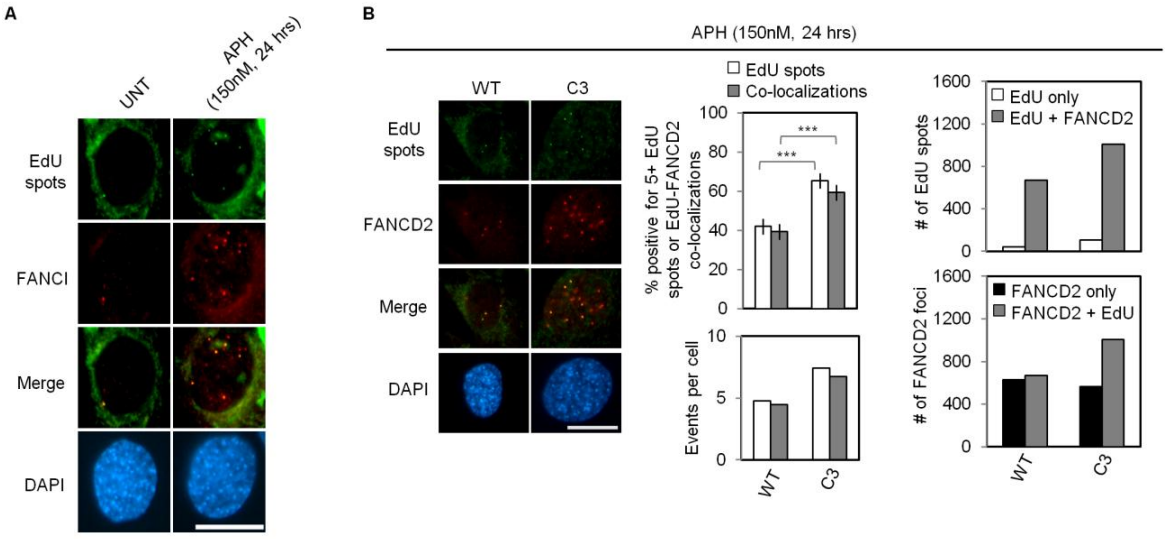
A
UNT
APH (150nM, 24 hrs)
EdU spots
FANCI
Merge
DAPI
B
APH (150nM, 24 hrs)
WT
C3
EdU spots
FANCD2
Merge
DAPI
EdU spots
Co-localizations
% positive for 5+ EdU spots or EdU-FANCD2 co-localizations
***
***
Events per cell
WT
C3
# of EdU spots
EdU only
EdU + FANCD2
# of FANCD2 foci
FANCD2 only
FANCD2 + EdU

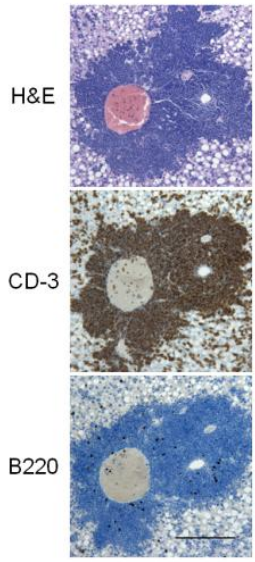
H&E
CD-3
B220

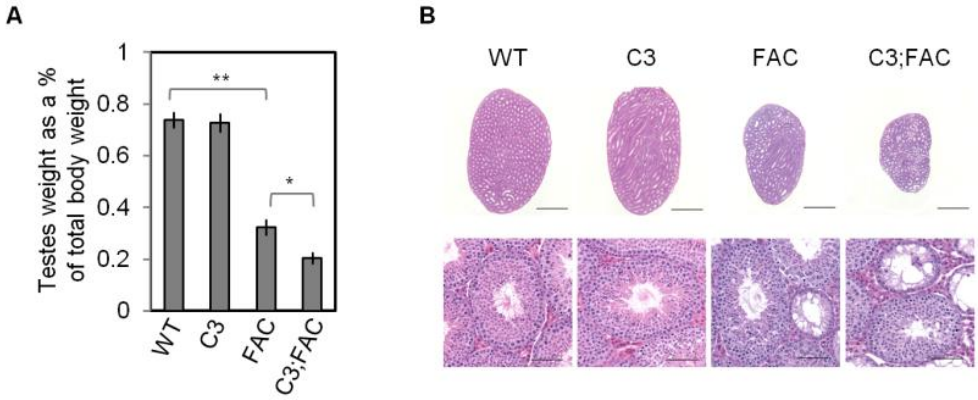
A
Testes weight as a % of total body weight
1
0.8
0.6
0.4
0.2
0
**
*
WT
C3
FAC
C3;FAC
B
WT
C3
FAC
C3;FAC

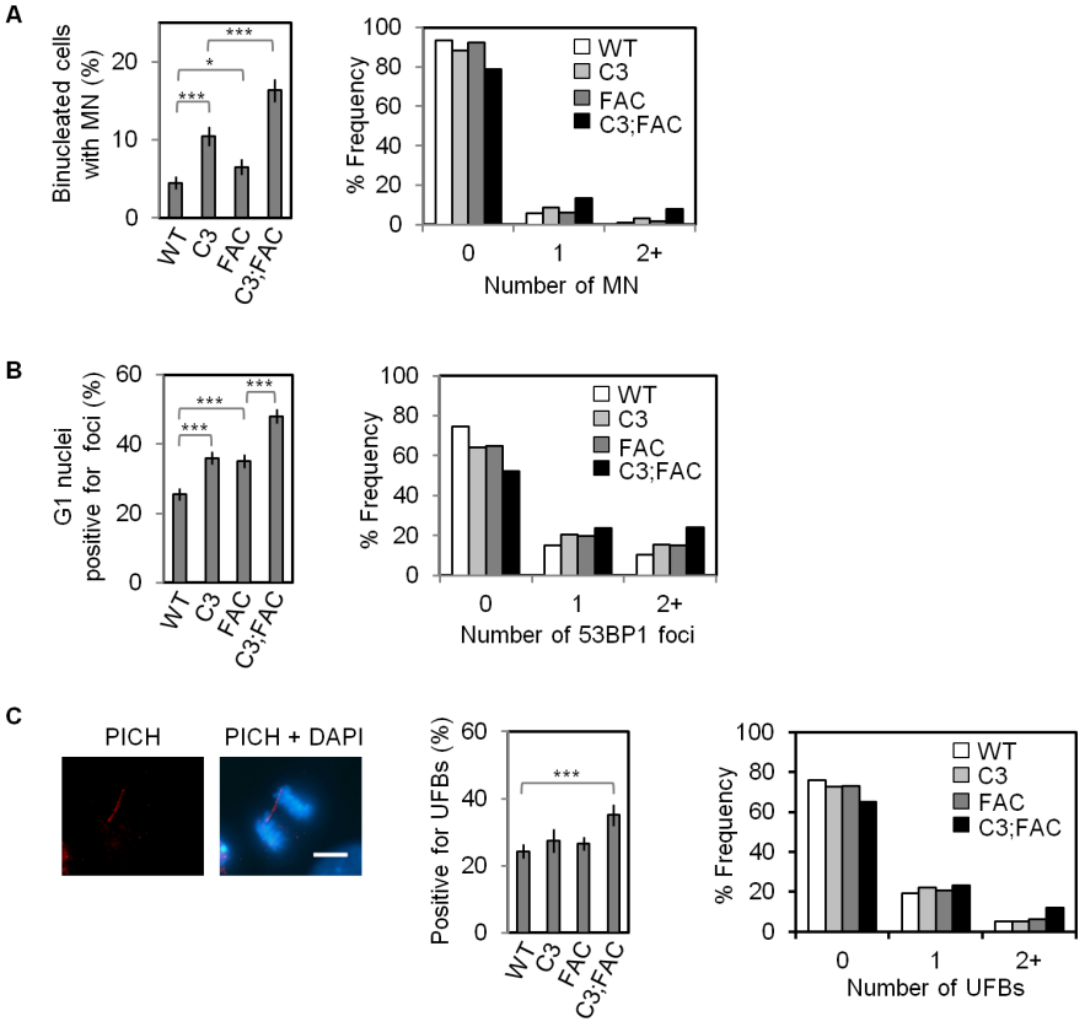
A
Binucleated cells with MN (%)
0
10
20
***
*
***
WT
C3
FAC
C3;FAC
% Frequency
0
20
40
60
80
100
WT
C3
FAC
C3;FAC
0
1
2+
Number of MN
B
G1 nuclei positive for foci (%)
0
20
40
60
***
***
***
WT
C3
FAC
C3;FAC
% Frequency
0
20
40
60
80
100
WT
C3
FAC
C3;FAC
0
1
2+
Number of 53BP1 foci
C
PICH
PICH + DAPI
Positive for UFBs (%)
0
20
40
60
***
WT
C3
FAC
C3;FAC
% Frequency
0
20
40
60
80
100
WT
C3
FAC
C3;FAC
0
1
2+
Number of UFBs

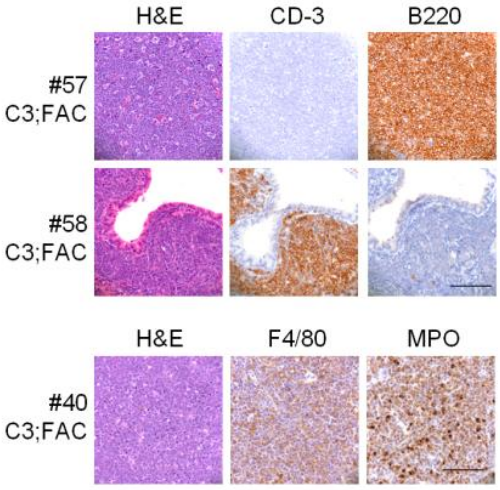
H&E
CD-3
B220
#57
C3;FAC
#58
C3;FAC
H&E
F4/80
MPO
#40
C3;FAC

References

1 Yekezare, M., Gómez-González, B. & Diffley, J. F. X. Controlling DNA replication origins in response to DNA damage – inhibit globally, activate locally. *Journal of Cell Science* **126**, 1297-1306 (2013).

2 Blow, J. J. & Dutta, A. Preventing re-replication of chromosomal DNA. *Nat Rev Mol Cell Biol* **6**, 476-486 (2005).

3 Sclafani, R. A. & Holzen, T. M. Cell Cycle Regulation of DNA Replication. *Annual Review of Genetics* **41**, 237-280 (2007).

4 Labib, K., Tercero, J. A. & Diffley, J. F. X. Uninterrupted MCM2-7 Function Required for DNA Replication Fork Progression. *Science* **288**, 1643-1647 (2000).

5 Pacek, M. & Walter, J. C. A requirement for MCM7 and Cdc45 in chromosome unwinding during eukaryotic DNA replication. *EMBO J* **23**, 3667-3676 (2004).

6 Shechter, D., Ying, C. Y. & Gautier, J. DNA Unwinding Is an MCM Complex-dependent and ATP Hydrolysis-dependent Process. *Journal of Biological Chemistry* **279**, 45586-45593 (2004).

7 Moyer, S. E., Lewis, P. W. & Botchan, M. R. Isolation of the Cdc45/Mcm2–7/GINS (CMG) complex, a candidate for the eukaryotic DNA replication fork helicase. *Proceedings of the National Academy of Sciences* **103**, 10236-10241 (2006).

8 Ilves, I., Petojevic, T., Pesavento, J. J. & Botchan, M. R. Activation of the MCM2-7 Helicase by Association with Cdc45 and GINS Proteins. *Molecular Cell* **37**, 247-258 (2010).

9 Burkhart, R. *et al.* Interactions of Human Nuclear Proteins P1Mcm3 and P1Cdc46. *European Journal of Biochemistry* **228**, 431-438 (1995).

10 Rowles, A. *et al.* Interaction between the Origin Recognition Complex and the Replication Licensing Systemin Xenopus. *Cell* **87**, 287-296 (1996).

11 Mahbubani, H. M., Chong, J. P. J., Chevalier, S., Thömmes, P. & Blow, J. J. Cell Cycle Regulation of the Replication Licensing System: Involvement of a Cdk-dependent Inhibitor. *The Journal of Cell Biology* **136**, 125-135 (1997).

12 Edwards, M. C. *et al.* MCM2–7 Complexes Bind Chromatin in a Distributed Pattern Surrounding the Origin Recognition Complex in Xenopus Egg Extracts. *Journal of Biological Chemistry* **277**, 33049-33057 (2002).

13 Woodward, A. M. *et al.* Excess Mcm2–7 license dormant origins of replication that can be used under conditions of replicative stress. *The Journal of Cell Biology* **173**, 673-683 (2006).

14 Ge, X. Q., Jackson, D. A. & Blow, J. J. Dormant origins licensed by excess Mcm2–7 are required for human cells to survive replicative stress. *Genes & Development* **21**, 3331-3341 (2007).

15 Ibarra, A., Schwob, E. & Méndez, J. Excess MCM proteins protect human cells from replicative stress by licensing backup origins of replication. *Proceedings of the National Academy of Sciences* **105**, 8956-8961 (2008).

16 Kawabata, T. *et al.* Stalled Fork Rescue via Dormant Replication Origins in Unchallenged S Phase Promotes Proper Chromosome Segregation and Tumor Suppression. *Molecular Cell* **41**, 543-553 (2011).
17 Shima, N. *et al.* A viable allele of Mcm4 causes chromosome instability and mammary adenocarcinomas in mice. *Nat Genet* **39**, 93-98 (2007).
18 Blow, J. J., Ge, X. Q. & Jackson, D. A. How dormant origins promote complete genome replication. *Trends in Biochemical Sciences* **36**, 405-414 (2011).
19 Crossan, G. P. & Patel, K. J. The Fanconi anaemia pathway orchestrates incisions at sites of crosslinked DNA. *The Journal of Pathology* **226**, 326-337 (2012).
20 Kottemann, M. C. & Smogorzewska, A. Fanconi anaemia and the repair of Watson and Crick DNA crosslinks. *Nature* **493**, 356-363 (2013).
21 Kashiyama, K. *et al.* Malfunction of Nuclease ERCC1-XPF Results in Diverse Clinical Manifestations and Causes Cockayne Syndrome, Xeroderma Pigmentosum, and Fanconi Anemia. *The American Journal of Human Genetics* **92**, 807-819 (2013).
22 Bogliolo, M. *et al.* Mutations in ERCC4, Encoding the DNA-Repair Endonuclease XPF, Cause Fanconi Anemia. *The American Journal of Human Genetics* **92**, 800-806 (2013).
23 Constantinou, A. Rescue of replication failure by Fanconi anaemia proteins. *Chromosoma* **121**, 21-36 (2012).
24 Kee, Y. & D'Andrea, A. D. Expanded roles of the Fanconi anemia pathway in preserving genomic stability. *Genes & Development* **24**, 1680-1694 (2010).
25 Langevin, F., Crossan, G. P., Rosado, I. V., Arends, M. J. & Patel, K. J. Fancd2 counteracts the toxic effects of naturally produced aldehydes in mice. *Nature* **475**, 53-58 (2011).
26 Garcia-Higuera, I. *et al.* Interaction of the Fanconi Anemia Proteins and BRCA1 in a Common Pathway. *Molecular Cell* **7**, 249-262 (2001).
27 Sims, A. E. *et al.* FANCI is a second monoubiquitinated member of the Fanconi anemia pathway. *Nat Struct Mol Biol* **14**, 564-567 (2007).
28 Smogorzewska, A. *et al.* Identification of the FANCI Protein, a Monoubiquitinated FANCD2 Paralog Required for DNA Repair. *Cell* **129**, 289-301 (2007).
29 Taniguchi, T. *et al.* S-phase–specific interaction of the Fanconi anemia protein, FANCD2, with BRCA1 and RAD51. *Blood* **100**, 2414-2420 (2002).
30 Sobeck, A. *et al.* Fanconi Anemia Proteins Are Required To Prevent Accumulation of Replication-Associated DNA Double-Strand Breaks. *Molecular and Cellular Biology* **26**, 425-437 (2006).
31 Ikegami, S., Taguchi, T., Ohashi, M., Nagano, H. & Mano, Y. Aphidicolin prevents mitotic cell division by interfering with the activity of DNA polymerase-alpha. *Nature* **275**, 458-460 (1978).
32 Howlett, N. G., Taniguchi, T., Durkin, S. G., D'Andrea, A. D. & Glover, T. W. The Fanconi anemia pathway is required for the DNA replication stress response

and for the regulation of common fragile site stability. *Human Molecular Genetics* **14**, 693-701 (2005).

33 Chan, K. L., Palmai-Pallag, T., Ying, S. & Hickson, I. D. Replication stress induces sister-chromatid bridging at fragile site loci in mitosis. *Nat Cell Biol* **11**, 753-760 (2009).

34 Naim, V. & Rosselli, F. The FANC pathway and BLM collaborate during mitosis to prevent micro-nucleation and chromosome abnormalities. *Nat Cell Biol* **11**, 761-768 (2009).

35 Durkin, S. G. & Glover, T. W. Chromosome Fragile Sites. *Annual Review of Genetics* **41**, 169-192 (2007).

36 Letessier, A. *et al.* Cell-type-specific replication initiation programs set fragility of the FRA3B fragile site. *Nature* **470**, 120-123 (2011).

37 Ozeri-Galai, E. *et al.* Failure of Origin Activation in Response to Fork Stalling Leads to Chromosomal Instability at Fragile Sites. *Molecular Cell* **43**, 122-131 (2011).

38 Whitney, M. *et al.* Germ cell defects and hematopoietic hypersensitivity to gamma- interferon in mice with a targeted disruption of the Fanconi anemia C gene. *Blood* **88**, 49-58 (1996).

39 Kawabata, T. *et al.* A reduction of licensed origins reveals strain-specific replication dynamics in mice. *Mammalian Genome* **22**, 506-517 (2011).

40 Luebben, S. W. *et al.* Helq acts in parallel to Fancc to suppress replication-associated genome instability. *Nucleic Acids Research* (2013).

41 Lukas, C. *et al.* 53BP1 nuclear bodies form around DNA lesions generated by mitotic transmission of chromosomes under replication stress. *Nat Cell Biol* **13**, 243-253 (2011).

42 Harrigan, J. A. *et al.* Replication stress induces 53BP1-containing OPT domains in G1 cells. *The Journal of Cell Biology* **193**, 97-108 (2011).

43 Baumann, C., Körner, R., Hofmann, K. & Nigg, E. A. PICH, a Centromere-Associated SNF2 Family ATPase, Is Regulated by Plk1 and Required for the Spindle Checkpoint. *Cell* **128**, 101-114 (2007).

44 Carreau, M. Not-so-novel phenotypes in the Fanconi anemia group D2 mouse model. *Blood* **103**, 2430 (2004).

45 Wang, L. C., Stone, S., Hoatlin, M. E. & Gautier, J. Fanconi anemia proteins stabilize replication forks. *DNA Repair* **7**, 1973-1981 (2008).

46 Schlacher, K., Wu, H. & Jasin, M. A Distinct Replication Fork Protection Pathway Connects Fanconi Anemia Tumor Suppressors to RAD51-BRCA1/2. *Cancer Cell* **22**, 106-116 (2012).

47 Chaudhury, I., Sareen, A., Raghunandan, M. & Sobeck, A. FANCD2 regulates BLM complex functions independently of FANCI to promote replication fork recovery. *Nucleic Acids Research* **41**, 6444-6459 (2013).

48 Zou, L. & Elledge, S. J. Sensing DNA Damage Through ATRIP Recognition of RPA-ssDNA Complexes. *Science* **300**, 1542-1548 (2003).

49 Byun, T. S., Pacek, M., Yee, M.-c., Walter, J. C. & Cimprich, K. A. Functional uncoupling of MCM helicase and DNA polymerase activities activates the ATR-dependent checkpoint. *Genes & Development* **19**, 1040-1052 (2005).

50 Rogakou, E. P., Pilch, D. R., Orr, A. H., Ivanova, V. S. & Bonner, W. M. DNA Double-stranded Breaks Induce Histone H2AX Phosphorylation on Serine 139. *Journal of Biological Chemistry* **273**, 5858-5868 (1998).

51 Chuang, C.-H., Wallace, M. D., Abratte, C., Southard, T. & Schimenti, J. C. Incremental Genetic Perturbations to MCM2-7 Expression and Subcellular Distribution Reveal Exquisite Sensitivity of Mice to DNA Replication Stress. *PLoS Genet* **6**, e1001110 (2010).

52 Bergoglio, V. *et al.* DNA synthesis by Pol η promotes fragile site stability by preventing under-replicated DNA in mitosis. *The Journal of Cell Biology* **201**, 395-408 (2013).

53 Naim, V., Wilhelm, T., Debatisse, M. & Rosselli, F. ERCC1 and MUS81–EME1 promote sister chromatid separation by processing late replication intermediates at common fragile sites during mitosis. *Nat Cell Biol* **15**, 1008-1015 (2013).

54 Casper, A. M., Nghiem, P., Arlt, M. F. & Glover, T. W. ATR Regulates Fragile Site Stability. *Cell* **111**, 779-789 (2002).

55 Fenech, M. Cytokinesis-block micronucleus cytome assay. *Nat. Protocols* **2**, 1084-1104 (2007).

56 Freie, B. *et al.* Fanconi anemia type C and p53 cooperate in apoptosis and tumorigenesis. *Blood* **102**, 4146-4152 (2003).

57 Wallace, M. D., Southard, T. L., Schimenti, K. J. & Schimenti, J. C. Role of DNA damage response pathways in preventing carcinogenesis caused by intrinsic replication stress. *Oncogene* (2013).

58 Niedzwiedz, W. *et al.* The Fanconi Anaemia Gene FANCC Promotes Homologous Recombination and Error-Prone DNA Repair. *Molecular Cell* **15**, 607-620 (2004).

59 Mirchandani, K. D., McCaffrey, R. M. & D'Andrea, A. D. The Fanconi anemia core complex is required for efficient point mutagenesis and Rev1 foci assembly. *DNA Repair* **7**, 902-911 (2008).

60 Kim, H., Yang, K., Dejsuphong, D. & D'Andrea, A. D. Regulation of Rev1 by the Fanconi anemia core complex. *Nat Struct Mol Biol* **19**, 164-170 (2012).

61 Lossaint, G. *et al.* FANCD2 Binds MCM Proteins and Controls Replisome Function upon Activation of S Phase Checkpoint Signaling. *Molecular Cell* **51**, 678-690 (2013).

62 Ying, S. *et al.* MUS81 promotes common fragile site expression. *Nat Cell Biol* **15**, 1001-1007 (2013).

63 Parmar, K., D'Andrea, A. & Niedernhofer, L. J. Mouse models of Fanconi anemia. *Mutation Research/Fundamental and Molecular Mechanisms of Mutagenesis* **668**, 133-140 (2009).

64 Tischkowitz, M. & Winqvist, R. Using mouse models to investigate the biological and physiological consequences of defects in the Fanconi anaemia/breast cancer DNA repair signalling pathway. *The Journal of Pathology* **224**, 301-305 (2011).

65 Hughes, C. R. *et al.* MCM4 mutation causes adrenal failure, short stature, and natural killer cell deficiency in humans. *The Journal of Clinical Investigation* **122**, 814-820 (2012).

66 Gineau, L. *et al.* Partial MCM4 deficiency in patients with growth retardation, adrenal insufficiency, and natural killer cell deficiency. *The Journal of Clinical Investigation* **122**, 821-832 (2012).

67 Hendzel, M. J. *et al.* Mitosis-specific phosphorylation of histone H3 initiates primarily within pericentromeric heterochromatin during G2 and spreads in an ordered fashion coincident with mitotic chromosome condensation. *Chromosoma* **106**, 348-360 (1997).

CHAPTER IV: *Helq* Acts in Parallel to *Fancc* to Suppress Replication-associated Genome Instability

My contributions to this chapter

Figures 1-6

Table 1

Figures S2-7

This chapter is a replicate of a publication in *Nucleic Acids Research* (2013). Spencer W. Luebben, Tsuyoshi Kawabata, Monica K. Akre, Wai Long Lee, Charles S. Johnson, M. Gerard O'Sullivan and Naoko Shima.

Summary

HELQ is a superfamily 2 DNA helicase found in archaea and metazoans. It has been implicated in processing stalled replication forks and in repairing DNA double-strand breaks and inter-strand crosslinks. Though previous studies have suggested the possibility that HELQ is involved in the Fanconi anemia (FA) pathway, a dominant mechanism for inter-strand crosslink repair in vertebrates, this connection remains elusive. Here, we investigated this question in mice using the *Helq*^{gt} and *Fancc*$^{-}$ strains. Compared with *Fancc*$^{-/-}$ mice lacking FANCC, a component of the FA core complex, *Helq*$^{gt/gt}$ mice exhibited a mild of form of FA-like phenotypes including hypogonadism and cellular sensitivity to the crosslinker mitomycin C. However, unlike *Fancc*$^{-/-}$ primary fibroblasts, *Helq*$^{gt/gt}$ cells had intact FANCD2 mono-ubiquitination and focus formation. Notably, for all traits examined, *Helq* was non-epistatic with *Fancc*, as *Helq*$^{gt/gt}$*;Fancc*$^{-/-}$ double mutants displayed significantly worsened phenotypes than either single mutant. Importantly, this was most noticeable for the suppression of spontaneous chromosome instability such as micronuclei and 53BP1 nuclear bodies, known consequences of persistently stalled replication forks. These findings suggest that mammalian HELQ contributes to genome stability in unchallenged conditions through a mechanism distinct from the function of FANCC.

Introduction

Maintaining genome stability is critical for cells, given that the genome is under constant attack by numerous exogenous and endogenous agents[1]. It is inevitable that cells will have to proceed with genome duplication using damaged template DNA, which can perturb the normal progression of replication forks. To cope with this problem, organisms have developed multiple mechanisms to allow the rescue of stalled replication forks[2]. Such mechanisms include firing of dormant origins, translesion synthesis with error-prone DNA polymerases and homology-directed fork recovery[3-5]. Evidence suggests that the latter two mechanisms are in part coordinated by the concerted work of proteins that are mutated in Fanconi anemia (FA)[6], a rare polygenic human genetic disorder[7]. FA patients exhibit genome instability, congenital abnormalities, bone marrow failure, hypogonadism and a heightened predisposition to cancer[7,8]. FA is uniquely characterized by its cellular hypersensitivity to agents that induce DNA inter-strand crosslinks (ICLs)[7,9], although it is unclear how ICL repair is functionally linked with stalled fork recovery in unchallenged conditions.

The DNA helicase HELQ was first discovered in the human and mouse genomes through its homology to MUS308[10], a DNA repair enzyme required for ICL resistance in *Drosophila melanogaster*[11,12]. Although it is unlikely that its vertebrate ortholog POLQ plays a major role in ICL repair[13-15], together they make up a unique family of DNA polymerases that possess a helicase domain in the N-terminus in addition to a C-terminal polymerase domain[16-18]. Unlike its paralog POLQ, HELQ lacks a polymerase domain,

and several lines of evidence indicate that HELQ performs a distinct function from POLQ. *HELQ* is an ortholog of the Drosophila *mus301* gene[19], which is allelic to the female-sterile mutation *spindle-C* (*spn-C*)[20]. Mutations in *spn-C* result in the failed repair of meiotic double-strand breaks (DSB) and activation of the meiotic checkpoint[20], which was not observed in *mus308* mutants. In line with this observation, it was also reported that the *Caenorhabditis elegans* ortholog *helq-1* plays a role in meiotic DSB repair by promoting postsynaptic RAD-51 filament disassembly[21]. These findings suggest that HELQ has a role in meiotic DSB repair through homologous recombination (HR) in these species. In humans, *HELQ* is expressed in the testes, ovaries, heart and skeletal muscle[22]. However, its function is largely unknown.

Biochemically, human HELQ exhibits ATP-dependent 3'-5' DNA helicase activity *in vitro*[10,23]. A recent study demonstrated that human HELQ preferentially unwinds the parental strands of forked structures with a nascent lagging strand, and that this activity is stimulated by replication protein A (RPA)[23]. These findings suggest that HELQ is likely to participate in the recovery of stalled or collapsed replication forks. Several studies have suggested that this role of HELQ is closely linked with the FA pathway. A genetic study in *C. elegans* demonstrated that *helq-1* is required for ICL repair and is epistatic to *fcd-2*[24], an ortholog of *FANCD2* whose product is mono-ubiquitinated by the FA core complex as a key step in this pathway[25]. However, *C. elegans* contains only a few FA proteins and lacks multiple members comprising the FA core complex[26]. HELQ may belong to a primitive FA pathway in *C. elegans*, but its

evolution seems to have taken a complex path. Paradoxically, disruption of *Helq* in chicken DT40 cells, which contain all of the FA proteins, did not confer hypersensitivity to ICL inducing agents[14]. In human cells, HELQ depletion confers hypersensitivity to the crosslinker mitomycin C (MMC) and HR deficiency, the latter reported to be epistatic to FANCD2[27]. Consistent with this observation, exogenously expressed GFP-tagged HELQ co-localizes with RAD51 foci as well as FANCD2 foci after treatment with the topoisomerase I inhibitor camptothecin (CPT)[23]. There is little information about the link between HELQ and the FA pathway in mammals, particularly in the absence of exogenous DNA damage.

To decipher the enigmatic connection between HELQ and the FA pathway, we have generated *Helq* deficient mice using a gene-trap allele named *Helq*^{gt} for phenotypic comparisons to mice deficient for *Fancc*, encoding FANCC, a component of the FA core complex[28] in the same genetic background. For all traits examined including hypogonadism and MMC sensitivity, we found that loss of *Helq* results in phenotypes considerably milder than *Fancc* deficiency. Moreover, our data show that combined loss of *Helq* and *Fancc* leads to further severe phenotypes than single mutants, presenting no evidence for epistasis. Importantly, the strongest inter-dependence for *Helq* and *Fancc* was observed for the suppression of spontaneous genome instability derived from replication fork failures rather than MMC resistance. These findings collectively suggest that HELQ contributes to genome stability in unperturbed conditions in a manner that is distinct from the function of FANCC.

Materials and methods

Mouse strains and MEFs

All experiments were performed using mice from a C57BL/6J background and were approved by the Institutional Animal Care and Use Committee (IACUC). MEFs were generated from 12.5-14.5 dpc embryos and cultured using standard procedures as described previously[29]. All mice were genotyped by PCR. The primers used are available upon request.

Quantitative RT-PCR

RNA was isolated from either cultured MEFs or testes tissue using the PureLink RNA Mini Kit (Ambion, Life Technologies) and the RNeasy Kit (QIAGEN). cDNA was then synthesized using the Superscript VILO cDNA Synthesis Kit (Invitrogen, Life Technologies). q-PCR analysis was performed on the LightCycler 480 (Roche) using primer pairs specific for exons 1-2, exons 11-12 and the chimeric mutant transcript spanning between exon 11 and the inserted vector. Expression was normalized to glyceraldehydes 3-phosphate dehydrogenase (GAPDH).

Western Blotting and Immunofluorescence Microscopy

Western blotting and immunofluorescence staining were carried out using standard procedures as described previously[29].

Antibodies

For immunofluorescence and western blotting procedures, we used anti-phospho-histone H3, anti-RPA32, anti-γH2AX, anti-CENP-A, anti-phospho-CHK1 (Cell Signaling; #9706, #2208, #2577, #2048, #2341, respectively), anti-FANCD2 for foci staining, anti-FANCI, anti-53BP1, anti-MCM4 (Abcam; ab2187 or ab108928, ab74332, ab36823, ab4459, respectively), anti-FANCA (Bethyl Laboratories; #A301-980A), anti-CHK1 (Santa Cruz; sc-8408), anti-FANCD2 for western blots (Epitomics; #2986-1) and anti-HELQ (MyBioSource; #MBS120320). For the DNA Fiber assay, anti-digoxigenin antibody conjugated with rhodamine from Roche (11207750910) and the streptavidin-AlexaFluor488 from Invitrogen (S-32354) were used.

siRNA transfection in MEFs, HEK 293T and PD331 cells

One million cells were seeded per well in a six-well dish followed by transfection with either 50nM (MEFs) or 25 nM (HEK 293T, PD331) of non-targeted control small interfering RNA (siRNA) (#D-001206-13-20, siGENOME Smart pool), HELQ siRNA (#M-015379-01-0005, siGENOME Smart pool) or FANCA siRNA (#M-019283-02-

0005, siGENOME Smart pool) from Dharmacon. This was performed using OPTI-MEM and Lipofectamine RNAiMAX (Life technologies) transfection reagents. Twenty-four hours later, a second round of transfection was performed using the same concentration of siRNA, followed by 24 h culture. Cells were then re-plated according to the analysis performed. The PD331 cell lines were obtained from the Oregon Health & Science University Fanconi Anemia Cell Repository (Portland, Oregon).

Metaphase Analysis

MEFs were treated with 600 nM MMC for 2 h and allowed 22 h to recover before harvest. For experiments using the HEK 293T cell line, cells were treated with 300 nM MMC for 24 h before harvest. In all experiments, cells were treated with colcemid for 1-2 h prior to harvest. Following hypotonic treatment, cells were fixed with fixative (3:1 methanol: acetic acid in volume) and dropped on slides in a humidified environment to optimize spreading. Slides were mounted in 1X 4',6-diamidino-2-phenylindole, dihydrochloride (DAPI) anti-fade solution the following day and blinded for analysis. Only metaphases with 38-41 chromosomes (MEFs) or 64-72 chromosomes (HEK 293T cells) were included in the analysis. Chromosome aberrations including radials, gaps/breaks, fragments and ring chromosomes were scored for all experiments. HEK 293T cells were cultured using the same procedures used for MEFs.

DNA Fiber Assay

All techniques and methods of analysis used were performed as described previously[29,30]. Briefly, replication forks were sequentially labeled with deoxyuridine triphosphates (dUTPs) conjugated with digoxigenin (digoxigenin-dUTPs) for 20 min and with biotin-dUTPs for 30 min. Labeled cells were dropped onto slides, fixed, and dipped into lysis buffer for the release and extension of DNA fibers. Incorporated dUTPs were visualized by anti-digoxigenin rhodamine conjugate (Roche, Branford, CT) and streptavidin, -Alexa Fluor 488 (Invitrogen, Carlsbad, CA).

Colony Formation Assay

Five hundred cells were plated in 6 cm dishes along with the corresponding doses of MMC. For HEK 293T cells, the bottoms of the dishes were coated with poly-L-lysine beforehand to aid in cell adhesion. Colonies were stained using crystal violet after a period of 1 week (HEK 293T) or 2 weeks (PD331 and PD331+FANCC) and counted.

MTT Assay

The Vybrant MTT (3-(4,5-dimethylthiazol-2-yl)-2,5-diphenyltetrazolium bromide) Cell Proliferation Assay Kit (Life Technologies) was used. Briefly, 5×10^4 (experiments with MEFs) or 1×10^4 (experiments with PD331 cell lines) cells of each genotype were plated per well in a 96-well plate. The next day, cells were either treated with the corresponding

drug or left untreated for 5 days before the assay was performed according to the manufacturer's instructions. A_{570} was used to measure relative cell proliferation while A_{670} was used as a reference for background absorbance.

Cytokinesis-Block Micronucleus Assay and G1 Phase Cell Analyses

The cytokinesis-block micronucleus (MN) assay was performed as described previously[29,31], except that cells were treated with cytochalasin B (0.72 μg/ml) for 4-5 h. The same procedure was used for all analyses of G1 cells.

Measuring HR events using the fluorescent yellow direct repeat transgenic locus system

Wildtype and *Helq*$^{gt/gt}$ MEFs carrying the *FYDR* transgenic locus[32] in the hemizygous state were generated as described above. Cells at passage 2 were plated, grown for three days and then re-plated into three separate dishes. The corresponding drug treatments (untreated, MMC, CPT) were then administered the following day and washed out after 24 hours. After a 48-hour recovery period, cells were analyzed by flow cytometry using the FL1-H and FL2-H channels of the FACSCalibur (BD Biosciences).

Results

Helq deficient mice carry a gene-trap allele that generates HELQΔ-β-Geo

To generate a mouse *Helq* mutant, we searched the BayGenomics database for mutant mouse embryonic stem (ES) cell clones[33,34]. Gene-trap vectors are designed to have a splice acceptor site upstream of a reporter gene, typically β-Geo, a fusion gene of the β-galactosidase and neomycin resistance genes. We found that the ES cell clone RRF112 has an insertion of the gene-trap vector pGT0Lxf in the intron between exons 11 and 12 of the *Helq* locus (Supplementary Figure S1A). This gene-trap allele was named $Helq^{gt}$. The $Helq^{gt}$ allele is expected to create a chimeric transcript containing exons 1-11 of *Helq* and β-Geo (Figure 1A), producing a truncated HELQ protein that is fused with β-Geo at its C-terminal end (Figure 1B). This mutant protein still retains its helicase domain but lacks the three C-terminal domains with highly conserved motifs thorough archaea to metazoans[35,36]. It has been demonstrated that these domains are required for normal helicase activity in other species[36-38]. To generate mice that carry the $Helq^{gt}$ allele, we microinjected RRF112 ES cells into blastocysts from an inbred strain of C57BL/6J (B6) females using a standard method. High-percentage chimera males were mated with B6 inbred females to produce carriers of the $Helq^{gt}$ allele, which were identified by genomic PCR using primer pairs that amplify the boundary sequences of the insertion site (Supplementary Figure S1B). $Helq^{gt}$ heterozygous ($Helq^{gt/+}$) carriers appear normal in every aspect and are undistinguishable from wildtype (WT) mice (data not shown). A congenic line of $Helq^{gt}$ has been established by backcrossing $Helq^{gt/+}$ mice to inbred B6

mice at least 10 generations. This B6 congenic *Helq*^{gt} line was used for the following studies unless otherwise indicated.

WT *Helq* mRNA and protein are virtually undetectable in *Helq*^{gt} homozygous cells

Helq$^{gt/+}$ mice were timed-mated to generate mouse embryonic fibroblasts (MEFs). We extracted total RNA from WT and *Helq*^{gt} homozygous (*Helq*$^{gt/gt}$) MEFs for reverse-transcription (RT)-PCR and verified the presence of the chimeric message in *Helq*$^{gt/gt}$ MEFs and the wildtype mRNA in WT MEFs (Figure 1A) by sequencing the RT-PCR products (Supplementary Figure S1C). Furthermore, quantitative (q-)RT-PCR on RNA from WT and *Helq*$^{gt/gt}$ cells revealed that the WT transcript containing exons 11-12 was nearly absent in *Helq*$^{gt/gt}$ cells (less than 1 % of WT) that predominantly express the chimeric transcript containing exon 11 and β-Geo sequences (Figure 1C). As we found no difference between WT and *Helq*$^{gt/gt}$ cells for the levels of transcript containing exons 1-2 far upstream of the insertion site, the presence of the gene-trap vector likely has no effect on *Helq* expression. Next, we performed western blots on whole cell extracts from WT and *Helq*$^{gt/gt}$ MEFs (Figure 1D). Consistent with the q-RT-PCR results, WT HELQ (~120kD) was undetectable in *Helq*$^{gt/gt}$ cells. Instead, they predominantly express the mutant HELQ protein (HELQΔ-β-Geo). A semi-quantitative analysis indicated that *Helq*$^{gt/gt}$ cells express WT HELQ protein less than 10% of the levels seen in WT cells, if any at all (Figure 1E). These data suggest that the splice acceptor site at the *Helq*^{gt} allele

is very efficient, leading to very little expression of normal, full-length HELQ in *Helq*$^{gt/gt}$ cells.

Helq deficiency causes a mild form of hypogonadism, which is not epistatic to *Fancc*

As previous studies suggested an intriguing connection of HELQ to the FA pathway[23,24,27], we generated *Helq*$^{gt/gt}$ mice along with WT control mice to examine hypogonadism, one of the most consistent phenotypes seen in the FA mouse models[39]. We found that *Helq*$^{gt/gt}$ males have significantly smaller testes (p<0.005, t-test), ~62% of WT males by weight at 6 weeks of age (0.165g±0.01 and 0.102g±0.01 for the average WT and *Helq*$^{gt/gt}$ testes weights, respectively, Figure 2A). Histological analysis revealed that approximately 10~20% seminiferous tubules in *Helq*$^{gt/gt}$ males are atrophied and devoid of spermatocytes and spermatogonia (Figure 2B). This mosaic pattern of normal and empty seminiferous tubules is very similar to what has been seen in a number of FA mouse models[40-48]. For comparison, we also generated mice homozygous for a *Fancc* allele (*Fancc*$^{-}$)[28] in the same background. As reported earlier[28,49,50], *Fancc*$^{-/-}$ males had extremely small testes weighing an average of only 0.027g±0.001 (only 16% of WT by weight, p<0.0001, t-test) with >90% of seminiferous tubules exhibiting atrophy or hypotrophy (Figure 2A and B). When compared to *Helq*$^{gt/gt}$ males, *Fancc*$^{-/-}$ testes were only 26% of *Helq*$^{gt/gt}$ testes by weight (p<0.0001, t-test). These data suggest that the hypogonadism observed in *Helq*$^{gt/gt}$ testes is not as severe as in *Fancc*$^{-/-}$ testes. To test for an epistatic relationship between *Helq* and *Fancc* for this trait, we generated mice doubly

homozygous for *Helq*^{gt} and *Fancc*$^{-}$. Testes from *Helq*$^{gt/gt}$;*Fancc*$^{-/-}$ males were even smaller (the average 0.021g±0.002) than those from *Fancc*$^{-/-}$ males (p<0.05, t-test), having all seminiferous tubules completely devoid of spermatogonia and spermatocytes. While *Fancc*$^{-/-}$ and *Helq*$^{gt/gt}$;*Fancc*$^{-/-}$ mice are significantly smaller in size than WT and *Helq*$^{gt/gt}$ mice, these observations still hold true after taking this into consideration (Supplementary Figures S2A and B). Collectively, these findings indicate that mutations in *Helq* and *Fancc* are not epistatic to each other in causing hypogonadism.

Female-specific sub-fertility in *Helq*$^{gt/gt}$ mice is consistent with germ cell hypoplasia during embryogenesis

It has been reported that hypogonadism in FA mouse models is attributed to severely compromised proliferation of primordial germ cells[40,41,45,51]. This leads to sterility in a significant fraction of *Fancc*$^{-/-}$ mice[28,49]. However, as hypogonadism in *Helq*$^{gt/gt}$ males is very modest, they are fertile, producing litters at size comparable to *Helq*$^{gt/+}$ males (Supplementary Table S1). It should be noted that younger *Helq*$^{gt/gt}$ males have a greatly increased fraction (>50%) of seminiferous tubules exhibiting atrophy or hypotrophy (Supplementary Figure S2C). However, as they get older, the number of such tubules decreases. This is most likely because surviving germ cells in *Helq*$^{gt/gt}$ males can repopulate as spermatogonial stem cells and support fertility as previously seen in FA mouse models[42]. Therefore, much like the FA genes, *Helq* is required for normal proliferation of germ cells during embryogenesis but has no effect on spermatogonial

stem cells at later stages. Different from males, *Helq*$^{gt/gt}$ females were more severely affected with hypogonadism (see Figure 2C and D). The number of ova per ovary was reduced to 6±0.61 in *Helq*$^{gt/gt}$ females compared to 31±3.2 in WT females (p<0.0001, t-test). When initially tested in a 129/B6 mixed background, four of seven *Helq*$^{gt/gt}$ females were sterile. Fertile *Helq*$^{gt/gt}$ females tended to have small litters, with an average litter size of only 3.5 (n=6). This female-specific sub-fertility is consistent with germ cell hypoplasia during embryogenesis, as it is believed that the total oocyte pool is determined at this stage. Taken together, while *Helq*$^{gt/gt}$ mice exhibit hypogonadsim that is phenotypically similar to FA mouse models, its underlying mechanism is distinct given the non-epistatic relationship between *Helq* and *Fancc*.

Helq$^{gt/gt}$ mice are born in the expected Mendelian ratio, showing no growth retardation

As *Helq*$^{gt/gt}$ males are fertile, we performed crosses between *Helq*$^{gt/gt}$;*Fancc*$^{+/-}$ males and *Helq*$^{gt/+}$;*Fancc*$^{+/-}$ females to efficiently generate *Helq*$^{gt/gt}$;*Fancc*$^{-/-}$ mice in the B6 background. A total of 105 mice were genotyped at 3 weeks of age (Supplementary Table S2). While *Helq*$^{gt/gt}$ mice were found at the expected ratio, the number of *Fancc*$^{-/-}$ mice in this background was reduced to ~65% of the expected number (17 vs 26.25, p<0.05, χ2-test) as described previously[52]. Only 7 *Helq*$^{gt/gt}$;*Fancc*$^{-/-}$ mice were observed at this age but this number was not statistically different from 13.125, the expected number (p>0.05, χ2-test). This relatively small number of *Helq*$^{gt/gt}$;*Fancc*$^{-/-}$ mice is most

likely attributed to the sub-lethality of *Fancc*$^{-/-}$ mice in this background. As shown in Figure 2E, we also found that *Fancc*$^{-/-}$ mice are significantly smaller in size (average weight of 7.4g±0.61) compared to WT (8.7g±0.15) and *Helq*$^{gt/gt}$ mice (8.8g±0.39). *Helq*$^{gt/gt}$;*Fancc*$^{-/-}$ mice were even smaller than *Fancc*$^{-/-}$ mice, weighing 6.0g±0.71 on average, though this difference did not reach statistical significance likely due to the small number of mice examined. Overall, *Helq*$^{gt/gt}$ mice are quite healthy, exhibiting phenotypes milder than *Fancc*$^{-/-}$ mice. It was reported that *Fancc*$^{-/-}$ mice in the B6 background are essentially tumor-free[53]. Similarly, a small-scale aging study with 11 *Helq*$^{gt/gt}$ mice (5 males and 6 females) in this background showed no significant increase in spontaneous tumor incidence up to 21 months of age. This was not surprising, given the milder phenotypes of *Helq*$^{gt/gt}$ mice compared to *Fancc*$^{-/-}$ mice.

Mono-ubiquitination and focus formation of FANCD2 are intact in *Helq*$^{gt/gt}$ cells

Our data so far did not support epistasis between *Helq* and *Fancc.* Therefore, we next tested the role of *Helq* in FANCD2 focus formation, a signature of FA pathway activation[25]. For this purpose, we used primary WT and *Helq*$^{gt/gt}$ MEFs, as *Fancc*$^{-/-}$ and *Helq*$^{gt/gt}$;*Fancc*$^{-/-}$ cells, both lacking a functional FA core complex, do not form FANCD2 foci[25]. As shown in Figure 3A and B, no significant difference was observed in the percentage of cells positive for FANCD2 foci between WT and *Helq*$^{gt/gt}$ cells even after treatment with the crosslinker MMC. The same was true after treatment with aphidicolin (APH), a replication inhibitor and robust inducer of FANCD2 and FANCI foci[54] (Figure

3C and D). Focus formation of FANCD2/FANCI at prophase, markers of unresolved replication intermediates[55], were also unchanged between these two genotypes in response to MMC or APH (Supplementary Figure S3A and B). Agreeing with these data, mono-ubiquitination of FANCD2 was also robustly induced in *Helq*$^{gt/gt}$ cells following treatment with either MMC or APH (Figures 3E and F). In comparison, no mono-ubiquitinated FANCD2 could be detected in *Fancc*$^{-/-}$ and *Helq*$^{gt/gt}$;*Fancc*$^{-/-}$ cells. These data collectively suggest that *Helq* is not required for FANCD2 mono-ubiquitination or focus formation.

HELQ plays a minor role in MMC resistance in a manner non-epistatic with FANCC

Previous studies reported that HELQ is required for ICL resistance in worms and humans[24,27] but not in chicken DT40 cells[14]. Therefore, we tested *Helq*$^{gt/gt}$ cells for MMC hypersensitivity, another hallmark of FA cells[6]. For this line of experiments, we used primary MEFs with the following four genotypes, WT, *Helq*$^{gt/gt}$, *Fancc*$^{-/-}$, and *Helq*$^{gt/gt}$;*Fancc*$^{-/-}$. First, we examined MMC-induced chromosome aberrations. Representative metaphase spreads for each genotype after MMC treatment are shown in Figure 4A. Although we scored 120 metaphases per experimental group, the total number of MMC-induced chromosome aberrations was not statistically different between *Helq*$^{gt/gt}$ and WT cells (Figure 4B and C). However, *Helq*$^{gt/gt}$ cells did exhibit a slight but significant increase in radials (9.2%±2.6 as opposed to 5.0%±2.0 in WT), a type of complex chromosome aberrations that occur frequently in MMC-treated FA cells (Figure

4A and D). Consistent with their hypersensitivity to MMC, the majority of *Fancc*$^{-/-}$ cells exhibited chromosome aberrations (72.5%±4.09, Figure 4B) with a drastic increase in radials (36.7%±4.42, Figure 4D). Intriguingly, *Helq*$^{gt/gt}$*;Fancc*$^{-/-}$ cells showed statistically higher levels of chromosome aberrations including radials (84.5%±3.35 and 46.7%±4.57 in Figure 4B and D, respectively) compared to *Fancc*$^{-/-}$ cells. These data suggest that *Helq*$^{gt/gt}$ cells are not as extremely sensitive to MMC as *Fancc*$^{-/-}$ cells. However, as *Helq*$^{gt/gt}$*;Fancc*$^{-/-}$ cells showed a significantly higher number of MMC-induced chromosome aberrations than *Fancc*$^{-/-}$ cells, HELQ contributes to MMC resistance through a mechanism that is distinct from the function of FANCC. Given the mild sensitivity of *Helq*$^{gt/gt}$ cells to MMC, this mechanism is likely to be a secondary alternative to the FA pathway. Finally, we tested the effect of MMC on the proliferation of these cells using a MTT assay. In agreement with the metaphase analysis, a 5 days culture in multiple low doses of MMC significantly reduced the proliferation of *Fancc*$^{-/-}$ and *Helq*$^{gt/gt}$*;Fancc*$^{-/-}$, but not *Helq*$^{gt/gt}$, cells (Figure 4E). While *Helq*$^{gt/gt}$*;Fancc*$^{-/-}$ cells appeared to display an even greater reduction in proliferation than *Fancc*$^{-/-}$ cells, this did not reach statistical significance. Together, these data are consistent with the idea of HELQ performing a minor role in MMC resistance.

HELQ depletion leads to only mild MMC sensitivity compared with FANCA-depleted/FANCC-deficient human cells

Although *Helq*$^{gt/gt}$ cells apparently lack normal full-length HELQ, they do express the mutant HELQΔ-β-Geo protein. Therefore, we wondered whether the mild MMC sensitivity of *Helq*$^{gt/gt}$ cells truly reflects a consequence of HELQ deficiency. To test this possibility, we depleted *HELQ* and/or *FANCA*, another FA core complex member[56], in human HEK 293T cells via small interfering RNAs (siRNA, see Supplementary Figure S4A). At two different doses, *FANCA* depletion, but not *HELQ* depletion, led to MMC hypersensitivity as measured by colony formation assay (Supplementary Figure S4B). Similar results were obtained for MMC-induced chromosome aberrations (Supplementary Figures S4C and D). To further confirm these results, we also performed siRNA-mediated depletion of *HELQ* in PD331 cells (Supplementary Figure S4E), a human cell line deficient for *FANCC*, or their complemented counterparts (PD331+FANCC). In a colony formation assay, *HELQ*-depleted PD331+FANCC cells exhibited modestly decreased survival following MMC treatment (at 300nM) compared to control siRNA-treated counterparts, though this was still very mild compared with that of the PD331 cells (Supplementary Figure S4F). Only when measured by MTT assay (5 days culture, 15-45 nM doses) could we observe a clear non-epistatic relationship between *HELQ* and *FANCC* (Supplementary Figure S4G). Together, these data collectively support the idea that HELQ plays a minor, backup role in MMC resistance in mammalian cells that is most likely non-epistatic to *FANCC*.

A loss of HELQ and/or FANCC alters the distribution of replication fork speed in unperturbed S phase, increasing persistent stalled forks

Several studies have suggested that HELQ and its orthologs have a role in the recovery of stalled or collapsed replication forks[23,38,57]. As we noticed a modest but significant increase in spontaneous chromosome aberrations in *Fancc*$^{-/-}$ and *Helq*$^{gt/gt}$*;Fancc*$^{-/-}$ cells (Figure 4B), we examined replication fork speed in WT, *Helq*$^{gt/gt}$, *Fancc*$^{-/-}$, and *Helq*$^{gt/gt}$*;Fancc*$^{-/-}$ cells in unperturbed S phase using the DNA fiber technique (Supplementary Figure S5A)[29]. Although the mean fork speeds were not different among the four genotypes (Figure 5A), the distributions of fork speed values were significantly different (p<0.001, Kolmogorov-Smirnov test, Supplementary Figure S5B). Categorizing fork speeds into three ranges (slow, mid and fast), we found that compared to WT cells, *Helq*$^{gt/gt}$ cells exhibited a slight increase of forks in mid-range speed and a decrease in slow forks (Figure 5B). *Fancc*$^{-/-}$ cells had a higher frequency of faster forks with a decrease of mid-speed forks. Increases in mid-speed and faster forks in these cells might have contributed to faster median fork speeds in these cells (Figure 5A). *Helq*$^{gt/gt}$*;Fancc*$^{-/-}$ cells displayed increases in both faster and slower fork speeds, indicating that their fork movement is greatly altered from WT cells even in unchallenged S phase. Although counterintuitive, an increase in faster forks may suggest an increase in fork stalling events, as we previously reported[29]. This is due to the number of fork termination events. Faster forks that terminate within the duration of the assay likely

escape detection. Thus, an increase in fork stalling leads to a decreased number of fork termination events, thereby leaving a greater number of faster forks visible for measurement. To address if this was the case, we next looked at RPA32 foci, markers of stalled replication forks (Figure 5C)[58,59]. Compared to WT cells (7.06%±0.61), increased percentages of *Helq*$^{gt/gt}$ and *Fancc*$^{-/-}$ cells (9.20%±0.61 and 12.5%±0.88, respectively) were positive for RPA32 foci (Figure 5D), with an even further increase observed in *Helq*$^{gt/gt}$*;Fancc*$^{-/-}$ cells (15.6%±0.98). These differences were all significant to one another (p<0.001, χ^2-test). The number of RPA32 foci co-localizing with γH2AX foci, a marker of DSBs[60], was also significantly increased in *Helq*$^{gt/gt}$ and *Fancc*$^{-/-}$ cells (5.46%±0.48 and 7.44%±0.70, respectively) compared to WT cells (4.08%±0.47). However, unlike RPA32 foci, there was no significant increase in RPA/γH2AX co-localizing foci in *Helq*$^{gt/gt}$*;Fancc*$^{-/-}$ cells (8.02%±0.73) compared to *Fancc*$^{-/-}$ cells. These data present a new line of evidence that *Helq* and *Fancc* are not epistatic to each other in the recovery of stalled/collapsed replication forks even in unchallenged S phase.

<u>*Helq* and *Fancc* are independently required to prevent the formation of spontaneous MN</u>

Persistent stalled forks can lead to micronucleus (MN) formation if unresolved before M phase entry[29,61]. Therefore, we measured spontaneous MN levels using the cytokinesis-block MN assay (Figure 6A), a standard assay for this purpose[31]. Compared to WT cells (4.33%±0.48, see Figure 6B), significantly increased numbers of *Helq*$^{gt/gt}$ (9.56%±0.98)

and *Fancc*$^{-/-}$ (14.0%±1.16) cells contained spontaneous MN (p<0.001, χ^2-test for both). *Helq*$^{gt/gt}$*;Fancc*$^{-/-}$ cells exhibited a >6-fold increase (26.1%±1.47) compared to WT cells and this number was also statistically higher than that of *Fancc*$^{-/-}$ cells (p<0.001, χ^2-test). These data indicate that *Helq* and *Fancc* function in a non-epistatic manner to prevent spontaneous MN likely through contributing to the recovery of stalled forks. We exploited this modest but significant increase in spontaneous MN in *Helq*$^{gt/gt}$ cells to validate that this allele accurately reflects the consequences of loss of HELQ function. We performed siRNA-mediated knockdown of *Helq* (or *Helq*^{gt}) transcripts in WT and *Helq*$^{gt/gt}$ MEFs, respectively (Supplementary Figures S6A and B). This resulted in significantly increased spontaneous MN levels in WT cells (p<0.001, χ^2-test) but not *Helq*$^{gt/gt}$ cells (Supplementary Figure S6C), suggesting that the HELQΔ-β-Geo mutant protein is likely devoid of any activity. Unresolved replication intermediates can cause the formation of MN through two mechanisms; non-disjunction of sister chromatids and chromosome/chromatid breaks. These two mechanisms can be distinguished by staining MN for the centromeric marker CENP-A[62] (Supplementary Figure S6D). We found that both types of MN were increased in these mutant cells with similar ratios (Supplementary Figure S6E). We also measured MMC-induced MN in these cells. Because of the relatively higher levels of spontaneous MN in mutant cells, we subtracted spontaneous MN frequency values from those in the MMC treatment to obtained differences (numbers in the white bars in Figure 6B). These were then compared to evaluate the effect of MMC on MN formation. Such values were very similar between WT and *Helq*$^{gt/gt}$ cells

(7.44 and 7.22, respectively), while *Fancc*$^{-/-}$ cells showed a 2-fold larger value (14.1) at the same dose used for the metaphase analysis (Figure 4). These findings are consistent with the idea that the FA pathway is a major pathway for MMC resistance for which HELQ performs only a minor role. *Helq*$^{gt/gt}$*;Fancc*$^{-/-}$ cells showed a value (15.0) that was not much higher than that of *Fancc*$^{-/-}$ cells. We think this may be due to the extreme sensitivity of *Helq*$^{gt/gt}$*;Fancc*$^{-/-}$ cells to MMC. As the majority of them have multiple abnormal metaphase chromosomes (Figure 4C), a fraction of them may not complete M phase to form MN in the subsequent G1 phase, making this value smaller. Unlike spontaneous conditions, MMC increased exclusively CENP-A- MN (Supplementary Figure S6E). We also examined CPT-induced MN (Supplementary Figure S6F). Both *Helq*$^{gt/gt}$ and *Fancc*$^{-/-}$ cells showed significantly increased levels of CPT-induced MN (14.2 and 14.2, respectively) compared to WT cells (9.93). The largest increase was observed in *Helq*$^{gt/gt}$*;Fancc*$^{-/-}$ cells (16.2). However, we were unable to determine epistasis for this, due to the limited sensitivity of the MN assay.

<u>*Helq* and *Fancc* are not epistatic to suppress the formation of 53BP1 nuclear bodies</u>

Recently, it was shown that unresolved replication intermediates can rupture during passage through M phase, leading to the formation of what are known as 53BP1 nuclear bodies (53BP1-NB) in G1 phase cells[63,64]. Interestingly, such bodies are often exquisitely symmetrical in terms of their appearance within the daughter nuclei (Figure 6C). To score 53BP1-NB, G1 phase cells are typically identified as cyclin A negative[63,64].

However, owing to the lack of a cyclin A antibody that works well for mouse cells, we used the cytokinesis-blocking reagent, cytochalasin B, to identify G1 phase daughter nuclei as those contained within binucleated cells (Figure 6C). Although there was no significant difference in the percentage of 53BP1-NB positive nuclei between WT and *Helq*$^{gt/gt}$ cells (33.3%±1.67 and 34.2%±1.68, respectively), the number of nuclei containing 53BP1-NB was statistically higher in *Fancc*$^{-/-}$ cells (37.8%±1.71, $p<0.01$, χ^2 test) (Figure 6D). Much like spontaneous MN formation (Figure 6B), *Helq*$^{gt/gt}$*;Fancc*$^{-/-}$ cells showed a drastic increase in 53BP1-NB containing nuclei (54.1%±1.77) compared to *Fancc*$^{-/-}$ cells ($p<0.001$, χ^2 test) with more nuclei containing multiple 53BP1-NB (Figure 6E). These data are consistent with the non-epistatic relationship between *Helq* and *Fancc* in preventing genome instability derived from persistent stalled forks.

Helq$^{gt/gt}$ cells display recombinant frequencies at the *FYDR* locus that are comparable with wildtype

Given its involvement in meiotic DSB repair in flies and worms[20,21], we postulated that HELQ may function downstream of the FA pathway in HR, similar to other proteins such as BRCA2 and PALB2[65,66]. Supporting this idea, it has been reported that depletion of *HELQ* in human cells lowers HR efficiency[27]. To test this, we used the *FYDR* transgenic locus system[32] to measure the levels of spontaneous, MMC-induced and CPT-induced HR events in *Helq*$^{gt/gt}$ MEFs (Supplementary Figures S7A and B). Under all conditions

tested, *Helq*$^{gt/gt}$ cells showed levels of recombination that were comparable with WT (Figure 6F and Supplementary Figure S7C), suggesting the possibility that HELQ is not a major player in HR.

Discussion

In this study, we have investigated a possible involvement of HELQ in the FA pathway using the *Helq*^{gt} strain as a model. We showed that primary *Helq*$^{gt/gt}$ MEFs are capable of FANCD2 mono-ubiquitination and focus formation (Figure 3). By phenotypic comparison to *Fancc*$^{-/-}$ mice/cells in the same genetic background, we found that *Helq*$^{gt/gt}$ mice/cells exhibit a mild form of FA-like phenotypes such as hypogonadism (Figure 2) and MMC sensitivity (Figure 4). Importantly, double mutants for *Helq*^{gt} and *Fancc*$^{-}$ had more severe phenotypes than single mutants (Table 1). These findings are in stark contrast to the complete epistasis reported for *Fanca/Fancc* and *Fanca/Fancg* in mice[50,67]. Collectively, our data show that *Helq* and *Fancc* are not epistatic to one another for any trait tested.

Although our data strongly indicate that HELQ and FANCC function in parallel, it remains possible that HELQ could function in HR as a downstream step in the FA pathway. If this is the case, then the non-epistatic relationship between *Helq* and *Fancc* implicates that the FA core complex and HR machinery have a complicated, non-linear relationship as seen previously for *fancc* and *brca2* in chicken DT40 cells[68]. However, using the *FYDR* transgenic locus system, we found that HELQ's role in HR is likely to be non-essential or minor (Figure 6F). This is further supported by the fact that (i) *Helq*$^{gt/gt}$ mice are fully viable as opposed to early embryonic lethality seen for disruption of major HR genes[69], (ii) loss of HELQ results in only modest sensitivity to MMC (Figure 4), and (iii) *Helq*$^{gt/gt}$ males are fertile, showing no apparent meiosis defects. Alternatively, it may

be that the role of HELQ in HR is only visible when a major player in HR is compromised. Thus, the precise role of HELQ in HR requires further investigation.

Our data show that loss of *Helq* in mice results in phenotypes considerably milder compared with those seen in *Fancc*$^{-/-}$ mice (Table 1). This observation was not limited to *Helq*^{gt} homozygosity, as *HELQ* depletion in human HEK 293T cells did not cause a statistically higher level of MMC-induced chromosome aberrations or affect cellular survival as measured by colony formation assay (Supplementary Figure S4A-D). Furthermore, *HELQ*-depleted PD331+FANCC cells exhibited only modestly reduced cellular survival at 300 nM MMC (colony formation assay) (Supplementary Figure S4F). Although our data show a consistent trend towards HELQ and FANCA/FANCC being non-epistatic in human cells, the minor role of HELQ in MMC resistance may have prevented it from being manifested as statistically significant, except in the MTT assay (Supplementary Figure S4G).

It is noteworthy that HELQ orthologs do not exist in bacteria or yeast but archaea have HELQ-like helicases (HELQa)[70]. Atomic structures of HELQa from three species revealed the presence of five structural domains in HELQ, which are also conserved in HELQ in metazoans[36,38,71]. Mutagenesis studies have demonstrated that normal helicase activity requires the three C-terminal domains[36,72], which are missing from HELQΔ-β-Geo in *Helq*$^{gt/gt}$ mice (Figure 1B). Therefore, it is likely that HELQΔ-β-Geo is also devoid of helicase activity. Furthermore, the presence of β-Geo is also likely to

jeopardize its enzymatic activity. In line with this, siRNA-mediated knockdown of the *Helq*^{gt} transcript in *Helq*$^{gt/gt}$ cells did not lead to increased levels of spontaneous MN (Supplementary Figure S6C). Furthermore, given the normal phenotypes of *Helq*$^{gt/+}$ mice, we do not think that this allele confers any dominant-negative effect. Future studies using a null allele may give definitive answers for these issues.

Although there are definitely certain differences, HELQa and mammalian HELQ share similar biochemical properties with preference for structures resembling stalled replication forks, suggesting their role in stalled fork recovery[23,57,73]. Consistent with this idea, loss of HELQ caused an increase in stalled forks even in unchallenged conditions, and this role of HELQ was not epistatic to *Fancc* (Figure 5D). The non-epistatic relationship for *Helq* and *Fancc* is much clearer for the formation of spontaneous MN and 53BP1-NB (Figure 6), which are derived from persistent stalled forks, rather than MMC-induced chromosome aberrations (Figure 4). Therefore, we propose that the major role of HELQ is the rescue of stalled forks in normal S phase. Given that HELQ and the FA core complex function in parallel, elucidating such a role of HELQ may provide clues to decipher the function of the FA pathway in physiological conditions beyond ICL repair. Furthermore, as HELQ remains functional in FA mutant cells, it could potentially be exploited to provide a therapeutic benefit against cancers with FA pathway disruption.

Recent genome-wide associations studies have identified single nucleotide polymorphisms at loci within or near *HELQ* that are associated with increased risks for several different cancers including upper aerodigestive tract cancers and head and neck

cancers[74-77]. Our study was unable to detect an increased incidence of spontaneous tumors in *Helq*$^{gt/gt}$ mice. This could be due to several different factors, such as genetic background and species difference. The majority of FA mouse models do not show a strong cancer phenotype, despite the FA pathway's tumor suppressive role in humans[39]. Therefore, it may be necessary to test the role of *Helq* in tumor suppression in a sensitized background.

Acknowledgements

The authors thank Dr John Schimenti's Laboratory for initial support for this study, Dr Markus Grompe for providing them with the *Fancc*$^{-}$ strain, Dr Bevin Engelward for providing the *FYDR* strain, Dr Alexandra Sobeck for her critical reading of this manuscript and Drs Hung-Ji Tsai and Matt Anderson for their assistance with qRT-PCR experiments.

Table and figure legends

Table 1

Summary of phenotypes following *Helq* and/or *Fancc* disruption. "-" indicates no significant change from wildtype, while "+", "++" & "+++" refer to progressively more severe phenotypes. "+/-" refers to a small but significant effect. N.D. means not determined.

Figure 1

Characterization of the $Helq^{gt}$ allele. Diagrams (drawn to scale) depicting the transcripts (A) and resulting peptides (B) for the wildtype (WT) *Helq* and $Helq^{gt}$ alleles. The HELQ protein is split into five domains, the first two of which contain the well conserved motifs of the DEAD/DEAH helicase box. The $Helq^{gt}$ allele has most of domain 3 and all of domains 4 and 5 replaced by β-Geo. (C) qRT-PCR analysis using total RNA extracted from WT or $Helq^{gt/gt}$ ($H^{gt/gt}$) MEFs is shown. Data for the wildtype transcript containing exons 11 and 12 (top), the chimeric transcript containing exon 11 and the gene-trap vector (middle), and transcript containing exons 1 and 2 upstream of the insertion site (bottom) are shown. $Helq^{gt/gt}$ MEFs have less than $1/100^{th}$ of the levels of the wildtype *Helq* mRNA compared to WT cells (see top). Experiments were duplicated using RNA samples from different MEF lines to confirm reproducibility. A representative qRT-PCR data set is shown. (D) Western blotting shows no detectable levels of wildtype HELQ

protein in *Helq*$^{gt/gt}$ MEFs. A band corresponding to the HELQ$^{\Delta}$-β-Geo fusion peptide appears at the predicted molecular weight of ~230kDa only in the lysate from *Helq*$^{gt/gt}$ cells. (E) Loading differing ratios of protein reveals that the amount of wildtype HELQ protein (indicated by arrow) is extremely low in *Helq*$^{gt/gt}$ MEFs. Asterisk indicates non-specific bands. A stained membrane was used as a loading control for (D) and (E).

Figure 2

Helq$^{gt/gt}$ mice exhibit a hypogonadism phenotype reminiscent of mouse models of Fanconi anemia. (A) *Helq*$^{gt/gt}$, *Fancc*$^{-/-}$ and *Helq*$^{gt/gt}$*;Fancc*$^{-/-}$ males show significantly reduced testes weights at 6 weeks of age. At least 5 males were observed per genotype. (B) Histological analysis by hematoxylin and eosin (H&E) staining shows a mosaic pattern of normal and empty seminiferous tubules in *Helq*$^{gt/gt}$, *Fancc*$^{-/-}$ and *Helq*$^{gt/gt}$*;Fancc*$^{-/-}$ mice, with the respective phenotypes becoming increasingly worse. Scale bars are 1500 µm for the whole testis sections (top) and 75 µm for the enlarged images (bottom). (C) *Helq*$^{gt/gt}$ females exhibit smaller ovaries with a reduced number of follicles at 3 weeks of age. Six ovaries from 3 wildtype females and 10 ovaries from 5 *Helq*$^{gt/gt}$ females were observed. (D) H&E staining of ovaries from wildtype and *Helq*$^{gt/gt}$ females. Example ova-containing follicles are indicated by arrows. Scale bars are 500 µm. (E) *Helq*$^{gt/gt}$ mice display normal body weights at weaning age, unlike *Fancc*$^{-/-}$ and *Helq*$^{gt/gt}$*;Fancc*$^{-/-}$ mice which are significantly smaller. In (A), (C) and (E), error bars represent the standard error of the means (SEMs) and significance was determined by *t*-

test. Statistical significance at $p<0.05$, $p<0.01$, and $p<0.001$ are indicated as *, ** and ***, respectively. WT, $H^{gt/gt}$, $Fac^{-/-}$ and $H^{gt/gt};Fac^{-/-}$ refer to wildtype, $Helq^{gt/gt}$, $Fancc^{-/-}$ and $Helq^{gt/gt};Fancc^{-/-}$, respectively.

Figure 3

FANCD2 mono-ubiquitination and focus formation remain intact in $Helq^{gt/gt}$ cells. Shown are representative images of FANCD2 foci (green) in response to MMC (A) or APH (C) in WT and $Helq^{gt/gt}$ cells. Cells were harvested immediately following treatment except for the 2 hours treatment of 1200nM MMC, in which cells were given 22 hours of recovery time before harvest. Nuclei were stained with DAPI (blue). Scale bar is 10 μm. The average percentages of cells positive for FANCD2 foci in response to MMC or APH are shown in (B) and (D), respectively. (E) Western blotting shows that $Helq^{gt/gt}$ cells exhibit normal FANCD2 mono-ubiquitination in response to MMC. The defect observed in $Fancc^{-/-}$ and $Helq^{gt/gt};Fancc^{-/-}$ cells is shown for a better comparison. (F) $Helq^{gt/gt}$ cells do not display any defect in FANCD2 mono-ubiquitination in response to APH. Cells were treated with 300 nM APH for either 4 hrs (4H) or 24 hrs (24H) prior to harvest. Error bars (B, D) represent the binomial error for the combined data set. A stained membrane and MCM4 were used as loading controls in (E) and (F), respectively. W, H, F and H;F in (E, F) refer to wildtype, $Helq^{gt/gt}$, $Fancc^{-/-}$ and $Helq^{gt/gt};Fancc^{-/-}$ cells, respectively. UNT refers to untreated cells.

Figure 4

Helq$^{gt/gt}$ cells display modest sensitivity to MMC. (A) Shown are representative images of DAPI-stained metaphase spreads from all genotypes following MMC treatment (600 nM MMC for 2 hrs followed by 22-hr recovery before harvest). White arrowheads indicate chromosome aberrations. Enlarged images of radial structures from the *Fancc*$^{-/-}$ and *Helq*$^{gt/gt}$*;Fancc*$^{-/-}$ samples are shown at bottom. Scale bar is 10 μm. (B) Shown are the average percentages of metaphases positive for chromosomal aberrations in the untreated (left) or MMC-treated (right) conditions. For each experimental group, 120 metaphases were scored. (C) A histogram displaying the number of aberrations per metaphase for each genotype after MMC treatment is shown. (D) The average percentages of metaphases positive for radial structures after MMC treatment are shown. (E) The MTT assay reveals that *Helq*$^{gt/gt}$ cells display little, if any MMC sensitivity compared to *Fancc*$^{-/-}$ or *Helq*$^{gt/gt}$*;Fancc*$^{-/-}$ cells. Cells were treated with the indicated doses of MMC for 5 days prior to analysis. Error bars show either the binomial error of the combined data set (B, D) or the SEMs for at least three independent experiments (E). Significance was determined by either χ^2-test (B, D) or *t*-test (E). Statistical significance at $p<0.05$, $p<0.01$, and $p<0.001$ is indicated as *, ** and ***, respectively. WT, *H*$^{gt/gt}$, *Fac*$^{-/-}$ and *H*$^{gt/gt}$*;Fac*$^{-/-}$ refer to wildtype, *Helq*$^{gt/gt}$, *Fancc*$^{-/-}$, and *Helq*$^{gt/gt}$*;Fancc*$^{-/-}$ respectively.

Figure 5

A combined loss of *Helq* and *Fancc* greatly alters the distribution of replication fork speeds and leads to increased levels of RPA/γH2AX foci. (A) Box plots show the range of fork speed values for the four genotypes. The line through the middle of the shaded box represents the median while the "+" sign shows the location of the mean (values shown at bottom along with the number of tracts, N, analyzed). (B) Separating fork speed values into slow, mid and fast forks reveals statistically significant differences among the ratios of the four genotypes ($p<0.001$, χ^2-test). Error bars show the binomial error. (C) Shown are representative images of cells from all four genotypes co-stained for RPA (green) and γH2AX (red). Nuclei were stained with DAPI (blue). For RPA foci analysis, cells were pre-extracted prior to fixation using a 0.5% Triton X-100 solution. Scale bar is 10 μm. (D) The average percentages of cells positive for RPA foci (top) or RPA/γH2AX co-localization events (bottom) are shown. Error bars show the binomial error for the combined data set. Statistical significance (determined by χ^2-test) at $p<0.01$ and $p<0.001$ are indicated as ** and ***, respectively. WT, $H^{gt/gt}$, $Fac^{-/-}$ and $H^{gt/gt}$;$Fac^{-/-}$ refer to wildtype, $Helq^{gt/gt}$, $Fancc^{-/-}$, and $Helq^{gt/gt}$;$Fancc^{-/-}$ respectively.

Figure 6

Helq suppresses multiple forms of spontaneous genome instability in a manner that is not epistatic with *Fancc*, while $Helq^{gt/gt}$ cells show levels of recombination comparable to

wildtype. (A) Shown are representative images of binucleated cells with or without micronuclei (MN, indicated by white arrows). Nuclei and MN were stained with DAPI (blue). Scale bar is 10 µm. (B) Shown are the average percentages of binucleated cells positive for spontaneous MN (left) or MMC-induced MN (right). For the latter, the levels for the untreated condition are shown in gray with numbers in the white box showing the increase after MMC treatment. At least three independent experiments were performed and a total of >900 cells were observed per experimental group. (C) Simultaneous disruption of *Helq* and *Fancc* results in a significant increase in 53BP1-NB. Shown are representative images of binucleated cells with or without nuclei positive for 53BP1-NB (red). Nuclei were stained with DAPI (blue). Scale bar is 10 µm. (D) Shown are the average percentages of nuclei positive for 53BP1-NB. (E) A histogram detailing the number of 53BP1-NB per nucleus is shown. Four independent experiments were performed and a total of >750 cells were observed per experimental group. (F) No significant difference in the number of HR events was detected between wildtype and $Helq^{gt/gt}$ MEFs as measured by the *FYDR* transgenic locus system. Shown are the average numbers of $EYFP^{+}$ recombinants per 10^6 cells analyzed. Scale bars in (B,D) show the binomial error of the combined data sets while those in (F) show the SEMs for data obtained from at least 7 different embryos per genotype. Statistical significance was determined by either χ^2-test (B,D) or *t*-test (F). $p<0.05$, $p<0.01$ and $p<0.001$ are indicated as*, ** and ***, respectively. WT, $H^{gt/gt}$, $Fac^{-/-}$ and $H^{gt/gt};Fac^{-/-}$ refer to wildtype, $Helq^{gt/gt}$, $Fancc^{-/-}$, and $Helq^{gt/gt};Fancc^{-/-}$ respectively.

Table 1 Luebben et al., 2013

Trait	Wildtype	*Helq*$^{gt/gt}$	*Fancc*$^{-/-}$	*Helq*$^{gt/gt}$*;Fancc*$^{-/-}$
Sub-lethality	-	-	+	+
Growth retardation	-	-	+	++?
Tumor	-	-	-[53]	N.D.
Hypogonadism	-	+	++	+++
MMC sensitivity	-	+/-	++	+++
MN formation	-	+	++	+++
53BP1-NB formation	-	-	+	++
HR (measured by *FYDR*)	-	-	N.D.	N.D.

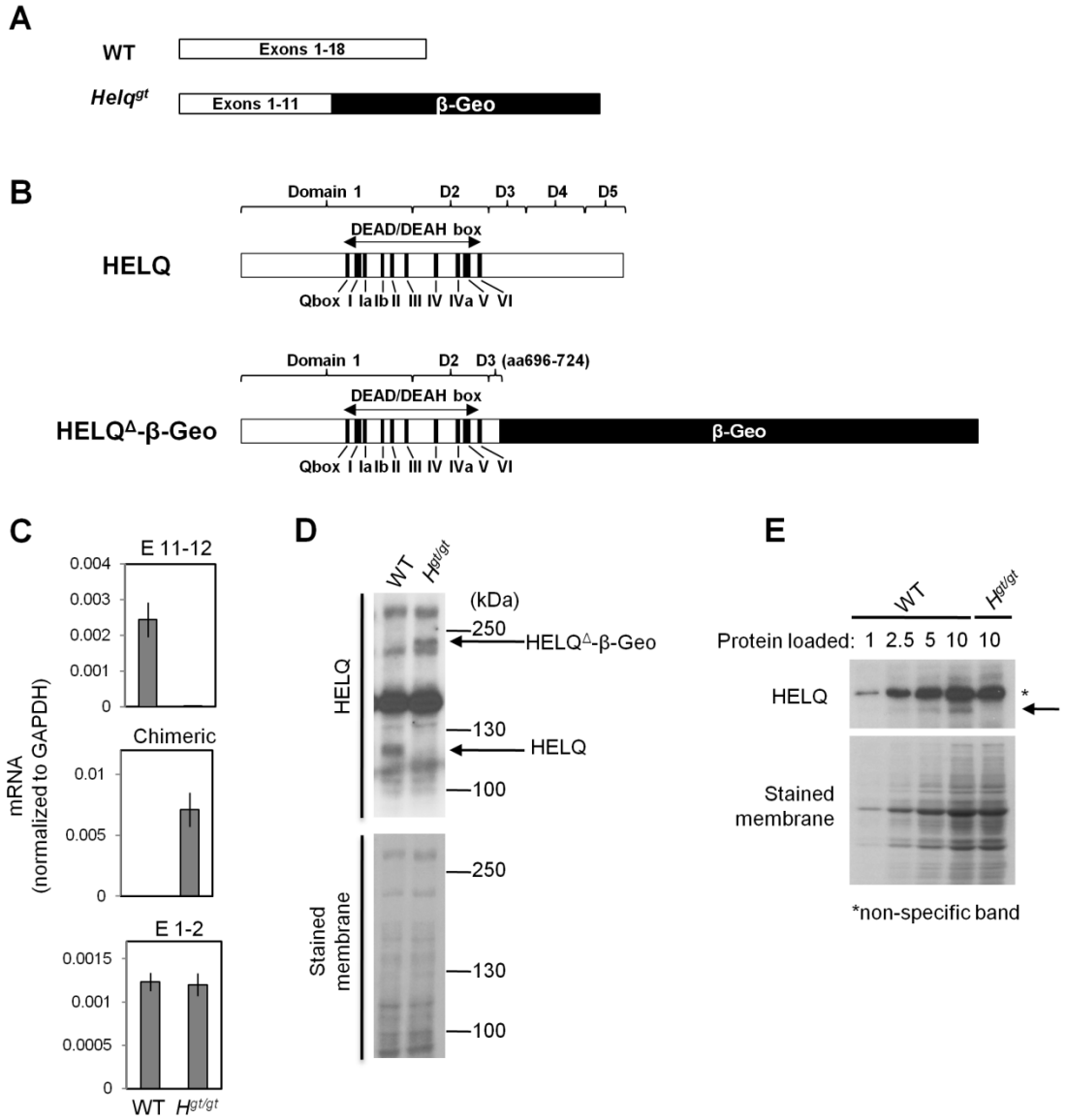
A
WT
Exons 1-18
Helq^gt
Exons 1-11
β-Geo
B
Domain 1
D2
D3
D4
D5
DEAD/DEAH box
HELQ
Qbox I Ia Ib II III IV IVa V VI
Domain 1
D2
D3 (aa696-724)
DEAD/DEAH box
HELQ^Δ-β-Geo
β-Geo
Qbox I Ia Ib II III IV IVa V VI
C
E 11-12
Chimeric
E 1-2
mRNA (normalized to GAPDH)
0.004
0.003
0.002
0.001
0
0.01
0.005
0.0015
0.0005
WT
H^gt/gt
D
WT
H^gt/gt
(kDa)
250
HELQ^Δ-β-Geo
130
HELQ
100
HELQ
Stained membrane
250
130
100
E
WT
H^gt/gt
Protein loaded: 1 2.5 5 10 10
HELQ
*
Stained membrane
*non-specific band

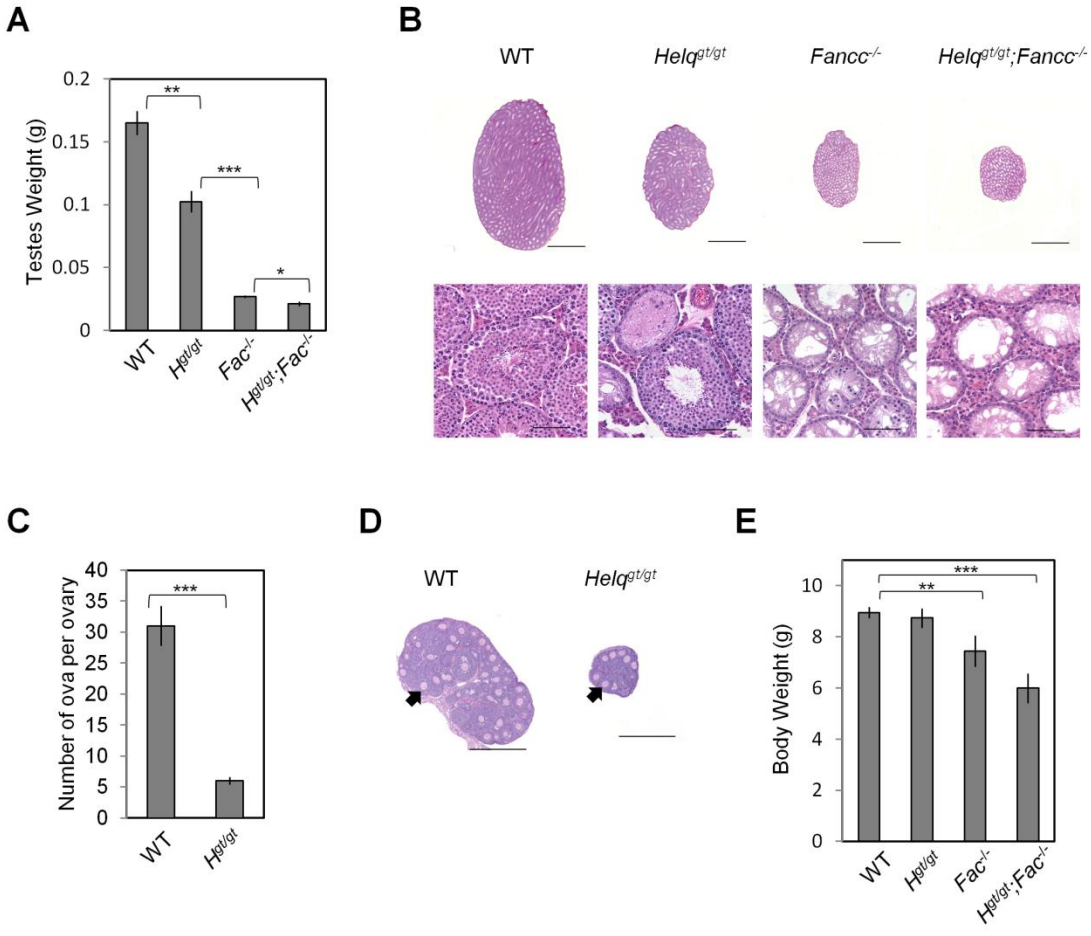
A
Testes Weight (g)
0.2
0.15
0.1
0.05
0
**
***
*
WT
Helq gt/gt
Fac -/-
Helq gt/gt;Fac -/-
B
WT
Helq gt/gt
Fancc -/-
Helq gt/gt;Fancc -/-
C
Number of ova per ovary
40
35
30
25
20
15
10
5
0
***
WT
Helq gt/gt
D
WT
Helq gt/gt
E
Body Weight (g)
10
8
6
4
2
0
***
**
WT
Helq gt/gt
Fac -/-
Helq gt/gt;Fac -/-

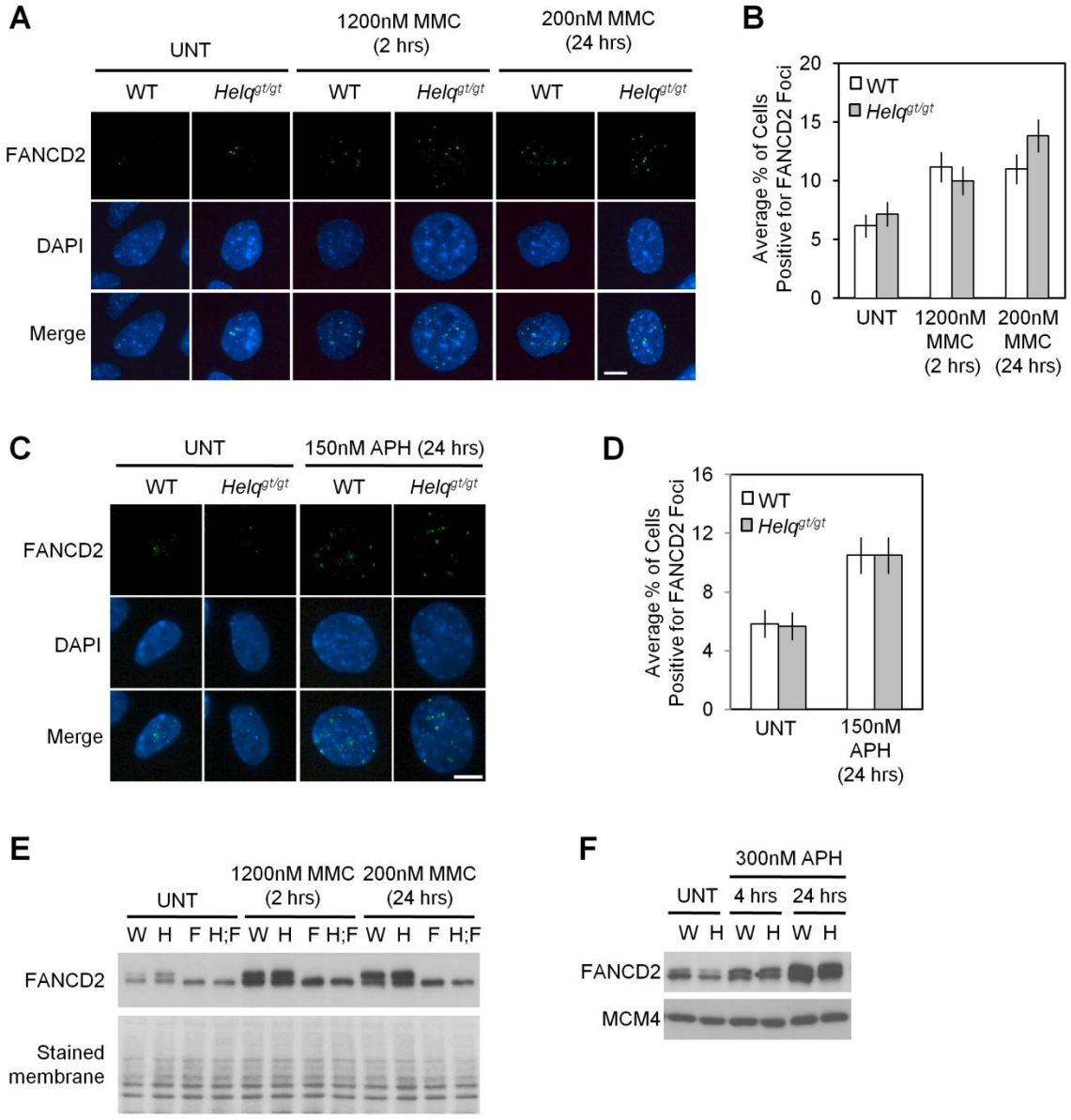
A
UNT
1200nM MMC (2 hrs)
200nM MMC (24 hrs)
WT
Helq gt/gt
FANCD2
DAPI
Merge
B
Average % of Cells Positive for FANCD2 Foci
WT
Helq gt/gt
UNT
1200nM MMC (2 hrs)
200nM MMC (24 hrs)
C
UNT
150nM APH (24 hrs)
D
150nM APH (24 hrs)
E
W H F H;F
Stained membrane
F
300nM APH
4 hrs
24 hrs
MCM4

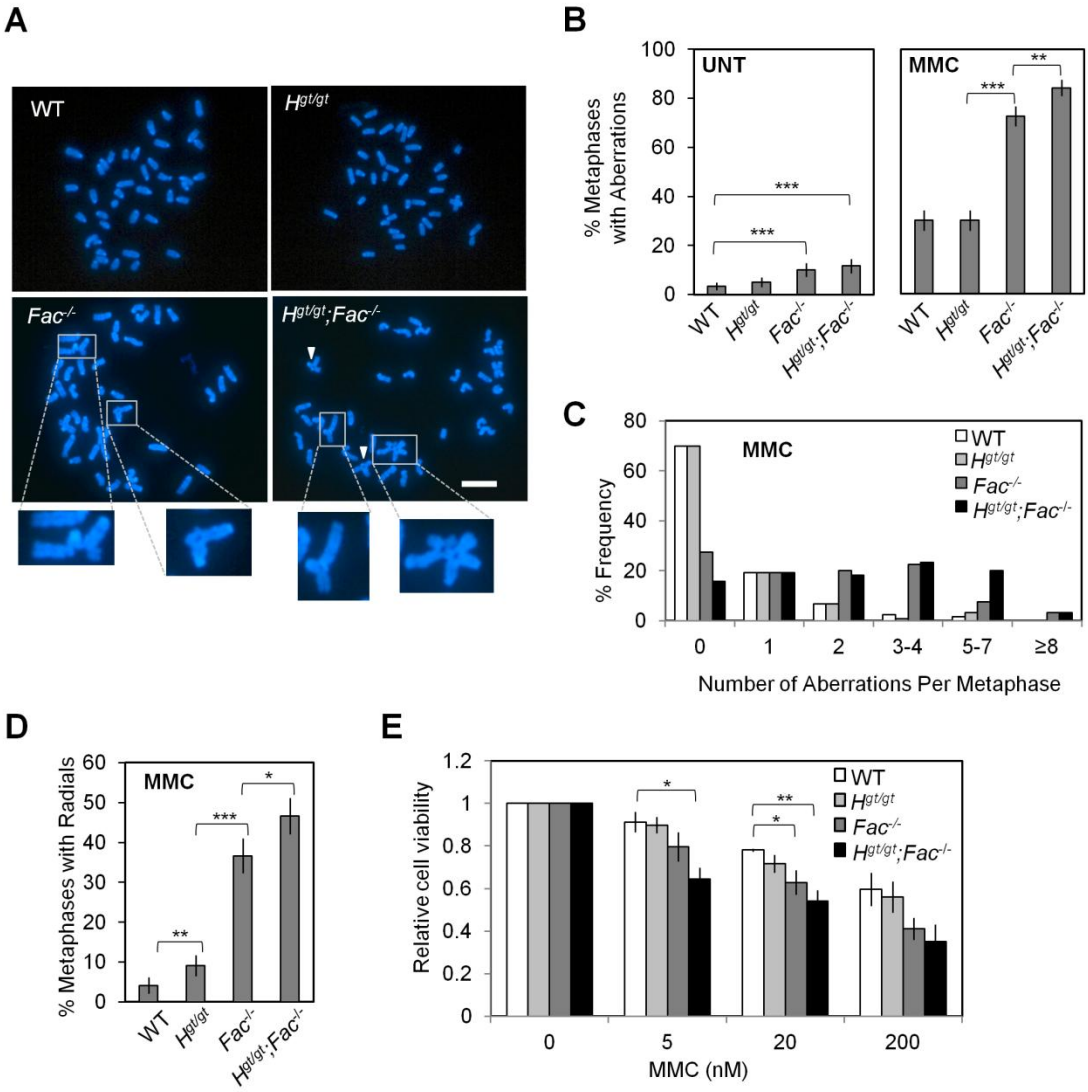
A
WT
Hgt/gt
Fac-/-
Hgt/gt;Fac-/-
B
UNT
MMC
% Metaphases with Aberrations
WT
Hgt/gt
Fac-/-
Hgt/gt;Fac-/-
C
MMC
% Frequency
Number of Aberrations Per Metaphase
D
MMC
% Metaphases with Radials
E
Relative cell viability
MMC (nM)

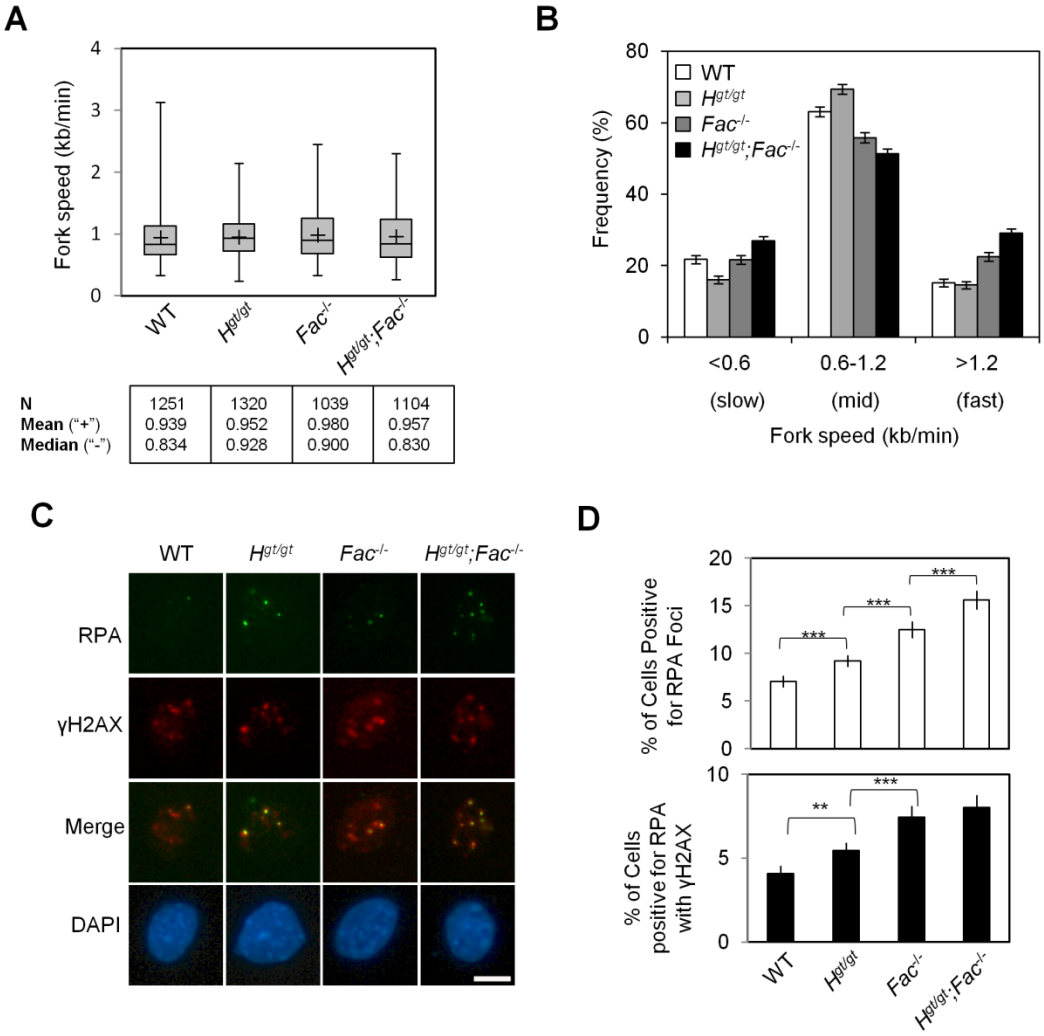
A
Fork speed (kb/min)
WT
Hgt/gt
Fac-/-
Hgt/gt;Fac-/-
N 1251 1320 1039 1104
Mean ("+") 0.939 0.952 0.980 0.957
Median ("-") 0.834 0.928 0.900 0.830
B
Frequency (%)
WT
Hgt/gt
Fac-/-
Hgt/gt;Fac-/-
<0.6 (slow)
0.6-1.2 (mid)
>1.2 (fast)
Fork speed (kb/min)
C
WT
Hgt/gt
Fac-/-
Hgt/gt;Fac-/-
RPA
γH2AX
Merge
DAPI
D
% of Cells Positive for RPA Foci
% of Cells positive for RPA with γH2AX
WT
Hgt/gt
Fac-/-
Hgt/gt;Fac-/-

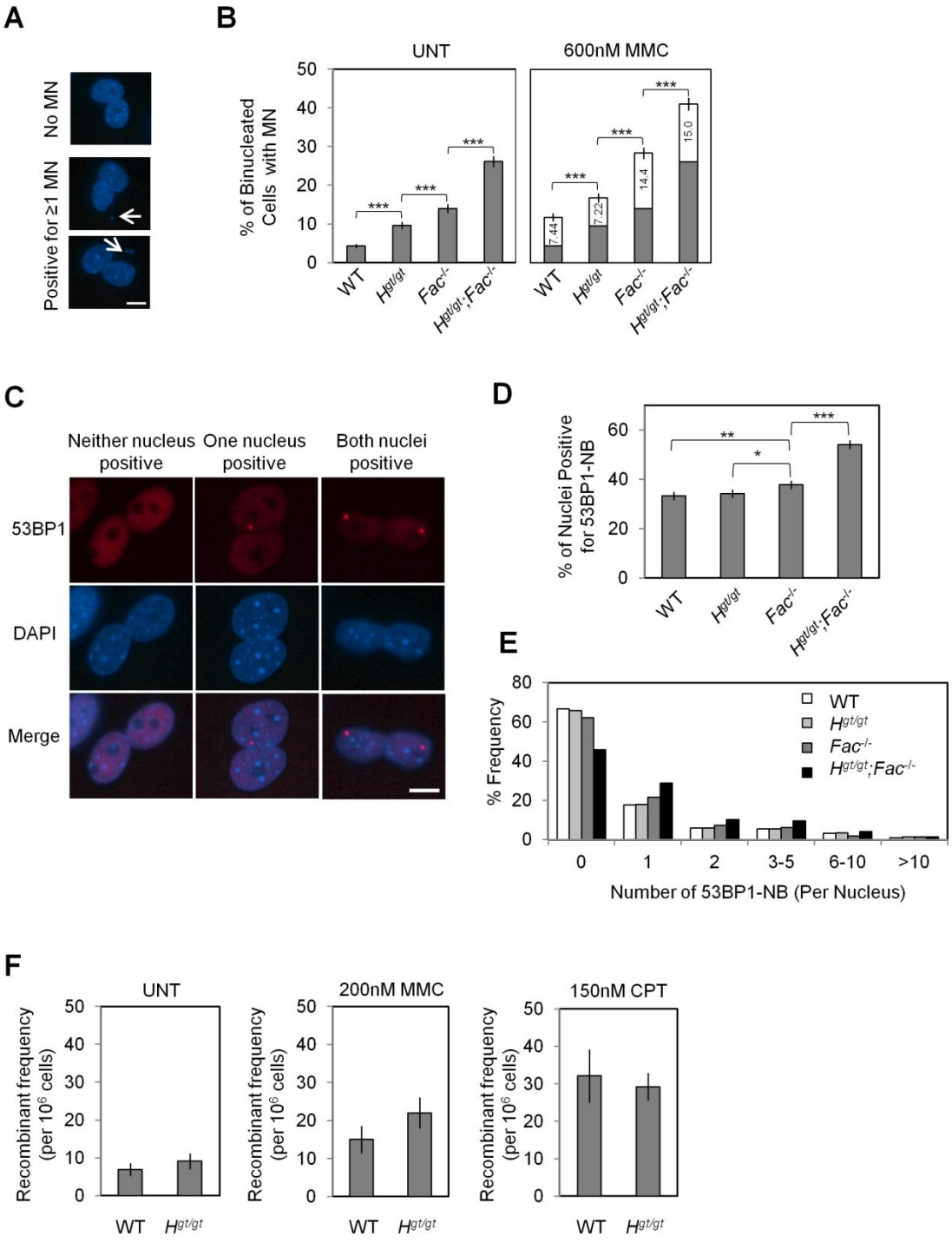
A
No MN
Positive for ≥1 MN
B
UNT
600nM MMC
% of Binucleated Cells with MN
WT
Hgt/gt
Fac-/-
Hgt/gt;Fac-/-
7.44
7.22
14.4
15.0
C
Neither nucleus positive
One nucleus positive
Both nuclei positive
53BP1
DAPI
Merge
D
% of Nuclei Positive for 53BP1-NB
E
% Frequency
Number of 53BP1-NB (Per Nucleus)
F
Recombinant frequency (per 10^6 cells)
UNT
200nM MMC
150nM CPT

Supplementary table and figure legends

Supplementary Table S1

Helq$^{gt/gt}$ males are fertile, producing about the same average litter size as *Helq*$^{gt/+}$ males.

Supplementary Table S2

Helq$^{gt/gt}$ mice are born in the expected Mendelian ratio but *Fancc*$^{-/-}$ mice show sub-lethality.

Supplementary Figure S1

Structure of the *Helq*^{gt} allele. (A) A diagram (drawn to scale) depicting the insertion of the gene-trap vector (pGT0Lxf) into the mouse *Helq* locus is shown. Exons are shown as rectangles and the coding region is filled with black. The region corresponding to the DEAD/DEAH box is indicated by the thick double-sided arrow. The gene-trap vector consists of the En2 (engrail 2) intron and the subsequent splice acceptor site (SA), as well as a β-Geo reporter gene followed by a polyadenylation signal (pA). (B) PCR using genomic DNA from *Helq*$^{gt/gt}$ mice reveals the insertion of the gene-trap vector (8.6kb) within the intron between exons 11-12. Sequencing chromatograms are shown with the shaded area highlighting sequence from the vector. Primer pairs p1 & p3 and p5 & p6 indicated in (A) were used to map the beginning and end of the insertion, respectively. Right after the end of the vector insertion, a 13-bp sequence in the intron was replaced

with an 8-bp sequence of unknown origin. (C) RT-PCR on total RNA from testes shows the presence of the wildtype (with exons 11 and 12) and chimeric transcripts. The sequencing chromatogram on the left is sequence from the wildtype transcript showing the junction between exons 11 and 12 (amplified with primers p1 and p2). On the right is the sequence of the junction between exon 11 and the vector amplified using primers p1 and p4. Shaded areas indicate the end of the exon 11 sequence. Information on all primers is available upon request.

Supplementary Figure S2

Helq$^{gt/gt}$ mice are normal in size but display a significant reduction in testes size. (A) Shown are the average body weights of mice from the four genotypes at the age of testes analysis (6 weeks of age). (B) Shown is the average testes weight as a percentage of total body weight for the four genotypes. Bars in (A) and (B) show the SEMs for ≥ 5 mice. Statistical significance (determined by t-test) at $p<0.05$, $p<0.01$ and $p<0.001$ are indicated as *, ** and **, respectively. WT, *H*$^{gt/gt}$, *Fac*$^{-/-}$, *H*$^{gt/gt}$*;Fac*$^{-/-}$ refers to wildtype, *Helq*$^{gt/gt}$, *Fancc*$^{-/-}$, *Helq*$^{gt/gt}$*;Fancc*$^{-/-}$, respectively. (C) The mosaic pattern of seminiferous tubules is more apparent in testes of *Helq*$^{gt/gt}$ mice at 3 weeks of age. Shown are H&E images of whole testis (top) and seminiferous tubules (bottom) from widltype (WT) and *Helq*$^{gt/gt}$ mice. Scale bars are 1500 μm for the whole testis sections and 75 μm for the enlarged images.

Supplementary Figure S3

Helq$^{gt/gt}$ cells show normal levels of FANCD2 and FANCI focus formation in prophase. Shown are the average percentages of cells positive for ≥2 FANCD2 (A) or FANCI (B) foci at prophase. Prophase cells were identified as those which displayed bright staining for phospho-Histone H3 (Ser10) and had not yet proceeded to prometaphase. APH treatment was 150 nM for 24 hrs. MMC treatment was 1.2 μM for 2 hrs followed by 22-hr recovery in fresh media. Experiments were repeated twice with different MEF lines. At least 140 prophases were scored per experimental group. Bars show the binomial error for the combined data set.

Supplementary Figure S4

HELQ depletion causes only mild MMC sensitivity compared to FA core complex-depletion/deficiency in human cell lines. (A) Western blotting shows that siRNA pools targeting HELQ (siHELQ) and/or FANCA (siFANCA) efficiently deplete HELQ and FANCA, respectively, to sub-detectable levels in HEK 293T cells, while a control siRNA pool (siCONT) has no effect. (B) Depletion of HELQ does not confer MMC hypersensitivity in HEK 293T cells. Shown are the results of two independently performed colony formation assays at the indicated doses of MMC. Treatment with MMC was for 2 hours, followed by a one-week culture period. (C) Shown are representative images of metaphase spreads from HEK 293T cells following 24 hours treatment with 300nM MMC. Enlarged images show representative radial structures

observed in the siFANCA (bottom left) and siHELQ;siFANCA (bottom right) samples. Scale bar is 10 μm. (D) FANCA depletion, but not HELQ depletion, leads to a statistically significant increase in metaphase chromosomal aberrations in response to MMC. Shown are the average percentages of metaphases positive for chromosomal aberrations (top) or radial structures (middle). The average number of aberrations per metaphase is shown at bottom. At least 40 metaphases were scored per experimental group. (E) siHELQ efficiently depletes HELQ to sub-detectable levels in the PD331 (or PD331+FANCC complemented) cell lines, while siCONT has no effect. (F) Depletion of HELQ confers modest MMC hypersensitivity in the PD331+FANCC cell line. Shown are the results of two independently performed colony formation assays at the indicated doses of MMC. Treatment with MMC was for 2 hours, followed by a two-week culture period. (G) An MTT assay reveals that HELQ depletion further decreases the proliferation of PD331 (*FANCC*-deficient) cells, suggesting non-epistasis between *HELQ* and *FANCC*. MMC treatment was for 5 days at the indicated doses. A stained membrane was used as a loading control in (A,E). Error bars in (B, F, G) show the SEMs for at least three independent experiments while those in (D) indicate the binomial error. Statistical significance was determined by either t-test (B, F, G) or χ^2-test (D). Significance at $p<0.01$ and $p<0.001$ are indicated as ** and ***, respectively.

Supplementary Figure S5

(A) A diagram depicting the DNA fiber assay is shown. In this assay, ongoing replication forks are observed via the sequential incorporation of digoxigenin- (red) or biotin (green)-conjugated dUTPs. Fork speed measurements are then made by measuring the distance between the start of the red tract to the start of the green tract. (B) The distributions of fork speed values for the four genotypes are shown. Slightly different patterns between the four genotypes result in statistically significant differences as measured by Kolmogorov-Smirnov test. (p<0.001 indicated as ***). WT, $H^{gt/gt}$, $Fac^{-/-}$, $H^{gt/gt}$;$Fac^{-/-}$ refers to wildtype, $Helq^{gt/gt}$, $Fancc^{-/-}$, $Helq^{gt/gt}$;$Fancc^{-/-}$, respectively.

Supplementary Figure S6

(A) qRT-PCR analysis using total RNA reveals that siHELQ was able to efficiently deplete both the wildtype *Helq* transcript (E 11-12, top) in wildtype MEFs as well as the chimeric mutant transcript (Chimeric, bottom) in $Helq^{gt/gt}$ MEFs by ~70% compared to siCONT-treated cells. Experiments were duplicated using RNA samples from different MEF lines to confirm reproducibility. A representative qRT-PCR data set is shown. (B) Western blotting shows that siHELQ depletes HELQ or $HELQ^{\Delta}$-β-Geo to sub-detectable levels in wildtype or $Helq^{gt/gt}$ MEFs, respectively. A stained membrane was used as a loading control. (C) Depletion of $HELQ^{\Delta}$-β-Geo does not have any effect on the levels of spontaneous MN in $Helq^{gt/gt}$ MEFs. The average percentages of binucleated cells positive for MN are shown. Experiments were repeated using different MEF lines so that

600 cells were observed per experimental group. (D) Shown are representative images of binucleated cells with MN (stained with DAPI, blue) that are either positive for CENP-A staining (CENP-A+, red) or negative for CENP-A staining (CENP-A-). White arrows point to MN. Scale bar is 10 μm. (E) Compared to WT cells, *Helq*$^{gt/gt}$, *Fancc*$^{-/-}$ and *Helq*$^{gt/gt}$*;Fancc*$^{-/-}$ cells display an increase in both types of MN in untreated conditions (left), but an increase of CENP-A- MN in *Helq*$^{gt/gt}$ cells is not statistically significant. MMC treatment (600 nM for 2 hrs followed by 22-hr recovery) leads primarily to a higher number of CENP-A- MN (right). (F) The average percentages of binucleated cells positive for MN are shown after CPT treatment (250nM for 6 hrs followed by 18-hr recovery). The levels for the untreated condition are duplicated on the right in gray for better comparison. Numbers in the white box show the increase above untreated conditions. Experiments were repeated at least three times using different MEF lines so that >600 cells were observed per experimental group. Error bars in (C, E, F) show the binomial error for the combined data set. Significance (determined by χ^2-test) at $p<0.05$, $p<0.01$, and $p<0.001$ are indicated as *, ** and ***, respectively. WT, *H*$^{gt/gt}$, *Fac*$^{-/-}$ and *H*$^{gt/gt}$*;Fac*$^{-/-}$ refer to wildtype, *Helq*$^{gt/gt}$, *Fancc*$^{-/-}$, and *Helq*$^{gt/gt}$*;Fancc*$^{-/-}$ respectively.

Supplementary Figure S7

Helq$^{gt/gt}$ cells do not display any significant changes in recombinant frequencies at the *FYDR* locus compared to wildtype cells. (A) The *FYDR* transgenic locus contains two tandem repeats of incomplete eYFP expression cassettes (jagged lines indicate deleted

sequence information). An HR event at this locus can restore eYFP expression following either of two different methods of resolution: gene conversion as the result of a non-crossover event (top) or unequal sister chromatid exchange as the result of a crossover (bottom). Using wildtype and *Helq*$^{gt/gt}$ MEFs that carry this locus in the hemizygous state allows for the detection of HR events only during and/or after this locus has replicated. (B) Shown are sample flow cytometry plots from wildtype *FYDR* non-carrier MEFs (left) and wildtype hemizygous *FYDR* carrier MEFs (right). eYFP signals were detected using the FL1-H and FL2-H channels and counted using the "R2" gate. (C) The distributions of the number of eYFP^{+} recombinants (per 10^{6} cells analyzed) from are shown. Two samples were excluded from the data as outliers (number of recombinants in the untreated condition >25).

Supplementary Table S1 Luebben et al., 2013

Cross	Number of pairs	Number of litters	Average litter size
Helq$^{gt/+}$ female x *Helq*$^{gt/+}$ male	4	5	7.6±0.75*
Helq$^{gt/+}$ female x *Helq*$^{gt/gt}$ male	6	15	6.3±0.62*

*No significant difference was observed between the average litter sizes by t-test.

Supplementary Table S2 Luebben et al., 2013

Genotype	*Fancc*$^{+/+}$ or *Fancc*$^{+/-}$	*Fancc*$^{-/-}$	Total number	Expected number
Helq$^{gt/+}$	40	10	50	52.5
Helq$^{gt/gt}$	48	7	55	52.5
Total number	88	17*	105	
Expected number	78.75	26.25*		

* The observed number of 17 was significantly different from the expected number of 26.25 ($p<0.05$ χ^2-test).

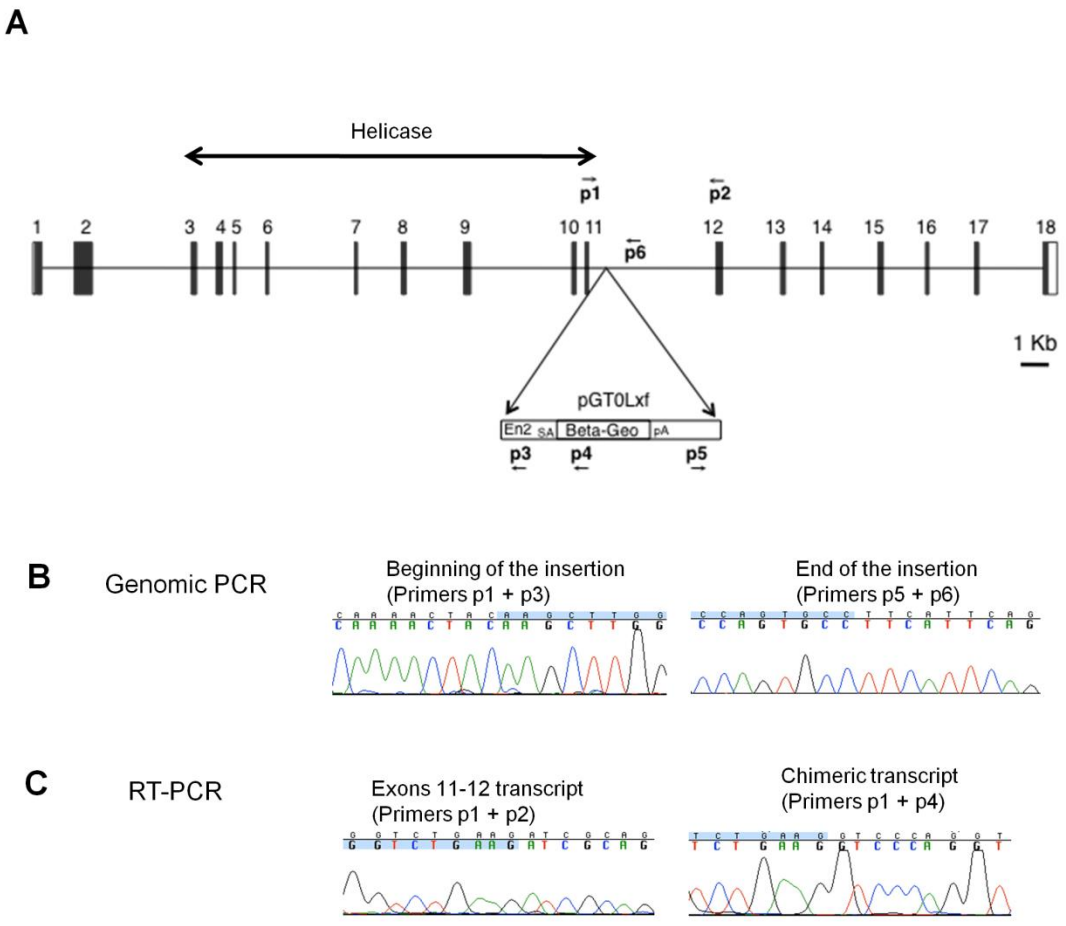
A
Helicase
p1
p2
1 2 3 4 5 6 7 8 9 10 11 12 13 14 15 16 17 18
p6
1 Kb
pGT0Lxf
En2 SA
Beta-Geo
pA
p3
p4
p5
B
Genomic PCR
Beginning of the insertion
(Primers p1 + p3)
End of the insertion
(Primers p5 + p6)
C
RT-PCR
Exons 11-12 transcript
(Primers p1 + p2)
Chimeric transcript
(Primers p1 + p4)

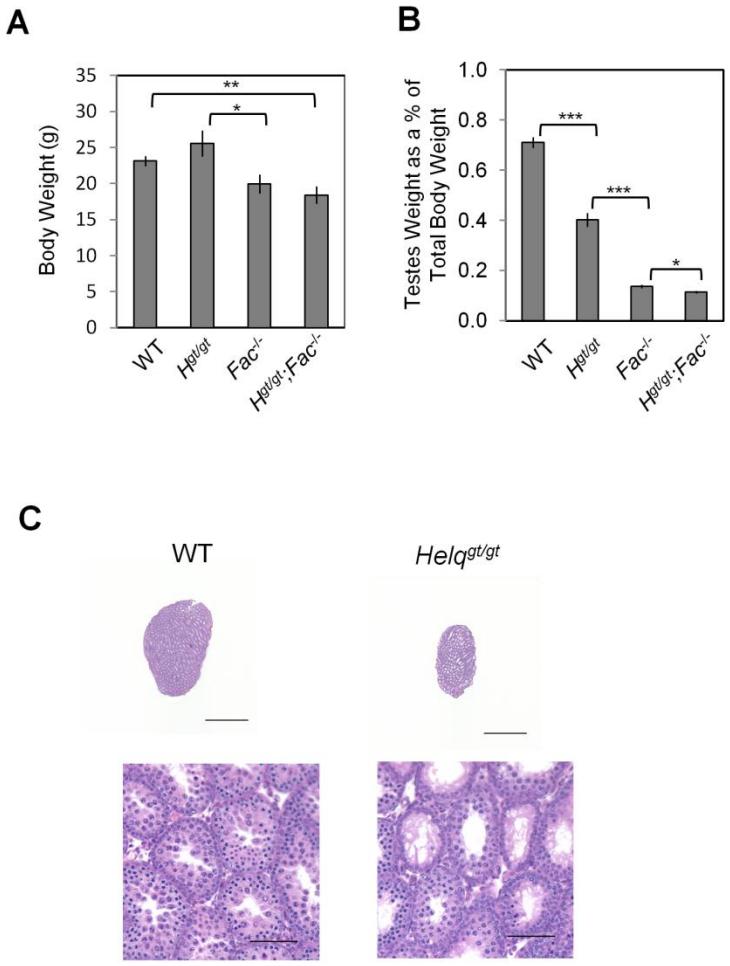
A
Body Weight (g)
35
30
25
20
15
10
5
0
**
*
WT
Hgt/gt
Fac-/-
Hgt/gt;Fac-/-
B
Testes Weight as a % of Total Body Weight
1.0
0.8
0.6
0.4
0.2
0.0
***
***
*
WT
Hgt/gt
Fac-/-
Hgt/gt;Fac-/-
C
WT
Helqgt/gt

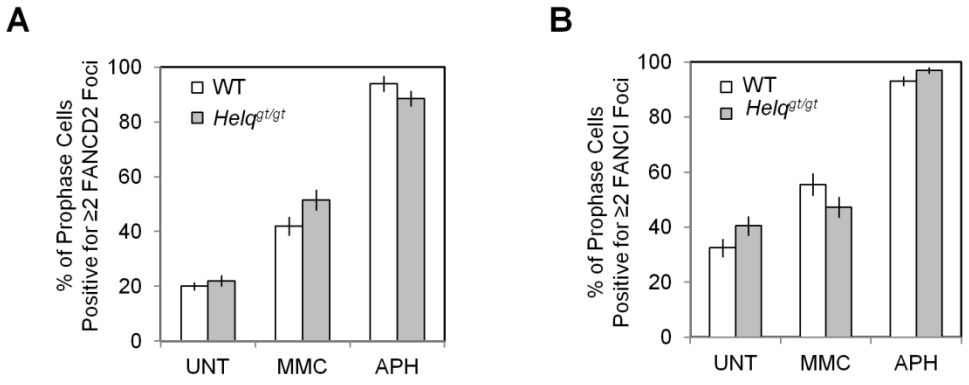
A
% of Prophase Cells
Positive for ≥2 FANCD2 Foci
100
80
60
40
20
0
WT
Helq gt/gt
UNT
MMC
APH
B
% of Prophase Cells
Positive for ≥2 FANCI Foci
100
80
60
40
20
0
WT
Helq gt/gt
UNT
MMC
APH

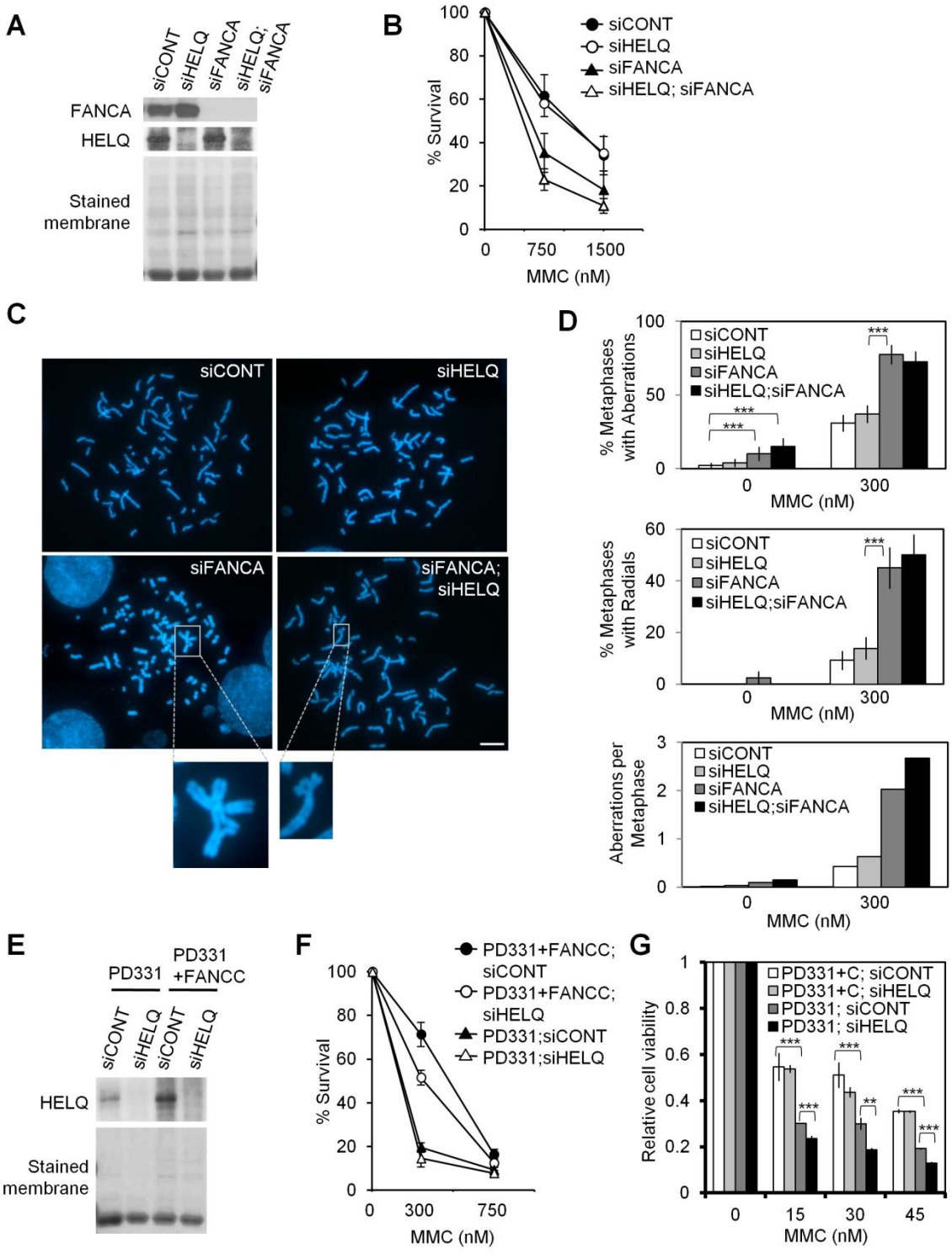
A
siCONT
siHELQ
siFANCA
siHELQ; siFANCA
FANCA
HELQ
Stained membrane
B
siCONT
siHELQ
siFANCA
siHELQ; siFANCA
% Survival
MMC (nM)
C
siCONT
siHELQ
siFANCA
siFANCA; siHELQ
D
% Metaphases with Aberrations
% Metaphases with Radials
Aberrations per Metaphase
siCONT
siHELQ
siFANCA
siHELQ;siFANCA
MMC (nM)
E
PD331
PD331 +FANCC
siCONT
siHELQ
HELQ
Stained membrane
F
PD331+FANCC; siCONT
PD331+FANCC; siHELQ
PD331;siCONT
PD331;siHELQ
% Survival
MMC (nM)
G
PD331+C; siCONT
PD331+C; siHELQ
PD331; siCONT
PD331; siHELQ
Relative cell viability
MMC (nM)

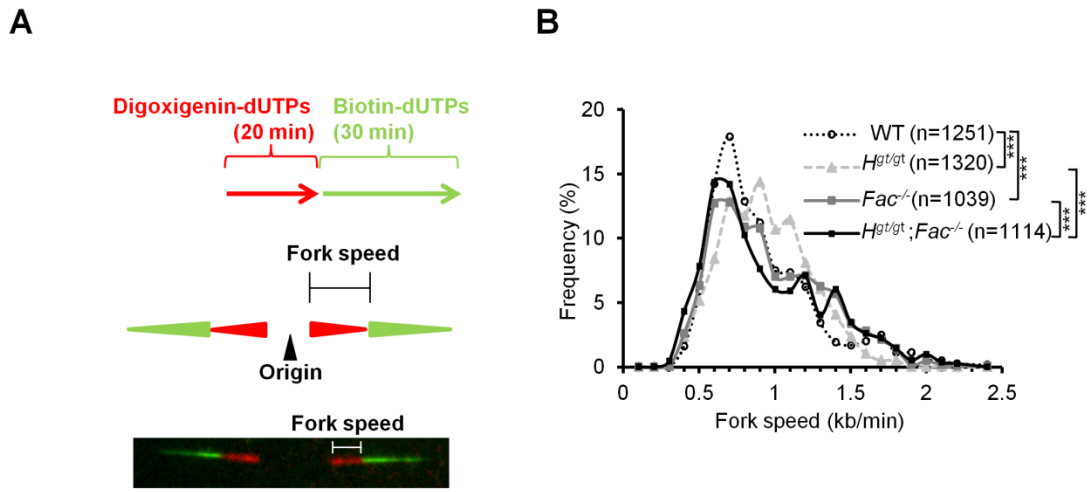
A
Digoxigenin-dUTPs
(20 min)
Biotin-dUTPs
(30 min)
Fork speed
Origin
Fork speed
B
WT (n=1251)
Hgt/gt (n=1320)
Fac-/- (n=1039)
Hgt/gt;Fac-/- (n=1114)
***
***
***
***
Frequency (%)
20
15
10
5
0
0
0.5
1
1.5
2
2.5
Fork speed (kb/min)

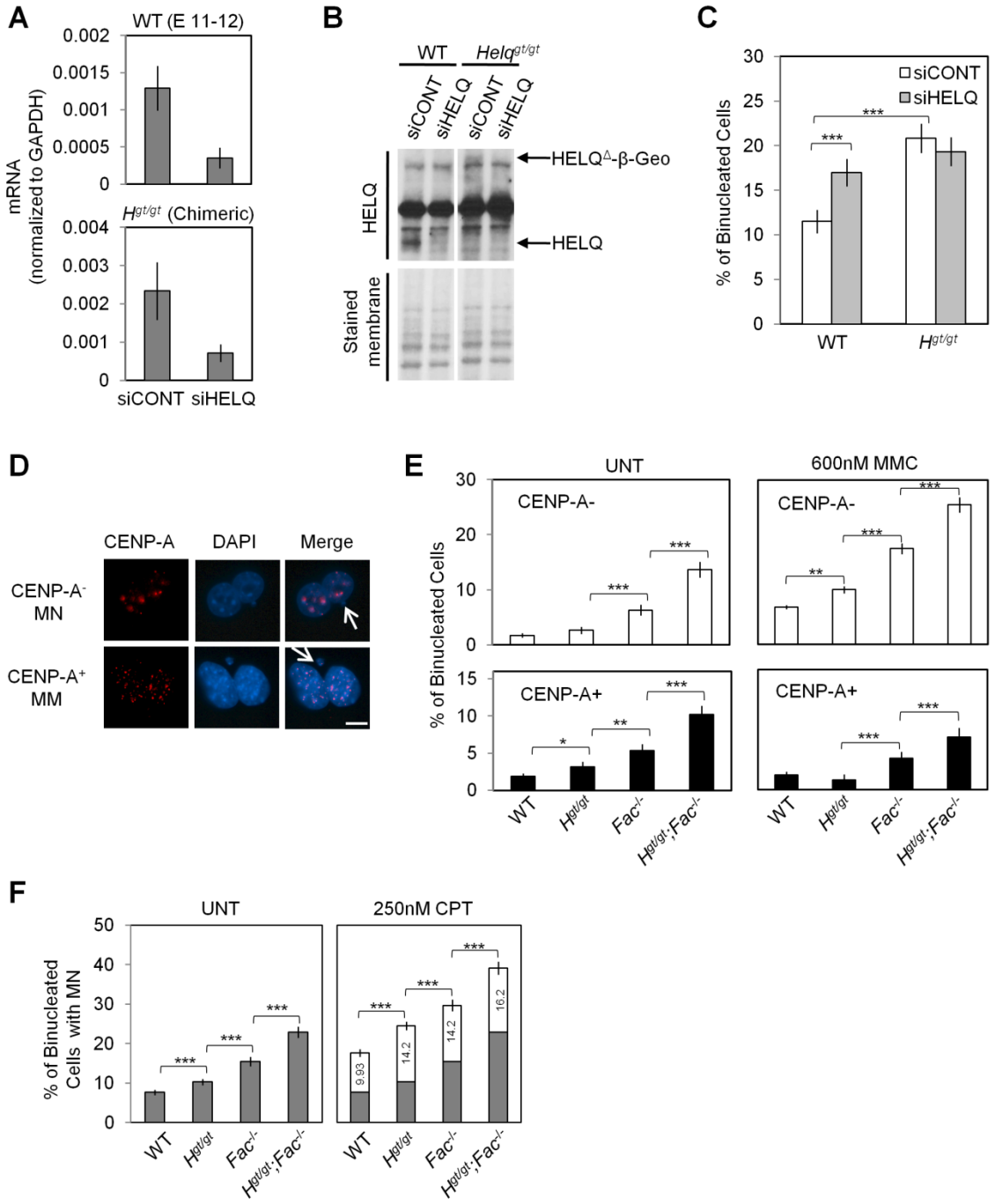
A
WT (E 11-12)
mRNA (normalized to GAPDH)
0.002
0.0015
0.001
0.0005
0
Hgt/gt (Chimeric)
0.004
0.003
0.002
0.001
0
siCONT siHELQ
B
WT
Helqgt/gt
siCONT siHELQ siCONT siHELQ
HELQ
HELQΔ-β-Geo
HELQ
Stained membrane
C
% of Binucleated Cells
siCONT
siHELQ
WT
Hgt/gt
D
CENP-A DAPI Merge
CENP-A- MN
CENP-A+ MM
E
UNT
600nM MMC
CENP-A-
CENP-A+
% of Binucleated Cells
WT
Hgt/gt
Fac-/-
Hgt/gt;Fac-/-
F
UNT
250nM CPT
% of Binucleated Cells with MN
9.93
14.2
14.2
16.2

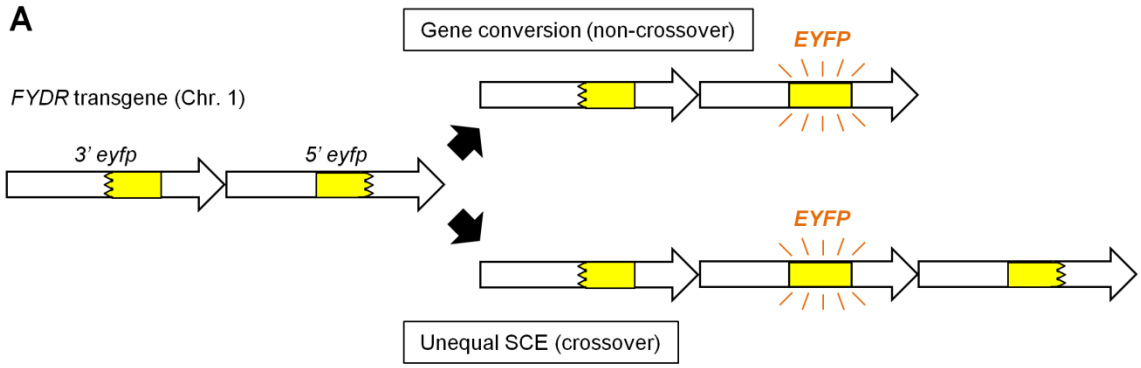
A
Gene conversion (non-crossover)
EYFP
FYDR transgene (Chr. 1)
3' eyfp
5' eyfp
EYFP
Unequal SCE (crossover)

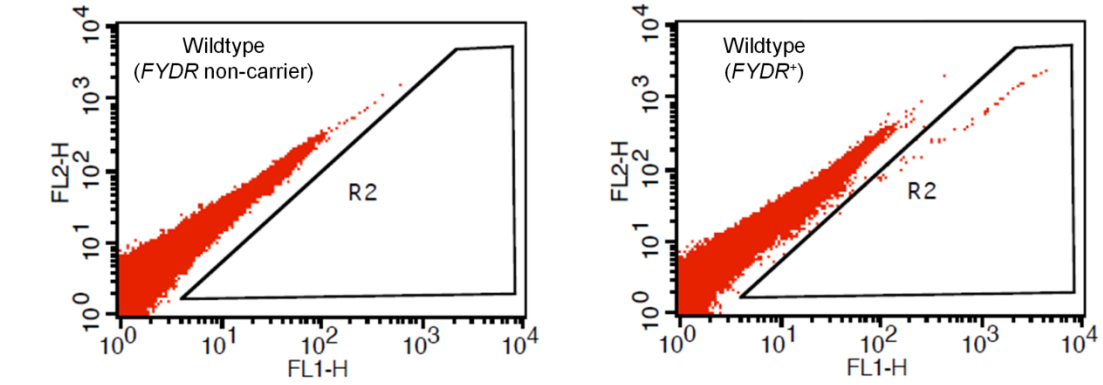
B
Wildtype
(FYDR non-carrier)
R2
FL2-H
FL1-H
Wildtype
(FYDR+)
R2
FL2-H
FL1-H

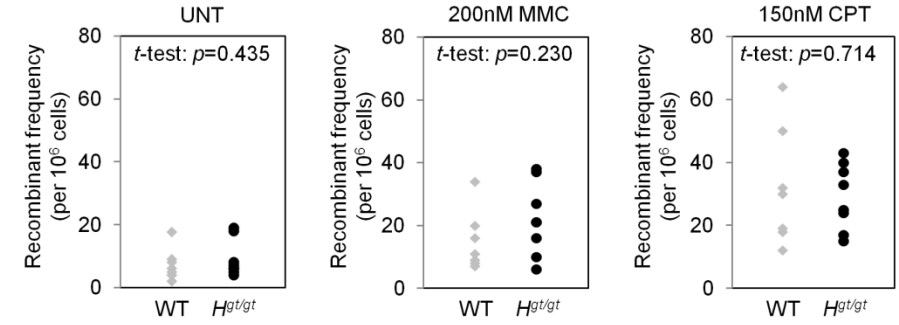
C
UNT
t-test: p=0.435
200nM MMC
t-test: p=0.230
150nM CPT
t-test: p=0.714
Recombinant frequency (per 10^6 cells)
WT
Hgt/gt

References

1 Ciccia, A. & Elledge, S. J. The DNA Damage Response: Making It Safe to Play with Knives. *Molecular Cell* **40**, 179-204 (2010).

2 Branzei, D. & Foiani, M. Maintaining genome stability at the replication fork. *Nat Rev Mol Cell Biol* **11**, 208-219 (2010).

3 Blow, J. J. & Ge, X. Q. A model for DNA replication showing how dormant origins safeguard against replication fork failure. *EMBO Rep* **10**, 406-412 (2009).

4 Petermann, E. & Helleday, T. Pathways of mammalian replication fork restart. *Nat Rev Mol Cell Biol* **11**, 683-687 (2010).

5 Sale, J. E., Lehmann, A. R. & Woodgate, R. Y-family DNA polymerases and their role in tolerance of cellular DNA damage. *Nat Rev Mol Cell Biol* **13**, 141-152 (2012).

6 Kim, H. & D'Andrea, A. D. Regulation of DNA cross-link repair by the Fanconi anemia/BRCA pathway. *Genes Dev* **26**, 1393-1408 (2012).

7 Kottemann, M. C. & Smogorzewska, A. Fanconi anaemia and the repair of Watson and Crick DNA crosslinks. *Nature* **493**, 356-363 (2013).

8 Crossan, G. P. & Patel, K. J. The Fanconi anaemia pathway orchestrates incisions at sites of crosslinked DNA. *The Journal of Pathology* **226**, 326-337 (2012).

9 Kee, Y. & D'Andrea, A. D. Expanded roles of the Fanconi anemia pathway in preserving genomic stability. *Genes & Development* **24**, 1680-1694 (2010).

10 Marini, F. & Wood, R. D. A Human DNA Helicase Homologous to the DNA Cross-link Sensitivity Protein Mus308. *Journal of Biological Chemistry* **277**, 8716-8723 (2002).

11 Boyd, J. B., Sakaguchi, K. & Harris, P. V. mus308 mutants of Drosophila exhibit hypersensitivity to DNA cross-linking agents and are defective in a deoxyribonuclease. *Genetics* **125**, 813-819 (1990).

12 Leonhardt, E. A., Henderson, D. S., Rinehart, J. E. & Boyd, J. B. Characterization of the mus308 gene in Drosophila melanogaster. *Genetics* **133**, 87-96 (1993).

13 Shima, N., Munroe, R. J. & Schimenti, J. C. The Mouse Genomic Instability Mutation chaos1 Is an Allele of Polq That Exhibits Genetic Interaction with Atm. *Molecular and Cellular Biology* **24**, 10381-10389 (2004).

14 Yoshimura, M. *et al.* Vertebrate POLQ and POLβ Cooperate in Base Excision Repair of Oxidative DNA Damage. *Molecular Cell* **24**, 115-125 (2006).

15 Yousefzadeh, M. J. & Wood, R. D. DNA polymerase POLQ and cellular defense against DNA damage. *DNA Repair (Amst)* **12**, 1-9 (2013).

16 Harris, P. V. *et al.* Molecular cloning of Drosophila mus308, a gene involved in DNA cross-link repair with homology to prokaryotic DNA polymerase I genes. *Mol Cell Biol* **16**, 5764-5771 (1996).

17 Seki, M., Marini, F. & Wood, R. D. POLQ (Pol theta), a DNA polymerase and DNA-dependent ATPase in human cells. *Nucleic Acids Res* **31**, 6117-6126 (2003).

18 Shima, N. *et al.* Phenotype-based identification of mouse chromosome instability mutants. *Genetics* **163**, 1031-1040 (2003).

19 Laurencon, A. *et al.* A large-scale screen for mutagen-sensitive loci in Drosophila. *Genetics* **167**, 217-231, doi:167/1/217 (2004).

20 McCaffrey, R., St Johnston, D. & González-Reyes, A. Drosophila mus301/spindle-C Encodes a Helicase With an Essential Role in Double-Strand DNA Break Repair and Meiotic Progression. *Genetics* **174**, 1273-1285 (2006).

21 Ward, J. D. *et al.* Overlapping Mechanisms Promote Postsynaptic RAD-51 Filament Disassembly during Meiotic Double-Strand Break Repair. *Molecular Cell* **37**, 259-272 (2010).

22 Marini, F., Kim, N., Schuffert, A. & Wood, R. D. POLN, a nuclear PolA family DNA polymerase homologous to the DNA cross-link sensitivity protein Mus308. *J Biol Chem* **278**, 32014-32019 (2003).

23 Tafel, A. A., Wu, L. & McHugh, P. J. Human HEL308 Localizes to Damaged Replication Forks and Unwinds Lagging Strand Structures. *Journal of Biological Chemistry* **286**, 15832-15840 (2011).

24 Muzzini, D. M., Plevani, P., Boulton, S. J., Cassata, G. & Marini, F. Caenorhabditis elegans POLQ-1 and HEL-308 function in two distinct DNA interstrand cross-link repair pathways. *DNA Repair* **7**, 941-950 (2008).

25 Garcia-Higuera, I. *et al.* Interaction of the Fanconi Anemia Proteins and BRCA1 in a Common Pathway. *Molecular Cell* **7**, 249-262 (2001).

26 Youds, J. L., Barber, L. J. & Boulton, S. J. C. elegans: A model of Fanconi anemia and ICL repair. *Mutation Research/Fundamental and Molecular Mechanisms of Mutagenesis* **668**, 103-116 (2009).

27 Moldovan, G.-L. *et al.* DNA Polymerase POLN Participates in Cross-Link Repair and Homologous Recombination. *Molecular and Cellular Biology* **30**, 1088-1096 (2010).

28 Whitney, M. *et al.* Germ cell defects and hematopoietic hypersensitivity to gamma- interferon in mice with a targeted disruption of the Fanconi anemia C gene. *Blood* **88**, 49-58 (1996).

29 Kawabata, T. *et al.* Stalled fork rescue via dormant replication origins in unchallenged S phase promotes proper chromosome segregation and tumor suppression. *Molecular Cell* **41**, 543-553 (2011).

30 Sugimura, K., Takebayashi, S.-i., Ogata, S., Taguchi, H. & Okumura, K. Non-Denaturing Fluorescence in Situ Hybridization to Find Replication Origins in a Specific Genome Region on the DNA Fiber. *Bioscience, Biotechnology, and Biochemistry* **71**, 627-632 (2007).

31 Fenech, M. Cytokinesis-block micronucleus cytome assay. *Nat. Protocols* **2**, 1084-1104 (2007).

32 Hendricks, C. A. *et al.* Spontaneous mitotic homologous recombination at an enhanced yellow fluorescent protein (EYFP) cDNA direct repeat in transgenic mice. *Proc Natl Acad Sci U S A* **100**, 6325-6330 (2003).

33 Stryke, D. *et al.* BayGenomics: a resource of insertional mutations in mouse embryonic stem cells. *Nucleic Acids Research* **31**, 278-281 (2003).

34 Stanford, W. L., Cohn, J. B. & Cordes, S. P. Gene-trap mutagenesis: past, present and beyond. *Nat Rev Genet* **2**, 756-768 (2001).

35 Fujikane, R., Komori, K., Shinagawa, H. & Ishino, Y. Identification of a Novel Helicase Activity Unwinding Branched DNAs from the Hyperthermophilic Archaeon, Pyrococcus furiosus. *Journal of Biological Chemistry* **280**, 12351-12358 (2005).

36 Buttner, K., Nehring, S. & Hopfner, K. P. Structural basis for DNA duplex separation by a superfamily-2 helicase. *Nat Struct Mol Biol* **14**, 647-652 (2007).

37 Woodman, I. L., Briggs, G. S. & Bolt, E. L. Archaeal Hel308 Domain V Couples DNA Binding to ATP Hydrolysis and Positions DNA for Unwinding Over the Helicase Ratchet. *Journal of Molecular Biology* **374**, 1139-1144 (2007).

38 Richards, J. D. *et al.* Structure of the DNA Repair Helicase Hel308 Reveals DNA Binding and Autoinhibitory Domains. *Journal of Biological Chemistry* **283**, 5118-5126 (2008).

39 Parmar, K., D'Andrea, A. & Niedernhofer, L. J. Mouse models of Fanconi anemia. *Mutation Research/Fundamental and Molecular Mechanisms of Mutagenesis* **668**, 133-140 (2009).

40 Wong, J. C. Y. *et al.* Targeted disruption of exons 1 to 6 of the Fanconi Anemia group A gene leads to growth retardation, strain-specific microphthalmia, meiotic defects and primordial germ cell hypoplasia. *Human Molecular Genetics* **12**, 2063-2076 (2003).

41 Agoulnik, A. I. *et al.* A novel gene, Pog, is necessary for primordial germ cell proliferation in the mouse and underlies the germ cell deficient mutation, gcd. *Human Molecular Genetics* **11**, 3047-3053 (2002).

42 Lu, B. & Bishop, C. E. Late Onset of Spermatogenesis and Gain of Fertility in POG-Deficient Mice Indicate that POG Is Not Necessary for the Proliferation of Spermatogonia. *Biology of Reproduction* **69**, 161-168 (2003).

43 Yang, Y. *et al.* Targeted disruption of the murine Fanconi anemia gene,Fancg/Xrcc9. *Blood* **98**, 3435-3440 (2001).

44 Crossan, G. P. *et al.* Disruption of mouse Slx4, a regulator of structure-specific nucleases, phenocopies Fanconi anemia. *Nat Genet* **43**, 147-152 (2011).

45 Holloway, J. K. *et al.* Mammalian BTBD12 (SLX4) protects against genomic instability during mammalian spermatogenesis. *PLoS Genet* **7**, e1002094 (2011).

46 Bakker, S. T. *et al.* Fancm-deficient mice reveal unique features of Fanconi anemia complementation group M. *Human Molecular Genetics* **18**, 3484-3495, doi:10.1093/hmg/ddp297 (2009).

47 Bakker, S. T. *et al.* Fancf-deficient mice are prone to develop ovarian tumours. *J Pathol* **226**, 28-39, doi:10.1002/path.2992 (2012).

48 Houghtaling, S. *et al.* Epithelial cancer in Fanconi anemia complementation group D2 (Fancd2) knockout mice. *Genes & Development* **17**, 2021-2035 (2003).

49 Chen, M. *et al.* Inactivation of Fac in mice produces inducible chromosomal instability and reduced fertility reminiscent of Fanconi anaemia. *Nat Genet* **12**, 448-451 (1996).

50 Noll, M. *et al.* Fanconi anemia group A and C double-mutant mice: Functional evidence for a multi-protein Fanconi anemia complex. *Experimental Hematology* **30**, 679-688 (2002).

51 Nadler, J. J. & Braun, R. E. Fanconi anemia complementation group C is required for proliferation of murine primordial germ cells. *Genesis* **27**, 117-123 (2000).

52 Carreau, M. Not-so-novel phenotypes in the Fanconi anemia group D2 mouse model. *Blood* **103**, 2430 (2004).

53 Freie, B. *et al.* Fanconi anemia type C and p53 cooperate in apoptosis and tumorigenesis. *Blood* **102**, 4146-4152 (2003).

54 Howlett, N. G., Taniguchi, T., Durkin, S. G., D'Andrea, A. D. & Glover, T. W. The Fanconi anemia pathway is required for the DNA replication stress response and for the regulation of common fragile site stability. *Hum Mol Genet* **14**, 693-701 (2005).

55 Chan, K. L., Palmai-Pallag, T., Ying, S. & Hickson, I. D. Replication stress induces sister-chromatid bridging at fragile site loci in mitosis. *Nat Cell Biol* **11**, 753-760 (2009).

56 Foe, J. R. *et al.* Expression cloning of a cDNA for the major Fanconi anaemia gene, FAA. *Nat Genet* **14**, 488 (1996).

57 Guy, C. P. & Bolt, E. L. Archaeal Hel308 helicase targets replication forks in vivo and in vitro and unwinds lagging strands. *Nucleic Acids Research* **33**, 3678-3690 (2005).

58 Zou, L. & Elledge, S. J. Sensing DNA damage through ATRIP recognition of RPA-ssDNA complexes. *Science* **300**, 1542-1548 (2003).

59 Byun, T. S., Pacek, M., Yee, M. C., Walter, J. C. & Cimprich, K. A. Functional uncoupling of MCM helicase and DNA polymerase activities activates the ATR-dependent checkpoint. *Genes Dev* **19**, 1040-1052 (2005).

60 Rogakou, E. P., Pilch, D. R., Orr, A. H., Ivanova, V. S. & Bonner, W. M. DNA double-stranded breaks induce histone H2AX phosphorylation on serine 139. *J Biol Chem* **273**, 5858-5868 (1998).

61 Naim, V. & Rosselli, F. The FANC pathway and BLM collaborate during mitosis to prevent micro-nucleation and chromosome abnormalities. *Nat Cell Biol* **11**, 761-768 (2009).

62 Howman, E. V. *et al.* Early disruption of centromeric chromatin organization in centromere protein A (Cenpa) null mice. *Proc Natl Acad Sci U S A* **97**, 1148-1153 (2000).

63 Lukas, C. *et al.* 53BP1 nuclear bodies form around DNA lesions generated by mitotic transmission of chromosomes under replication stress. *Nat Cell Biol* **13**, 243-253 (2011).

64 Harrigan, J. A. *et al.* Replication stress induces 53BP1-containing OPT domains in G1 cells. *The Journal of Cell Biology* **193**, 97-108 (2011).

65 Howlett, N. G. *et al.* Biallelic Inactivation of BRCA2 in Fanconi Anemia. *Science* **297**, 606-609 (2002).

66 Reid, S. *et al.* Biallelic mutations in PALB2 cause Fanconi anemia subtype FA-N and predispose to childhood cancer. *Nat Genet* **39**, 162-164 (2007).

67 van de Vrugt, H. J. *et al.* Evidence for complete epistasis of null mutations in murine Fanconi anemia genes Fanca and Fancg. *DNA Repair* **10**, 1252-1261 (2011).

68 Kitao, H. *et al.* Functional Interplay between BRCA2/FancD1 and FancC in DNA Repair. *Journal of Biological Chemistry* **281**, 21312-21320 (2006).

69 Friedberg, E. C. & Meira, L. B. Database of mouse strains carrying targeted mutations in genes affecting biological responses to DNA damage Version 7. *DNA Repair* **5**, 189-209 (2006).

70 Woodman, I. L. & Bolt, E. L. Molecular biology of Hel308 helicase in archaea. *Biochem Soc Trans* **37**, 74-78 (2009).

71 Oyama, T. *et al.* Atomic structures and functional implications of the archaeal RecQ-like helicase Hjm. *BMC Struct Biol* **9**, 2 (2009).

72 Zhang, C. *et al.* Genetic manipulation in Sulfolobus islandicus and functional analysis of DNA repair genes. *Biochem Soc Trans* **41**, 405-410 (2013).

73 Fujikane, R., Shinagawa, H. & Ishino, Y. The archaeal Hjm helicase has recQ-like functions, and may be involved in repair of stalled replication fork. *Genes to Cells* **11**, 99-110 (2006).

74 Li, W.-Q. *et al.* Genetic variants in DNA repair pathway genes and risk of esophageal squamous cell carcinoma and gastric adenocarcinoma in a Chinese population. *Carcinogenesis* **34**, 1536-1542 (2013).

75 Gao, Y. *et al.* Genetic variants at 4q21, 4q23 and 12q24 are associated with esophageal squamous cell carcinoma risk in a Chinese population. *Human Genetics*, 1-8 (2013).

76 Liang, C. *et al.* Gene–environment interactions of novel variants associated with head and neck cancer. *Head & Neck* **34**, 1111-1118 (2012).

77 McKay, J. D. *et al.* A Genome-Wide Association Study of Upper Aerodigestive Tract Cancers Conducted within the INHANCE Consortium. *PLoS Genet* **7**, e1001333 (2011).

CHAPTER V: Final Discussion and Future Directions

Final discussion

Dormant origins, genome instability and cancer

In contrast to previous studies, which suggested that dormant origins are only required under conditions of replicative stress[1-3], our findings using the *Mcm4*^{chaos3} mouse model have clearly shown their integral role in chromosome stability and tumor suppression even in unchallenged conditions. These functions are apparently achieved through two distinct mechanisms. First, dormant origins can be activated adjacent to stalled forks as the simplest form of fork recovery. This role overlaps with several different mechanisms, such as the FA pathway, which work in parallel. Second, dormant origins also preclude the presence of long, origin-poor loci that would otherwise be unable to finish replication prior to mitosis. This function is unique and cannot be fully compensated by other mechanisms.

This latter finding was made possible by closely investigating the intrinsic FA pathway activation that occurs in *Mcm4*$^{chaos3/chaos3}$ cells. In our original study (Kawabata et al., 2011) we assumed that the elevated number of FANCD2 foci in prophase was an indication of persistently stalled forks, as proposed by others[4,5]. However, our later analysis (Luebben et al., 2014) clearly showed that this increase in FANCD2 foci can be attributed solely to those that co-localize with EdU incorporation. This indicates that such sites are very late-replicating rather than completely stalled, and may remain unreplicated before chromosome segregation at anaphase. We interpret this finding such that the ~60% reduction in chromatin-bound MCMs caused by *Mcm4*^{chaos3} homozygosity

results in long stretches of the genome that are devoid of any origins and cannot be replicated except by distant incoming forks.

These observations fit well with a pair of studies showing that fragility at the FRA3B and FRA16C loci is dictated by a paucity of origin initiation events[6] or an inability to activate additional origins following fork stalling[7], respectively. It is thus easy to imagine how *Mcm4*^{chaos3} homozygosity could generate additional "fragile sites" at genomic regions where origin levels are already limiting. Indeed, initial studies characterizing the *Mcm4*^{chaos3} model found a significant increase in chromosome breaks following APH treatment[8]. Based on our findings, it will be important to determine if there is a significant correlation between site-specific fragility and the levels of chromatin-bound MCMs.

Although the *Mcm4*^{chaos3} model represents a unique case, what it has taught us about dormant origins may have major implications toward our understanding of human cancers. It is now understood that oncogene-induced replication stress, which disrupts normal DNA replication kinetics, is a major source of cancer-driving chromosome instability[9]. This includes genetic changes that deregulate the G1/S transition, as seen in the majority of human cancers[10,11]. It may therefore be that an accelerated G1/S transition during the early stages of cancer could leave the chromatin under-licensed[12,13], leading to under-replication as seen in the context of *Mcm4*^{chaos3} homozygosity.

As cancer cells progress into later stages, the expression of MCM proteins is very often upregulated to help them maintain their high proliferative status[14-16]. Meanwhile, in

normal cells, entry into S phase is inhibited by a "licensing checkpoint" only when the number of licensed origins is extremely low (5-10% of normal levels)[17-20]. Putting these ideas together, it is tempting to speculate that an acute, modest reduction in licensing could be used to selectively kill cancer cells. In fact, it has been shown that licensing inhibition can achieve the efficient killing of cancer cells while having negligible effects on normal cells[17,21,22]. Therefore, it seems likely that a temporary, substantial knockdown of MCMs could exploit the replication stress in late-stage cancer cells as an effective therapeutic strategy. We believe the *Mcm4*^{chaos3} model provides a useful model to test this hypothesis.

Finally, it is worth noting that mutations in human *MCM4* were recently found to be responsible for a rare, recessive genetic disorder causing growth retardation, adrenal failure and natural killer cell deficiency[23-25]. Cells derived from these patients were shown to display a higher number of chromosome breaks after treatment with replication inhibitors[25], similar to what was seen in *Mcm4*$^{chaos3/chaos3}$ cells[8]. However, they also exhibited normal levels of chromatin-bound MCMs, suggesting that the causative mutations may confer a very different defect on MCM4 function. We therefore think it is important for these patients to be carefully monitored for cancer development throughout their lifetimes.

A loss of dormant origins reveals roles of the FA pathway in stalled fork recovery and replication completion

To determine the functional significance of the intrinsic FA pathway activation in *Mcm4*$^{chaos3/chaos3}$ cells, we disrupted the FA pathway in this background via a null allele of *Fancc* (*Fancc*$^{-}$). As expected, *Mcm4*$^{chaos3/chaos3}$*;Fancc*$^{-/-}$ double mutant cells revealed a distinct, overlapping function of FANCC in the recovery of spontaneously stalled forks. This function proved to be even more important in the absence of HELQ or upon a reduction in the number of dormant origins, highlighting how cells utilize a multi-layered system to maintain fork progression. Several studies have confirmed the FA pathway's role in protecting stalled forks from breakage and MRE11-mediated degradation[26-28], though how exactly this is achieved remains a mystery. One possibility is that the binding of monoubiquitinated FANCD2/FANCI to stalled forks starting at mid-S phase simply provides a protective function until mitosis. Another possibility is that the FA pathway plays a direct role in fork rescue/restart. For example, the loss of FANCC could compromise the FA core complex's unique role in stimulating efficient TLS[29-31]. Recent work has also revealed that FANCD2 is required for BLM-mediated fork restart[32], though the role of the FA core complex in this process has yet to be determined.

Our studies have brought to light a novel, yet perhaps related function of the FA pathway: replication completion. While recent work by Bergoglio et al. found that FANCD2 foci localized to mitotic EdU spots[33], our study is the first to show that an increased number of EdU spots occurs in prophase cell nuclei when FA pathway activation is compromised. This function was only revealed under conditions of

replicative stress, including a loss of dormant origins or low levels of APH treatment. This could perhaps be a manifestation of the FA core complex's role in recruiting TLS enzymes, as deficiency for Pol η led to a similar increase in mitotic EdU spots[33]. The authors of this study found that this was because Pol η was more efficient at synthesizing past difficult-to-replicate CFS sequences than the replicative polymerases. It could also be that FANCD2 itself plays a yet underappreciated role in the recruitment of TLS enzymes[34]. Finally, it was shown that FANCD2 displays *in vitro* nucleosome-assembly activity in response to ICLs[35]. This function of FANCD2 might allow for replication to resume at late replication intermediates during the G2/M phases. For now, more biochemical studies are needed to determine the precise role(s) of the FA pathway in replication completion.

Finally, two recent studies revealed exciting new information that mitotic FANCD2 foci co-localize with the structure-specific endonucleases MUS81-EME1 and XPF-ERCC1[36,37]. These groups found that down-regulation of these nucleases led to a lack of CFS breaks, and that this paradoxically increased the levels of genomic instability manifesting as MN, anaphase brides, UFBs and 53BP1-NBs. Therefore, it appears that CFS breakage is a programmed cellular event in which unresolved replication intermediates can be enzymatically processed to prevent potentially more severe forms of genomic instability. Seeing as FANCD2 localizes at these sites during mitosis and has been observed to regulate other nucleases[38-42], it might have been easy to imagine the FA pathway as being necessary for this processing. However, it was clearly shown that cells

deficient for *FANCC* had no defect in the mitotic localization of MUS81 or ERCC1[36], indicating that the FA pathway likely doesn't directly regulate this step.

One very important question still remains. How does the role(s) of the FA pathway in replication relate to the clinical phenotypes of FA? Could under-replication be the underlying factor causing bone marrow failure or cancer predisposition? Intriguingly, it is now well-understood that CFSs occur in a cell type-specific manner[6,43], suggesting that cellular differentiation programs might lead to certain chromosomal regions having a lower number of initiation events in certain cell types. Indeed, we observed that double homozygosity for $Mcm4^{chaos3}$ and $Fancc^{-}$ led to extremely high perinatal lethality in an inbred C57BL/6J background, which has an intrinsically lower density of active origins[44]. It is therefore tempting to postulate that perhaps hematopoietic stem cells could have a unique hyper-dependence upon the FA pathway to finish replication, the loss of which triggers cell death and manifests as bone marrow failure. Furthermore, based on the accelerated tumor latency observed in $Mcm4^{chaos3/chaos3}$;$Fancc^{-/-}$ mice, it may be even more likely that this has a role in FA-associated cancers, whereby the cell types in which malignancy originates (e.g. myeloid cells in AML, squamous epithelial cells in head and neck cancers) could also suffer from under-replication in the absence of the FA pathway.

HELQ plays an important role in suppressing replication-associated genome instability

After utilizing the *Helq*^{gt} mouse model to investigate the function of mammalian HELQ, one role that stands out is its requirement for the recovery of spontaneously stalled replication forks. This role proved essential for the suppression of MN and 53BP1-NBs and works in parallel to the FA pathway component FANCC. These findings were in agreement with the study of Adelman et al.[45], who reported that cells derived from the same mouse model (called *Helq*$^{\Delta C/\Delta C}$ in their study) displayed a significantly higher number of MN as well as asymmetric replication tract lengths, a measure of fork stalling events. Because this function can be observed under normal, physiological conditions, it may best explain the hypogonadism phenotype clearly observed by both groups. So while *HELQ* is unlikely to be one of the unassigned complementation groups of FA, it may still have very important roles in human health, such as that described recently for *REV7*[46]. Future studies investigating why certain stem cell types are prone to replication-associated genome instability will be very important to understanding both the role of HELQ and the clinical manifestations of FA.

The roles of HELQ in ICL repair, HR and tumor suppression remain unclear

While Adelman et al. reported on the characterization of the exact same *Helq* mouse model, a third study by Takata et al. investigated the role of human *HELQ* using knockout cell lines[47]. In general, both groups uncovered many findings very similar to ours, including HELQ's role in ICL resistance and germ cell maintenance, with

Helq/*HELQ* being non-epistatic to *Fancd2*/*FANCD2* for either phenotype. In addition to our data, both studies also identified interacting partners of HELQ by mass spectrometry, including ATR, RPA, the FANCD2-FANCI heterodimer and the RAD51 paralogs, which are required for efficient HR[48-51].

Despite these similarities, there were also several discrepancies between these three studies that merit closer examination. First, there were marked differences in the extent to which *Helq*/*HELQ* deficiency was reported to confer ICL hypersensitivity. While we showed that both $Helq^{gt/gt}$ cells as well as *HELQ* siRNA-treated human cells were only modestly sensitive to MMC, Adelman et al. reported striking hypersensitivity in the very same mouse model as well as with siRNA-treated human cells. Using their knockout human cell lines, Takata et al. reported modest hypersensitivities that seem to more closely resemble our findings. Together, it appears that HELQ probably does not play a major role in ICL repair in mammals, acting only as a backup to the FA pathway.

A second major difference can be seen in regards to HELQ's role in HR. Adelman et al. provided multiple lines of evidence to suggest that HELQ is an important HR factor, including the persistence of MMC-induced DSBs in $Helq^{\Delta C/\Delta C}$ cells, reduced HR efficiency in *HELQ* siRNA-treated human cells as measured by a GFP reporter assay and the hypersensitivity of both cell types to poly-ADP ribose polymerase (PARP) inhibitors, a signature of HR-deficient cells[52,53]. On the contrary, our *in vivo* analysis using the *FYDR* transgenic locus system clearly showed that the absence of *Helq* does not overtly affect spontaneous or damage-induced HR levels in mice. In addition, the human

HELQ knockout cell lines used by Takata et al. did not show any reduction in the levels of spontaneous or MMC-induced sister chromatid exchange, a measure of crossover events resulting from HR. Together with the fact that, unlike *Helq*, most major HR genes are embryonic lethal in mice[54] and that *Helq*$^{gt/gt}$ males do not exhibit any meiotic defect, it is very difficult to imagine *Helq*/*HELQ* being a major HR gene at this time. A minor or backup role of HELQ should be tested in the future.

Finally, in contrast to our finding that *Helq*$^{gt/gt}$ mice exhibit no observable cancer phenotype, Adelman et al. reported that the same mouse model in their hands displayed a significant number of ovarian tumors and pituitary adenomas. Upon closer examination, however, this phenotype was actually very mild as the vast majority of the mice exhibited tumor-free survival beyond 500 days of age. Furthermore, a significant fraction of the wildtype mice in their study exhibited the same types of tumors at reduced frequencies. The fact that their mouse model was maintained in a mixed genetic background rather than a pure, inbred background like the C57BL/6J background we used could also explain some of the discrepancies between our studies. Still, a possible tumor suppressive role of *HELQ* in humans should not be overlooked as many FA genes which have little effect on mouse tumorigenesis[55] are found mutated in several sporadic human cancers[56]. Indeed, multiple genome-wide association studies have already identified SNPs in *HELQ* that are associated with upper-aerodigestive tract cancers and head and neck cancers[57-61].

The frequency of EdU spots, not MN, correlates more closely with cancer development

One thought-provoking observation from these studies is the lack of correlation between MN and cancer development. For example, while *Fancc*$^{-/-}$ (and especially *Helq*$^{gt/gt}$*;Fancc*$^{-/-}$) MEFs exhibited even higher MN frequencies than *Mcm4*$^{chaos3/chaos3}$ cells, these mice did not display any significant tumor phenotypes. This is interesting as the *Mcm4*^{chaos3} allele was originally identified in a genetic screen for increased levels of MN in erythrocytes with the idea that such chromosome instability might be an accurate marker of cancer susceptibility[62]. Since then, other studies have suggested that the defective replication and reintegration of micronucleus DNA could be a significant driver of the aneuploidy and/or chromosome pulverization observed in cancer[63]. However, our results in mice do not support this.

Rather, what distinguished *Mcm4*$^{chaos3/chaos3}$ cells from others was the number of late-replicating loci, manifesting as EdU spots in prophase. It is thus tempting to speculate that an inability to finish replication at these sites could lead to deletions in the resulting daughter cells, which may not otherwise be detected by the MN or 53BP1-NBs assays. Over time, such deletions could lead to the loss of tumor suppressor genes or cause other genetic alterations that drive *Mcm4*^{chaos3} tumorigenesis.

Future directions

What are the consequences of late-replicating loci?

Our findings indicate that the cancer phenotype of *Mcm4*$^{chaos3/chaos3}$ correlates better with an increased number of EdU spots rather than an increase in MN *per se*. This suggests that late-replicating/un-replicated regions may lead to a different form of genomic instability that has serious consequences for cancer progression. We have begun to test this by developing a series of pulse-chase experiments to determine the fate of late-replicating regions after prophase. By treating cells with a 10 minute pulse of EdU labeling and then waiting 90 minutes prior to fixation, we found that EdU detection could be achieved on metaphase spreads. Strikingly, we found that EdU spots can often be observed to co-localize at chromosome breaks and radial structures. Importantly, the frequency of such events was significantly elevated in *Mcm4*$^{chaos3/chaos3}$ and *Mcm4*$^{chaos3/chaos3}$*;Fancc*$^{-/-}$ mutant cells, and the majority of breaks in APH-treated cells contained EdU staining. Furthermore, dual labeling with fluorescent probes targeting mouse-specific fragile sites shows that a number of EdU-associated breaks occur at these sites. These preliminary findings strongly indicate that late-replicating regions, rather than stalled forks *per se*, are the major precursor to chromosome breakage at CFSs, in agreement with recent findings[36].

We have also utilized EdU pulse-labeling to determine the relationship between EdU spots and G1 phase markers of chromosome instability, namely MN and 53BP1-NBs. After a 10 minute pulse-labeling with EdU, cells were given 4 hours to progress

into G1 phase. G1 phase nuclei were then easily identified as those contained within binucleated cells using a protocol similar to the cytokinesis-block MN assay. Punctate EdU spots were observed in wildtype, *Mcm4*$^{chaos3/chaos3}$, *Fancc*$^{-/-}$ and *Mcm4*$^{chaos3/chaos3}$*;Fancc*$^{-/-}$ cells in similar ratios to those observed at prophase. However, the vast majority of these spots did not reside in the MN or 53BP1-NBs of these cells, suggesting that the majority of either of these markers do not arise directly from late-replicating/un-replicating regions. In addition, it is possible that EdU spots could manifest as a different form of genomic instability all together, like large deletions. While not as easily detectable as MN and 53BP1-NBs, such significant losses of genetic information could have a much greater effect on driving *Mcm4*^{chaos3} tumorigenesis. Future studies using array-based comparative genomic hybridization technology may be able to adequately address this intriguing possibility.

What are the distinct functions of the FA core complex and FANCD2?

Although the FA pathway is usually described as being one linear pathway, there is an abundance of evidence to suggest otherwise. As additional interactions and functions are identified for each component, this pathway grows more and more complex, blurring our understanding of what FA pathway functions correspond to FA disease phenotypes. For example, one study reported that the levels of genomic instability are higher in *Fancd2*$^{-/-}$ mice when compared to *Fancg*$^{-/-}$ mice, and that double homozygosity for these alleles results in embryonic lethality[64]. Therefore, distinguishing the separate

roles of individual FA pathway components is essential for us to more fully understand the FA pathway's role in genome stability.

One important study that could be done would be to test the effects of *Fancd2* nullizygosity in a *Mcm4*$^{chaos3/chaos3}$ mutant background, as we have done for *Fancc*. This would allow us to determine if the fork recovery mechanism performed by FANCC is mediated by FANCD2 or if it involves a distinct pathway (like FA core complex-stimulated TLS). We have already used such a strategy to test the genetic interaction between *Mcm4*^{chaos3} and *Brca2*$^{\Delta 27}$, a hypomorphic truncation allele of *Brca2*[65], revealing a synthetic lethal interaction between the two. It would be interesting to see if *Mcm4*$^{chaos3/chaos3}$*;Fancd2*$^{-/-}$ mice are viable in a C57BL/6J inbred genetic background and if their tumor latency is significantly different than that of *Mcm4*$^{chaos3/chaos3}$*;Fancc*$^{-/-}$ mice.

Is HELQ part of the downstream FA pathway?

Our data clearly indicate that HELQ is dispensable for FANCD2 monoubiquitination and is unlikely to be part of the FA core complex. However, this does not rule out the possibility of HELQ being a part of the downstream FA pathway. This would not be difficult to imagine seeing as the majority of the downstream FA members play a critical role in HR and that multiple studies (excluding our own) have implicated HELQ as either playing a role in HR[45,66-68] or associating with HR factors[45,47]. As a preliminary investigation, we have recently generated mice doubly mutant for the *Helq*^{gt} and *Brca2*$^{\Delta 27}$ alleles to test for epistasis. Thus far, the data indicate that the two

are non-epistatic for germ cell maintenance as well as suppressing replication-associated genome instability (MN and 53BP1-NBs). Although this does not completely rule out a potential role of HELQ in HR, this coincides with all our previous findings that HELQ is unlikely to be an essential HR factor or to function within the FA pathway.

Does *Helq* have any significant tumor-suppressive role in mice?

Because $Helq^{gt/gt}$ mice did not exhibit any tumor phenotype in our hands, we hypothesized that a more sensitized background, such as $Mcm4^{chaos3}$ homozygosity, might reveal a significant tumor suppressive role of *Helq*, much like it did for *Fancc*. However, our preliminary results clearly show that $Mcm4^{chaos3/chaos3}$;$Helq^{gt/gt}$ double mutants do not display any significant difference in tumor latency compared to $Mcm4^{chaos3/chaos3}$ single mutants. These data make it more difficult to implicate *Helq* as having a significant role in suppressing murine tumorigenesis at this time.

Can manipulation of HELQ activity provide a therapeutic benefit for FA patients?

Though it appears unlikely that *HELQ* is another FA gene, our findings do provide an intriguing possibility that it could be a therapeutic target for treating FA, as HELQ should be present in the cells of FA patients and work in parallel to the FA pathway to maintain genome stability. Our data suggest that down-regulation or disruption of *HELQ* as a method of killing cancer cells in FA would probably not be an

effective strategy, as *Helq*$^{gt/gt}$*;Fancc*$^{-/-}$ cells were fully viable and exhibited even greater genomic instability. However, strategies to up-regulate *HELQ* expression have potential to mitigate genomic instability in FA patient cells, as *HELQ* is normally so lowly expressed in humans[69]. Importantly, it seems unlikely that this would have any negative effect on cells. Transfecting FA patient cells with a robust *HELQ* expression vector and measuring its effects on genomic instability would be an effective first step in testing this possibility. Finally, it should be investigated whether the proteins found to interact with HELQ (such as the RAD51 paralogs) are also needed for stalled fork recovery in a manner that is non-epistatic to FA pathway members, as these also could be targeted for therapeutic benefit.

References

1 Woodward, A. M. *et al.* Excess Mcm2–7 license dormant origins of replication that can be used under conditions of replicative stress. *The Journal of Cell Biology* **173**, 673-683 (2006).

2 Ge, X. Q., Jackson, D. A. & Blow, J. J. Dormant origins licensed by excess Mcm2–7 are required for human cells to survive replicative stress. *Genes & Development* **21**, 3331-3341 (2007).

3 Ibarra, A., Schwob, E. & Méndez, J. Excess MCM proteins protect human cells from replicative stress by licensing backup origins of replication. *Proceedings of the National Academy of Sciences* **105**, 8956-8961 (2008).

4 Chan, K. L., Palmai-Pallag, T., Ying, S. & Hickson, I. D. Replication stress induces sister-chromatid bridging at fragile site loci in mitosis. *Nat Cell Biol* **11**, 753-760 (2009).

5 Naim, V. & Rosselli, F. The FANC pathway and BLM collaborate during mitosis to prevent micro-nucleation and chromosome abnormalities. *Nat Cell Biol* **11**, 761-768 (2009).

6 Letessier, A. *et al.* Cell-type-specific replication initiation programs set fragility of the FRA3B fragile site. *Nature* **470**, 120-123, doi:10.1038/nature09745 (2011).

7 Ozeri-Galai, E. *et al.* Failure of Origin Activation in Response to Fork Stalling Leads to Chromosomal Instability at Fragile Sites. *Molecular Cell* **43**, 122-131 (2011).

8 Shima, N. *et al.* A viable allele of Mcm4 causes chromosome instability and mammary adenocarcinomas in mice. *Nat Genet* **39**, 93-98 (2007).

9 Halazonetis, T. D., Gorgoulis, V. G. & Bartek, J. An oncogene-induced DNA damage model for cancer development. *Science* **319**, 1352-1355 (2008).

10 Sherr, C. J. The Pezcoller Lecture: Cancer Cell Cycles Revisited. *Cancer Research* **60**, 3689-3695 (2000).

11 Malumbres, M. & Barbacid, M. To cycle or not to cycle: a critical decision in cancer. *Nat Rev Cancer* **1**, 222-231 (2001).

12 Sidorova, J. M. & Breeden, L. L. Precocious G1/S transitions and genomic instability: the origin connection. *Mutat Res* **532**, 5-19 (2003).

13 Ekholm-Reed, S. *et al.* Deregulation of cyclin E in human cells interferes with prereplication complex assembly. *The Journal of Cell Biology* **165**, 789-800 (2004).

14 Bailis, J. M. & Forsburg, S. L. MCM proteins: DNA damage, mutagenesis and repair. *Current Opinion in Genetics & Development* **14**, 17-21 (2004).

15 Blow, J. J. & Gillespie, P. J. Replication licensing and cancer--a fatal entanglement? *Nat Rev Cancer* **8**, 799-806 (2008).

16 Gonzalez, M. A., Tachibana, K. E., Laskey, R. A. & Coleman, N. Control of DNA replication and its potential clinical exploitation. *Nat Rev Cancer* **5**, 135-141 (2005).

17 Shreeram, S., Sparks, A., Lane, D. P. & Blow, J. J. Cell type-specific responses of human cells to inhibition of replication licensing. *Oncogene* **21**, 6624-6632, doi:10.1038/sj.onc.1205910 (2002).
18 Nevis, K. R., Cordeiro-Stone, M. & Cook, J. G. Origin licensing and p53 status regulate Cdk2 activity during G1. *Cell Cycle* **8**, 1952-1963 (2009).
19 Quan Ge, X. & Blow, J. The licensing checkpoint opens up. *Cell Cycle* **8**, 2319-2323 (2009).
20 McIntosh, D. & Blow, J. J. Dormant Origins, the Licensing Checkpoint, and the Response to Replicative Stresses. *Cold Spring Harbor Perspectives in Biology* **4** (2012).
21 Feng, D., Tu, Z., Wu, W. & Liang, C. Inhibiting the Expression of DNA Replication-Initiation Proteins Induces Apoptosis in Human Cancer Cells. *Cancer Research* **63**, 7356-7364 (2003).
22 Zimmerman, K. M., Jones, R. M., Petermann, E. & Jeggo, P. A. Diminished Origin-Licensing Capacity Specifically Sensitizes Tumor Cells to Replication Stress. *Molecular Cancer Research* **11**, 370-380 (2013).
23 Casey, J. P., Nobbs, M., McGettigan, P., Lynch, S. & Ennis, S. Recessive mutations in MCM4/PRKDC cause a novel syndrome involving a primary immunodeficiency and a disorder of DNA repair. *Journal of Medical Genetics* **49**, 242-245 (2012).
24 Hughes, C. R. *et al.* MCM4 mutation causes adrenal failure, short stature, and natural killer cell deficiency in humans. *The Journal of Clinical Investigation* **122**, 814-820 (2012).
25 Gineau, L. *et al.* Partial MCM4 deficiency in patients with growth retardation, adrenal insufficiency, and natural killer cell deficiency. *The Journal of Clinical Investigation* **122**, 821-832 (2012).
26 Sobeck, A. *et al.* Fanconi Anemia Proteins Are Required To Prevent Accumulation of Replication-Associated DNA Double-Strand Breaks. *Molecular and Cellular Biology* **26**, 425-437 (2006).
27 Wang, L. C., Stone, S., Hoatlin, M. E. & Gautier, J. Fanconi anemia proteins stabilize replication forks. *DNA Repair* **7**, 1973-1981 (2008).
28 Schlacher, K., Wu, H. & Jasin, M. A Distinct Replication Fork Protection Pathway Connects Fanconi Anemia Tumor Suppressors to RAD51-BRCA1/2. *Cancer Cell* **22**, 106-116 (2012).
29 Niedzwiedz, W. *et al.* The Fanconi Anaemia Gene FANCC Promotes Homologous Recombination and Error-Prone DNA Repair. *Molecular Cell* **15**, 607-620 (2004).
30 Mirchandani, K. D., McCaffrey, R. M. & D'Andrea, A. D. The Fanconi anemia core complex is required for efficient point mutagenesis and Rev1 foci assembly. *DNA Repair* **7**, 902-911 (2008).
31 Kim, H., Yang, K., Dejsuphong, D. & D'Andrea, A. D. Regulation of Rev1 by the Fanconi anemia core complex. *Nat Struct Mol Biol* **19**, 164-170 (2012).

32 Chaudhury, I., Sareen, A., Raghunandan, M. & Sobeck, A. FANCD2 regulates BLM complex functions independently of FANCI to promote replication fork recovery. *Nucleic Acids Research* **41**, 6444-6459 (2013).
33 Bergoglio, V. *et al.* DNA synthesis by Pol η promotes fragile site stability by preventing under-replicated DNA in mitosis. *The Journal of Cell Biology* **201**, 395-408 (2013).
34 Fu, D. *et al.* Recruitment of DNA polymerase eta by FANCD2 in the early response to DNA damage. *Cell Cycle* **12**, 803-809 (2013).
35 Sato, K. *et al.* Histone chaperone activity of Fanconi anemia proteins, FANCD2 and FANCI, is required for DNA crosslink repair. *EMBO J* **31**, 3524-3536 (2012).
36 Naim, V., Wilhelm, T., Debatisse, M. & Rosselli, F. ERCC1 and MUS81–EME1 promote sister chromatid separation by processing late replication intermediates at common fragile sites during mitosis. *Nat Cell Biol* **15**, 1008-1015 (2013).
37 Ying, S. *et al.* MUS81 promotes common fragile site expression. *Nat Cell Biol* **15**, 1001-1007 (2013).
38 Kratz, K. *et al.* Deficiency of FANCD2-Associated Nuclease KIAA1018/FAN1 Sensitizes Cells to Interstrand Crosslinking Agents. *Cell* **142**, 77-88 (2010).
39 Liu, T., Ghosal, G., Yuan, J., Chen, J. & Huang, J. FAN1 Acts with FANCI-FANCD2 to Promote DNA Interstrand Cross-Link Repair. *Science* **329**, 693-696 (2010).
40 MacKay, C. *et al.* Identification of KIAA1018/FAN1, a DNA Repair Nuclease Recruited to DNA Damage by Monoubiquitinated FANCD2. *Cell* **142**, 65-76 (2010).
41 Smogorzewska, A. *et al.* A Genetic Screen Identifies FAN1, a Fanconi Anemia-Associated Nuclease Necessary for DNA Interstrand Crosslink Repair. *Molecular Cell* **39**, 36-47 (2010).
42 Klein Douwel, D. *et al.* XPF-ERCC1 Acts in Unhooking DNA Interstrand Crosslinks in Cooperation with FANCD2 and FANCP/SLX4. *Molecular Cell* **54**, 460-471 (2014).
43 Le Tallec, B. *et al.* Common Fragile Site Profiling in Epithelial and Erythroid Cells Reveals that Most Recurrent Cancer Deletions Lie in Fragile Sites Hosting Large Genes. *Cell Reports* **4**, 420-428 (2013).
44 Kawabata, T. *et al.* A reduction of licensed origins reveals strain-specific replication dynamics in mice. *Mammalian Genome* **22**, 506-517 (2011).
45 Adelman, C. A. *et al.* HELQ promotes RAD51 paralogue-dependent repair to avert germ cell loss and tumorigenesis. *Nature* **502**, 381-384 (2013).
46 Watanabe, N. *et al.* The REV7 Subunit of DNA Polymerase ζ Is Essential for Primordial Germ Cell Maintenance in the Mouse. *Journal of Biological Chemistry* **288**, 10459-10471 (2013).
47 Takata, K., Reh, S., Tomida, J., Person, M. D. & Wood, R. D. Human DNA helicase HELQ participates in DNA interstrand crosslink tolerance with ATR and RAD51 paralogs. *Nat Commun* **4**, 2338 (2013).

48 Masson, J.-Y. *et al.* Identification and purification of two distinct complexes containing the five RAD51 paralogs. *Genes & Development* **15**, 3296-3307 (2001).
49 Johnson, R. D., Liu, N. & Jasin, M. Mammalian XRCC2 promotes the repair of DNA double-strand breaks by homologous recombination. *Nature* **401**, 397-399 (1999).
50 Takata, M. *et al.* The Rad51 Paralog Rad51B Promotes Homologous Recombinational Repair. *Molecular and Cellular Biology* **20**, 6476-6482 (2000).
51 Takata, M. *et al.* Chromosome Instability and Defective Recombinational Repair in Knockout Mutants of the Five Rad51 Paralogs. *Molecular and Cellular Biology* **21**, 2858-2866 (2001).
52 Bryant, H. E. *et al.* Specific killing of BRCA2-deficient tumours with inhibitors of poly(ADP-ribose) polymerase. *Nature* **434**, 913-917 (2005).
53 Huehls, A. M., Wagner, J. M., Huntoon, C. J. & Karnitz, L. M. Identification of DNA Repair Pathways That Affect the Survival of Ovarian Cancer Cells Treated with a Poly(ADP-Ribose) Polymerase Inhibitor in a Novel Drug Combination. *Molecular Pharmacology* **82**, 767-776 (2012).
54 Friedberg, E. C. & Meira, L. B. Database of mouse strains carrying targeted mutations in genes affecting biological responses to DNA damage Version 7. *DNA Repair* **5**, 189-209 (2006).
55 Bakker, S. T., de Winter, J. P. & Riele, H. t. Learning from a paradox: recent insights into Fanconi anaemia through studying mouse models. *Disease Models & Mechanisms* **6**, 40-47 (2013).
56 Valeri, A., Martinez, S., Casado, J. A. & Bueren, J. A. Fanconi anaemia: from a monogenic disease to sporadic cancer. *Clin Transl Oncol* **13**, 215-221 (2011).
57 McKay, J. D. *et al.* A Genome-Wide Association Study of Upper Aerodigestive Tract Cancers Conducted within the INHANCE Consortium. *PLoS Genet* **7**, e1001333 (2011).
58 Liang, C. *et al.* Gene–environment interactions of novel variants associated with head and neck cancer. *Head & Neck* **34**, 1111-1118 (2012).
59 Gao, Y. *et al.* Genetic variants at 4q21, 4q23 and 12q24 are associated with esophageal squamous cell carcinoma risk in a Chinese population. *Human Genetics*, 1-8 (2013).
60 Li, W.-Q. *et al.* Genetic variants in DNA repair pathway genes and risk of esophageal squamous cell carcinoma and gastric adenocarcinoma in a Chinese population. *Carcinogenesis* **34**, 1536-1542 (2013).
61 Babron, M.-C. *et al.* Genetic variants in DNA repair pathways and risk of upper aerodigestive tract cancers: combined analysis of data from two genome-wide association studies in European populations. *Carcinogenesis* (2014).
62 Shima, N. *et al.* Phenotype-Based Identification of Mouse Chromosome Instability Mutants. *Genetics* **163**, 1031-1040 (2003).
63 Crasta, K. *et al.* DNA breaks and chromosome pulverization from errors in mitosis. *Nature* **482**, 53-58 (2012).

64 Reliene, R., Yamamoto, M. L., Rao, P. N. & Schiestl, R. H. Genomic Instability in Mice Is Greater in Fanconi Anemia Caused by Deficiency of Fancd2 than Fancg. *Cancer Research* **70**, 9703-9710 (2010).

65 McAllister, K. A. *et al.* Cancer Susceptibility of Mice with a Homozygous Deletion in the COOH-Terminal Domain of the Brca2 Gene. *Cancer Research* **62**, 990-994 (2002).

66 Ward, J. D. *et al.* Overlapping Mechanisms Promote Postsynaptic RAD-51 Filament Disassembly during Meiotic Double-Strand Break Repair. *Molecular Cell* **37**, 259-272 (2010).

67 Moldovan, G.-L. *et al.* DNA Polymerase POLN Participates in Cross-Link Repair and Homologous Recombination. *Molecular and Cellular Biology* **30**, 1088-1096 (2010).

68 McCaffrey, R., St Johnston, D. & González-Reyes, A. Drosophila mus301/spindle-C Encodes a Helicase With an Essential Role in Double-Strand DNA Break Repair and Meiotic Progression. *Genetics* **174**, 1273-1285 (2006).

69 Marini, F., Kim, N., Schuffert, A. & Wood, R. D. POLN, a Nuclear PolA Family DNA Polymerase Homologous to the DNA Cross-link Sensitivity Protein Mus308. *Journal of Biological Chemistry* **278**, 32014-32019 (2003).

Bibliography

1 Ciccia, A. & Elledge, S. J. The DNA Damage Response: Making It Safe to Play with Knives. Molecular Cell 40, 179-204 (2010).

2 Branzei, D. & Foiani, M. Maintaining genome stability at the replication fork. Nat Rev Mol Cell Biol 11, 208-219 (2010).

3 Méchali, M. Eukaryotic DNA replication origins: many choices for appropriate answers. Nat Rev Mol Cell Biol 11, 728-738 (2010).

4 Huberman, J. A. & Riggs, A. D. Autoradiography of chromosomal DNA fibers from Chinese hamster cells. Proc Natl Acad Sci U S A 55, 599-606 (1966).

5 Blow, J. J. & Dutta, A. Preventing re-replication of chromosomal DNA. Nat Rev Mol Cell Biol 6, 476-486 (2005).

6 Bell, S. P. & Stillman, B. ATP-dependent recognition of eukaryotic origins of DNA replication by a multiprotein complex. Nature 357, 128-134 (1992).

7 Coleman, T. R., Carpenter, P. B. & Dunphy, W. G. The Xenopus Cdc6 protein is essential for the initiation of a single round of DNA replication in cell-free extracts. Cell 87, 53-63 (1996).

8 Cocker, J. H., Piatti, S., Santocanale, C., Nasmyth, K. & Diffley, J. F. An essential role for the Cdc6 protein in forming the pre-replicative complexes of budding yeast. Nature 379, 180-182 (1996).

9 Perkins, G. & Diffley, J. F. Nucleotide-dependent prereplicative complex assembly by Cdc6p, a homolog of eukaryotic and prokaryotic clamp-loaders. Mol Cell 2, 23-32 (1998).

10 Randell, J. C., Bowers, J. L., Rodriguez, H. K. & Bell, S. P. Sequential ATP hydrolysis by Cdc6 and ORC directs loading of the Mcm2-7 helicase. Mol Cell 21, 29-39 (2006).

11 Nishitani, H., Lygerou, Z., Nishimoto, T. & Nurse, P. The Cdt1 protein is required to license DNA for replication in fission yeast. Nature 404, 625-628 (2000).

12 Whittaker, A. J., Royzman, I. & Orr-Weaver, T. L. Drosophila double parked: a conserved, essential replication protein that colocalizes with the origin recognition complex and links DNA replication with mitosis and the down-regulation of S phase transcripts. Genes Dev 14, 1765-1776 (2000).

13 Maiorano, D., Moreau, J. & Mechali, M. XCDT1 is required for the assembly of pre-replicative complexes in Xenopus laevis. Nature 404, 622-625 (2000).

14 Ishimi, Y. A DNA helicase activity is associated with an MCM4, -6, and -7 protein complex. J Biol Chem 272, 24508-24513 (1997).

15 Lee, J. K. & Hurwitz, J. Isolation and characterization of various complexes of the minichromosome maintenance proteins of Schizosaccharomyces pombe. J Biol Chem 275, 18871-18878 (2000).

16 Schwacha, A. & Bell, S. P. Interactions between two catalytically distinct MCM subgroups are essential for coordinated ATP hydrolysis and DNA replication. Mol Cell 8, 1093-1104 (2001).

17 You, Z., Ishimi, Y., Masai, H. & Hanaoka, F. Roles of Mcm7 and Mcm4 subunits in the DNA helicase activity of the mouse Mcm4/6/7 complex. J Biol Chem 277, 42471-42479 (2002).

18 Kaplan, D. L., Davey, M. J. & O'Donnell, M. Mcm4,6,7 uses a "pump in ring" mechanism to unwind DNA by steric exclusion and actively translocate along a duplex. J Biol Chem 278, 49171-49182 (2003).

19 Ying, C. Y. & Gautier, J. The ATPase activity of MCM2-7 is dispensable for pre-RC assembly but is required for DNA unwinding. EMBO J 24, 4334-4344 (2005).

20 Maine, G. T., Sinha, P. & Tye, B.-K. Mutants of S. Cerevisiae Defective in the Maintenance of Minichromosomes. Genetics 106, 365-385 (1984).

21 Remus, D. et al. Concerted Loading of Mcm2–7 Double Hexamers around DNA during DNA Replication Origin Licensing. Cell 139, 719-730 (2009).

22 Evrin, C. et al. A double-hexameric MCM2-7 complex is loaded onto origin DNA during licensing of eukaryotic DNA replication. Proceedings of the National Academy of Sciences 106, 20240-20245 (2009).

23 Gambus, A., Khoudoli, G. A., Jones, R. C. & Blow, J. J. MCM2-7 Form Double Hexamers at Licensed Origins in Xenopus Egg Extract. Journal of Biological Chemistry 286, 11855-11864 (2011).

24 Edwards, M. C. et al. MCM2–7 Complexes Bind Chromatin in a Distributed Pattern Surrounding the Origin Recognition Complex in Xenopus Egg Extracts. Journal of Biological Chemistry 277, 33049-33057 (2002).

25 Ge, X. Q., Jackson, D. A. & Blow, J. J. Dormant origins licensed by excess Mcm2–7 are required for human cells to survive replicative stress. Genes & Development 21, 3331-3341 (2007).

26 Ibarra, A., Schwob, E. & Méndez, J. Excess MCM proteins protect human cells from replicative stress by licensing backup origins of replication. Proceedings of the National Academy of Sciences 105, 8956-8961 (2008).

27 Donovan, S., Harwood, J., Drury, L. S. & Diffley, J. F. X. Cdc6p-dependent loading of Mcm proteins onto pre-replicative chromatin in budding yeast. Proceedings of the National Academy of Sciences 94, 5611-5616 (1997).

28 Bowers, J. L., Randell, J. C. W., Chen, S. & Bell, S. P. ATP Hydrolysis by ORC Catalyzes Reiterative Mcm2-7 Assembly at a Defined Origin of Replication. Molecular Cell 16, 967-978 (2004).

29 Cortez, D., Glick, G. & Elledge, S. J. Minichromosome maintenance proteins are direct targets of the ATM and ATR checkpoint kinases. Proceedings of the National Academy of Sciences of the United States of America 101, 10078-10083 (2004).

30 Woodward, A. M. et al. Excess Mcm2–7 license dormant origins of replication that can be used under conditions of replicative stress. The Journal of Cell Biology 173, 673-683 (2006).

31 Hyrien, O., Marheineke, K. & Goldar, A. Paradoxes of eukaryotic DNA replication: MCM proteins and the random completion problem. BioEssays 25, 116-125 (2003).

32 Perkins, G., Drury, L. S. & Diffley, J. F. Separate SCF(CDC4) recognition elements target Cdc6 for proteolysis in S phase and mitosis. EMBO J 20, 4836-4845 (2001).

33 Labib, K., Diffley, J. F. & Kearsey, S. E. G1-phase and B-type cyclins exclude the DNA-replication factor Mcm4 from the nucleus. Nat Cell Biol 1, 415-422 (1999).

34 Nguyen, V. Q., Co, C. & Li, J. J. Cyclin-dependent kinases prevent DNA re-replication through multiple mechanisms. Nature 411, 1068-1073 (2001).

35 Drury, L. S., Perkins, G. & Diffley, J. F. X. The cyclin-dependent kinase Cdc28p regulates distinct modes of Cdc6p proteolysis during the budding yeast cell cycle. Current Biology 10, 231-240 (2000).

36 McGarry, T. J. & Kirschner, M. W. Geminin, an inhibitor of DNA replication, is degraded during mitosis. Cell 93, 1043-1053 (1998).

37 Wohlschlegel, J. A. et al. Inhibition of eukaryotic DNA replication by geminin binding to Cdt1. Science 290, 2309-2312 (2000).

38 Tada, S., Li, A., Maiorano, D., Mechali, M. & Blow, J. J. Repression of origin assembly in metaphase depends on inhibition of RLF-B/Cdt1 by geminin. Nat Cell Biol 3, 107-113 (2001).

39 Cook, J. G., Chasse, D. A. & Nevins, J. R. The regulated association of Cdt1 with minichromosome maintenance proteins and Cdc6 in mammalian cells. J Biol Chem 279, 9625-9633 (2004).

40 Lee, C. et al. Structural basis for inhibition of the replication licensing factor Cdt1 by geminin. Nature 430, 913-917 (2004).

41 Zhong, W., Feng, H., Santiago, F. E. & Kipreos, E. T. CUL-4 ubiquitin ligase maintains genome stability by restraining DNA-replication licensing. Nature 423, 885-889 (2003).

42 Higa, L. A., Mihaylov, I. S., Banks, D. P., Zheng, J. & Zhang, H. Radiation-mediated proteolysis of CDT1 by CUL4-ROC1 and CSN complexes constitutes a new checkpoint. Nat Cell Biol 5, 1008-1015 (2003).

43 Hu, J., McCall, C. M., Ohta, T. & Xiong, Y. Targeted ubiquitination of CDT1 by the DDB1-CUL4A-ROC1 ligase in response to DNA damage. Nat Cell Biol 6, 1003-1009 (2004).

44 Rape, M., Reddy, S. K. & Kirschner, M. W. The Processivity of Multiubiquitination by the APC Determines the Order of Substrate Degradation. Cell 124, 89-103 (2006).

45 Arias, E. E. & Walter, J. C. PCNA functions as a molecular platform to trigger Cdt1 destruction and prevent re-replication. Nat Cell Biol 8, 84-90 (2006).

46 Senga, T. et al. PCNA is a cofactor for Cdt1 degradation by CUL4/DDB1-mediated N-terminal ubiquitination. J Biol Chem 281, 6246-6252 (2006).

47 Tercero, J. A., Labib, K. & Diffley, J. F. DNA synthesis at individual replication forks requires the essential initiation factor Cdc45p. EMBO J 19, 2082-2093 (2000).

48 Labib, K., Tercero, J. A. & Diffley, J. F. X. Uninterrupted MCM2-7 Function Required for DNA Replication Fork Progression. Science 288, 1643-1647 (2000).

49 Pacek, M. & Walter, J. C. A requirement for MCM7 and Cdc45 in chromosome unwinding during eukaryotic DNA replication. EMBO J 23, 3667-3676 (2004).

50 Gambus, A. et al. GINS maintains association of Cdc45 with MCM in replisome progression complexes at eukaryotic DNA replication forks. Nat Cell Biol 8, 358-366 (2006).

51 Moyer, S. E., Lewis, P. W. & Botchan, M. R. Isolation of the Cdc45/Mcm2–7/GINS (CMG) complex, a candidate for the eukaryotic DNA replication fork helicase. Proceedings of the National Academy of Sciences 103, 10236-10241 (2006).

52 Pacek, M., Tutter, A. V., Kubota, Y., Takisawa, H. & Walter, J. C. Localization of MCM2-7, Cdc45, and GINS to the Site of DNA Unwinding during Eukaryotic DNA Replication. Molecular Cell 21, 581-587 (2006).

53 Ilves, I., Petojevic, T., Pesavento, J. J. & Botchan, M. R. Activation of the MCM2-7 Helicase by Association with Cdc45 and GINS Proteins. Molecular Cell 37, 247-258 (2010).

54 Zou, L. & Stillman, B. Formation of a Preinitiation Complex by S-phase Cyclin CDK-Dependent Loading of Cdc45p onto Chromatin. Science 280, 593-596 (1998).

55 Masai, H. et al. Phosphorylation of MCM4 by Cdc7 Kinase Facilitates Its Interaction with Cdc45 on the Chromatin. Journal of Biological Chemistry 281, 39249-39261 (2006).

56 Tsuji, T., Ficarro, S. B. & Jiang, W. Essential Role of Phosphorylation of MCM2 by Cdc7/Dbf4 in the Initiation of DNA Replication in Mammalian Cells. Molecular Biology of the Cell 17, 4459-4472 (2006).

57 Sheu, Y.-J. & Stillman, B. Cdc7-Dbf4 Phosphorylates MCM Proteins via a Docking Site-Mediated Mechanism to Promote S Phase Progression. Molecular Cell 24, 101-113 (2006).

58 Sheu, Y. J. & Stillman, B. The Dbf4-Cdc7 kinase promotes S phase by alleviating an inhibitory activity in Mcm4. Nature 463, 113-117 (2010).

59 Masumoto, H., Muramatsu, S., Kamimura, Y. & Araki, H. S-Cdk-dependent phosphorylation of Sld2 essential for chromosomal DNA replication in budding yeast. Nature 415, 651-655 (2002).

60 Yabuuchi, H. et al. Ordered assembly of Sld3, GINS and Cdc45 is distinctly regulated by DDK and CDK for activation of replication origins. EMBO J 25, 4663-4674 (2006).

61 Tanaka, S. et al. CDK-dependent phosphorylation of Sld2 and Sld3 initiates DNA replication in budding yeast. Nature 445, 328-332 (2007).

62 Zegerman, P. & Diffley, J. F. Phosphorylation of Sld2 and Sld3 by cyclin-dependent kinases promotes DNA replication in budding yeast. Nature 445, 281-285 (2007).

63 Muramatsu, S., Hirai, K., Tak, Y.-S., Kamimura, Y. & Araki, H. CDK-dependent complex formation between replication proteins Dpb11, Sld2, Pol ε, and GINS in budding yeast. Genes & Development 24, 602-612 (2010).

64 Merchant, A. M., Kawasaki, Y., Chen, Y., Lei, M. & Tye, B. K. A lesion in the DNA replication initiation factor Mcm10 induces pausing of elongation forks

through chromosomal replication origins in Saccharomyces cerevisiae. Molecular and Cellular Biology 17, 3261-3271 (1997).

65 Wohlschlegel, J. A., Dhar, S. K., Prokhorova, T. A., Dutta, A. & Walter, J. C. Xenopus Mcm10 binds to origins of DNA replication after Mcm2-7 and stimulates origin binding of Cdc45. Molecular Cell 9, 233-240 (2002).

66 Balestrini, A., Cosentino, C., Errico, A., Garner, E. & Costanzo, V. GEMC1 is a TopBP1-interacting protein required for chromosomal DNA replication. Nat Cell Biol 12, 484-491 (2010).

67 Chowdhury, A. et al. The DNA Unwinding Element Binding Protein DUE-B Interacts with Cdc45 in Preinitiation Complex Formation. Molecular and Cellular Biology 30, 1495-1507 (2010).

68 Pefani, D.-E. et al. Idas, a Novel Phylogenetically Conserved Geminin-related Protein, Binds to Geminin and Is Required for Cell Cycle Progression. Journal of Biological Chemistry 286, 23234-23246 (2011).

69 Ricke, R. M. & Bielinsky, A. K. Mcm10 regulates the stability and chromatin association of DNA polymerase-α. Molecular Cell 16, 173-185 (2004).

70 Yan, H., Merchant, A. M. & Tye, B. K. Cell cycle-regulated nuclear localization of MCM2 and MCM3, which are required for the initiation of DNA synthesis at chromosomal replication origins in yeast. Genes & Development 7, 2149-2160 (1993).

71 Todorov, I. T., Attaran, A. & Kearsey, S. E. BM28, a human member of the MCM2-3-5 family, is displaced from chromatin during DNA replication. The Journal of Cell Biology 129, 1433-1445 (1995).

72 Krude, T., Musahl, C., Laskey, R. A. & Knippers, R. Human replication proteins hCdc21, hCdc46 and P1Mcm3 bind chromatin uniformly before S-phase and are displaced locally during DNA replication. Journal of Cell Science 109, 309-318 (1996).

73 Santocanale, C. & Diffley, J. F. ORC- and Cdc6-dependent complexes at active and inactive chromosomal replication origins in Saccharomyces cerevisiae. EMBO J 15, 6671-6679 (1996).

74 Gilbert, D. M. Replication timing and transcriptional control: beyond cause and effect. Current Opinion in Cell Biology 14, 377-383 (2002).

75 Tabancay Jr, A. P. & Forsburg, S. L. in Current Topics in Developmental Biology Vol. Volume 76 (ed P. Schatten Gerald) 129-184 (Academic Press, 2006).

76 Masai, H., Matsumoto, S., You, Z., Yoshizawa-Sugata, N. & Oda, M. Eukaryotic Chromosome DNA Replication: Where, When, and How? Annual Review of Biochemistry 79, 89-130 (2010).

77 Krasinska, L. et al. Cdk1 and Cdk2 activity levels determine the efficiency of replication origin firing in Xenopus. EMBO J 27, 758-769 (2008).

78 Patel, P. K. et al. The Hsk1(Cdc7) Replication Kinase Regulates Origin Efficiency. Molecular Biology of the Cell 19, 5550-5558 (2008).

79 Wu, P.-Y. J. & Nurse, P. Establishing the Program of Origin Firing during S Phase in Fission Yeast. Cell 136, 852-864 (2009).

80 Mantiero, D., Mackenzie, A., Donaldson, A. & Zegerman, P. Limiting replication initiation factors execute the temporal programme of origin firing in budding yeast. EMBO J 30, 4805-4814 (2011).

81 Tanaka, S., Nakato, R., Katou, Y., Shirahige, K. & Araki, H. Origin Association of Sld3, Sld7, and Cdc45 Proteins Is a Key Step for Determination of Origin-Firing Timing. Current Biology 21, 2055-2063 (2011).

82 Lei, M., Kawasaki, Y. & Tye, B. K. Physical interactions among Mcm proteins and effects of Mcm dosage on DNA replication in Saccharomyces cerevisiae. Molecular and Cellular Biology 16, 5081-5090 (1996).

83 Liang, D. T., Hodson, J. A. & Forsburg, S. L. Reduced dosage of a single fission yeast MCM protein causes genetic instability and S phase delay. Journal of Cell Science 112, 559-567 (1999).

84 Slater, M. L. Effect of Reversible Inhibition of Deoxyribonucleic Acid Synthesis on the Yeast Cell Cycle. Journal of Bacteriology 113, 263-270 (1973).

85 Santocanale, C. & Diffley, J. F. A Mec1- and Rad53-dependent checkpoint controls late-firing origins of DNA replication. Nature 395, 615-618 (1998).

86 Shirahige, K. et al. Regulation of DNA-replication origins during cell-cycle progression. Nature 395, 618-621 (1998).

87 Luciani, M. G., Oehlmann, M. & Blow, J. J. Characterization of a novel ATR-dependent, Chk1-independent, intra-S-phase checkpoint that suppresses initiation of replication in Xenopus. Journal of Cell Science 117, 6019-6030 (2004).

88 Maya-Mendoza, A., Petermann, E., Gillespie, D. A., Caldecott, K. W. & Jackson, D. A. Chk1 regulates the density of active replication origins during the vertebrate S phase. EMBO J 26, 2719-2731 (2007).

89 Ge, X. Q. & Blow, J. J. Chk1 inhibits replication factory activation but allows dormant origin firing in existing factories. The Journal of Cell Biology 191, 1285-1297 (2010).

90 Toledo, Luis I. et al. ATR Prohibits Replication Catastrophe by Preventing Global Exhaustion of RPA. Cell 155, 1088-1103 (2013).

91 Yekezare, M., Gómez-González, B. & Diffley, J. F. X. Controlling DNA replication origins in response to DNA damage – inhibit globally, activate locally. Journal of Cell Science 126, 1297-1306 (2013).

92 Shima, N. et al. Phenotype-Based Identification of Mouse Chromosome Instability Mutants. Genetics 163, 1031-1040 (2003).

93 Shima, N. et al. A viable allele of Mcm4 causes chromosome instability and mammary adenocarcinomas in mice. Nat Genet 39, 93-98 (2007).

94 Ikegami, S. et al. Aphidicolin prevents mitotic cell division by interfering with the activity of DNA polymerase-alpha. Nature 275, 458-460 (1978).

95 Cheng, C. H. & Kuchta, R. D. DNA polymerase epsilon: Aphidicolin inhibition and the relationship between polymerase and exonuclease activity. Biochemistry 32, 8568-8574 (1993).

96 Wright, G. E., Hübscher, U., Khan, N. N., Focher, F. & Verri, A. Inhibitor analysis of calf thymus DNA polymerases α, δ and ϵ. FEBS Letters 341, 128-130 (1994).

97 Pruitt, S. C., Bailey, K. J. & Freeland, A. Reduced Mcm2 Expression Results in Severe Stem/Progenitor Cell Deficiency and Cancer. Stem Cells 25, 3121-3132 (2007).

98 Kunnev, D. et al. DNA damage response and tumorigenesis in Mcm2-deficient mice. Oncogene 29, 3630-3638 (2010).

99 Kawabata, T. et al. A reduction of licensed origins reveals strain-specific replication dynamics in mice. Mammalian Genome 22, 506-517 (2011).

100 Chuang, C.-H., Wallace, M. D., Abratte, C., Southard, T. & Schimenti, J. C. Incremental Genetic Perturbations to MCM2-7 Expression and Subcellular Distribution Reveal Exquisite Sensitivity of Mice to DNA Replication Stress. PLoS Genet 6, e1001110 (2010).

101 Glover, T., Berger, C., Coyle, J. & Echo, B. DNA polymerase α inhibition by aphidicolin induces gaps and breaks at common fragile sites in human chromosomes. Human Genetics 67, 136-142 (1984).

102 Mrasek, K. et al. Global screening and extended nomenclature for 230 aphidicolin-inducible fragile sites, including 61 yet unreported ones. International Journal of Oncology 36, 929-940 (2010).

103 Letessier, A. et al. Cell-type-specific replication initiation programs set fragility of the FRA3B fragile site. Nature 470, 120-123 (2011).

104 Le Tallec, B. et al. Common Fragile Site Profiling in Epithelial and Erythroid Cells Reveals that Most Recurrent Cancer Deletions Lie in Fragile Sites Hosting Large Genes. Cell Reports 4, 420-428 (2013).

105 Zlotorynski, E. et al. Molecular Basis for Expression of Common and Rare Fragile Sites. Molecular and Cellular Biology 23, 7143-7151 (2003).

106 Shah, S. N., Opresko, P. L., Meng, X., Lee, M. Y. & Eckert, K. A. DNA structure and the Werner protein modulate human DNA polymerase delta-dependent replication dynamics within the common fragile site FRA16D. Nucleic Acids Res 38, 1149-1162 (2010).

107 Zhang, H. & Freudenreich, C. H. An AT-rich sequence in human common fragile site FRA16D causes fork stalling and chromosome breakage in S. cerevisiae. Mol Cell 27, 367-379 (2007).

108 Ozeri-Galai, E. et al. Failure of Origin Activation in Response to Fork Stalling Leads to Chromosomal Instability at Fragile Sites. Molecular Cell 43, 122-131 (2011).

109 Helmrich, A., Ballarino, M. & Tora, L. Collisions between Replication and Transcription Complexes Cause Common Fragile Site Instability at the Longest Human Genes. Molecular Cell 44, 966-977 (2011).

110 Le Beau, M. M. et al. Replication of a Common Fragile Site, FRA3B, Occurs Late in S Phase and is Delayed Further Upon Induction: Implications for the Mechanism of Fragile Site Induction. Human Molecular Genetics 7, 755-761 (1998).

111 Wang, L. et al. Allele-specific Late Replication and Fragility of the Most Active Common Fragile Site, FRA3B. Human Molecular Genetics 8, 431-437 (1999).

112 Palakodeti, A., Han, Y., Jiang, Y. & Le Beau, M. M. The role of late/slow replication of the FRA16D in common fragile site induction. Genes, Chromosomes and Cancer 39, 71-76 (2004).

113 Casper, A. M., Nghiem, P., Arlt, M. F. & Glover, T. W. ATR regulates fragile site stability. Cell 111, 779-789 (2002).

114 Casper, A. M., Durkin, S. G., Arlt, M. F. & Glover, T. W. Chromosomal Instability at Common Fragile Sites in Seckel Syndrome. The American Journal of Human Genetics 75, 654-660 (2004).

115 Durkin, S. G., Arlt, M. F., Howlett, N. G. & Glover, T. W. Depletion of CHK1, but not CHK2, induces chromosomal instability and breaks at common fragile sites. Oncogene 25, 4381-4388 (2006).

116 Howlett, N. G., Taniguchi, T., Durkin, S. G., D'Andrea, A. D. & Glover, T. W. The Fanconi anemia pathway is required for the DNA replication stress response and for the regulation of common fragile site stability. Human Molecular Genetics 14, 693-701 (2005).

117 Sobeck, A. et al. Fanconi Anemia Proteins Are Required To Prevent Accumulation of Replication-Associated DNA Double-Strand Breaks. Molecular and Cellular Biology 26, 425-437 (2006).

118 Wang, L. C., Stone, S., Hoatlin, M. E. & Gautier, J. Fanconi anemia proteins stabilize replication forks. DNA Repair 7, 1973-1981 (2008).

119 Schlacher, K., Wu, H. & Jasin, M. A Distinct Replication Fork Protection Pathway Connects Fanconi Anemia Tumor Suppressors to RAD51-BRCA1/2. Cancer Cell 22, 106-116 (2012).

120 Garcia-Higuera, I. et al. Interaction of the Fanconi Anemia Proteins and BRCA1 in a Common Pathway. Molecular Cell 7, 249-262 (2001).

121 Taniguchi, T. et al. S-phase–specific interaction of the Fanconi anemia protein, FANCD2, with BRCA1 and RAD51. Blood 100, 2414-2420 (2002).

122 Chan, K. L., Palmai-Pallag, T., Ying, S. & Hickson, I. D. Replication stress induces sister-chromatid bridging at fragile site loci in mitosis. Nat Cell Biol 11, 753-760 (2009).

123 Naim, V. & Rosselli, F. The FANC pathway and BLM collaborate during mitosis to prevent micro-nucleation and chromosome abnormalities. Nat Cell Biol 11, 761-768 (2009).

124 Baumann, C., Körner, R., Hofmann, K. & Nigg, E. A. PICH, a Centromere-Associated SNF2 Family ATPase, Is Regulated by Plk1 and Required for the Spindle Checkpoint. Cell 128, 101-114 (2007).

125 Chan, K. L., North, P. S. & Hickson, I. D. BLM is required for faithful chromosome segregation and its localization defines a class of ultrafine anaphase bridges. EMBO J 26, 3397-3409 (2007).

126 Lukas, C. et al. 53BP1 nuclear bodies form around DNA lesions generated by mitotic transmission of chromosomes under replication stress. Nat Cell Biol 13, 243-253 (2011).

127 Blackford, A. N. et al. The DNA translocase activity of FANCM protects stalled replication forks. Human Molecular Genetics 21, 2005-2016 (2012).

128 Vinciguerra, P., Godinho, S. A., Parmar, K., Pellman, D. & D'Andrea, A. D. Cytokinesis failure occurs in Fanconi anemia pathway–deficient murine and human bone marrow hematopoietic cells. The Journal of Clinical Investigation 120, 3834-3842 (2010).

129 Rosenberg, P. S., Tamary, H. & Alter, B. P. How high are carrier frequencies of rare recessive syndromes? Contemporary estimates for Fanconi Anemia in the United States and Israel. American Journal of Medical Genetics Part A 155, 1877-1883 (2011).

130 Crossan, G. P. & Patel, K. J. The Fanconi anaemia pathway orchestrates incisions at sites of crosslinked DNA. The Journal of Pathology 226, 326-337 (2012).

131 Kottemann, M. C. & Smogorzewska, A. Fanconi anaemia and the repair of Watson and Crick DNA crosslinks. Nature 493, 356-363 (2013).

132 Bogliolo, M. et al. Mutations in ERCC4, Encoding the DNA-Repair Endonuclease XPF, Cause Fanconi Anemia. The American Journal of Human Genetics 92, 800-806 (2013).

133 Kashiyama, K. et al. Malfunction of Nuclease ERCC1-XPF Results in Diverse Clinical Manifestations and Causes Cockayne Syndrome, Xeroderma Pigmentosum, and Fanconi Anemia. The American Journal of Human Genetics 92, 807-819 (2013).

134 Schroeder, T. M., Anschütz, F. & Knopp, A. Spontane Chromosomenaberrationen bei familiärer Panmyelopathie. Humangenetik 1, 194-196 (1964).

135 Kubbies, M., Schindler, D., Hoehn, H., Schinzel, A. & Rabinovitch, P. S. Endogenous blockage and delay of the chromosome cycle despite normal recruitment and growth phase explain poor proliferation and frequent edomitosis in Fanconi anemia cells. Am J Hum Genet 37, 1022-1030 (1985).

136 Sasaki, M. S. & Tonomura, A. A high susceptibility of Fanconi's anemia to chromosome breakage by DNA cross linking agents. Cancer Research 33, 1829-1836 (1973).

137 Zamble, D. B. & Lippard, S. J. Cisplatin and DNA repair in cancer chemotherapy. Trends in Biochemical Sciences 20, 435-439 (1995).

138 Auerbach, A. D., Rogatko, A. & Schroeder-Kurth, T. M. International Fanconi Anemia Registry: Relation of clinical symptoms to diepoxybutane sensitivity. Blood 73, 391-396 (1989).

139 Auerbach, A. D. Fanconi anemia diagnosis and the diepoxybutane (DEB) test. Experimental Hematology 21, 731-733 (1993).

140 Singh, T. R. et al. MHF1-MHF2, a Histone-Fold-Containing Protein Complex, Participates in the Fanconi Anemia Pathway via FANCM. Molecular Cell 37, 879-886 (2010).

141 Meetei, A. R. et al. A novel ubiquitin ligase is deficient in Fanconi anemia. Nat Genet 35, 165-170 (2003).

142 Smogorzewska, A. et al. Identification of the FANCI Protein, a Monoubiquitinated FANCD2 Paralog Required for DNA Repair. Cell 129, 289-301 (2007).

143 Sims, A. E. et al. FANCI is a second monoubiquitinated member of the Fanconi anemia pathway. Nat Struct Mol Biol 14, 564-567 (2007).

144 Wooster, R. et al. Localization of a breast cancer susceptibility gene, BRCA2, to chromosome 13q12-13. Science 265, 2088-2090 (1994).

145 Rafnar, T. et al. Mutations in BRIP1 confer high risk of ovarian cancer. Nat Genet 43, 1104-1107 (2011).

146 Seal, S. et al. Truncating mutations in the Fanconi anemia J gene BRIP1 are low-penetrance breast cancer susceptibility alleles. Nat Genet 38, 1239-1241 (2006).

147 Rahman, N. et al. PALB2, which encodes a BRCA2-interacting protein, is a breast cancer susceptibility gene. Nat Genet 39, 165-167 (2007).

148 Tischkowitz, M. et al. Analysis of PALB2/FANCN-associated breast cancer families. Proc Natl Acad Sci U S A 104, 6788-6793 (2007).

149 Meindl, A. et al. Germline mutations in breast and ovarian cancer pedigrees establish RAD51C as a human cancer susceptibility gene. Nat Genet 42, 410-414 (2010).

150 Räschle, M. et al. Mechanism of Replication-Coupled DNA Interstrand Crosslink Repair. Cell 134, 969-980 (2008).

151 Knipscheer, P. et al. The Fanconi Anemia Pathway Promotes Replication-Dependent DNA Interstrand Cross-Link Repair. Science 326, 1698-1701 (2009).

152 Zhang, J. & Walter, J. C. Mechanism and regulation of incisions during DNA interstrand cross-link repair. DNA Repair 19, 135-142 (2014).

153 Klein Douwel, D. et al. XPF-ERCC1 Acts in Unhooking DNA Interstrand Crosslinks in Cooperation with FANCD2 and FANCP/SLX4. Molecular Cell 54, 460-471 (2014).

154 Hodskinson, Michael R. G. et al. Mouse SLX4 Is a Tumor Suppressor that Stimulates the Activity of the Nuclease XPF-ERCC1 in DNA Crosslink Repair. Molecular Cell 54, 472-484 (2014).

155 Long, D. T., Räschle, M., Joukov, V. & Walter, J. C. Mechanism of RAD51-Dependent DNA Interstrand Cross-Link Repair. Science 333, 84-87 (2011).

156 Lindahl, T. & Barnes, D. E. Repair of Endogenous DNA Damage. Cold Spring Harbor Symposia on Quantitative Biology 65, 127-134 (2000).

157 Ceccaldi, R. et al. Bone Marrow Failure in Fanconi Anemia Is Triggered by an Exacerbated p53/p21 DNA Damage Response that Impairs Hematopoietic Stem and Progenitor Cells. Cell Stem Cell 11, 36-49 (2012).

158 Langevin, F., Crossan, G. P., Rosado, I. V., Arends, M. J. & Patel, K. J. Fancd2 counteracts the toxic effects of naturally produced aldehydes in mice. Nature 475, 53-58 (2011).

159 Rosado, I. V., Langevin, F., Crossan, G. P., Takata, M. & Patel, K. J. Formaldehyde catabolism is essential in cells deficient for the Fanconi anemia DNA-repair pathway. Nat Struct Mol Biol 18, 1432-1434 (2011).

160 Wang, M. et al. Identification of DNA Adducts of Acetaldehyde. Chemical Research in Toxicology 13, 1149-1157 (2000).

161 Stein, S., Lao, Y., Yang, I. Y., Hecht, S. S. & Moriya, M. Genotoxicity of acetaldehyde- and crotonaldehyde-induced 1,N2-propanodeoxyguanosine DNA adducts in human cells. Mutat Res 608, 1-7 (2006).

162 Cheng, G. et al. Reactions of Formaldehyde Plus Acetaldehyde with Deoxyguanosine and DNA: Formation of Cyclic Deoxyguanosine Adducts and Formaldehyde Cross-Links. Chemical Research in Toxicology 16, 145-152 (2003).

163 Agoulnik, A. I. et al. A novel gene, Pog, is necessary for primordial germ cell proliferation in the mouse and underlies the germ cell deficient mutation, gcd. Human Molecular Genetics 11, 3047-3053 (2002).

164 Nadler, J. J. & Braun, R. E. Fanconi anemia complementation group C is required for proliferation of murine primordial germ cells. Genesis 27, 117-123 (2000).

165 Parmar, K., D'Andrea, A. & Niedernhofer, L. J. Mouse models of Fanconi anemia. Mutation Research/Fundamental and Molecular Mechanisms of Mutagenesis 668, 133-140 (2009).

166 Bakker, S. T., de Winter, J. P. & Riele, H. t. Learning from a paradox: recent insights into Fanconi anaemia through studying mouse models. Disease Models & Mechanisms 6, 40-47 (2013).

167 Wong, J. C. et al. Targeted disruption of exons 1 to 6 of the Fanconi Anemia group A gene leads to growth retardation, strain-specific microphthalmia, meiotic defects and primordial germ cell hypoplasia. Hum Mol Genet 12, 2063-2076 (2003).

168 Carreau, M. Not-so-novel phenotypes in the Fanconi anemia group D2 mouse model. Blood 103, 2430 (2004).

169 Houghtaling, S. et al. Epithelial cancer in Fanconi anemia complementation group D2 (Fancd2) knockout mice. Genes & Development 17, 2021-2035 (2003).

170 Crossan, G. P. et al. Disruption of mouse Slx4, a regulator of structure-specific nucleases, phenocopies Fanconi anemia. Nat Genet 43, 147-152 (2011).

171 Boyd, J. B., Golino, M. D., Shaw, K. E. S., Osgood, C. J. & Green, M. M. Third-Chromosome Mutagen-Sensitive Mutants of Drosophila Melanogaster. Genetics 97, 607-623 (1981).

172 McCaffrey, R., St Johnston, D. & González-Reyes, A. Drosophila mus301/spindle-C Encodes a Helicase With an Essential Role in Double-Strand DNA Break Repair and Meiotic Progression. Genetics 174, 1273-1285 (2006).

173 Muzzini, D. M., Plevani, P., Boulton, S. J., Cassata, G. & Marini, F. Caenorhabditis elegans POLQ-1 and HEL-308 function in two distinct DNA interstrand cross-link repair pathways. DNA Repair 7, 941-950 (2008).

174 Ward, J. D. et al. Overlapping Mechanisms Promote Postsynaptic RAD-51 Filament Disassembly during Meiotic Double-Strand Break Repair. Molecular Cell 37, 259-272 (2010).

175 Moldovan, G.-L. et al. DNA Polymerase POLN Participates in Cross-Link Repair and Homologous Recombination. Molecular and Cellular Biology 30, 1088-1096 (2010).

176 Tafel, A. A., Wu, L. & McHugh, P. J. Human HEL308 Localizes to Damaged Replication Forks and Unwinds Lagging Strand Structures. Journal of Biological Chemistry 286, 15832-15840 (2011).

177 Nowell, P. C. The clonal evolution of tumor cell populations. Science 194, 23-28 (1976).

178 Loeb, L. A. Mutator phenotype may be required for multistage carcinogenesis. Cancer Res 51, 3075-3079 (1991).

179 Kinzler, K. W. & Vogelstein, B. Cancer-susceptibility genes. Gatekeepers and caretakers. Nature 386, 761, 763 (1997).

180 Negrini, S., Gorgoulis, V. G. & Halazonetis, T. D. Genomic instability--an evolving hallmark of cancer. Nat Rev Mol Cell Biol 11, 220-228 (2010).

181 Sjoblom, T. et al. The consensus coding sequences of human breast and colorectal cancers. Science 314, 268-274 (2006).

182 Wood, L. D. et al. The genomic landscapes of human breast and colorectal cancers. Science 318, 1108-1113 (2007).

183 Jones, S. et al. Core signaling pathways in human pancreatic cancers revealed by global genomic analyses. Science 321, 1801-1806 (2008).

184 Parsons, D. W. et al. An integrated genomic analysis of human glioblastoma multiforme. Science 321, 1807-1812 (2008).

185 Bartkova, J. et al. DNA damage response as a candidate anti-cancer barrier in early human tumorigenesis. Nature 434, 864-870 (2005).

186 Gorgoulis, V. G. et al. Activation of the DNA damage checkpoint and genomic instability in human precancerous lesions. Nature 434, 907-913 (2005).

187 Bartkova, J. et al. Oncogene-induced senescence is part of the tumorigenesis barrier imposed by DNA damage checkpoints. Nature 444, 633-637 (2006).

188 Di Micco, R. et al. Oncogene-induced senescence is a DNA damage response triggered by DNA hyper-replication. Nature 444, 638-642 (2006).

189 Halazonetis, T. D., Gorgoulis, V. G. & Bartek, J. An oncogene-induced DNA damage model for cancer development. Science 319, 1352-1355 (2008).

190 Beroukhim, R. et al. The landscape of somatic copy-number alteration across human cancers. Nature 463, 899-905 (2010).

191 Bignell, G. R. et al. Signatures of mutation and selection in the cancer genome. Nature 463, 893-898 (2010).

192 Sclafani, R. A. & Holzen, T. M. Cell Cycle Regulation of DNA Replication. Annual Review of Genetics 41, 237-280 (2007).

193 Forsburg, S. L. Eukaryotic MCM Proteins: Beyond Replication Initiation. Microbiol. Mol. Biol. Rev. 68, 109-131 (2004).

194 Tye, B. K. MCM Proteins in DNA Replication. Annual Review of Biochemistry 68, 649-686 (1999).

195 Gilbert, D. M. In search of the holy replicator. Nat Rev Mol Cell Biol 5, 848-855 (2004).

196 Ha, S.-A. et al. Cancer-Associated Expression of Minichromosome Maintenance 3 Gene in Several Human Cancers and Its Involvement in Tumorigenesis. Clinical Cancer Research 10, 8386-8395 (2004).

197 Ishimi, Y. et al. Enhanced expression of Mcm proteins in cancer cells derived from uterine cervix. European Journal of Biochemistry 270, 1089-1101 (2003).

198 Sugimura, K., Takebayashi, S.-i., Ogata, S., Taguchi, H. & Okumura, K. Non-Denaturing Fluorescence in Situ Hybridization to Find Replication Origins in a Specific Genome Region on the DNA Fiber. Bioscience, Biotechnology, and Biochemistry 71, 627-632 (2007).

199 Byun, T. S., Pacek, M., Yee, M.-c., Walter, J. C. & Cimprich, K. A. Functional uncoupling of MCM helicase and DNA polymerase activities activates the ATR-dependent checkpoint. Genes & Development 19, 1040-1052 (2005).

200 Zou, L. & Elledge, S. J. Sensing DNA Damage Through ATRIP Recognition of RPA-ssDNA Complexes. Science 300, 1542-1548 (2003).

201 Bao, S. et al. ATR/ATM-mediated phosphorylation of human Rad17 is required for genotoxic stress responses. Nature 411, 969-974 (2001).

202 Wang, X. et al. Rad17 Phosphorylation Is Required for Claspin Recruitment and Chk1 Activation in Response to Replication Stress. Molecular Cell 23, 331-341 (2006).

203 Tsao, C. C., Geisen, C. & Abraham, R. T. Interaction between human MCM7 and Rad17 proteins is required for replication checkpoint signaling. EMBO J 23, 4660-4669 (2004).

204 Rogakou, E. P., Pilch, D. R., Orr, A. H., Ivanova, V. S. & Bonner, W. M. DNA Double-stranded Breaks Induce Histone H2AX Phosphorylation on Serine 139. Journal of Biological Chemistry 273, 5858-5868 (1998).

205 Petermann, E., Orta, M. L., Issaeva, N., Schultz, N. & Helleday, T. Hydroxyurea-Stalled Replication Forks Become Progressively Inactivated and Require Two Different RAD51-Mediated Pathways for Restart and Repair. Molecular Cell 37, 492-502 (2010).

206 Bugreev, D. V., Yu, X., Egelman, E. H. & Mazin, A. V. Novel pro- and anti-recombination activities of the Bloom's syndrome helicase. Genes & Development 21, 3085-3094 (2007).

207 Davies, S. L., North, P. S. & Hickson, I. D. Role for BLM in replication-fork restart and suppression of origin firing after replicative stress. Nat Struct Mol Biol 14, 677-679 (2007).

208 Gibson, S. I., Surosky, R. T. & Tye, B. K. The phenotype of the minichromosome maintenance mutant mcm3 is characteristic of mutants defective in DNA replication. Molecular and Cellular Biology 10, 5707-5720 (1990).

209 Li, X. C., Schimenti, J. C. & Tye, B. K. Aneuploidy and improved growth are coincident but not causal in a yeast cancer model. PLoS Biol 7, e1000161 (2009).

210 Hendricks, C. A. et al. Spontaneous mitotic homologous recombination at an enhanced yellow fluorescent protein (EYFP) cDNA direct repeat in transgenic mice. Proc Natl Acad Sci U S A 100, 6325-6330 (2003).

211 Saleh-Gohari , N. et al. Spontaneous Homologous Recombination Is Induced by Collapsed Replication Forks That Are Caused by Endogenous DNA Single-Strand Breaks. Molecular and Cellular Biology 25, 7158-7169 (2005).

212 Howman, E. V. et al. Early disruption of centromeric chromatin organization in centromere protein A (Cenpa) null mice. Proceedings of the National Academy of Sciences 97, 1148-1153 (2000).

213 Williams, B. R. et al. Aneuploidy affects proliferation and spontaneous immortalization in mammalian cells. Science 322, 703-709 (2008).

214 Blackwell, B.-N., Bucci, T. J., Hart, R. W. & Turturro, A. Longevity, Body Weight, and Neoplasia in Ad Libitum-Fed and Diet-Restricted C57BL6 Mice Fed NIH-31 Open Formula Diet. Toxicologic Pathology 23, 570-582 (1995).

215 Pileri, S. A. et al. Tumours of histiocytes and accessory dendritic cells: an immunohistochemical approach to classification from the International Lymphoma Study Group based on 61 cases. Histopathology 41, 1-29 (2002).

216 Paulsen, R. D. & Cimprich, K. A. The ATR pathway: Fine-tuning the fork. DNA Repair 6, 953-966 (2007).

217 Orr, S. J. et al. Reducing MCM levels in human primary T cells during the G(0)-->G(1) transition causes genomic instability during the first cell cycle. Oncogene 29, 3803-3814 (2010).

218 Liang, D. T., Hodson, J. A. & Forsburg, S. L. Reduced dosage of a single fission yeast MCM protein causes genetic instability and S phase delay. Journal of Cell Science 112, 559-567 (1999).

219 Lee, J. A., Carvalho, C. M. B. & Lupski, J. R. A DNA Replication Mechanism for Generating Nonrecurrent Rearrangements Associated with Genomic Disorders. Cell 131, 1235-1247 (2007).

220 Prakash, S., Johnson, R. E. & Prakash, L. Eukaryotic translesion synthesis DNA polymerases: specificity of structure and function. Annu Rev Biochem 74, 317-353, doi:10.1146/annurev.biochem.74.082803.133250 (2005).

221 Chan, K. L. & Hickson, I. D. On the origins of ultra-fine anaphase bridges. Cell Cycle 8, 3065-3066 (2009).

222 Sherr, C. J. The Pezcoller Lecture: Cancer Cell Cycles Revisited. Cancer Research 60, 3689-3695 (2000).

223 Fenech, M. Cytokinesis-block micronucleus cytome assay. Nat. Protocols 2, 1084-1104 (2007).

224 Shi, Q. & King, R. W. Chromosome nondisjunction yields tetraploid rather than aneuploid cells in human cell lines. Nature 437, 1038-1042 (2005).

225 Zellner, E., Herrmann, T., Schulz, C. & Grummt, F. Site-specific interaction of the murine pre-replicative complex with origin DNA: assembly and disassembly during cell cycle transit and differentiation. Nucleic Acids Res 35, 6701-6713 (2007).

226 Sotillo, R. et al. Mad2 overexpression promotes aneuploidy and tumorigenesis in mice. Cancer Cell 11, 9-23 (2007).

227 Farkash-Amar, S. et al. Global organization of replication time zones of the mouse genome. Genome Res 18, 1562-1570 (2008).

228 Bochman, M. L., Bell, S. P. & Schwacha, A. Subunit organization of Mcm2-7 and the unequal role of active sites in ATP hydrolysis and viability. Mol Cell Biol 28, 5865-5873 (2008).

229 Shechter, D., Ying, C. Y. & Gautier, J. DNA Unwinding Is an MCM Complex-dependent and ATP Hydrolysis-dependent Process. Journal of Biological Chemistry 279, 45586-45593 (2004).

230 Burkhart, R. et al. Interactions of Human Nuclear Proteins P1Mcm3 and P1Cdc46. European Journal of Biochemistry 228, 431-438 (1995).

231 Rowles, A. et al. Interaction between the Origin Recognition Complex and the Replication Licensing Systemin Xenopus. Cell 87, 287-296 (1996).

232 Mahbubani, H. M., Chong, J. P. J., Chevalier, S., Thömmes, P. & Blow, J. J. Cell Cycle Regulation of the Replication Licensing System: Involvement of a Cdk-dependent Inhibitor. The Journal of Cell Biology 136, 125-135 (1997).

233 Kawabata, T. et al. Stalled Fork Rescue via Dormant Replication Origins in Unchallenged S Phase Promotes Proper Chromosome Segregation and Tumor Suppression. Molecular Cell 41, 543-553 (2011).

234 Blow, J. J., Ge, X. Q. & Jackson, D. A. How dormant origins promote complete genome replication. Trends in Biochemical Sciences 36, 405-414 (2011).

235 Constantinou, A. Rescue of replication failure by Fanconi anaemia proteins. Chromosoma 121, 21-36 (2012).

236 Kee, Y. & D'Andrea, A. D. Expanded roles of the Fanconi anemia pathway in preserving genomic stability. Genes & Development 24, 1680-1694 (2010).

237 Ikegami, S., Taguchi, T., Ohashi, M., Nagano, H. & Mano, Y. Aphidicolin prevents mitotic cell division by interfering with the activity of DNA polymerase-alpha. Nature 275, 458-460 (1978).

238 Durkin, S. G. & Glover, T. W. Chromosome Fragile Sites. Annual Review of Genetics 41, 169-192 (2007).

239 Whitney, M. et al. Germ cell defects and hematopoietic hypersensitivity to gamma-interferon in mice with a targeted disruption of the Fanconi anemia C gene. Blood 88, 49-58 (1996).

240 Kawabata, T. et al. A reduction of licensed origins reveals strain-specific replication dynamics in mice. Mammalian Genome 22, 506-517 (2011).

241 Luebben, S. W. et al. Helq acts in parallel to Fancc to suppress replication-associated genome instability. Nucleic Acids Research (2013).

242 Harrigan, J. A. et al. Replication stress induces 53BP1-containing OPT domains in G1 cells. The Journal of Cell Biology 193, 97-108 (2011).

243 Chaudhury, I., Sareen, A., Raghunandan, M. & Sobeck, A. FANCD2 regulates BLM complex functions independently of FANCI to promote replication fork recovery. Nucleic Acids Research 41, 6444-6459 (2013).

244 Bergoglio, V. et al. DNA synthesis by Pol η promotes fragile site stability by preventing under-replicated DNA in mitosis. The Journal of Cell Biology 201, 395-408 (2013).

245 Naim, V., Wilhelm, T., Debatisse, M. & Rosselli, F. ERCC1 and MUS81–EME1 promote sister chromatid separation by processing late replication intermediates at common fragile sites during mitosis. Nat Cell Biol 15, 1008-1015 (2013).

246 Freie, B. et al. Fanconi anemia type C and p53 cooperate in apoptosis and tumorigenesis. Blood 102, 4146-4152 (2003).

247 Wallace, M. D., Southard, T. L., Schimenti, K. J. & Schimenti, J. C. Role of DNA damage response pathways in preventing carcinogenesis caused by intrinsic replication stress. Oncogene (2013).

248 Niedzwiedz, W. et al. The Fanconi Anaemia Gene FANCC Promotes Homologous Recombination and Error-Prone DNA Repair. Molecular Cell 15, 607-620 (2004).

249 Mirchandani, K. D., McCaffrey, R. M. & D'Andrea, A. D. The Fanconi anemia core complex is required for efficient point mutagenesis and Rev1 foci assembly. DNA Repair 7, 902-911 (2008).

250 Kim, H., Yang, K., Dejsuphong, D. & D'Andrea, A. D. Regulation of Rev1 by the Fanconi anemia core complex. Nat Struct Mol Biol 19, 164-170 (2012).

251 Lossaint, G. et al. FANCD2 Binds MCM Proteins and Controls Replisome Function upon Activation of S Phase Checkpoint Signaling. Molecular Cell 51, 678-690 (2013).

252 Ying, S. et al. MUS81 promotes common fragile site expression. Nat Cell Biol 15, 1001-1007 (2013).

253 Tischkowitz, M. & Winqvist, R. Using mouse models to investigate the biological and physiological consequences of defects in the Fanconi anaemia/breast cancer DNA repair signalling pathway. The Journal of Pathology 224, 301-305 (2011).

254 Hughes, C. R. et al. MCM4 mutation causes adrenal failure, short stature, and natural killer cell deficiency in humans. The Journal of Clinical Investigation 122, 814-820 (2012).

255 Gineau, L. et al. Partial MCM4 deficiency in patients with growth retardation, adrenal insufficiency, and natural killer cell deficiency. The Journal of Clinical Investigation 122, 821-832 (2012).

256 Hendzel, M. J. et al. Mitosis-specific phosphorylation of histone H3 initiates primarily within pericentromeric heterochromatin during G2 and spreads in an ordered fashion coincident with mitotic chromosome condensation. Chromosoma 106, 348-360 (1997).

257 Blow, J. J. & Ge, X. Q. A model for DNA replication showing how dormant origins safeguard against replication fork failure. EMBO Rep 10, 406-412 (2009).

258 Petermann, E. & Helleday, T. Pathways of mammalian replication fork restart. Nat Rev Mol Cell Biol 11, 683-687 (2010).

259 Sale, J. E., Lehmann, A. R. & Woodgate, R. Y-family DNA polymerases and their role in tolerance of cellular DNA damage. Nat Rev Mol Cell Biol 13, 141-152 (2012).

260 Kim, H. & D'Andrea, A. D. Regulation of DNA cross-link repair by the Fanconi anemia/BRCA pathway. Genes Dev 26, 1393-1408 (2012).

261 Marini, F. & Wood, R. D. A Human DNA Helicase Homologous to the DNA Cross-link Sensitivity Protein Mus308. Journal of Biological Chemistry 277, 8716-8723 (2002).

262 Boyd, J. B., Sakaguchi, K. & Harris, P. V. mus308 mutants of Drosophila exhibit hypersensitivity to DNA cross-linking agents and are defective in a deoxyribonuclease. Genetics 125, 813-819 (1990).

263 Leonhardt, E. A., Henderson, D. S., Rinehart, J. E. & Boyd, J. B. Characterization of the mus308 gene in Drosophila melanogaster. Genetics 133, 87-96 (1993).

264 Shima, N., Munroe, R. J. & Schimenti, J. C. The Mouse Genomic Instability Mutation chaos1 Is an Allele of Polq That Exhibits Genetic Interaction with Atm. Molecular and Cellular Biology 24, 10381-10389 (2004).

265 Yoshimura, M. et al. Vertebrate POLQ and POLβ Cooperate in Base Excision Repair of Oxidative DNA Damage. Molecular Cell 24, 115-125 (2006).

266 Yousefzadeh, M. J. & Wood, R. D. DNA polymerase POLQ and cellular defense against DNA damage. DNA Repair (Amst) 12, 1-9 (2013).

267 Harris, P. V. et al. Molecular cloning of Drosophila mus308, a gene involved in DNA cross-link repair with homology to prokaryotic DNA polymerase I genes. Mol Cell Biol 16, 5764-5771 (1996).

268 Seki, M., Marini, F. & Wood, R. D. POLQ (Pol theta), a DNA polymerase and DNA-dependent ATPase in human cells. Nucleic Acids Res 31, 6117-6126 (2003).

269 Laurencon, A. et al. A large-scale screen for mutagen-sensitive loci in Drosophila. Genetics 167, 217-231, doi:167/1/217 (2004).

270 Marini, F., Kim, N., Schuffert, A. & Wood, R. D. POLN, a nuclear PolA family DNA polymerase homologous to the DNA cross-link sensitivity protein Mus308. J Biol Chem 278, 32014-32019 (2003).

271 Youds, J. L., Barber, L. J. & Boulton, S. J. C. elegans: A model of Fanconi anemia and ICL repair. Mutation Research/Fundamental and Molecular Mechanisms of Mutagenesis 668, 103-116 (2009).

272 Stryke, D. et al. BayGenomics: a resource of insertional mutations in mouse embryonic stem cells. Nucleic Acids Research 31, 278-281 (2003).

273 Stanford, W. L., Cohn, J. B. & Cordes, S. P. Gene-trap mutagenesis: past, present and beyond. Nat Rev Genet 2, 756-768 (2001).

274 Fujikane, R., Komori, K., Shinagawa, H. & Ishino, Y. Identification of a Novel Helicase Activity Unwinding Branched DNAs from the Hyperthermophilic Archaeon, Pyrococcus furiosus. Journal of Biological Chemistry 280, 12351-12358 (2005).

275 Buttner, K., Nehring, S. & Hopfner, K. P. Structural basis for DNA duplex separation by a superfamily-2 helicase. Nat Struct Mol Biol 14, 647-652 (2007).

276 Woodman, I. L., Briggs, G. S. & Bolt, E. L. Archaeal Hel308 Domain V Couples DNA Binding to ATP Hydrolysis and Positions DNA for Unwinding Over the Helicase Ratchet. Journal of Molecular Biology 374, 1139-1144 (2007).

277 Richards, J. D. et al. Structure of the DNA Repair Helicase Hel308 Reveals DNA Binding and Autoinhibitory Domains. Journal of Biological Chemistry 283, 5118-5126 (2008).

278 Lu, B. & Bishop, C. E. Late Onset of Spermatogenesis and Gain of Fertility in POG-Deficient Mice Indicate that POG Is Not Necessary for the Proliferation of Spermatogonia. Biology of Reproduction 69, 161-168 (2003).

279 Yang, Y. et al. Targeted disruption of the murine Fanconi anemia gene,Fancg/Xrcc9. Blood 98, 3435-3440 (2001).

280 Bakker, S. T. et al. Fancm-deficient mice reveal unique features of Fanconi anemia complementation group M. Human Molecular Genetics 18, 3484-3495, doi:10.1093/hmg/ddp297 (2009).

281 Bakker, S. T. et al. Fancf-deficient mice are prone to develop ovarian tumours. J Pathol 226, 28-39, doi:10.1002/path.2992 (2012).

282 Chen, M. et al. Inactivation of Fac in mice produces inducible chromosomal instability and reduced fertility reminiscent of Fanconi anaemia. Nat Genet 12, 448-451 (1996).

283 Noll, M. et al. Fanconi anemia group A and C double-mutant mice: Functional evidence for a multi-protein Fanconi anemia complex. Experimental Hematology 30, 679-688 (2002).

284 Foe, J. R. et al. Expression cloning of a cDNA for the major Fanconi anaemia gene, FAA. Nat Genet 14, 488 (1996).

285 Guy, C. P. & Bolt, E. L. Archaeal Hel308 helicase targets replication forks in vivo and in vitro and unwinds lagging strands. Nucleic Acids Research 33, 3678-3690 (2005).

286 Howlett, N. G. et al. Biallelic Inactivation of BRCA2 in Fanconi Anemia. Science 297, 606-609 (2002).

287 Reid, S. et al. Biallelic mutations in PALB2 cause Fanconi anemia subtype FA-N and predispose to childhood cancer. Nat Genet 39, 162-164 (2007).

288 van de Vrugt, H. J. et al. Evidence for complete epistasis of null mutations in murine Fanconi anemia genes Fanca and Fancg. DNA Repair 10, 1252-1261 (2011).

289 Kitao, H. et al. Functional Interplay between BRCA2/FancD1 and FancC in DNA Repair. Journal of Biological Chemistry 281, 21312-21320 (2006).

290 Friedberg, E. C. & Meira, L. B. Database of mouse strains carrying targeted mutations in genes affecting biological responses to DNA damage Version 7. DNA Repair 5, 189-209 (2006).

291 Woodman, I. L. & Bolt, E. L. Molecular biology of Hel308 helicase in archaea. Biochem Soc Trans 37, 74-78 (2009).

292 Oyama, T. et al. Atomic structures and functional implications of the archaeal RecQ-like helicase Hjm. BMC Struct Biol 9, 2 (2009).

293 Zhang, C. et al. Genetic manipulation in Sulfolobus islandicus and functional analysis of DNA repair genes. Biochem Soc Trans 41, 405-410 (2013).

294 Fujikane, R., Shinagawa, H. & Ishino, Y. The archaeal Hjm helicase has recQ-like functions, and may be involved in repair of stalled replication fork. Genes to Cells 11, 99-110 (2006).

295 Li, W.-Q. et al. Genetic variants in DNA repair pathway genes and risk of esophageal squamous cell carcinoma and gastric adenocarcinoma in a Chinese population. Carcinogenesis 34, 1536-1542 (2013).

296 Gao, Y. et al. Genetic variants at 4q21, 4q23 and 12q24 are associated with esophageal squamous cell carcinoma risk in a Chinese population. Human Genetics, 1-8 (2013).

297 Liang, C. et al. Gene–environment interactions of novel variants associated with head and neck cancer. Head & Neck 34, 1111-1118 (2012).

298 McKay, J. D. et al. A Genome-Wide Association Study of Upper Aerodigestive Tract Cancers Conducted within the INHANCE Consortium. PLoS Genet 7, e1001333 (2011).

299 Malumbres, M. & Barbacid, M. To cycle or not to cycle: a critical decision in cancer. Nat Rev Cancer 1, 222-231 (2001).

300 Sidorova, J. M. & Breeden, L. L. Precocious G1/S transitions and genomic instability: the origin connection. Mutat Res 532, 5-19 (2003).

301 Ekholm-Reed, S. et al. Deregulation of cyclin E in human cells interferes with prereplication complex assembly. The Journal of Cell Biology 165, 789-800 (2004).

302 Bailis, J. M. & Forsburg, S. L. MCM proteins: DNA damage, mutagenesis and repair. Current Opinion in Genetics & Development 14, 17-21 (2004).

303 Blow, J. J. & Gillespie, P. J. Replication licensing and cancer--a fatal entanglement? Nat Rev Cancer 8, 799-806 (2008).

304 Gonzalez, M. A., Tachibana, K. E., Laskey, R. A. & Coleman, N. Control of DNA replication and its potential clinical exploitation. Nat Rev Cancer 5, 135-141 (2005).

305 Shreeram, S., Sparks, A., Lane, D. P. & Blow, J. J. Cell type-specific responses of human cells to inhibition of replication licensing. Oncogene 21, 6624-6632, doi:10.1038/sj.onc.1205910 (2002).

306 Nevis, K. R., Cordeiro-Stone, M. & Cook, J. G. Origin licensing and p53 status regulate Cdk2 activity during G1. Cell Cycle 8, 1952-1963 (2009).

307 Quan Ge, X. & Blow, J. The licensing checkpoint opens up. Cell Cycle 8, 2319-2323 (2009).

308 McIntosh, D. & Blow, J. J. Dormant Origins, the Licensing Checkpoint, and the Response to Replicative Stresses. Cold Spring Harbor Perspectives in Biology 4 (2012).

309 Feng, D., Tu, Z., Wu, W. & Liang, C. Inhibiting the Expression of DNA Replication-Initiation Proteins Induces Apoptosis in Human Cancer Cells. Cancer Research 63, 7356-7364 (2003).

310 Zimmerman, K. M., Jones, R. M., Petermann, E. & Jeggo, P. A. Diminished Origin-Licensing Capacity Specifically Sensitizes Tumor Cells to Replication Stress. Molecular Cancer Research 11, 370-380 (2013).

311 Casey, J. P., Nobbs, M., McGettigan, P., Lynch, S. & Ennis, S. Recessive mutations in MCM4/PRKDC cause a novel syndrome involving a primary immunodeficiency and a disorder of DNA repair. Journal of Medical Genetics 49, 242-245 (2012).

312 Fu, D. et al. Recruitment of DNA polymerase eta by FANCD2 in the early response to DNA damage. Cell Cycle 12, 803-809 (2013).

313 Sato, K. et al. Histone chaperone activity of Fanconi anemia proteins, FANCD2 and FANCI, is required for DNA crosslink repair. EMBO J 31, 3524-3536 (2012).

314 Kratz, K. et al. Deficiency of FANCD2-Associated Nuclease KIAA1018/FAN1 Sensitizes Cells to Interstrand Crosslinking Agents. Cell 142, 77-88 (2010).

315 Liu, T., Ghosal, G., Yuan, J., Chen, J. & Huang, J. FAN1 Acts with FANCI-FANCD2 to Promote DNA Interstrand Cross-Link Repair. Science 329, 693-696 (2010).

316 MacKay, C. et al. Identification of KIAA1018/FAN1, a DNA Repair Nuclease Recruited to DNA Damage by Monoubiquitinated FANCD2. Cell 142, 65-76 (2010).

317 Smogorzewska, A. et al. A Genetic Screen Identifies FAN1, a Fanconi Anemia-Associated Nuclease Necessary for DNA Interstrand Crosslink Repair. Molecular Cell 39, 36-47 (2010).

318 Adelman, C. A. et al. HELQ promotes RAD51 paralogue-dependent repair to avert germ cell loss and tumorigenesis. Nature 502, 381-384 (2013).

319 Watanabe, N. et al. The REV7 Subunit of DNA Polymerase ζ Is Essential for Primordial Germ Cell Maintenance in the Mouse. Journal of Biological Chemistry 288, 10459-10471 (2013).

320 Takata, K., Reh, S., Tomida, J., Person, M. D. & Wood, R. D. Human DNA helicase HELQ participates in DNA interstrand crosslink tolerance with ATR and RAD51 paralogs. Nat Commun 4, 2338 (2013).

321 Masson, J.-Y. et al. Identification and purification of two distinct complexes containing the five RAD51 paralogs. Genes & Development 15, 3296-3307 (2001).

322 Johnson, R. D., Liu, N. & Jasin, M. Mammalian XRCC2 promotes the repair of DNA double-strand breaks by homologous recombination. Nature 401, 397-399 (1999).

323 Takata, M. et al. The Rad51 Paralog Rad51B Promotes Homologous Recombinational Repair. Molecular and Cellular Biology 20, 6476-6482 (2000).

324 Takata, M. et al. Chromosome Instability and Defective Recombinational Repair in Knockout Mutants of the Five Rad51 Paralogs. Molecular and Cellular Biology 21, 2858-2866 (2001).

325 Bryant, H. E. et al. Specific killing of BRCA2-deficient tumours with inhibitors of poly(ADP-ribose) polymerase. Nature 434, 913-917 (2005).

326 Huehls, A. M., Wagner, J. M., Huntoon, C. J. & Karnitz, L. M. Identification of DNA Repair Pathways That Affect the Survival of Ovarian Cancer Cells Treated with a Poly(ADP-Ribose) Polymerase Inhibitor in a Novel Drug Combination. Molecular Pharmacology 82, 767-776 (2012).

327 Valeri, A., Martinez, S., Casado, J. A. & Bueren, J. A. Fanconi anaemia: from a monogenic disease to sporadic cancer. Clin Transl Oncol 13, 215-221 (2011).

328 Babron, M.-C. et al. Genetic variants in DNA repair pathways and risk of upper aerodigestive tract cancers: combined analysis of data from two genome-wide association studies in European populations. Carcinogenesis (2014).

329 Crasta, K. et al. DNA breaks and chromosome pulverization from errors in mitosis. Nature 482, 53-58 (2012).

330 Reliene, R., Yamamoto, M. L., Rao, P. N. & Schiestl, R. H. Genomic Instability in Mice Is Greater in Fanconi Anemia Caused by Deficiency of Fancd2 than Fancg. Cancer Research 70, 9703-9710 (2010).

331 McAllister, K. A. et al. Cancer Susceptibility of Mice with a Homozygous Deletion in the COOH-Terminal Domain of the Brca2 Gene. Cancer Research 62, 990-994 (2002).